Vegetation–Water Dynamics in the Australian Landscape

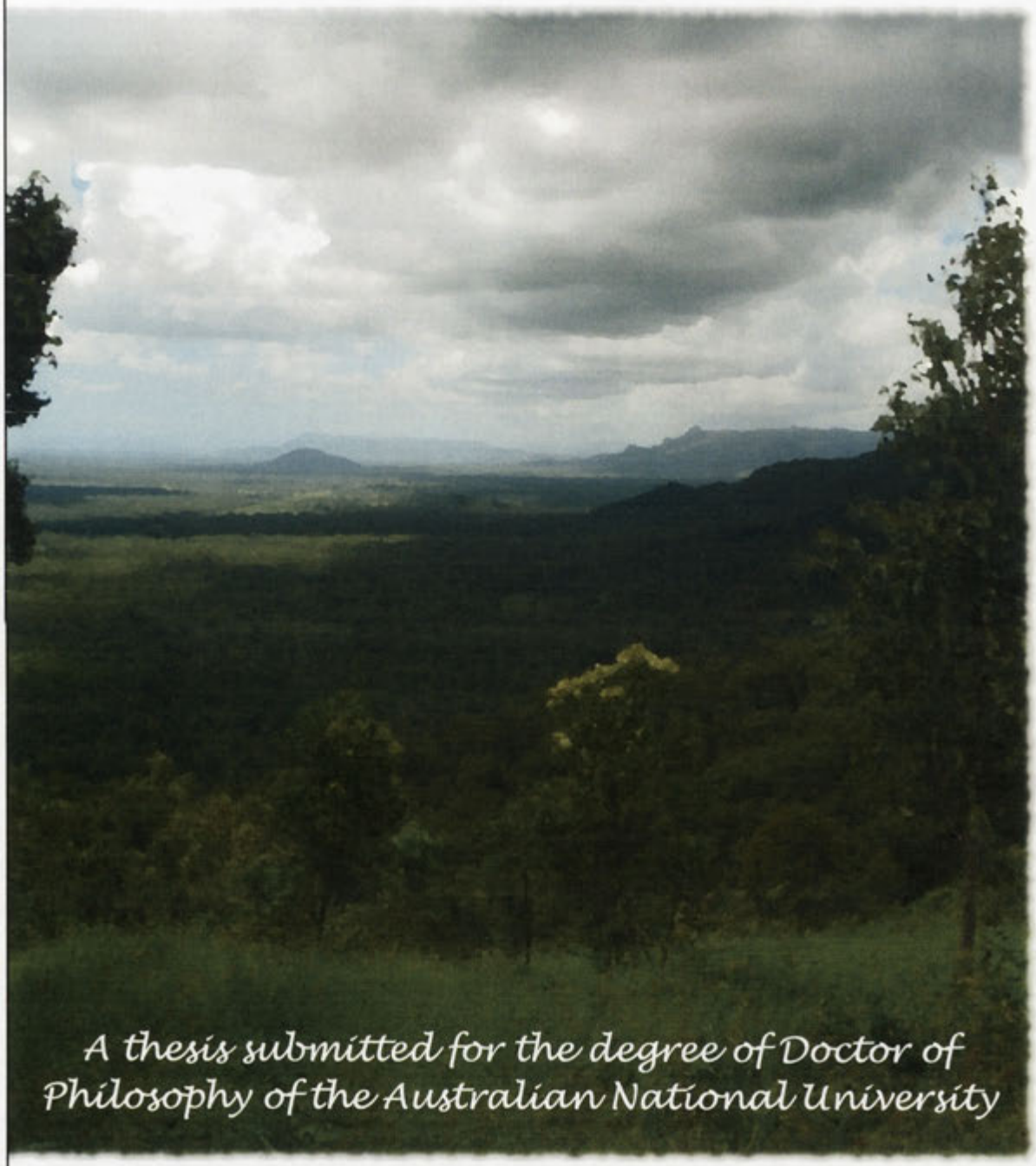

A thesis submitted for the degree of Doctor of Philosophy of the Australian National University

Randall James Donohue

December 2009

The work presented in this thesis is my own unless otherwise stated.

Randall J Donohue

1 December 2009

Acknowledgements

My two supervisors, Dr Michael Roderick and Dr Tim McVicar, have been superb. Both have taught me valuable lessons of science and shown me different perspectives and approaches to research. Each has freely given of their time and knowledge and friendship. Any success with which this thesis meets is because of their excellence as supervisors. I am very grateful to them.

The Research School of Biological Sciences, of the Australian National University, kindly provided me with a PhD position and scholarship. CSIRO Land and Water very generously provided a CLW Top-up Scholarship without which this research would not have been possible. In the latter stages of the degree the support of CLW, and Tim in particular, have been critical and is much appreciated.

Many have helped in this research in different ways. I would like to thank my supervisory panel for their time, which consisted of Pr. Graham Farquhar (chair), Dr Sandy Berry, Dr Lu Zhang, Dr Brendan Mackey and Dr Kim Ritman. Of those people who kindly provided comments on drafts of the material presented in this thesis I particularly wish to acknowledge Tom Van Niel and Sandy Berry.

The achievements of the past five or so years of which I am most proud are my three daughters, Olivia, Adelaide and *in utero*. Taryn, my wife, has supported me whole-heartedly, endured my foibles and given me her love. Nice one, gorgeous.

Table of Contents

* Note that the page numbering within Chapters 2–4 is the numbering assigned by the journals in which each chapter's research has been published. Such numbering is presented in italics. The numbering of the remaining chapters, as well as the title pages of the afore-mentioned chapters, follow the '1-1' format outlined in the Table of Contents.

Abstract

The study of the interactions between vegetation and water is an important research field in water-limited environments such as typically occur across Australia. Vegetation functioning and water availability are intimately linked in drier environments, generally existing in a dynamic equilibrium. The research presented herein utilises the concept of vegetation equilibrium to examine whether satellite-derived vegetation cover information can be used to enhance current understanding of ecohydrological processes.

Two research hypotheses are tested. The **first hypothesis** states that the observed changes in growing conditions across Australia over the past two and a half decades will have increased Australia's average vegetation cover and that such changes should be evident in satellite-derived fPAR data (the fraction of Photosynthetically Active Radiation absorbed by vegetation, which is proportional to the fraction of green cover). A consistent, long-term record of remotely sensed fPAR data, spanning 1981–2006, is created using a novel method developed herein. In this method, Advanced Very High Resolution Radiometer red and near infra-red reflectance data are linearly transformed to ensure the position of the vegetation cover triangle is temporally stable in reflectance space. The first hypothesis is tested by identifying linear trends in total, persistent and recurrent fPAR (the latter two variables approximate the cover of perennial and annual vegetation types, respectively, and are derived here using a newly developed technique). Results show that an average increase in total fPAR has occurred (an increase of 8%), due to large increases in persistent fPAR (up 21%) and despite decreases in recurrent fPAR (down 7%). Results also show that increases in persistent fPAR were not always linked to changes in precipitation, leading to the possibility that some of the observed 'greening' may be due to higher concentrations of atmospheric CO_2. Overall, this research implies that Australia has, on average, become effectively wetter over the past 2–3 decades.

A variety of processes can perturb the hydrological cycle including dynamics in vegetation cover (via associated changes in water use) and the roles of persistent and recurrent vegetation dynamics have not previously been considered in catchment hydrological models. The **second hypothesis** of this research is that the incorporation of fPAR data into Budyko's hydrological model can improve this model's accuracy, especially at smaller spatial and shorter temporal scales. Alongside stream flow,

precipitation and fPAR data, estimates of potential evaporation are required as an input to the Budyko modelling. No Australian long-term, fully dynamic potential evaporation data existed prior to this research. Consequently, five representations of potential evaporation are generated and assessed as to how well each captures the annual, seasonal and long-term temporal dynamics in evaporative demand over the study period. The Penman formulation, calculated using remotely sensed surface albedo and a new wind speed dataset developed for this research, is identified as the most appropriate formulation for use in the Budyko modelling. In testing the second hypothesis, it was found that the incorporation of fPAR data into the Budyko model, whilst improving stream flow predictions at the long-term annual average time-scale, did not improve predictions at the shorter annual time-scale. It is speculated that this is because fPAR data were unable to account for changes in water storage as hypothesised. Future research may yet prove that vegetation dynamics are a key ecohydrological forcing at small time-scales if water storage effects can be first addressed.

Publication of research

Donohue RJ, Roderick ML and McVicar TR (2007) On the importance of including vegetation dynamics in Budyko's hydrological model. *Hydrology and Earth System Sciences*, 11, 983-995.

Donohue RJ, Roderick ML and McVicar TR (2008) Deriving consistent long-term vegetation information from AVHRR reflectance data using a cover-triangle-based framework. *Remote Sensing of Environment*, 112, 2938-2949 DOI:10.1016/j.rse.2008.02.008.

Donohue RJ, McVicar TR and Roderick ML (2009) Climate-related trends in Australian vegetation cover as inferred from satellite observations, 1981–2006. *Global Change Biology*, 15, 1025-1039. DOI: 10.1111/j.1365-2486.2008.01746.x

Donohue RJ, McVicar TR and Roderick ML (2009) Assessing the ability of potential evaporation formulations to capture the dynamics in evaporative demand within a changing climate. *Journal of Hydrology*, Submitted manuscript.

Donohue RJ, Roderick ML and McVicar TR (2009) Can dynamic vegetation information improve the accuracy of Budyko's hydrological model? *Journal of Hydrology*, Submitted manuscript.

CHAPTER 1

Vegetation–water dynamics in the Australian landscape

1.1 Vegetation–water dynamics in the Australian landscape

In dry landscapes, such as typically occur across Australia, vegetation cover is generally a function of water availability (Nix, 1982; Specht, 1981). The distribution and productivity of Australia's vegetation closely reflects that of precipitation and climatic dryness (Figure 1). It has been long-established that vegetation is dependent on the availability of resources needed for growth, that is, solar radiation, water, nutrients and atmospheric gases (namely CO_2 but also O_2) (Forman, 1964; Holdridge, 1947; Field et al., 1992; Austin, 1980) and that it dynamically responds to changes in the availability of such resources—particularly those that are most limiting (e.g., Nix, 1978; Blackman, 1905). The study of vegetation–water dynamics is the focus of the relatively young and emerging field of ecohydrology.

Ecohydrology is an important research field for countries such as Australia where the supply of water is scarce and the productivity of landscapes is intimately tied to water dynamics. As vegetation is the primary medium of land management, improving understanding of ecohydrological processes is crucial for natural resource management. Uncertainty (and even confusion) about the likely effects of climate change further complicates this picture. Consequently there is an increasing need for greater understanding of ecohydrological processes.

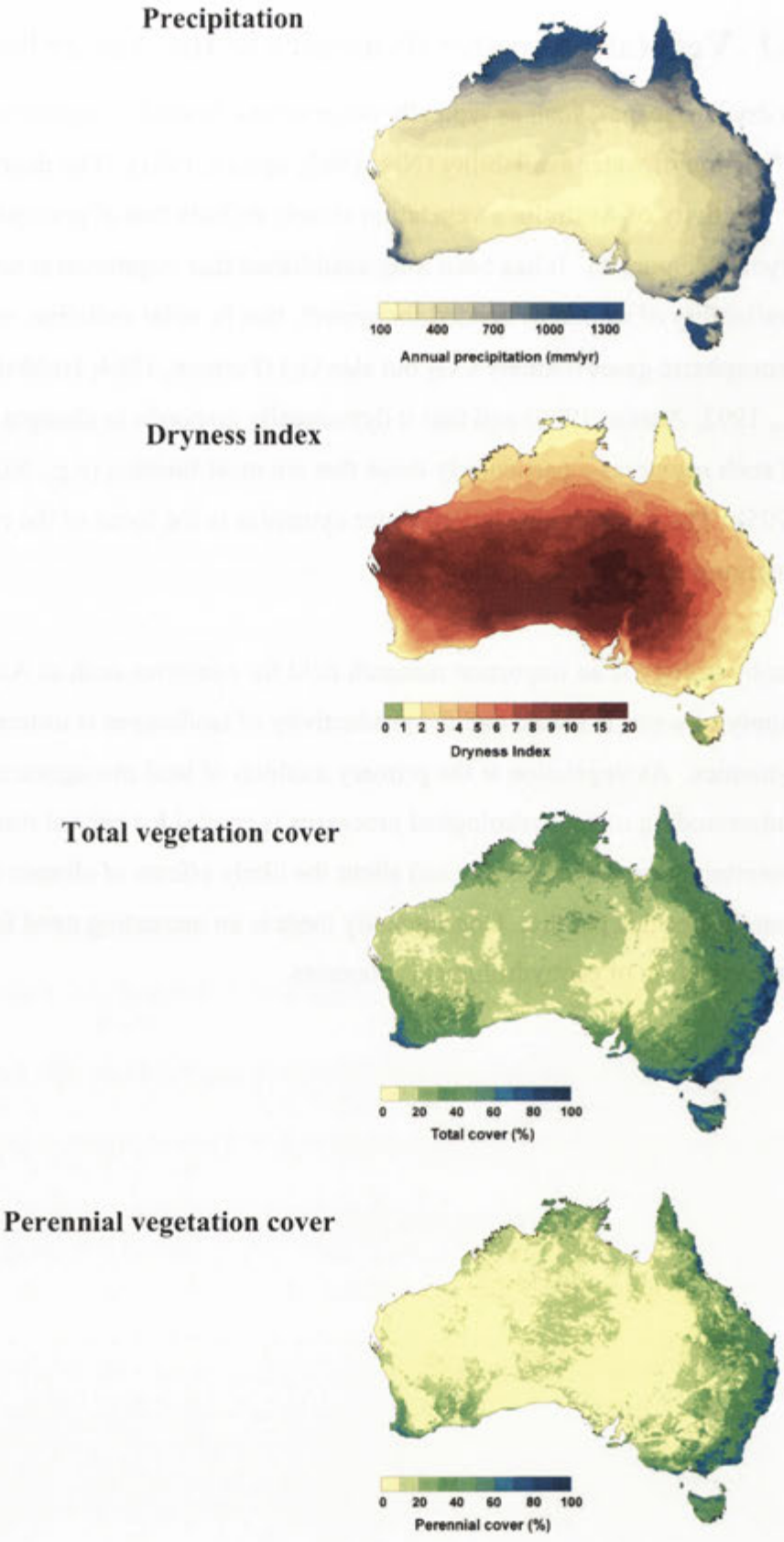

Figure 1. Long-term average precipitation, climatic dryness and vegetation cover across Australia. Averages are of the period 1981–2006. The dryness index is the ratio of precipitation to potential evaporation. Sources: precipitation data are from Jones et al. (2009); the dryness index is derived from precipitation data and the Penman potential evaporation data of Donohue et al. (2009a); vegetation cover data are from Donohue et al. (2008).

Australian landscapes are strongly water-limited and this is an important context for ecohydrological studies in this country. Budyko (1974) established a framework of supply and demand limitations which links average energy and water balances and describes the effects of limitations in these two resources on the partitioning of precipitation (P) into actual evaporation (E_a) and stream flow (Q)—given that $P = E_a + Q$ at steady state. Over a given timescale, a water-limited environment is described as one where the energy available for evaporation (i.e., the evaporative demand, typically represented as potential evaporation, E_p) exceeds the availability of water for evaporation (i.e., P). An energy-limited environment experiences the reverse situation. Hence, in water-limited environments, E_a approaches P and in energy-limited environments E_a approaches E_p (Figure 2). As transpiration is often the largest component of E_a (e.g., Choudhury and DiGirolamo, 1998; Huxman et al., 2005), this framework implicitly incorporates the effects of biological processes and provides a powerful means of analysing the different ecohydrological processes that occur in different environments.

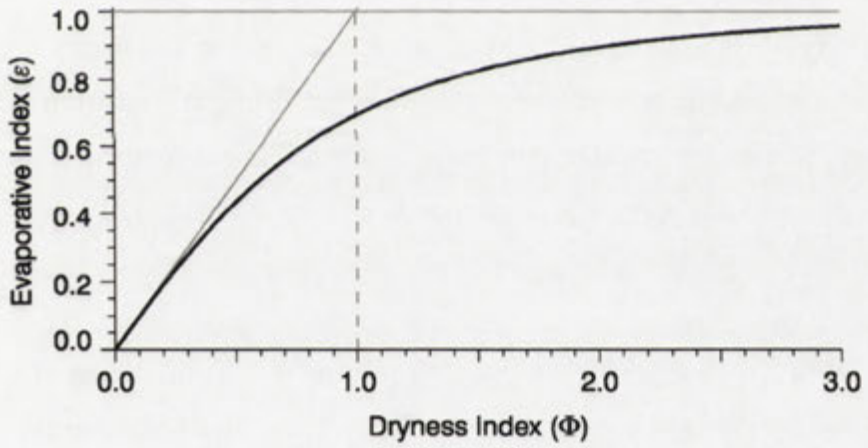

Figure 2. The Budyko curve and the supply–demand framework. The Budyko curve (black) describes the relation between the long-term catchment averages in ε (the ratio of E_a to P) and Φ (the ratio of E_p to P). The horizontal grey line is the water-limit, where 100% of P becomes E_a, and the diagonal grey line is the energy-limit, where 100% of available evaporative energy (i.e., E_p) is converted to latent heat. To the left of the dashed line are energy-limited conditions, and to the right are water-limited conditions.

Vegetation equilibrium is a concept that was originally championed in the ecological arena by Specht (1972) and later in the hydrological arena by Eagleson (1982) in his related theory of vegetation optimality. The process underlying this equilibrium is that vegetation will dynamically adapt to environmental changes in ways that maintain maximum net energy (i.e., carbon) capture (e.g., Schymanski et al., 2007). If water is

the most limiting resource, this implies that water use will be also maximised over the long-term (as per Specht, 1972; Kerkhoff et al., 2004). As a consequence, Specht (1972) observed that, within water-limited landscapes, the cover of natural perennial vegetation exists in dynamic equilibrium with the supply of water. Vegetation equilibrium implies that changes in the supply of plant-available water—be they seasonal or annual changes—will be accompanied by changes in the cover of the associated vegetation such that the equilibrium between water supply and water use is maintained. This link is highly significant as fractional cover can be measured via remote sensing using the closely related measure of fPAR (the fraction of Photosynthetically Active Radiation absorbed by vegetation, Asrar et al., 1984).

As well as responding to changes in growing conditions, changes in vegetation itself can also drive changes in local growing conditions, most notably the availability of water (Farley et al., 2005; Jackson et al., 2005; Pierce et al., 1993; Vertessy, 1998). Acknowledging this 'forcing' role of vegetation is of great practical significance as it is primarily through vegetation that landscapes are managed and manipulated. Hence, as well as enabling inferences to be made about vegetation characteristics based on knowledge of the underlying water balance dynamics, vegetation equilibrium theory can, at least in principle, be used to make inferences about water characteristics from associated vegetation dynamics, particularly in intensively managed landscapes. Currently, vegetation equilibrium theory is an under-explored idea in the field of ecohydrology.

This two-way linkage between dynamics in water and vegetation is a manifestation of the fact that all processes operating in vegetation-water systems (i.e., landscapes) are inter-related and are contained within a complex network of feedbacks. No single process is independent and any given process can act as both a forcing and a response variable. The time-scales over which system feedbacks operate can vary from minutes to decades. Quantifying these complexities between system forcings, responses and feedbacks is a central challenge of ecohydrology.

The term vegetation equilibrium is used here to refer specifically to the linkage between water availability and vegetation cover (via water use) and, defined as such, this term is particular to water-limited systems. It is a dynamic equilibrium in that water availability is continually changing and therefore so is the vegetation cover, typically

with reasonably short response times (for example, the response time for Eucalypt forests is in the order of several months, Pook, 1985). Implicit in this concept is that the forcings are climatic. If perturbations in these climatic forcings are large enough (i.e., the system is no longer water-limited) a shift in the equilibrium will occur such that the equilibrium is no longer driven by water availability, but perhaps by nutrient or energy availability, for example. However, non-climatic forcings also operate (e.g., vegetation disturbance processes which include land management activities) and these generally disrupt the dynamic equilibrium. Whilst the response times can be immediate, the time it takes for the system to establish a new equilibrium can vary from months to decades and even centuries (Kuczera, 1987) depending on the magnitude of the forcing. The study of such disequilibrium states can also reveal a wealth of information about ecohydrological processes.

The equilibrium between ecohydrological processes can be quantified by expressing each response variable as a function of all relevant forcing variables. For example, E_a can be expressed generally as:

$$E_a = f\left(P, E_p, CO_2, F_p, F_r, \ldots\right). \tag{1}$$

Here the role total fPAR (F_t) plays in determining E_a is split into its constituent persistent (F_p) and recurrent (F_r) fPAR components (Donohue et al., 2009b):

$$F_t = F_p + F_r \tag{2}$$

F_p and F_r approximate the separate contributions to F_t of perennial, non-deciduous vegetation types and of deciduous, annual and ephemeral vegetation types, respectively. Incorporating stored water (S_w) changes, Q can be expressed as:

$$Q = P - E_a - \frac{dS_w}{dt}. \tag{3}$$

The response of vegetation cover to forcings can be expressed through F_p and F_r as a function of the four primary forcing variables that determine plant growth: solar radiation (R_s), soil water (W), nutrients (N) and CO_2 (e.g., Forman, 1964; Holdridge, 1947):

$$F_p = f(R_s, W, N, CO_2, ...) \quad (4)$$

$$F_r = f(R_s, W, N, CO_2, ...) \quad (5)$$

Expressing the responses of these variables to perturbations in the relevant forcing variables becomes complex as the many interactions between forcing variables, as well as the feedbacks between response and forcing variables, should ideally be quantified.

A useful framework for building ecohydrological knowledge is presented in Table 1. This scheme attempts to simplify the complexities of vegetation–water interactions by examining forcing processes and response processes in isolation and without reference to system feedbacks. Hence, the effects of hypothetical changes in forcing variables on response variables are presented assuming all else is constant. In Table 1, P, E_p, atmospheric CO_2 concentration and F_t (via F_p and F_r) are considered to be forcing variables. E_a, Q and the three fPAR components are the response variables. Differentiation is made between the responses of variables in energy-limited environments to those in water-limited environments. As an example, an increase in P over time in energy-limited environments is likely to lead to a small increase in E_a, a large increase in Q and perhaps a small decrease in F_t. By contrast, in a water-limited environment the likely responses to an increase in P are for E_a and F_t to increase substantially and Q marginally. In both cases, the responses in F_p and F_r are uncertain. Broadly, the green sections of Table 1 relate to responses to dynamics in climatic forcings and the yellow sections relate to responses to vegetation forcings.

Table 1. A generalised outline of the likely responses of catchment water fluxes and vegetation cover to changes in climatic and vegetation forcings across environments with different supply limitations. The changes in forcing variables are presented as increases in the forcing; the opposite responses are expected for decreases in forcings. Large and small arrows indicate relative magnitude and direction of responses.

ENERGY-LIMITED* Change in response variable due to change in forcing variable					Change in forcing variable#	WATER-LIMITED Change in response variable due to change in forcing variable				
F_r	F_p	F_t	Q	E_a		Ea	Q	F_t	F_p	F_r
?	?	↓	↑	↑	P	↑	↑	↑	?	?
?	?	↑	↓	↑	E_p	↑	↓	↓	?	?
?	?	↑	↑	↓	CO_2	—	—	↑	?	?
			?	?	F_t	↑	↓			
			?	?	F_p	↑	↓			
			?	?	F_r	↓	↑			

* Energy-limited environments can be further split into radiation-limited (i.e., tropics) and temperature-limited (i.e., high latitudes and elevations) as per Nemani et al. (2003). These splits are particularly important as vegetation responses will differ across these two sub-classes of energy-limitation; here F_t is filled out for temperature-limited conditions (little change is expected in radiation-limited areas as cover will likely remain near 100% irrespective of changes in drivers). # The water balance responses due to changes in the fPAR variables in water-limited environments are according to Zhang et al. (2001).

Atmospheric CO_2 is included as a forcing variable in Table 1 as it is known to be increasing (Keeling et al., 2009) and much speculation surrounds its potential ecohydrological effects. Whilst it is established that the water use efficiency of photosynthesis increases with CO_2 such that less water is lost in transpiration for a given gain in CO_2 (Farquhar, 1997), how this effect will be manifest in actual landscapes is not certain (Polley, 1997; Poorter and Navas, 2003; Drake et al., 1997). The perspective presented in Table 1 is that this is likely to cause a reduction in transpiration (and therefore E_a) and an increase in Q in energy-limited landscapes (e.g., Gedney et al., 2006). However, in water-limited landscapes any increase in the efficiency of vegetation water use (the reduced transpiration per unit leaf area) should increase the leaf area that can be sustained for a given supply of water, as per the theory of dynamic equilibrium. Hence, the overall fluxes of water (e.g., E_a and Q) should

remain reasonably constant whilst the vegetation cover is expected to change (Berry and Roderick, 2006).

The current state of ecohydrological knowledge is such that the content of Table 1 is largely qualitative and contains a great deal of uncertainty for particular variables (Table 2). One of the over-arching aims of this thesis is to develop ways of populating this table quantitatively. The response of hydrological variables to dynamics in the supply of water and energy (the green areas in Table 2) can be estimated relatively quantitatively using a simple hydrological model, and throughout this thesis the framework developed by Budyko (1974) is used (see Figure 2).

Table 2. The relative certainty with which the dynamics between forcing and response ecohydrological variables in water-limited environments are understood. Those variables whose interactions are relatively well understood are highlighted in yellow; in orange are those moderately well understood and in red are those relatively poorly understood.

Change in forcing variable	**WATER-LIMITED** **Change in response variable due to change in forcing variable**				
	Ea	***Q***	***F_t***	***F_p***	***F_r***
P					
E_p					
CO_2					
F_t					
F_p					
F_r					

This thesis aims to develop greater insight into those vegetation–water dynamics which are currently poorly understood within water-limited environments (the orange and yellow areas in Table 2). Thus, two hypotheses are presented and tested here. The first relates to quantifying vegetation responses to dynamics in climatic forcings (i.e., filling in the orange section in Table 3) and the second to quantifying the influences of climatic and vegetation forcings on the water balance (filling in the blue in Table 3).

Table 3. The ecohydrological interactions that are the foci of the two hypotheses. In orange is the focus of Hypothesis I and in blue is that of Hypothesis II.

Change in forcing variable	WATER-LIMITED Change in response variable due to change in forcing variable				
	Ea	*Q*	F_t	F_p	F_r
P					
E_p					
CO_2					
F_t					
F_p					
F_r					

1.2 Two hypotheses

Hypothesis I

In water-limited environments, the structural complexity of natural perennial vegetation bears a direct relationship to the availability of water (e.g., Nemani and Running, 1989; Specht, 1972). Vegetation and water exist in a dynamic equilibrium—changes in the availability of water result in changes in the local vegetation, and changes to vegetation result in changes to the local water balance. Additionally, measures of the structure of a given area of natural vegetation can be used to infer the associated water balance, and vice versa.

Australian climatic conditions have been changing over the past 2-3 decades. Precipitation has increased on average (Bureau of Meteorology, 2007; Rotstayn et al., 2007) and pan evaporation—a measure of evaporative demand—has, on average, decreased (Roderick and Farquhar, 2004; Roderick et al., 2007). In addition, the expected effect of higher atmospheric CO_2 concentrations is to increase the water use efficiency of vegetation generally (Farquhar, 1997), most likely leading to higher levels of vegetation cover for a given precipitation in a dry environment. Each of these changes should have effectively increased the availability of water to vegetation generally, resulting in an increase in vegetation cover in Australia.

These above ideas lead to the first research hypothesis that ***observed changes in hydro-climatic conditions of the past 2–3 decades will have increased vegetation cover across Australia's predominantly water-limited environments, and such changes should be observable in satellite-based measures of fPAR***. Such a change in vegetation would be of great importance, showing that recent climatic changes have effectively increased water availability, affecting the productivity of natural and agricultural ecosystems, rates of carbon sequestration, the viability of plantation and revegetation activities and possibly even issues affecting sustainability such as salinity, soil carbon content and soil erosion.

Hypothesis II

The mass-energy balance framework developed by Budyko (1974) for describing long-term catchment water balances relates the dryness index to the evaporative index. This framework is useful as it shows, for a given climate, how long-term average catchment P is partitioned into E_a and Q. When examined within this framework, Budyko found that data from catchments at steady-state have a distinct curvilinear relation. This relation has subsequently become known as 'the Budyko curve'.

Budyko also noticed a degree of scatter around the curve (Figure 3). Such scatter indicates that, for any given climate, catchments vary in their ability to store surplus water, which itself determines how P is split into E_a, Q and dS_w/dt as per Eq. (3). Several authors have attempted to explain what causes this scatter (Table 4).

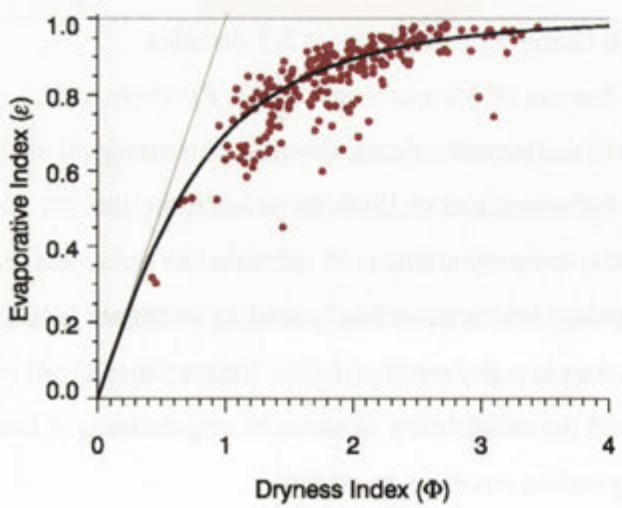

Figure 3. An example of the Budyko scatter—the scatter of values around the Budyko curve that typically occurs when using observational data. Values (red) are derived from long-term

annual average stream flow (Peel et al., 2000), precipitation (Jones et al., 2009) and potential evaporation (Donohue et al., 2009a) data from a selection of Australian catchments.

Table 4. Foci of previous studies investigating the causes of the Budyko scatter.

Cause of scatter	**Authors**
Phases of annual P and E_p cycles	Budyko (1974)
Relative soil water storage capacity	Milly (1994)
Intra-seasonal P variability/storminess	Milly (1994), Porporato et al. (2004)
Spatial variability of S_w	Milly (1994)
Seasonality of P and E_p	Hickel and Zhang (2006), Milly (1994), Potter and Zhang (2009)
Spatial and temporal scale of analyses	Choudhury (1999), Oudin et al. (2008), Zhang et al. (2008)
Plant available water capacity (e.g., rooting depth, soil characteristics)	Yang et al. (2007), Zhang et al. (2001)
Topography, e.g. slope, relief ratio	Yang et al. (2007)
Vegetation cover types	Zhang et al. (2001)
Infiltration-excess runoff	Potter et al. (2005)

The role of vegetation has not been considered in great depth in hydrological models, as is generally evidenced by Table 4. Yet the role of vegetation in determining the water balance is believed to be significant for a number of reasons. Vegetation changes the surface energy balance, it accesses stored water that is otherwise isolated from the atmosphere, and increases the surface area available for energy/mass transfer (via the high root and leaf areas per unit area of land surface). The flux of water at any point in space or time is determined by the interaction of both physical and biological processes.

However, if vegetation is a reflection of water availability in water-limited landscapes, then it is also the product of the many interacting processes that determine water availability. Conversely, any processes that act to limit vegetation growth are likely to also affect the partitioning of P into E_a, Q and ΔS_w. Hence, vegetation-related data should contain information about the observed variation in E_a and Q regardless of the source of that variation. Also, because of the link between vegetation functioning and water storage (and therefore steady-state conditions—see Chapter 2) and because vegetation is a reflection of the local water supply, vegetation information has the potential to explain hydrological variability at small temporal and spatial scales.

The second research hypothesis is that ***the incorporation of remotely sensed measures of fPAR into the Budyko model can improve the model's accuracy (i.e., reduce the scatter), especially at smaller spatial and temporal scales.*** Confirmation of this hypothesis would lead to the development of a model that is parsimonious. It would capture the effects of the processes that determine the water balance without needing to describe them explicitly. Additionally, because of the straightforward link to real-world vegetation characteristics provided by fPAR, the model is likely to be useful in land management arenas.

1.3 Thesis overview

The body of research of this thesis has been written as scientific articles that are either published in or submitted to various peer-reviewed, international journals. In total, five papers have been produced and are presented here, one per chapter, in the native format of the respective journals. They are given in the order in which they were submitted which is also the order in which the research progressed. Currently, three of the five papers have been published, and two are in review. Figure 4 diagrammatically shows these papers, the chapters they appear in, and how these are related. Following this current introductory chapter is Chapter 2, containing the paper which establishes the theoretical framework for Hypothesis II; Chapters 3 and 5 contain papers describing the development of two input datasets critical for the subsequent hypothesis testing; and Chapters 4 and 6 present the papers that test Hypotheses I and II, respectively. Finally, conclusions and recommendations stemming from this body of research are presented. Overviews of, and the inter-relations between, these papers are given below.

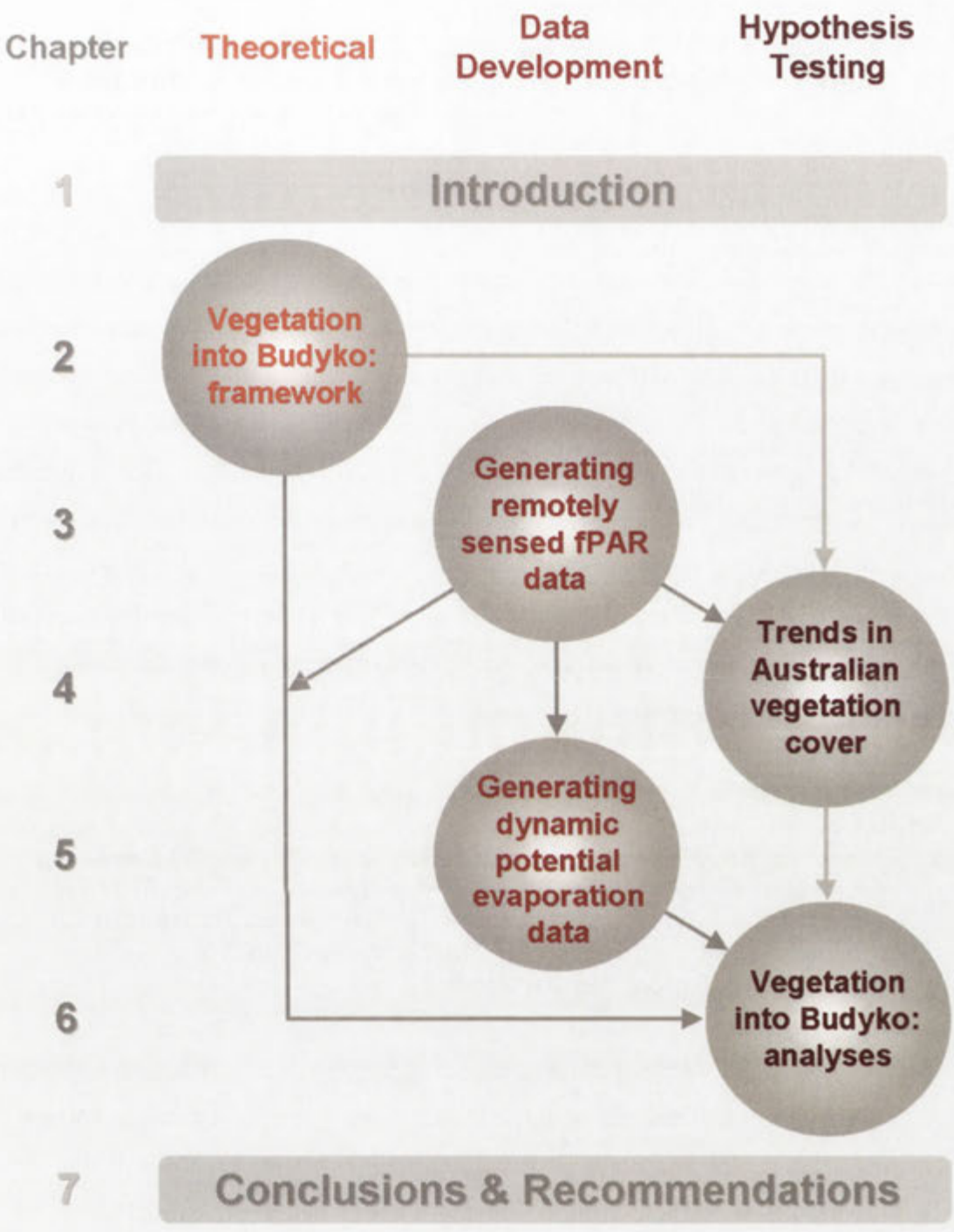

Figure 4. Diagram of the thesis structure highlighting the relations between the five papers and the chapters in which they are presented.

Chapter 2.

Donohue RJ, Roderick ML and McVicar TR (2007) On the importance of including vegetation dynamics in Budyko's hydrological model. Hydrology and Earth System Science , 11, 983-995.

An overview of Budyko's hydrological model (Budyko, 1974) is given in this paper with specific emphasis on the role of vegetation dynamics in determining hydrological variability, as well as on spatial and temporal scales of analysis. Key vegetation-related functions are examined that determine seasonal and annual variability and vegetation water use. Due to the close links between transpiration and leaf area, and between changes in both stored soil water and in rooting depth, it is hypothesised that a dynamic measure of vegetation should provide some explanation of the variability observed in hydrological processes not already explained by climate data alone. It is proposed that this vegetation measure is remotely sensed fPAR, which is linearly related to fractional green cover. This paper is the precursor to the final paper presented in this thesis (Chapter 6) in which Hypothesis II is tested.

Chapter 3.

Donohue RJ, Roderick ML and McVicar TR (2008) Deriving consistent long-term vegetation information from AVHRR reflectance data using a cover-triangle-based framework. Remote Sensing of Environment, 112, 2938-2949 DOI:10.1016/j.rse.2008.02.008.

This paper was driven by the need for consistent, long-term remotely sensed vegetation cover information suitable for the analysis of long-term vegetation dynamics. A new method is developed that accounts for the discontinuities often present within the Advanced Very High Resolution Radiometer (AVHRR) data record caused by variability in atmospheric conditions and instrument calibration. This method is simple, easily implemented and is based on biophysical principles. It is achieved by stabilising, through time, the position of the vegetation cover triangle when plotted in red and near infra-red reflectance space. From corrected reflectances, monthly, Australian wide grids of the Normalised Difference Vegetation Index (NDVI) and fPAR are generated. As this fPAR dataset covers all of Australia, is long-term and is spatially and temporally dynamic, it is *the fundamental input* to the analyses performed to test both Hypotheses I and II (Chapters 4 and 6, respectively), as well as to the generation of dynamic potential

evaporation data (Chapter 5). The period of these data (Jan 1981–Dec 2006) set the temporal extent of all subsequent analyses.

Chapter 4.

Donohue, R.J., McVicar, T.R. and Roderick, M.L., 2009. Climate-related trends in Australian vegetation cover as inferred from satellite observations, 1981–2006. Global Change Biology, 15(4): 1025-1039, DOI: 10.1111/j.1365-2486.2008.01746.x.

Hypothesis I is tested in this paper, which is to examine whether there is evidence within the fPAR dataset (see Chapter 3) of an increase in vegetation cover between 1981 and 2006. Total fPAR—the total green fractional vegetation cover—is split into its constituent perennial and recurrent components, which approximately represent the cover from non-deciduous perennial vegetation types and from deciduous, annual and ephemeral vegetation types, respectively. The observed annual and seasonal changes in these three fPAR variables are examined and compared with changes in *P* and US Class A pan evaporation (used as a surrogate for evaporative demand). Observed changes are interpreted within Budyko's energy–water limitation framework and different responses in perennial and non-perennial vegetation types are examined.

Chapter 5.

Donohue RJ, McVicar TR and Roderick ML (2009) Assessing the ability of potential evaporation formulations to capture the dynamics in evaporative demand within a changing climate. Journal of Hydrology.
Manuscript submitted 20th November 2009.

The research in this paper was prompted by the need—in order to later test Hypothesis II—for fully dynamic, Australia-wide grids of potential evaporation. For the hypothesis testing, it is crucial that the potential evaporation formulation is capable of capturing all possible effects of long-term changes on evaporative demand and so needs to treat all the key drivers of evaporative demand (i.e., net radiation, temperature, vapour pressure, and wind speed) as variables. Consequently, using daily, Australia-wide grids of air temperature and vapour pressure, and of AVHRR-derived albedo and vegetation cover (i.e., fPAR), plus a newly developed wind speed dataset, five different representations of potential evaporation were generated. Each dataset is tested as to how well it captures the annual, seasonal and long-term temporal dynamics in evaporative demand

that are expected to have occurred between 1981 and 2006. The generation of the underlying datasets is not described in this chapter, but is separately described in Donohue et al. (2009c). It is the testing of the temporal dynamics in potential evaporation data that is presented in Chapter 5.

Chapter 6.

Donohue RJ, Roderick ML and McVicar TR (2009). Can dynamic vegetation information improve the accuracy of Budyko's hydrological model? Journal of Hydrology. *Manuscript submitted 20th November 2009.*

The paper within Chapter 6 concludes the work presented in Chapter 2 in that it tests Hypothesis II in which it is proposed that dynamic vegetation information in the form of remotely sensed fPAR data can improve the accuracy of the Budyko hydrological model, especially at small spatial and temporal scales. This research uses the fPAR data of Chapter 3 and the potential evaporation data of Chapter 5. It also uses the persistent and recurrent fPAR components described in Chapter 4. Testing of Hypothesis II involves modelling of the 'scatter' that occurs within the Budyko framework (i.e., the variation in the evaporative index not accounted for by Budyko's original model formulation). Scatter was modelled as a linear relation of one of a number of variables, namely the annual values of P, E_p, and the three fPAR inputs, as well as metrics describing the inter-annual variability and seasonality in these variables. Models are developed at several different spatial and temporal scales to test the circumstances in which vegetation is important for improving the prediction of E_a and Q.

1.4 References

Asrar G, Fuchs M, Kanemasu ET and Hatfield JL (1984) Estimating absorbed photosynthetic radiation and leaf-area index from spectral reflectance in wheat. *Agronomy Journal*, 76, 300-306.

Austin MP (1980) Searching for a model for use in vegetation analysis. *Vegetatio*, 42, 11-21.

Berry SL and Roderick ML (2006) Changing Australian vegetation from 1788 to 1988: effects of CO2 and land-use change. *Australian Journal of Botany*, 54, 325-338.

Blackman FF (1905) Optima and limiting factors. *Annals of Botany*, 19, 281-296.

Budyko MI (1974) Climate and life. edition. Academic, New York, 508 pp.

Bureau of Meteorology (2007) Timeseries—Australian climate variability and change. Australian Government Bureau of Meteorology. Accessed May, 2007. Available at < http://www.bom.gov.au/cgi-bin/silo/reg/cli_chg/timeseries.cgi >

Choudhury BJ (1999) Evaluation of an empirical equation for annual evaporation using field observations and results from a biophysical model. *Journal of Hydrology*, 216, 99-110.

Choudhury BJ and DiGirolamo NE (1998) A biophysical process-based estimate of global land surface evaporation using satellite and ancillary data - I. Model description and comparison with observations. *Journal of Hydrology*, 205, 164-185.

Donohue RJ, McVicar TR and Roderick ML (2009a) Assessing the ability of potential evaporation formulations to capture the dynamics in evaporative demand within a changing climate. *Journal of Hydrology*, Submitted manuscript.

Donohue RJ, McVicar TR and Roderick ML (2009b) Climate-related trends in Australian vegetation cover as inferred from satellite observations, 1981–2006. *Global Change Biology*, 15, 1025-1039. DOI: 10.1111/j.1365-2486.2008.01746.x

Donohue RJ, McVicar TR and Roderick ML (2009c) Generating Australian potential evaporation data suitable for assessing the dynamics in evaporative demand within a changing climate. CSIRO: Water for a Healthy Country National Research Flagship, Canberra. Available at < http://www.clw.csiro.au/publications/waterforahealthycountry/2009/wfhc-evaporative-demand-dynamics.pdf >

Donohue RJ, Roderick ML and McVicar TR (2008) Deriving consistent long-term vegetation information from AVHRR reflectance data using a cover-triangle-based framework. *Remote Sensing of Environment*, 112, 2938-2949 DOI:10.1016/j.rse.2008.02.008.

Drake BG, Gonzalez-Meler MA and Long SP (1997) More efficient plants: a consequence of rising atmospheric CO2? *Annual Review of Plant Physiology and Plant Molecular Biology*, 48, 609-639. doi:10.1146/annurev.arplant.48.1.609.

Eagleson PS (1982) Ecological optimality in water-limited natural soil-vegetation systems .1. theory and hypothesis. *Water Resources Research*, 18, 325-340.

Farley KA, Jobbagy EG and Jackson RB (2005) Effects of afforestation on water yield: a global synthesis with implications for policy. *Global Change Biology*, 11, 1565-1576.

Farquhar GD (1997) Carbon dioxide and vegetation. *Science*, 278, 1411.

Field CB, Chapin FS, Matson PA and Mooney HA (1992) Responses of terrestrial ecosystems to the changing atmosphere - a resource-based approach. *Annual Review of Ecology and Systematics*, 23, 201-235.

Forman RTT (1964) Growth under controlled conditions to explain the hierarchical distributions of a moss, Tetraphis pellucida. *Ecological Monographs*, 34, 1-25.

Gedney N, Cox PM, Betts RA, Boucher O, Huntingford C and Stott PA (2006) Detection of a direct carbon dioxide effect in continental river runoff records. *Nature*, 439, 835-838.

Hickel K and Zhang L (2006) Estimating the impact of rainfall seasonality on mean annual water balance using a top-down approach. *Journal of Hydrology*, 331, 409-424.

Holdridge LR (1947) Determination of world plant formations from simple climatic data. *Science*, 105, 367-368.

Huxman TE, Wilcox BP, Breshears DD, Scott RL, Snyder KA, Small EE, Hultine K, Pockman WT and Jackson RB (2005) Ecohydrological implications of woody plant encroachment. *Ecology*, 86, 308-319.

Jackson RB, Jobbagy EG, Avissar R, Roy SB, Barrett DJ, Cook CW, Farley KA, le Maitre DC, McCarl BA and Murray BC (2005) Trading water for carbon with biological sequestration. *Science*, 310, 1944-1947.

Jones DA, Wang W and Fawcett R (2009) High-quality Spatial Climate Data Sets for Australia. *Australian Meteorological and Oceanographic Journal*, In press.

Keeling RF, Piper SC, Bollenbacher AF and Walker SJ (2009) Atmospheric CO2 Records from Sites in the SIO Air Sampling Network. Scripps Institution of Oceanography, University of California, La Jolla. Accessed October, 2009. Available at < http://cdiac.ornl.gov/trends/co2/sio-keel.html >

Kerkhoff AJ, Martens SN and Milne BT (2004) An ecological evaluation of Eagleson's optimality hypotheses. *Functional Ecology*, 18, 404-413.

Kuczera G (1987) Prediction of water yield reductions following a bushfire in ash-mixed species eucalypt forest. *Journal of Hydrology*, 94, 215-236.

Milly PCD (1994) Climate, soil water storage, and the average annual water balance. *Water Resources Research*, 30, 2143-2156.

Nemani RR, Keeling CD, Hashimoto H, Jolly WM, Piper SC, Tucker CJ, Myneni RB and Running SW (2003) Climate-driven increases in global terrestrial net primary production from 1982 to 1999. *Science*, 300, 1560-1563.

Nemani RR and Running SW (1989) Testing a theoretical climate soil leaf-area hydrologic equilibrium of forests using satellite data and ecosystem simulation. *Agricultural and Forest Meteorology*, 44, 245-260.

Nix H (1982) Environmental determinants of biogeography and evolution in Terra Australis. In: Evolution of the flora and fauna of arid Australia (eds Barker WR and Greensdale PJM). Peacock, Sydney.

Nix HA (1978) Determinants of environmental tolerance limits in plants. In: Biology and quaternary environments (eds Walker D and Guppy JC), pp. 195-206. Australian Academy of Science, Canberra.

Oudin L, Andreassian V, Lerat J and Michel C (2008) Has land cover a significant impact on mean annual streamflow? An international assessment using 1508 catchments. *Journal of Hydrology*, 357, 303-316.

Peel MC, Chiew FHS, Western AW and McMahon TA (2000) Extension of unimpaired monthly streamflow data and regionalisation of parameter values to estimate streamflow in ungauged catchments. National Land and Water Resources Audit, Canberra. Available at < http://audit.ea.gov.au/anra/water/docs/national/Streamflow/Streamflow.pdf >

Pierce LL, Walker J, Dowling TI, McVicar TR, Hatton TJ, Running SW and Coughlan JC (1993) Ecohydrological changes in the Murray-Darling Basin .3. A simulation of regional hydrological changes. *Journal of Applied Ecology*, 30, 283-294.

Polley HW (1997) Implications of rising atmospheric carbon dioxide concentration for rangelands. *Journal of Range Management*, 50, 562-577.

Pook EW (1985) Canopy dynamics of Eucalyptus-maculata Hook. 3. Effects of drought. *Australian Journal of Botany*, 33, 65-79.

Poorter H and Navas ML (2003) Plant growth and competition at elevated CO2: on winners, losers and functional groups. *New Phytologist*, 157, 175-198.

Porporato A, Daly E and Rodriguez-Iturbe I (2004) Soil water balance and ecosystem response to climate change. *American Naturalist*, 164, 625-632.

Potter NJ and Zhang L (2009) Interannual variability of catchment water balance in Australia. *Journal of Hydrology*, 369, 120-129.

Potter NJ, Zhang L, Milly PCD, McMahon TA and Jakeman AJ (2005) Effects of rainfall seasonality and soil moisture capacity on mean annual water balance for

Australian catchments. *Water Resources Research*, 41. DOI: 10.1029/2004WR003697.

Roderick ML and Farquhar GD (2004) Changes in Australian pan evaporation from 1970 to 2002. *International Journal of Climatology*, 24, 1077-1090.

Roderick ML, Rotstayn LD, Farquhar GD and Hobbins MT (2007) On the attribution of changing pan evaporation. *Geophysical Research Letters*, 34. DOI: 10.1029/2007GL031166

Rotstayn LD, Cai WJ, Dix MR, Farquhar GD, Feng Y, Ginoux P, Herzog M, Ito A, Penner JE, Roderick ML and Wang MH (2007) Have Australian rainfall and cloudiness increased due to the remote effects of Asian anthropogenic aerosols? *Journal of Geophysical Research-Atmospheres*, 112, D09202. DOI:10.1029/2006JD007712.

Schymanski SJ, Roderick ML, Sivapalan M, Hutley LB and Beringer J (2007) A test of the optimality approach to modelling canopy properties and CO2 uptake by natural vegetation. *Plant Cell and Environment*, 30, 1586-1598.

Specht RL (1972) Water use by perennial evergreen plant communities in Australia and Papua New Guinea. *Australian Journal of Botany*, 20, 273-299.

Specht RL (1981) Major vegetation formations in Australia. In: Ecological biogeography of Australia Vol. 1 (ed Keast A), pp. 163-298. Dr. W. Junk, The Hague.

Vertessy RA (1998) Predicting water yield from mountain ash forest catchments. 98/4. Cooperative Research Centre for Catchment Hydrology.

Yang DW, Sun FB, Liu ZY, Cong ZT, Ni GH and Lei ZD (2007) Analyzing spatial and temporal variability of annual water-energy balance in nonhumid regions of China using the Budyko hypothesis. *Water Resources Research*, 43. DOI: 10.1029/2006WR005224

Zhang L, Dawes WR and Walker GR (2001) Response of mean annual evapotranspiration to vegetation changes at catchment scale. *Water Resources Research*, 37, 701-708.

Zhang L, Potter N, Hickel K, Zhang YQ and Shao QX (2008) Water balance modeling over variable time scales based on the Budyko framework - Model development and testing. *Journal of Hydrology*, 360, 117-131. DOI: 10.1016/j.jhydrol.2008.07.021

CHAPTER 2

On the importance of including vegetation dynamics in Budyko's hydrological model

Hydrol. Earth Syst. Sci., 11, 983–995, 2007
www.hydrol-earth-syst-sci.net/11/983/2007/

Hydrology and Earth System Sciences

On the importance of including vegetation dynamics in Budyko's hydrological model

R. J. Donohue[1,2], M. L. Roderick[1], and T. R. McVicar[2]

[1]Environmental Biology Group, Research School of Biological Sciences, Australian National University, Canberra, ACT 0200, Australia
[2]CSIRO Land and Water and eWater Cooperative Research Centre, GPO Box 1666, Canberra, ACT 2601, Australia

Received: 20 January 2006 – Published in Hydrol. Earth Syst. Sci. Discuss.: 12 July 2006
Revised: 10 October 2006 – Accepted: 5 March 2007 – Published: 13 March 2007

Abstract. The Budyko curve describes the patterns observed between between climate, evapotranspiration and run-off and has proven to be a useful model for predicting catchment energy and water balances. In this paper we review the Budyko curve's underlying framework and, based on the literature, present an argument for why it is important to include vegetation dynamics into the framework for some purposes. The Budyko framework assumes catchments are at steady-state and are driven by the macro-climate, two conditions dependent on the scales of application, such that the framework's reliability is greatest when applied using long-term averages ($\gg$1 year) and to large catchments ($>10\,000\,km^2$). At these scales previous experience has shown that the hydrological role of vegetation does not need to be explicitly considered within the framework. By demonstrating how dynamics in the leaf area, photosynthetic capacity and rooting depth of vegetation affect not only annual and seasonal vegetation water use, but also steady-state conditions, we argue that it is necessary to explicitly include vegetation dynamics into the Budyko framework before it is applied at small scales. Such adaptations would extend the framework not only to applications at small timescales and/or small catchments but to operational activities relating to vegetation and water management.

1 Introduction

Efforts to better understand the components of the catchment water balance have traditionally been the realm of the hydrological community. Investigations have used models predominantly based on physical processes and applications have generally remained in the same arena. Very few catchment-scale hydrological models incorporate vegetation or, in those that do, it is often included generically or in abstract terms that are difficult to measure across space and through time. This is beginning to change with the recognition by the hydrological community that biological processes play a key role in the catchment water balance (Rodriguez-Iturbe and Porporato, 2005; Montaldo et al., 2004). One key feature of this role is that transpiration, a major component of the catchment water balance, and biological productivity are intimately coupled (Berry et al., 2005). The fields of hydrology and ecology will benefit from a more integrated understanding of catchment behaviour. This is the central challenge of ecohydrology.

In order to characterise the components of catchment water balances, Budyko (1974) developed what is now one of the most enduring frameworks that links climate to catchment run-off and evapotranspiration. It is simple to interpret and plainly links basic physical principles governing the catchment water balance. The resulting relationship, widely known as the "Budyko curve", partitions average precipitation into average run-off and average evapotranspiration. Deviations around this relationship are observed and considerable work has been done to explain these deviations, attributing them to variability and seasonality in climate, to soil characteristics, to vegetation type and to the scales of analyses.

It seems likely that the quantitative integration of measures of key vegetation characteristics might enhance the Budyko framework. If true, then the applicability of the framework might be extended to a variety of land management applications. The purpose of this paper is to review the Budyko framework with particular reference to vegetation and, by highlighting the dynamic role vegetation often plays in catchment behaviour, to argue the importance of including spatially and temporally dynamic measures of vegetation into Budyko's framework. More specifically, this review:

1. explicitly quantifies some of the assumptions inherent in the water balance as formulated by Budyko, particularly

Correspondence to: R. J. Donohue
(randall.donohue@csiro.au)

Published by Copernicus GmbH on behalf of the European Geosciences Union.

those relating to steady-state conditions (Sect. 2);

2. examines the Budyko-related literature focusing on how vegetation processes and dynamics can affect the assumption of steady-state conditions within the framework as well as the components of the water balance itself (Sect. 3);

3. collates information from the literature that demonstrates the magnitude to which vegetation dynamics can affect the water balance and the timescales over which these effects can operate (Sect. 4); and

4. suggests some potential ways forward for investigating how time-series remote sensing may enable vegetation dynamics to be incorporated into the Budyko framework (Sect. 5).

2 The Budyko framework and curve

In the middle of last century Budyko (1958, 1974) published a framework describing the partitioning of average precipitation into average evapotranspiration and average run-off based on simple physical relationships. This is now known as the "Budyko curve" and is described below.

2.1 Catchment water and energy balances

Budyko described the hydrology of a catchment using a supply-demand framework and a simple bucket model where net drainage is assumed to be negligible. The water balance was defined as:

$$\frac{dS_w}{dt} = P - E - Q \tag{1}$$

where E, P and Q are catchment-wide estimates of evapotranspiration, precipitation and run-off fluxes, respectively (in SI units, which will be the units used henceforth, these are all kg s^{-1}), and S_w (kg) is the soil water storage. A catchment is in steady-state when changes in S_w are zero. In reality, $\frac{dS_w}{dt}$ is almost continually varying due to fluctuations in P, Q and E and steady-state conditions are typically established in analyses by integrating Eq. (1) over a finite time period (τ) that is larger than the time-scale of fluctuations in S_w:

$$\int_0^\tau \frac{dS_w}{dt}dt = \int_0^\tau P dt - \int_0^\tau E dt - \int_0^\tau Q dt \tag{2}$$

In finite form we have the catchment mass balance:

$$\Delta S_w = \overline{P}\tau - \overline{E}\tau - \overline{Q}\tau \tag{3}$$

or

$$\frac{\Delta S_w}{\tau} = \overline{P} - \overline{E} - \overline{Q} \tag{4}$$

We can convert to the familiar depth units by dividing both sides by the catchment area (A_c, m^2) and the density of liquid water (ρ_w, kg m^{-3}):

$$\frac{\Delta S_w}{\rho_w A_c \tau} = \frac{\overline{P} - \overline{E} - \overline{Q}}{\rho_w A_c} \tag{5}$$

The framework can be further extended by noting that soil water depends on the volume of the bucket (V, m^3) and the mass concentration of water in the bucket ($[S_w]$, kg m^{-3}):

$$S_w = V\ [S_w] \tag{6}$$

An upper limit to $[S_w]$ is set by the pore space within the soil which is a function of soil texture and structure (Craze and Hamilton, 1991). Soil water can change because of a change in the volume of the bucket or a change in mass concentration within the volume. To the first order we have:

$$\Delta S_W = [S_w]\ \Delta V + V\ \Delta [S_w] \tag{7}$$

The volume of the bucket depends on the catchment area and bucket depth (z, m):

$$V = A_c z \tag{8}$$

For a given catchment, the area is fixed and the volume of the bucket can only change because of the change in depth (Δz). With that, and combining Eqs. (5, 7 and 8):

$$\frac{1}{\rho_w}\left([S_w]\frac{\Delta z}{\tau} + z\frac{\Delta [S_w]}{\tau}\right) = \frac{\overline{P} - \overline{E} - \overline{Q}}{\rho_w A_c} \tag{9}$$

Formulating the water balance in this way allows links to be made (later in Sects. 3 and 4) between vegetation characteristics and the spatial analysis scales, as well as the "flux components" (RHS of Eq. 9, that is, $\overline{Q}$ and $\overline{E}$) and the "steady-state components" (LHS of Eq. 9) of the water balance. Even though this seems more complicated than Eq. (1) it has the advantage that it makes all the terms, especially A_c, τ and z, explicit. Firstly, A_c determines the spatial scale of analyses. Budyko only examined catchments with A_c well over 1000 km^2, partly to minimise the effect of any groundwater flow (i.e. to ensure the validity of the bucket model) as he assumed this to be negligible, and partly to minimise the effect of "local conditions" on $\overline{E}$ (see Sect. 2.2). Secondly, τ determines the timescale of analyses. In developing his framework, Budyko assumed catchments were at steady-state (i.e. LHS of Eq. (9)$\rightarrow$0). Budyko therefore a priori selected a value of τ to ensure that the steady-state assumptions would be reasonable. In doing that, Budyko found that ΔS_w can be as large as $\overline{E}$ or $\overline{Q}$ over a single year, and so set τ to be much greater than 1 year by using long-term averages. Lastly, z controls total possible S_w. However, under the assumption that groundwater flow is negligible, water loss from the bucket is via soil evaporation or plant transpiration. Thus rooting depth, z_r (m), determines the water potentially available to plants and therefore the effective bucket depth.

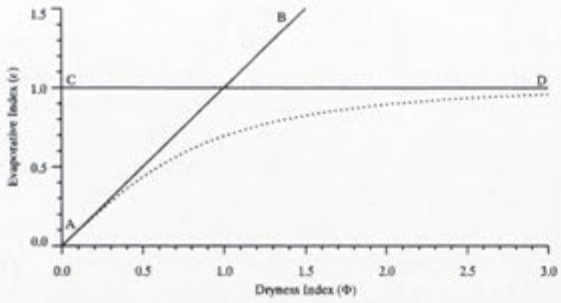

Fig. 1. Budyko's framework and curve. The curve (dotted line), defined by Eq. (12), describes the relationship between the dryness index (Φ; $\overline{R_n}/\lambda\overline{P}$) and the evaporative index (ε; $\overline{E}/\overline{P}$). Line A–B defines the energy-limit to evapotranspiration, and line C–D defines the water-limit.

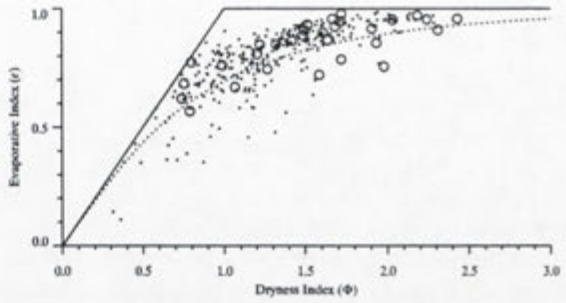

Fig. 2. Plot of mass balance data from 331 Australian catchments showing the deviations of values around the Budyko curve. Large, hollow circles denote the 30 moderate-sized catchments ($A_c \geq 1000\,\mathrm{km}^2$) and small circles denote the remaining 301 smaller catchments ($<1000\,\mathrm{km}^2$). Data are from Peel et al. (2000) and Raupach et al. (2001) calculated using Eq. (9) with $\tau \geq 8$ years.

Fluxes of both mass and energy are involved in evapotranspiration and this provides a critical link between the water and energy balances. The catchment-wide energy balance is given by:

$$\Delta S_e = R_n - \lambda E - H \tag{10}$$

where the change in energy storage (S_e) is the balance between net radiation (R_n) and the fluxes of latent (λE) and sensible (H) heat (all in $\mathrm{J\,s^{-1}}$) where λ ($\mathrm{J\,kg^{-1}}$) is the latent heat of vaporisation. Note that the sign convention used in Eq. (10) assumes that λE and H are positive away from the surface while R_n is positive into the surface. Using the same form as Eq. (9) gives:

$$[S_e]\frac{\Delta z_e}{\tau} + z_e\frac{\Delta[S_e]}{\tau} = \frac{\overline{R_n} - \lambda\overline{E} - \overline{H}}{A_c} \tag{11}$$

where z_e (m) is the depth to which energy can be stored. Over annual timescales energy storage can usually be omitted from the energy balance.

2.2 The framework and curve

Evapotranspiration is limited by the supply of either water or energy. At steady-state, when water is limiting ($\overline{R_n}/\lambda > \overline{P}$), the maximum possible $\overline{E}$ is $\overline{P}$, at which $\overline{Q}$=0 (Eq. 9). Similarly, the maximum possible $\overline{E}$ when energy is limiting is $\overline{R_n}/\lambda$ at which $\overline{H}$=0 (Eq. 11). Evapotranspiration approaches one of these two limits as water or energy, respectively, become increasingly limiting. This framework of mass and energy balances and supply and demand-limited evapotranspiration is the key component of Budyko's work. The type and degree of limitation is determined by the radiative index of dryness (Φ) which is the ratio of $\overline{R_n}/\lambda$ to $\overline{P}$. Values of $\Phi<1$ represent energy-limited environments, and >1 water-limited. Intermediate environments occur where $\Phi\sim1$.

If all available energy is converted to $\lambda\overline{E}$, then $\overline{E}=\overline{R_n}/\lambda$. Budyko considered this to represent "the greatest possible value of evaporation under given conditions" (Budyko, 1974, pp. 323). To avoid the need to define the widely used notion of "potential evaporation" (Granger, 1989), subsequent discussion will refer to the available energy simply as $\overline{R_n}/\lambda$. This seems like a reasonable simplification as Budyko found that, averaged over a year or longer, $\overline{H}$ is always positive (i.e. provides no net energy input) and that $\overline{R_n}$ alone is a good approximation of the available energy.

Catchment-scale annual (or longer) evapotranspiration is usually estimated for gauged catchments by assuming that ΔS_w is 0 and hence $\overline{E}$ is the difference between measured values of $\overline{P}$ and $\overline{Q}$ (Eq. 9). The need for a simple means of estimating $\overline{E}$ from ungauged catchments prompted Budyko to develop the "equation of relationship" that describes the dependency of $\overline{E}$ on the variables $\overline{P}$ and $\overline{R_n}/\lambda$:

$$\overline{E} = \left(\frac{\overline{R_n}\,\overline{P}}{\lambda}\tanh\frac{1}{\Phi}\left(1-\cosh\Phi+\sinh\Phi\right)\right)^{1/2} \tag{12}$$

This curvilinear relationship, which built on the works of Schreiber (1904) and Ol'dekop (1911), has become known as the Budyko curve (Fig. 1). Budyko often used the evaporative index (ε; which is $\overline{E}/\overline{P}$) to describe the partitioning of $\overline{P}$ into $\overline{E}$ and $\overline{Q}$. The curve approaches the water and energy limits as values of Φ become more extreme. $\overline{Q}$ is proportional to the vertical distance between the curve and the water limit and $\overline{H}$ is proportional to the vertical distance between the curve and the energy limit.

Budyko tested this relationship using measured values of $\overline{E}$ from 1200 moderate sized ($A_c>1000\,\mathrm{km}^2$) catchments and found that it explained about 90% of the variation in observed values. When limited to very large catchments ($A_c>10\,000\,\mathrm{km}^2$) the relation was even better. This improvement with catchment area was attributed to the (macro-) climate being the principle determinant of $\overline{E}$ over large areas. As A_c diminishes (i.e. as catchment size decreases), $\overline{E}$ "may

vary appreciably under the influence of local conditions of a non-climatic character" such as topography and vegetation (Budyko, 1974, pp. 318 and 330). The availability of energy, as described by $\overline{R_n}$, is a micro-climatic variable that is dependent on albedo and surface temperature (Oke, 1987). These, in turn, are affected by surface characteristics such as vegetation cover, slope and aspect which can vary over fine spatial scales (tens to hundreds of metres) depending on landscape complexity. Hence, we take Budyko's statement to mean that, the smaller the catchment area, the more sensitive estimates of $\overline{R_n}$ are likely to be to variations in local catchment surface characteristics and vice versa.

3 Understanding deviations from the Budyko curve

Budyko did note that systematic deviations occurred between actual and expected values and that it was most pronounced in intermediate climates (Fig. 2) and that these deviations were, in part, related to the seasonal cycles of P and R_n/λ (Budyko, 1974, pp. 326). When these are in phase, measured values of ε are slightly higher than expected and, when out of phase, are slightly lower. Budyko did not comment in any detail about the underlying processes.

3.1 Previous studies

A number of studies have examined the Budyko curve to find out what causes the deviations (e.g. Eagleson, 1978; Milly, 1994; Choudhury, 1999; Dooge et al., 1999; Koster and Suarez, 1999; Zhang et al., 2001; Sankarasubramanian and Vogel, 2002; Porporato et al., 2004; Potter et al., 2005). Many have focused on climatic and geophysical processes alone or have included vegetation but treated it as a constant. Several studies are of particular interest here as they have directly examined the effects of vegetation. Milly (1994) set out to explore reasons why Budyko's curve plots below the energy and water limits and what causes the deviations. Using a stochastic model, Milly found that, when the supplies of energy and water varied seasonally, the phase differences between R_n/λ and P where important. For example, when the supplies of R_n/λ and P were seasonal and out of phase there was proportionally less $\overline{E}$ (and more $\overline{Q}$) than when they were either non-seasonal or when seasonal and in phase. Soil water storage, which is partly a function of z_r, provides a buffer against this seasonal climate variability. In times of surplus, water can be stored in situ and is available to vegetation for use at a later time of deficit. Thus, Milly (1994) also found that $\overline{E}$ increases (and $\overline{Q}$ decreases) as potential S_w increases. Milly's analysis was grid-based, with a resolution of 0.5° (A_c~2500 km^2 at 35° latitude). When compared to observed values (represented as interpolated surfaces of equivalent resolution) the model explained 88% and 85% of the variation in $\overline{Q}$ and $\overline{E}$, respectively. Even though the model allowed for a dynamic z_r, Milly held this constant in the analyses.

Choudhury (1999) did not directly examined the effects of vegetation yet he did test the effects of spatial scales of analysis (A_c) on predictions of $\overline{E}$ which are significant from a vegetation perspective. Choudhury used Pike's (1964) equation which is numerically similar to Budyko's curve, except that it had an adjustable parameter, α:

$$\overline{E} = \frac{\overline{P}}{\left(1 + \left(\overline{P}\lambda/\overline{R_n}\right)^{\alpha}\right)^{1/\alpha}} \tag{13}$$

This relationship was tested using observations of $\overline{P}$, $\overline{R_n}$ and $\overline{E}$ derived from mass balances and micro-meteorology at field sites (A_c~1 km^2), and derived from a biophysical process model (Choudhury and DiGirolamo, 1998) for large basins (A_c>1 000 000 km^2). It was found that the dependence of $\overline{E}$ on $\overline{P}$ and $\overline{R_n}$ changes with A_c (α=2.6 for site based observations [r^2=0.99] and 1.8 for basins [r^2=0.97]). That is, the larger the basin area, the lower the α and the less evapotranspiration for a given Φ (Fig. 3). Choudhury did not stipulate exactly what physical processes were involved in this scale-dependence in α.

Zhang et al. (2001) focused on the role vegetation plays within the Budyko framework, acknowledging that a number of key vegetation characteristics affect evapotranspiration rates. Their aim was to adapt the Budyko framework so that it could be used to quantify the effect of long-term vegetation change on $\overline{E}$. They developed an equation similar to Budyko's and Choudhury's, also with an adjustable parameter, w, that they called the "plant available water coefficient":

$$\varepsilon = \frac{1 + w\Phi}{1 + w\Phi + \frac{1}{\Phi}} \tag{14}$$

They hypothesised that this parameter should reflect the role of vegetation, particularly z_r, on $\overline{E}$. In fitting this curve to mass balance data from forested and non-forested catchments, the best-fit values of w were found to be 2.0 [r^2=0.93] and 0.5 [r^2=0.90], respectively (Fig. 3). Hence, forested catchments (high w) have higher $\overline{E}$ and lower $\overline{Q}$ for a given Φ compared to grassed catchments (low w). Catchment sizes varied between 1 and 600 000 km^2. Whilst showing that $\overline{E}$ was related to vegetation, no quantitative link was made between these two variables. Zhang et al. (2004) noted that w represents the integrated effect of multiple catchment processes on evapotranspiration, of which vegetation is one, and that a priori estimations of w for a catchment are very difficult. An important point made by these authors (based on the work of Fu, 1981) was that evapotranspiration is most sensitive to variation in w under intermediate climates (Φ~1).

Building on the work of Milly (1994) and Rodriguez-Iturbe et al. (2001), Porporato et al. (2004) used a simple stochastic model to explore the effect that changes in both z_r and the temporal distribution of precipitation have on the

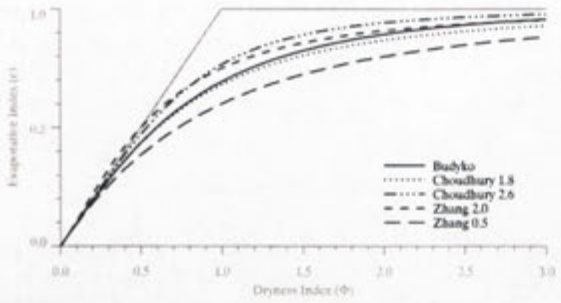

Fig. 3. Comparison of the Budyko curve (Eq. 12) with the curves of Choudhury (1999) (Eq. 13) and Zhang et al. (2001) (Eq. 14). Choudhury 1.8 is calculated using α=1.8 and describes ε from large catchments ($A_c > 1\times10^6$ km^2). Choudhury 2.6 uses α=2.6 and describes field plots ($A_c \sim 1$ km^2). Zhang 2.0 and Zhang 0.5 use w=2.0 and 0.5, respectively, and describe ε from forested and non-forested catchments, respectively.

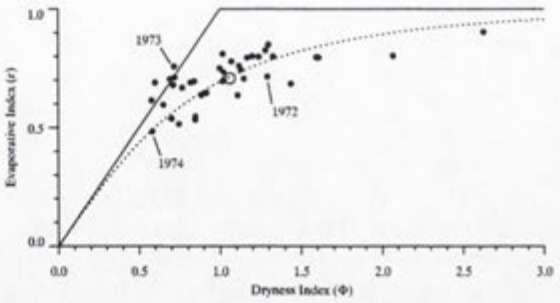

Fig. 4. Inter-annual mass balance data for the Upper Cotter catchment, showing several years with values of ε above the energy-limit. Values derived with Eq. (9) with A_c=148 km^2 and τ=1 year. The progression of ε and Φ from 1972 to 1974 is shown to highlight the ΔS_w between a dry year (1972; $\overline{P}$=780 mm, $\overline{Q}$=220 mm) and a very wet year (1973; $\overline{P}$=1320 mm, $\overline{Q}$=320 mm) and two very wet years (1973) and (1974; $\overline{P}$=1460 mm, $\overline{Q}$=750 mm). The hollow circle denotes the long-term (τ=39 years) value of ε. Data courtesy of Ecowise Services (Australia), Pty. Ltd.

soil water balance and associated ecological processes. Using the Budyko framework, they showed that ΔS_w has the inverse effect on ε as a change in average storm depth. That is, an increase in z_r shifts the Budyko curve up (increases ε) as does a decrease in average storm depth, holding all else constant. These results provide some confirmation of Zhang et al.'s (2001) hypothesis of the relationship between w and z_r. Porporato et al. (2004) then demonstrated how their reformulation of Budyko could be used to estimate the effect of long-term changes in average storm depth (for a given $\overline{P}$) on vegetation productivity, and changes in vegetation on evapotranspiration.

3.2 Interactions between analysis scale, vegetation and Budyko deviations

The only plant functional attribute considered in these previous studies is z_r. This attribute is generally treated as a constant, except by Porporato et al. (2004) who represent it as a temporally dynamic variable. It is a pragmatic approach to hold z_r constant as it is currently a very difficult attribute to measure. Ultimately, it would be extremely useful to integrate vegetation into the framework in a more comprehensive and spatio-temporally dynamic manner as it would enable the Budyko framework be applied to a wider range of ecological and hydrological issues.

The dependence of $\overline{E}$ on the long-term climatic parameters $\overline{P}$ and $\overline{R_n}/\lambda$ has been demonstrated by several authors using a variety of equations that represent variations of the Budyko curve. According to Budyko (1974), the numerical similarity of equations describing this relationship is inevitable. The advantage of the Choudhury (1999) and Zhang et al. (2001) equations is computational simplicity and the flexibility afforded by the adjustable parameters. These two adjustable parameters appear also to be functionally similar, possibly indicating a link between vegetation, A_c and variation in $\overline{E}$ and that such a link is most pronounced under intermediate climates.

Vegetation can affect the spatial scales to which the Budyko framework can be applied. Choudhury's (1999) work emphasised the importance of A_c in describing the dynamics of $\overline{E}$. As Budyko's curve considers only macroclimatic processes, its reliability is greatest where A_c exceeds 1000 km^2. This is confirmed by Budyko (1974) and Milly (1994) who, working at large scales, concluded that most variation in $\overline{E}$ could be explained by Φ. Alternatively, over half the catchments used by Zhang et al. (2001) were under 1000 km^2 and these authors concluded that vegetation does play an important role in partitioning $\overline{P}$ into $\overline{E}$ and $\overline{Q}$ at these scales. Thus, as A_c decreases, the more important it becomes to incorporate the catchment-specific effects of vegetation on the energy and water balances.

Vegetation can also affect the temporal scales appropriate for analysis. Applying the Budyko framework over small time-scales needs to be done carefully in order to maintain steady-state conditions as vegetation dynamics, and particularly net changes in vegetation (e.g. due to harvesting, wildfire and land-use change) can result in large ΔS_w even when τ is around 1 year. Several examples will illustrate this. Talsma and Gardner (1986) showed that some *Eucalyptus* species drew more heavily on stored water during the summer of a drought year than the summers of years with average precipitation, using 200 mm more soil water than average. Another example is given in Fig. 4, which shows evapotranspiration for the Upper Cotter catchment in the Australian Capital Territory (148°50′, 35°40′ S, 148 km^2) calculated using Eq. (9) with τ=1 year. Several years show evapotranspiration values above the energy limit. These years

had unexpectedly low $\overline{Q}$ given the high $\overline{P}$ and were each preceded by moderately dry years. This catchment contains *Sphagnum* bogs with large water holding capacities. The observed pattern implies that recharge/discharge of these bogs results in relatively large changes in S_w. When measured $\overline{P}$ and $\overline{Q}$ are used to estimate $\overline{E}$ using Eq. (9) in a non-steady-state catchment, the estimate of $\overline{E}$ inherently includes ΔS_w. Finally, Calder et al. (1997) reported that *Eucalyptus* plantations established on former croplands exploited substantial stored soil water resulting in unusually high $\overline{E}$ and that ΔS_w could be up to 50% of $\overline{P}$ for several years after planting (the opposite ΔS_w would be expected in the years following clearing of the same plantations). These examples demonstrate that vegetation dynamics can result in non-steady-state conditions, especially after net vegetation change, over periods of up to several years. The longer the period needed to establish steady-state conditions, the less useful the approach for catchment and land management applications.

Budyko's curve is based on long-term averages which remove short- to medium-term variability to establish steady-state conditions. Consequently, the reliability of Budyko's curve is diminished if used to address issues of short-term changes in the water balance. This is particularly pertinent to vegetated landscapes as the hydrological role of vegetation can be highly dynamic. It will be of great practical value to apply a Budyko-type framework to inter-annual (and even intra-annual) timeframes and therefore be able to use it to address landscape change.

Besides affecting the spatial and temporal scales to which Budyko can be applied, quantitative incorporation of hydrologically important vegetation characteristics into Budyko's model is also expected to open its scope to more ecologically-oriented applications such as vegetation productivity modelling (e.g. Porporato, 2004), to integrated vegetation and water management and to assessing possible impacts of climate change on catchment processes. A crucial aspect of achieving this is to ensure that the vegetation characteristics have relevance at catchment scales and be readily measured, preferably by some form of remote sensing.

4 The dynamic role of vegetation in the water balance

It is well established that vegetation plays an important role in the water balance (e.g. Jones, 1992; Calder, 1993; Arora, 2002; Lee et al., 2005) and that changes in vegetation extent and type are accompanied by changes in catchment evapotranspiration and run-off (Sharma, 1984; Vertessy et al., 2003). This was recently highlighted by Farley et al. (2005) and Jackson et al. (2005) in the context of the hydrological consequences of proposed afforestation for carbon sequestration. Although many plant physiological and structural characteristics affect $\overline{E}$, the three that dominate are: 1) leaf area; 2) photosynthetic rate; and 3) rooting depth (Pierce et al., 1993; Zhang et al., 2001; Arora, 2002; Eamus, 2003). These characteristics have rarely been incorporated into catchment-scale hydrological models (Arora, 2002) most likely because they can be difficult to measure at these scales. Nevertheless, it is important to understand how they each influence $\overline{E}$ in order to understand the nature of, and mechanisms driving, the different water use dynamics of different vegetation types.

4.1 Three key vegetation attributes

The first two vegetation characteristics - leaf area and photosynthetic rate - only directly affect the flux components of Eq. (9). Rooting depth, on the other hand, affects both the flux and the steady-state components of the water balance. Focusing on the evaporative flux, $\overline{E}$ can be separated into three fractions: transpiration ($\overline{E_t}$), evaporation from plant surfaces of intercepted precipitation ($\overline{E_i}$) and evaporation from soil and other non-vegetated surfaces ($\overline{E_s}$, all in $\mathrm{kg\,s^{-1}}$):

$$\overline{E} = \overline{E_t} + \overline{E_i} + \overline{E_s} \tag{15}$$

The leaf area of canopies is commonly represented using the leaf area index (L) which is the total projected leaf area per unit ground area:

$$L = \frac{\text{leaf area}}{\text{ground area}} \tag{16}$$

L is an important plant structural attribute that relates to both the energy and water fluxes (Nemani and Running, 1989; Pierce et al., 1993; Hatton and Wu, 1995). L is related to photosynthesis as it determines the fraction of Photosynthetically Active Radiation absorbed by foliage (fPAR). It alters albedo, and therefore R_n, as well as surface roughness which influences $\overline{E}$ (Arora, 2002). Of the three vegetation characteristics only L directly affects all three fractions of the evaporative flux. Broadly, $\overline{E_t}$ and $\overline{E_i}$ are related to L and $\overline{E_s}$ is inversely related to L. At low values of L common in drier environments ($\leq$3–5) increases in L are accompanied by proportional increases in $\overline{E_t}$ and decreases in $\overline{E_s}$ (Schulze et al., 1994, Law et al., 2002). As the climate becomes wetter and L increases further, $\overline{E_t}$ becomes less responsive to changes in L (Schulze et al., 1994) and the relationship between $\overline{E_i}$ and L becomes important, such that $\overline{E_i}$ can comprise 40–50% of $\overline{E}$ in energy-limited environments (Hutley et al., 1997; Barbour et al., 2005). Considering these relations, L bears a general relationship to $\overline{E}$ over most climates.

Leaf area is a highly dynamic vegetation characteristic. It varies with resource availability (Field et al., 1992; Whitehead and Beadle, 2004) being higher where conditions are more favourable for growth. Significant temporal variation occurs due to climate dynamics and the type and age of vegetation. Annual and deciduous species have extreme cyclical variation in L whilst evergreen species have more moderate values with medium-low seasonal variability. L can change inter-annually as a function of vegetation age: young vegetation quickly increases its leaf area which peaks before dropping to a lower and more constant value as it matures (Arora,

2002). Vegetation age is altered by the frequency of major disturbances (e.g. fires, storms, diseases) and management actions (e.g. destructive harvesting, crop establishment).

Photosynthetic rate (A_g, mol CO_2 s^{-1}) refers to the net carbon assimilation rate per unit leaf area (Salisbury and Ross, 1992; Larcher, 1995). A_g is related, via leaf conductance (Wong et al., 1979), to E_t as:

$$E_t = 0.018\left(\frac{A_g}{W_{ph}}\right) \quad (17)$$

where W_{ph} is the water use efficiency of photosynthesis and is the ratio of the number of moles CO_2 gained in photosynthesis to the number of moles H_2O lost in transpiration, expressed per unit leaf area. In this case, E_t is also per unit leaf area. A variety of methods can be used to approximately convert A_g to canopy or catchment scales (Norman, 1993) and W_{ph} can be expressed similarly (McVicar et al., 2002) allowing Eq. (17) to be expressed per unit ground area. It can be seen from Eq. (17) that, at a given W_{ph}, high A_g is accompanied by high rates of transpiration. A_g is highly dynamic, varying within and across species and vegetation types, with location and plant age. Highly fertile sites support vegetation with higher A_g than resource poor sites (Larcher, 1995; Eamus et al., 2001). There is a general relationship between A_g, the ratio of leaf area to leaf volume (Λ) and leaf longevity (Reich et al., 1997; Roderick et al., 2000). Short-lived, thin leaves (high Λ) typical of annual and deciduous species and the young foliage of evergreens, have high A_g compared with long-lived, thick leaves (low Λ) of mature evergreens, all else being equal. Also, A_g and L bear a general relationship as both are higher in resource-rich locations and become less as water and/or nutrients become scarce.

Rooting depth (z_r) is an extremely important plant characteristic as it alters the water balance in two ways. Firstly, z_r affects the flux components of the water balance (Eq. 9) by determining the soil water potentially available for transpiration. In the absence of roots (vegetation), little buffering of precipitation variability occurs and, considering that evaporation from bare soil rapidly diminishes after precipitation (Ritchie, 1972), the majority of precipitation eventually becomes run-off (Milly, 1994; Porporato et al., 2004). It is worth noting that z_r has different affects on S_w in different soil types due to differences in $[S_w]$ and that variations in $[S_w]$ can result from changes in vegetation and from management-induced changes in soil structure (Eldridge and Freudenberger, 2005; Craze and Hamilton, 1991). Secondly, z_r can affect the steady-state components of the water balance. Roots extend down some proportion of total soil depth. Even though soil depth at a site may be invariant (over typical timescales of interest, e.g. 100 years), z_r is not. It can vary inter-annually due to fluctuations in climate (Field et al., 1992), and even seasonally in concert with water table fluctuations (Knight, 1999; Pate and Bell, 1999). Of significance is the potentially rapid changes in z_r, and therefore in S_w (Eq. 9), due to vegetation change. Disturbances such as deforestation can almost instantly reduce the effective z_r (roots may remain but are generally inactive) whilst regeneration and revegetation can increase it over time. Hence, z_r not only affects $\overline{E_t}$ but can also alter ΔS_w and therefore the value of τ required to achieve steady-state conditions.

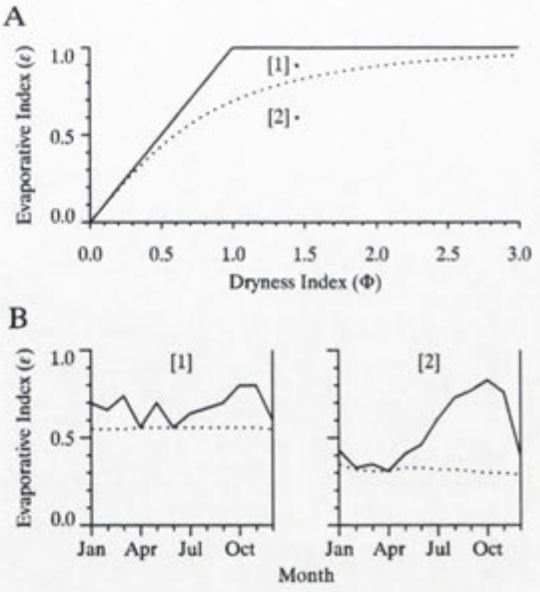

Fig. 5. The effect of seasonal vegetation dynamics on catchment evapotranspiration and run-off. For a given dryness index, catchments with a high proportion of persistent vegetation (e.g. [1]) have greater evapotranspiration fluxes and smaller run-off fluxes (and therefore plot higher on the Budyko curve) than catchments with a high proportion of recurrent vegetation (e.g. [2]).

(A): Indicative values of the evaporative index for catchments [1] and [2], both with $\Phi \sim 1.45$, demonstrating vertical deviations that are possible within the Budyko framework.

(B): Profiles of catchment fPAR showing seasonal vegetation dynamics. Catchment [1] has a higher total fPAR (solid line) and higher proportion of persistent fPAR (dotted line) compared to catchment [2]. Recurrent fPAR is the difference between total and persistent. Catchment [1] supports mostly open Eucalypt forest (149.725° E, 34.070° S). Catchment [2] supports agricultural pastures with patches of Eucalypt forest (147.369° E, 35.443° S). Derivations of fPAR and the persistent/recurrent components based on Roderick et al. (1999) using AVHRR Global Area Coverage NDVI data.

4.2 Seasonal vegetation dynamics

Budyko (1974) and Milly (1994) both noted that phase differences between the seasonal dynamics of R_n/λ and P are associated with differences that can occur in E and Q under a given climate. Such differences result in vertical deviations from the Budyko curve where, for a given Φ, a variety of values in ε can occur (Fig. 5a). As Zhang et al. (2001)

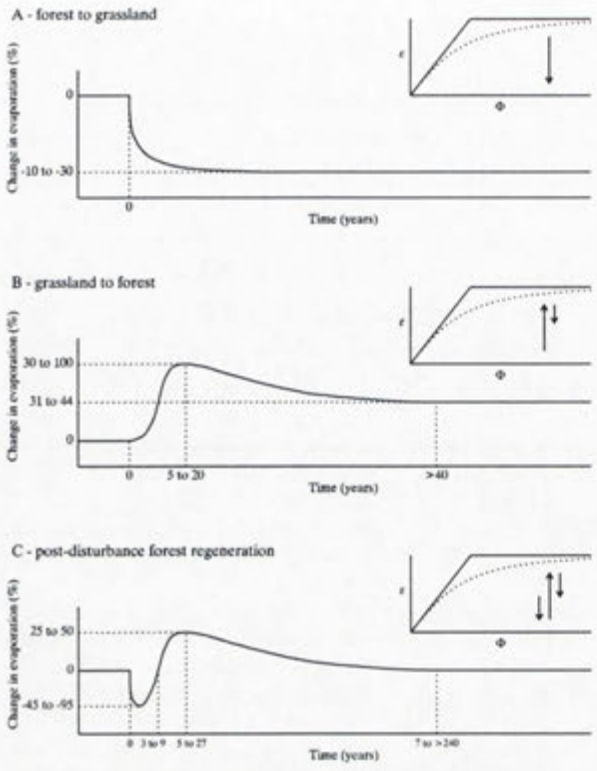

Fig. 6. Changes in catchment evapotranspiration following major vegetation changes.

(A): Conversion of forest to grassland. **(B)**: Conversion of grassland to forest. **(C)**: Forest disturbance and subsequent regeneration. Values given are predominantly based on Eucalypt forests and plantations in water-limited catchments (Langford, 1976; Van Lill et al., 1980; Kuczera, 1987; Pierce et al., 1993; Costa and Foley, 1997; Vertessy, 1998; Cornish and Vertessy, 2001; Gordon et al., 2003; Vertessy et al., 2003; Farley et al., 2005). The timing and magnitude of changes in evapotranspiration vary with annual average precipitation, species and the proportion of catchment undergoing change. Insets indicate vertical changes ($\Delta\varepsilon$ for a given Φ) in a catchment's location within the Budyko framework associated with each type of vegetation change.

and Porporato et al. (2004) have shown, these vertical deviations also relate to seasonal water use dynamics of different vegetation types. Further, seasonal vegetation dynamics and seasonal climate dynamics are coupled (Berry et al., 2005) – except where the vegetation has been heavily modified – such that it would be difficult to ascertain which of the two dynamics are most directly responsible for these deviations.

A useful classification of vegetation which captures these seasonal water use differences is persistent and recurrent functional types. This approach is useful because the functional types can be distinguished in time-series satellite imagery (DeFries et al., 1995; Roderick et al., 1999; Lu et al., 2003). Persistent vegetation is comprised of species that are active year-round and displays relatively little seasonal variation in canopy structure. This generally encompasses non-deciduous, perennial species. Recurrent vegetation is comprised of species that operate in continuous cycles of activity and dormancy and includes deciduous, annual and ephemeral species. These two types are characterised by differences in the seasonal dynamics of L and A_g. Also, if deciduous species are uncommon in a catchment, then the useful generalisation can be made that persistents have high and reasonably static z_r and recurrents have low z_r and this only during the growing season. One consequence of these dynamics is that, for a given climate, $\overline{E}$ from a catchment supporting mostly persistent vegetation should be relatively high and $\overline{Q}$ relatively low compared to that from a catchment with mostly recurrent vegetation (Hatton and Nulsen, 1999; Berry et al., 2005). On the Budyko curve, a persistent catchment is likely to plot above the curve and a recurrent catchment below the curve (Figs. 5a and b), as per Zhang et al. (2001). Describing vegetation simply as annual averages will not fully capture these important differences in $\overline{E}$ and $\overline{Q}$ associated with seasonal vegetation dynamics. Instead, some indication of the relative contributions of recurrent and persistent vegetation types to a catchment's water balance (e.g. Fig. 5b) will most likely explain more of the vertical deviations that occur around the Budyko curve.

4.3 Annual vegetation dynamics

Catchments experiencing net vegetation change between years will experience changes in catchment evapotranspiration. The position that such catchments plot on the Budyko curve can change over time even in the absence of changes in the macro-climate. For example, clearing of persistent vegetation means an instant reduction in z_r, A_g and L and, for a given Φ, is followed by a decrease in $\overline{E}$ and an increase in $\overline{Q}$. A change in S_w occurs as the soil profile fills in the absence of soil water extraction by deep roots. A new steady-state eventually re-establishes at a lower $\overline{E}$ associated with the replacement vegetation type typically being recurrent (Fig. 6a). This is the typical hydrological impact of clearing for agriculture (Calder, 1993; Pierce et al., 1993; Walker et al., 1993). These changes mean a catchment will progressively plot lower on the Budyko curve. The opposite vegetation change – the replacement of recurrent with persistent vegetation – initially produces a marked increase in $\overline{E}$ and drop in $\overline{Q}$ (Fig. 6b) due to the high L, A_g and rapid increases in z_r (up to 2.5 m/yr (Calder et al., 1997)) associated with young evergreen vegetation. Rapid extraction of S_w often occurs. As the vegetation ages, $\overline{E}$ moderates and a new steady-state establishes with higher overall $\overline{E}$ and lower $\overline{Q}$ than that of the original steady-state condition, which eventually locates the catchment higher on the Budyko curve. This is the typical hydrological pattern following

afforestation (Van Lill et al., 1980; Vertessy et al., 2003; Farley et al., 2005). Both these cycles are observed when persistent vegetation regenerates after disturbance (Fig. 6c) such as after fire (Vertessy, 1998) or after timber harvesting (Cornish and Vertessy, 2001). These examples demonstrate that dramatic vegetation change can disrupt steady-state conditions within catchments and alter the relative proportions of $\overline{Q}$ and $\overline{E}$ for years, and even decades, after large disturbances, ultimately changing a catchment's position within the Budyko framework.

In summary, Sects. 3 and 4 have demonstrated the potentially significant role vegetation plays in the hydrology of catchments. Vegetation dynamics can dictate the spatio-temporal scales appropriate for analyses. This is because the three key vegetation characteristics, L, A_g and z_r, are all spatially and temporarily dynamic. Each can influence the flux components of the water balance whilst z_r can also change steady-state conditions. When both τ and A_c are large, it has been found that it is not necessary to explicitly include vegetation in Budyko's framework to achieve reasonable predictions of catchment behaviour. However, as τ and/or A_c become smaller it becomes increasingly important to incorporate both the inter- and intra-annual vegetation dynamics into the framework. One potential way of achieving this may be to utilise remotely sensed vegetation information within the theoretical framework of ecohydrological equilibrium.

5 Using vegetation information in ecohydrology

5.1 Vegetation – the great landscape integrator

Vegetation directly affects the energy and water balances. However, vegetation grows in response to the combined affect of all conditions that limit growth (Odum, 1993), such as light, temperature, pH, nutrients and disturbances. In environments where the dominant limitation is water, vegetation grows in response to the multiple processes that affect the availability of water (Specht, 1972; Zhang et al., 2004) and may provide a shortcut to quantifying the local, micro-climatic factors affecting $\overline{E}$. As Nemani and Running (1989) suggested, vegetation is the great landscape integrator.

5.2 Ecohydrological equilibrium

In water-limited environments strong relationships have been found between water availability and mature, perennial vegetation, most particularly vegetation structure (Specht, 1972; Woodward, 1987). Perennial vegetation supports leaf areas that can be predicted from moisture availability and which vary in concert with it. This suggests an ecohydrological equilibrium, or steady-state (Eagleson, 1978, 1982; Nemani and Running, 1989; Pierce et al., 1993; Hatton and Nulsen, 1999), a dynamic condition that fluctuates with micro-climatic variations and only occurs in relatively undisturbed vegetation. Measures of such vegetation are expected to be correlated to the net effect of all processes affecting water availability and may bypass the need to measure each process individually (Zhang et al., 2004). Since L is an above-ground, structural characteristic and is therefore relatively easy to measure compared to z_r and A_g, it is the most useful of the three vegetation characteristics to incorporate into the Budyko model. As L fluctuates according to ecohydrological equilibrium theory, in some circumstances incorporation of L will account for the effects of z_r, and even changes in z_r (Specht, 1972), and may provide a surrogate measure of z_r. Additionally, L provides a link to land management as L is manipulated by management practices such as planting, harvesting and thinning of vegetation and by modifying site fertility.

5.3 Remotely-sensed measures of Leaf Area Index and the fraction of absorbed Photosynthetically Available Radiation (fPAR)

The easiest means of measuring L across large areas and repeatedly through time is by satellite-based remote sensing. Vegetation has a unique spectral signature (Jones, 1992) which forms the basis of a variety of remotely sensed vegetation indices, including the Simple Ratio (SR) and the more common Normalised Difference Vegetation Index (NDVI). Theory and measurements have shown that SR is linearly related to L whilst NDVI is non-linearly related to L above values of L around 2-4 (Nemani and Running, 1989; McVicar et al., 1996; Carlson, 1997; Lu et al., 2003). The NDVI-L relationship saturates with further increases in L. fPAR, on the other hand, is near-linearly related to NDVI (Kumar and Monteith, 1981; Asrar et al., 1984; Lu et al., 2003) and can be related to A_g and E_t through Monteith's light use efficiency model (Monteith, 1981; Roderick et al., 2001; Berry and Roderick, 2004). Considering the problematic NDVI-L relationship and that fPAR is functionally similar to L, from a remote sensing point of view fPAR would be an excellent alternative measure for describing the hydrological role of vegetation.

In applications, integrals of NDVI have often been used (e.g. Prince, 1991; McVicar and Jupp, 1998). Annual NDVI has been found to be linearly related to annual catchment $\overline{E}$ from both an energy-limited environment (Szilagyi, 2000) and a water-limited environment (Mora and Iverson, 1998). For more detailed work, the seasonal dynamics of the fPAR signal can be processed to estimate the persistent and recurrent vegetation types (Fig. 5b) (Roderick et al., 1999; Lu et al., 2003) which can then be used to estimate primary productivity and $\overline{E}$ of the separate types (Berry and Roderick, 2004). It is worth noting that before using fPAR data in applications, it is important to ensure potential sources of signal contamination are accounted for, such as the effects of satellite calibration, atmospheric and cloud interference, and Sun-target-sensor geometry (Gutman, 1999, Kaufman et al. 2000, Tanre et al., 1992).

6 Conclusion

The assumptions inherent in Budyko's hydrological model have been highlighted by explicitly restating the framework to include the temporal (τ) and spatial (A_c) scales of analysis. The first assumption is that catchments are at steady-state (that is, $\Delta S_w \approx 0$). To a large degree, this condition depends on τ. The second is that, at large spatial scales ($A_c \gg 1000\,km^2$), only macro-climatic variables are required to describe catchment water balances. When applied over long timescales and to large catchments, Budyko's curve reliably predicts catchment water balances. However, when applied to small spatio-temporal scales the inherent assumptions can be violated. It is in these circumstances that incorporating vegetation into the framework is expected to enhance the frameworks predictive capacity.

Vegetation is known to play a significant and highly dynamic role in determining catchment evapotranspiration. Vegetation accesses stored soil water, the potential volume of which is determined by z_r, and evaporates this water into the atmosphere at rates dependent on $L$and A_g amongst other things. The role of vegetation in the water balance is continually changing as z_r, L and A_g all vary with climatic conditions and with the type and age of vegetation. At small spatial and temporal scales ($A_c \leq 1000\,km^2$ and $\tau \leq 1$–5 years), which are scales arguably more relevant to management activities than those originally used by Budyko, vegetation becomes an important explanatory variable of catchment hydrological behaviour. This is particularly true for catchments experiencing net vegetation change as this means the relative proportions of $\overline{E}$ and $\overline{Q}$ are shifting and, because of changes in z_r, steady-state conditions are unlikely to exist in these catchments.

The theory of ecohydrological equilibrium is based on the idea that, in water-limited environments, vegetation is the integrated response to all processes affecting the availability of water. Consequently, incorporation of some key measure of vegetation into Budyko's model is expected to extend the model's ability to describe catchment behaviour to small-scale analyses. L is one such measure as it has been shown to vary with water availability according to ecohydrological equilibrium theory. It is difficult to measure L across large areas and repeatedly through time and so remotely-sensed estimates of fPAR can provide a useful alternative measure of vegetation. We expect that the integration of the temporally dynamic recurrent and persistent components of fPAR into the Budyko framework will extend the framework to be a reliable predictor of $\overline{E}$ and $\overline{Q}$ over small timescales and/or in small catchments, even when those catchments are experiencing significant vegetation change.

As far as we are aware, this proposal has not yet been tested. If such a modified Budyko framework can be developed, its use is expected to extend not only to application at small scales but also to practical applications such as predicting the hydrological effects of vegetation management activities. It is also expected to be a powerful tool for exploring the possible effects of short and long-term climate change on both vegetation and hydrology.

Acknowledgements. This research has been supported by the Research School of Biological Sciences, CSIRO Land and Water and eWater CRC. The ARC Earth System Science Network provided funding for attendance at the Sir Mark Oliphant Conference on Thresholds and Pattern Dynamics in Climate Driven Systems 3–7 July 2005. We particularly thank N. Potter, CSIRO Land and Water, for helpful comments. We also thank the three anonymous reviewers and the editor for their constructive contributions to the manuscript.

Edited by: C. Hinz

References

Arora, V.: Modeling vegetation as a dynamic component in soil-vegetation-atmosphere transfer schemes and hydrological models, Rev. Geophys., 40(2), doi:10.1029/2001RG000103, 2002.

Asrar, G., Fuchs, M., Kanemasu, E. T., and Hatfield, J. L.: Estimating absorbed photosynthetic radiation and leaf-area index from spectral reflectance in wheat, Agronomy J., 76, 300–306, 1984.

Barbour, M. M., Hunt, J. E., Walcroft, A. S., Rogers, G. N. D., McSeveny, T. M., and Whitehead, D.: Components of ecosystem evaporation in a temperate coniferous rainforest, with canopy transpiration scaled using sapwood density, New Phytologist, 165, 549–558, 2005.

Berry, S. L., Farquhar, G. D., and Roderick, M. L.: Co-evolution of climate, soil and vegetation, in: Encyclopaedia of hydrological sciences, edited by: Anderson M., John Wiley And Sons, Indianapolis, 2005.

Berry, S. L. and Roderick, M. L.: Gross primary productivity and transpiration flux of the Australian vegetation from 1788 to 1988 AD: effects of CO_2 and land use change, Global Change Biology, 10, 1884–1898, 2004.

Budyko, M. I.: The heat balance of the earth's surface, U.S. Dept. of Commerce, Washington, 1958.

Budyko, M. I.: Climate and life, Academic, New York, 1974.

Calder, I. R.: Hydrologic effects of land-use change, in: Handbook of hydrology, edited by: Maidment, D. R., McGraw Hill, Sydney, 1993.

Calder, I. R., Rosier, P. T. W., Prasanna, K. T., and Parameswarappa, S.: Eucalyptus water use greater than rainfall input-a possible explanation from southern India, Hydrol. Earth Syst. Sci., 1, 249–256, 1997, http://www.hydrol-earth-syst-sci.net/1/249/1997/.

Carlson, T. N., and Ripley, D. A.: On the relation between NDVI, fractional vegetation cover, and leaf area index, Remote Sens. Environ., 62, 241–252, 1997.

Choudhury, B. J.: Evaluation of an empirical equation for annual evaporation using field observations and results from a biophysical model., J. Hydrol., 216, 99–110, 1999.

Choudhury, B. J. and DiGirolamo, N. E.: A biophysical process-based estimate of global land surface evaporation using satellite and ancillary data – I. Model description and comparison with observations, J. Hydrol., 205, 164–185, 1998.

Cornish, P. M. and Vertessy, R. A.: Forest age-induced changes in evapotranspiration and water yield in a eucalypt forest, J. Hydrol., 242, 43–63, 2001.

Costa, M. H. and Foley, J. A.: Water balance of the Amazon Basin: dependence on vegetation cover and canopy conductance, J. Geophys. Res.-Atmos., 102, 23 973–23 989, 1997.

Craze, B., and Hamilton, G. J.: Soil physical properties, in: Soils - their properties and management, edited by: Charman, P. E. V. and Murphy, B. W., Sydney University Press, South Melbourne, 147–164, 1991.

DeFries, R., Hansen, M., and Townshend, J.: Global discrimination of land cover types from metrics derived from AVHRR pathfinder data, Remote Sens. Environ., 54, 209–222, 1995.

Dooge, J. C. I., Bruen, M., and Parmentier, B.: A simple model for estimating the sensitivity of runoff to long-term changes in precipitation without a change in vegetation, Advances in Water Resources, 23, 153–163, 1999.

Eagleson, P. S.: Climate, soil, and vegetation 4. Expected value of annual evapotranspiration, Water Resour. Res., 14, 731–739, 1978.

Eagleson, P. S.: Ecological optimality in water-limited natural soil-vegetation systems, 1. theory and hypothesis, Water Resour. Res., 18, 325–340, 1982.

Eamus, D.: How does ecosystem water balance affect net primary productivity of woody ecosystems?, Functional Plant Biology, 30, 187–205, 2003.

Eamus, D., Hutley, L. B., and O'Grady, A. P.: Daily and seasonal patterns of carbon and water fluxes above a north Australian savanna, Tree Physiology, 21, 977–988, 2001.

Eldridge, D. J., and Freudenberger, D.: Ecosystem wicks: woodland trees enhance water infiltration in a fragmented agricultural landscape in eastern Australia, Austral Ecology, 30, 336–347, 2005.

Farley, K. A., Jobbagy, E. G., and Jackson, R. B.: Effects of afforestation on water yield: a global synthesis with implications for policy, Global Change Biology, 11, 1565–1576, 2005.

Field, C. B., Chapin, F. S., Matson, P. A., and Mooney, H. A.: Responses of terrestrial ecosystems to the changing atmosphere – a resource-based approach, Ann. Rev. Ecol. Systematics, 23, 201–235, 1992.

Fu, B. P.: On the calculation of the evaporation from land surface (in Chinese), Scientia Atmospherica Sinica, 5, 23–31, 1981.

Gordon, L., Dunlop, M., and Foran, B.: Land cover change and water vapour flows: learning from Australia, Philosophical Transactions of the Royal Society of London Series B-Biological Sciences, 358, 1973–1984, 2003.

Granger, R. J.: An examination of the concept of potential evaporation, J. Hydrol., 111, 9–19, 1989.

Gutman, G. G.: On the use of long-term global data of land reflectances and vegetation indices derived from the advanced very high resolution radiometer, J. Geophys. Res.-Atmos., 104, 6241–6255, 1999.

Hatton, T. J. and Nulsen, R. A.: Towards achieving functional ecosystem mimicry with respect to water cycling in southern Australian agriculture, Agroforestry Systems, 45, 203–214, 1999.

Hatton, T. J. and Wu, H. I.: Scaling theory to extrapolate individual tree water-use to stand water-use, Hydrol. Processes, 9, 527–540, 1995.

Hutley, L. B., Doley, D., Yates, D. J., and Boonsaner, A.: Water balance of an Australian subtropical rainforest at altitude: The ecological and physiological significance of intercepted cloud and fog, Aust. J. Botany, 45, 311–329, 1997.

Jackson, R. B., Jobbagy, E. G., Avissar, R., Roy, S. B., Barrett, D. J., Cook, C. W., Farley, K. A., le Maitre, D. C., McCarl, B. A., and Murray, B. C.: Trading water for carbon with biological sequestration, Science, 310, 1944–1947, 2005.

Jones, H. G.: Plants and microclimate, Second edition, Cambridge University Press, Cambridge, 1992.

Kaufmann, R. K., Zhou, L.M., Knyazikhin, Y., Shabanov, N.V., Myneni, R.B., Tucker, C.J.: Effect of orbital drift and sensor changes on the time series of AVHRR vegetation index data, IEEE Transactions on Geoscience and Remote Sensing, 38, 2584–2597, 2000.

Knight, J. H.: Root distributions and water uptake patterns in Eucalypts and other species, in: The ways trees use water, p. 55–85, edited by: Landsberg, J., Rural Industries Research and Development Corporation, publication 99/37, project CSM-4A, Canberra, 1999.

Koster, R. D. and Suarez, M. J.: A simple framework for examining the interannual variability of land surface moisture fluxes, J. Climate, 12, 1911–1917, 1999.

Kuczera, G.: Prediction of water yield reductions following a bushfire in ash-mixed species eucalypt forest, J. Hydrol., 94, 215–236, 1987.

Kumar, M. and Monteith, J. L.: Remote sensing of crop growth, Academic press, New York, 1981.

Langford, K. J.: Change in yield of water following a bushfire in a forest of Eucalyptus regnans, J. Hydrol., 29, 87–114, 1976.

Larcher, W.: Physiological plant ecology: ecophysiology and stress physiology of functional groups, Third edition, Springer, Berlin, 1995.

Law, B. E., Falge, E., Gu, L., Baldocchi, D. D., Bakwin, P., Berbigier, P., Davis, K., Dolman, A. J., Falk, M., Fuentes, J. D., Goldstein, A., Granier, A., Grelle, A., Hollinger, D., Janssens, I. A., Jarvis, P., Jensen, N. O., Katul, G., Mahli, Y., Matteucci, G., Meyers, T., Monson, R., Munger, W., Oechel, W., Olson, R., Pilegaard, K., Paw, K. T., Thorgeirsson, H., Valentini, R., Verma, S., Vesala, T., Wilson, K., and Wofsy, S.: Environmental controls over carbon dioxide and water vapor exchange of terrestrial vegetation, Agric. For. Meteorol., 113, 97–120, 2002.

Lee, J. E., Oliveira, R. S., Dawson, T. E., and Fung, I.: Root functioning modifies seasonal climate., Proceedings of the National Academy of Sciences of United States of America, 102, 17 576–17 581, 2005.

Lu, H., Raupach, M. R., McVicar, T. R., and Barrett, D. J.: Decomposition of vegetation cover into woody and herbaceous components using AVHRR NDVI time series, Remote Sens. Environ., 86, 1–18, 2003.

McVicar, T. R. and Jupp, D. L. B.: The current and potential operational uses of remote sensing to aid decisions on drought exceptional circumstances in Australia: a review, Agricultural Systems, 57, 399–468, 1998.

McVicar, T. R., Walker, J., Jupp, D. L. B., Pierce, L. L., Byrne, G. T., and Dallwitz, R.: Relating AVHRR vegetation indices to in situ measurements of leaf area index, Technical memorandum 96.5, CSIRO Division of Water Resources, Canberra, 1996.

McVicar, T. R., Zhang, G. L., Bradford, A. S., Wang, H. X., Dawes,

W. R., Zhang, L., and Li, L. T.: Monitoring regional agricultural water use efficiency for Hebei Province on the North China Plain, Australian J. Agric. Res., 53, 55–76, 2002.

Milly, P. C. D.: Climate, soil water storage, and the average annual water balance, Water Resour. Res., 30, 2143–2156, 1994.

Montaldo, N., Rondena, R., Albertson, J. D., and Mancini, M.: Parsimonious modeling of vegetation dynamics for ecohydrologic studies of water-limited ecosystems, Water Resour. Res., 41, W10416, doi:10.1029/2005WR, 2005.

Monteith, J. L.: Evaporation and surface temperature, Quart. J. Roy. Meteorol. Soc., 107, 1–27, 1981.

Mora, F. and Iverson, L. R.: On the sources of vegetation activity variation, and their relation with water balance in Mexico, Int. J. Remote Sens., 19, 1843–1871, 1998.

Nemani, R. R. and Running, S. W.: Testing a theoretical climate soil leaf-area hydrologic equilibrium of forests using satellite data and ecosystem simulation, Agric. For. Meteorol., 44, 245–260, 1989.

Norman, J. M.: Scaling processes between leaf and canopy levels, in: Scaling physiological processes – leaf to globe, edited by: Ehleringer, J. R. and C. B., Field, Academic, San Diego, 41–76, 1993.

Odum, E. P.: Ecology and our endangered life-support systems, Second edition, Sinaver, Sunderland, 1993.

Oke, T. R.: Boundary layer climates, Second edition, Routledge, London, 1987.

Ol'dekop, E. M.: On evaporation from the surface of river basins., Transactions on meteorological observations., 4, 1911.

Pate, J. S. and Bell, T. L.: Application of the ecosystem mimic concept to the species-rich Banksia woodlands of Western Australia, Agroforestry Systems, 45, 303–341, 1999.

Peel, M. C., Chiew, F. H. S., Western, A. W., and McMahon, T. A.: Extension of unimpaired monthly streamflow data and regionalisation of parameter values to estimate streamflow in ungauged catchments, National Land and Water Resources Audit, Canberra, http://audit.ea.gov.au/anra/water/docs/national/Streamflow/Streamflow.pdf. 2000.

Pierce, L. L., Walker, J., Dowling, T. I., McVicar, T. R., Hatton, T. J., Running, S. W., and Coughlan, J. C.: Ecohydrological changes in the Murray-Darling Basin .3. A simulation of regional hydrological changes, J. Appl. Ecology, 30, 283–294, 1993.

Pike, J. G.: The estimation of annual run-off from meteorological data in a tropical climate, J. Hydrol., 2, 116–123, 1964.

Porporato, A., Daly, E., and Rodriguez-Iturbe, I.: Soil water balance and ecosystem response to climate change, American Naturalist, 164, 625–632, 2004.

Potter, N. J., Zhang, L., Milly, P. C. D., McMahon, T. A., and Jakeman, A. J.: Effects of rainfall seasonality and soil moisture capacity on mean annual water balance for Australian catchments, Water Resour. Res., 41, W02502, doi:10.1029/2003WR002710, 2005.

Prince, S. D.: A model of regional primary production for use with coarse resolution satellite data, Int. J. Remote Sens., 12, 1313–1330, 1991.

Raupach, M. R., Kirby, J. M., Barrett, D. J., and Briggs, P. R.: Balances of water, carbon, nitrogen and phosphorus in Australian landscapes: (1) Project description and results, Technical report 40/01, CSIRO Land and Water, Canberra, 2001.

Reich, P. B., Walters, M. B., and Ellsworth, D. S.: From tropics to tundra: global convergence in plant functioning, Proc. National Academy of Sciences of the United States of America, 94, 13 730–13 734, 1997.

Ritchie, J. T.: Model for predicting evaporation from a row crop with incomplete cover, Water Resour. Res., 8, 1204–1213, 1972.

Roderick, M. L., Berry, S. L., and Noble, I. R.: A framework for understanding the relationship between environment and vegetation based on the surface area to volume ratio of leaves., Functional Ecology, 14, 423–437, 2000.

Roderick, M. L., Farquhar, G. D., Berry, S. L., and Noble, I. R.: On the direct effect of clouds and atmospheric particles on the productivity and structure of vegetation., Oecologia, 129, 21–30, 2001.

Roderick, M. L., Noble, I. R., and Cridland, S. W.: Estimating woody and herbaceous vegetation cover from time series satellite observations, Global Ecology and Biogeography, 8, 501–508, 1999.

Rodriguez-Iturbe, I. and Porporato, A.: Ecohydrology of water-controlled ecosystems: soil moisture and plant dynamics, Cambridge University Press, Cambridge, 2004.

Rodriguez-Iturbe, I., Porporato, A., Laio, F., and Ridolfi, L.: Plants in water-controlled ecosystems: active role in hydrologic processes and response to water stress – I. Scope and general outline, Adv. Water Resour., 24, 695–705, 2001.

Salisbury, F. B. and Ross, C. W.: Plant physiology, Fourth edition, Wadsworth, Belmont, 1992.

Sankarasubramanian, A. and Vogel, R. M.: Annual hydroclimatology of the United States, Water Resour. Res., 38, 2002.

Schreiber, P.: Über die Beziehungen zwischen dem Niederschlag und der Wasserführung der Flüsse in Mitteleuropa, Meteorol. Z., 21, 1904.

Schulze, E.-D., Kelliher, F.M., Korner, C., Lloyd, J. and Leuning, R.: Relationships among maximum stomatal conductance, ecosystem surface conductance, carbon assimilation rate, and plant nutrition: A global ecology scaling exercise, Ann. Rev. Ecol. Syst., 25, 629–660, 1994.

Sharma, M. L.: Evapotranspiration from a Eucalyptus community, Agric. Water Manage., 8, 41–56, 1984.

Specht, R. L.: Water use by perennial evergreen plant communities in Australia and Papua New Guinea, Aust. J. Botany, 20, 273–299, 1972.

Szilagyi, J.: Can a vegetation index derived from remote sensing be indicative of areal transpiration?, Ecological Modelling, 127, 65–79, 2000.

Talsma, T. and Gardner, E. A.: Soil-water extraction by a mixed Eucalypt forest during a drought period, Aust. J. Soil Res., 24, 25–32, 1986.

Tanre, D., Holben, B. N., and Kaufman, Y. J.: Atmospheric correction algorithm for NOAA-AVHRR products – theory and application, IEEE Transactions on Geoscience and Remote Sensing, 30, 231–248, 1992.

Van Lill, W. S., Kruger, F. J., and Van Wyk, D. B.: The effect of afforestation with Eucalyptus-grandis Hill ex Maiden and Pinus-patula Schlecht et Cham on streamflow from experimental catchments at Mokobulaan, Transvaal, J. Hydrol., 48, 107–118, 1980.

Vertessy, R. A.: Predicting water yield from mountain ash forest catchments. Industry report 98/4, Cooperative Research Centre for Catchment Hydrology, 1998.

Vertessy, R. A., Zhang, L., and Dawes, W. R.: Plantations, river

flows and river salinity, Australian Forestry, 66, 55–61, 2003.
Walker, J., Bullen, F., and Williams, B. G.: Ecohydrological changes in the Murray-Darling Basin .1. The number of trees cleared over 2 centuries, J. Appl. Ecology, 30, 265–273, 1993.
Whitehead, D. and Beadle, C. L.: Physiological regulation of productivity and water use in Eucalyptus: a review, Forest Ecology and Management, 193, 113–140, 2004.
Wong, S. C., Cowan, I. R., and Farquhar, G. D.: Stomatal conductance correlates with photosynthetic capacity, Nature, 282, 424–426, 1979.
Woodward, F. I.: Climate and plant distribution, Cambridge University Press, Cambridge, 1987.
Zhang, L., Dawes, W. R., and Walker, G. R.: Response of mean annual evapotranspiration to vegetation changes at catchment scale, Water Resour. Res., 37, 701–708, 2001.
Zhang, L., Hickel, K., Dawes, W. R., Chiew, F. H. S., Western, A. W., and Briggs, P. R.: A rational function approach for estimating mean annual evapotranspiration, Water Resour. Res., 40, W02502, doi:10.1029/2003WR002710, 2004.

CHAPTER 3

Deriving consistent long-term vegetation information from AVHRR reflectance data using a cover-triangle-based framework

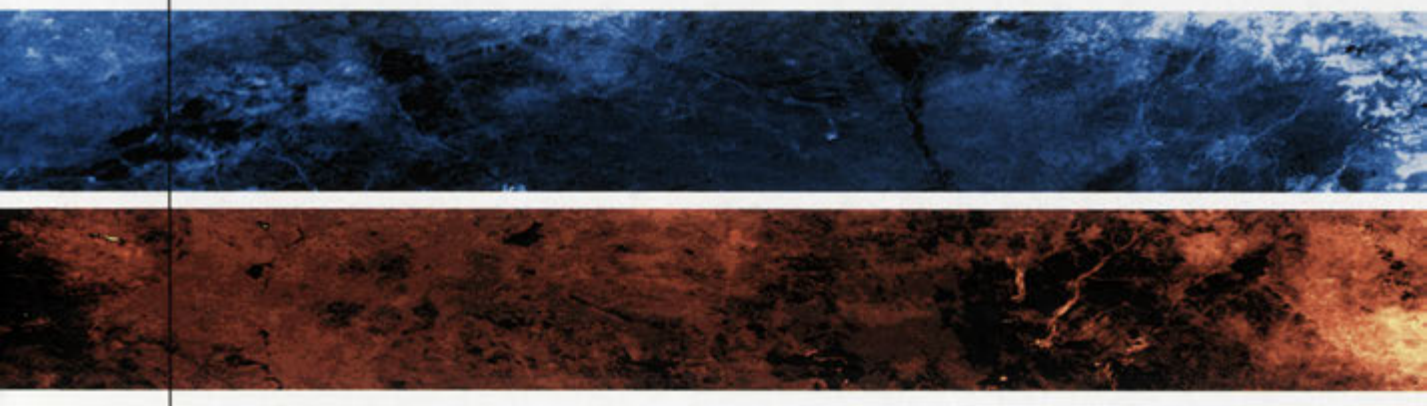

Remote Sensing of Environment 112 (2008) 2938–2949

Contents lists available at ScienceDirect

Remote Sensing of Environment

journal homepage: www.elsevier.com/locate/rse

Deriving consistent long-term vegetation information from AVHRR reflectance data using a cover-triangle-based framework

Randall J. Donohue [a,b,*], Michael L. Roderick [b], Tim R. McVicar [a]

[a] CSIRO Land and Water and eWater CRC, GPO Box 1666, Canberra ACT 2601, Australia
[b] Research School of Biological Sciences, Australian National University, GPO Box 475, Canberra ACT 2601, Australia

ARTICLE INFO

Article history:
Received 1 August 2007
Received in revised form 20 December 2007
Accepted 9 February 2008

Keywords:
Vegetation dynamics
Cover triangle
Soil line
Dark point
AVHRR
Reflectance
NDVI
fPAR
Atmospheric effects
Sensor calibration

ABSTRACT

Long-term vegetation dynamics associated with climatic changes can be assessed using Advanced Very High Resolution Radiometer (AVHRR) red and near-infrared reflectance data provided that the data have been processed to remove the effects of non-target signal variability, such as atmospheric and sensor calibration effects. Here we present a new method that performs a relative calibration of reflectance data to produce consistent long-term vegetation information. It is based on a simple biological framework that assumes that the position of the vegetation cover triangle is invariant in reflectance space. This assumption is in fact an intrinsic assumption behind the commonly used Normalised Difference Vegetation Index (NDVI) and is violated when the NDVI is calculated from inadequately corrected reflectance data. In this new method, any temporal variability in the position of the cover triangle is removed by geometrically transforming the observed reflectance data such that two features of the triangle—the soil line and the dark point—are stationary in reflectance space. The fraction of Photosynthetically Active Radiation absorbed by vegetation (fPAR; 0.0–0.95) is then calculated, via the NDVI, from calibrated reflectances. This method was tested using two distinct, monthly AVHRR products for Australia: (i) the coarse-resolution, fully calibrated, partially atmospherically corrected PAL data (1981–1994); and (ii) the fine-resolution, fully calibrated, non-atmospherically corrected HRPT data (1992–2004). Results show that, in the 20-month period when the two datasets overlap (1992–1994), the Australia-wide, root mean square difference between the two datasets improved from 0.098 to 0.027 fPAR units. The calibrations have produced two approximately equivalent datasets that can be combined as a single input into time-series analyses. The application of this method is limited to areas that have a wide-enough variety of land-cover types so that the soil line and dark point are evident in the cover triangle in every image of the time-series. Another limitation is that the methodology performs only bulk, relative calibrations and does not remove the absolute effects of observation uncertainties. The simplicity of the method means that the calibration procedure can be easily incorporated into near-real-time operational remote-sensing environments. Vegetation information produced using this invariant-cover-triangle method is expected to be well suited to the analysis of long-term vegetation dynamics and change.

1. Introduction

Remotely sensed data can be used to measure and monitor vegetation characteristics in high spatial and temporal detail across large areas. Historically, this has been achieved using vegetation indices derived from multi-temporal reflectance of red (0.6–0.7 μm) and near-infrared (NIR; 0.7–1.1 μm) radiation (e.g., Tucker, 1979; Running & Nemani, 1988; Nemani et al., 2003). Analyses of long-term vegetation dynamics require reflectance data that are not significantly affected by non-target signal variability associated with remotely sensed data (e.g., Gutman, 1999). Traditional methods for correcting reflectance data typically require ancillary data to drive atmospheric or directional reflectance models (e.g., Tanre et al., 1992; Los et al., 2005) or are delayed until publication of post-launch calibration coefficients (e.g., Mitchell, 1999). Across Australia, the application of traditional correction methods to Advanced Very High Resolution Radiometer (AVHRR) data is problematic because ancillary data (especially water vapour and aerosol data) that span both the country and the entire AVHRR observation period are generally unavailable. Additionally, traditional approaches do not lend themselves to real-time operational environments. For these reasons we developed, and present here, a simple, biologically oriented approach to calibrating broad-scale satellite reflectance data, akin to those of Hall et al. (1995) and Pickup et al. (1993), where knowledge of vegetation and soil reflectance characteristics is used to drive the calibration procedure. There are also similarities between this current method and the 'cover triangle' method of Gillies and Carlson (1995; see also Carlson (2007)) which standardises the Normalised Difference Vegetation Index

* Corresponding author. CSIRO Land and Water and eWater CRC, GPO Box 1666, Canberra ACT 2601, Australia.
E-mail address: Randall.Donohue@csiro.au (R.J. Donohue).

0034-4257/$ – see front matter © 2008 Elsevier Inc. All rights reserved.
doi:10.1016/j.rse.2008.02.008

(NDVI) and surface temperature values in order to estimate soil moisture. The basis of the method we present here is the assumption that key features of the cover triangle (described in Section 1.2) are spectrally invariant. Using these features, the relative temporal effects of non-target signal variability are minimised in the data, thereby producing consistent vegetation information suitable for long-term time-series analysis. In the remainder of this introduction, we review traditional methods of correcting AVHRR data and then present the rationale for the new calibration approach. Following the introduction, we present and discuss this new calibration methodology using, as a case study, two monthly AVHRR data products spanning continental Australia from June 1981 to December 2004.

1.1. Traditional approaches to correcting AVHRR reflectance data

The series of polar-orbiting environmental satellites operated by the National Oceanographic and Atmospheric Administration (NOAA) each carry an AVHRR sensor. These sensors measure spectral radiance using a number of bandwidths including 0.58–0.68 μm (Channel 1) and 0.725–1.1 μm (Channel 2) which measure red reflectance (ρ_R) and NIR reflectance (ρ_N), respectively. The available AVHRR data record is near-continuous from June 1981 and provides one of the longest useful remotely sensed records of the Earth's surface. For this reason these data are of exceptional value in the analysis of long-term variability in vegetation, especially those relating to land-use change (e.g., Graetz et al., 1995) and climate change (e.g., Nemani et al., 2003). The main obstacle to using AVHRR data in terrestrial applications is the presence of variability in the reflectance signal that originates not from the surface target but from atmospheric dynamics, from time-dependent changes in the sensors, and from variations in Sun-target-sensor geometry (Cracknell, 1997). In the absence of adequate corrections for this signal variability, time-series analyses can lead to inaccurate conclusions about vegetation dynamics and especially about long-term vegetation change (Gutman, 1999).

From a vegetation perspective, non-target signal variability constitutes uncertainties in the reflectance data. AVHRR data are susceptible to a variety of uncertainties, each having specific effects on ρ_R and ρ_N and on the resultant Normalised Difference Vegetation Index (NDVI). These uncertainties, shown in Table 1, can be broadly categorised as atmospheric effects and satellite sensor effects. The most important atmospheric effects originate from the scattering and absorption of radiation by gases and aerosols. Satellite sensor effects are more time dependent, originating from post-launch degradation of sensor calibrations and from changes in Sun-target-sensor geometry, caused, in part, by satellite orbital drift (Kaufman, 1989; Price, 1991).

Traditionally, atmospheric effects are corrected individually using models of atmospheric optical properties. Molecular scattering and ozone absorption effects are generally predictable over space and time and can be corrected for relatively simply (Kaufman, 1989). In contrast, the effects of aerosol scattering and water-vapour absorption are spatially and temporally dynamic and are therefore more difficult to correct for directly (El Saleous et al., 2000). Correction of sensor effects is particularly important prior to long-term time-series analyses of reflectance data as these effects can introduce artificial trends into reflectance data (Price, 1987; Gutman, 1999) as well as alter the magnitude of atmospheric effects (Kaufmann et al., 2000). Both sensor degradation and orbital drift effects are commonly corrected using invariant-target analysis (Che & Price, 1992; Gordon et al., 1988; Vermote & Kaufman, 1995; Gutman, 1999; Kaufman & Holben, 1993; Roderick et al., 1996b). In this type of analysis, dark and bright targets are identified in geographic space whose reflectances are assumed to be constant. Trends in measured reflectance from invariant targets are attributed to sensor effects and are removed from all reflectance data. Invariant-target analysis is retrospective, typically requiring several years of data collection prior to analysis. Illumination effects have been addressed using bidirectional reflectance distribution functions (BRDF) that correct reflectances to a standard Sun-target-sensor angle (e.g., Cihlar et al., 1997; Los et al., 2005; Bacour et al., 2006). However, many BRDF corrections require specification of land-surface parameters and, as these parameters can be highly dynamic, such corrections can be difficult to accomplish reliably over long time-periods and across large areas.

Another commonly used method of minimising atmospheric and sensor effects is Maximum Value Compositing (MVC; Holben, 1986). MVC was originally developed to minimise the effect of clouds on calculated NDVI but it also minimises any effect that reduces the NDVI including aerosol scattering and water-vapour absorption (Holben, 1986). Consequently, MVC preferentially selects measurements made through clear and dry atmospheres with minimum optical depths (Kaufman, 1989). The longer the compositing period the more effective MVC becomes in minimising atmospheric effects (Holben, 1986); indeed, in areas where aerosol and water-vapour effects are not large, even 10 day composites can render these effects insignificant (Kaufman & Tanre, 1992). Whilst traditional approaches to correcting AVHRR data are effective at removing uncertainties, they can be complex and there can be considerable delay after the remotely sensed data are acquired before full corrections can be implemented. One of the motivations behind the research presented here was to develop a calibration methodology that is effective and simple, and the idea of enforcing a stationary cover triangle holds potential as a means for achieving this.

1.2. A new approach for calibrating AVHRR reflectance data using the cover triangle

The vegetation cover triangle was first described by Kauth and Thomas (1976) who demonstrated that ρ_R and ρ_N (%) from a large geographic area form a characteristic 'tasselled cap', or triangle, when plotted in red–NIR space (Fig. 1). In this triangle, reflectance from bare soils plot linearly along the base of the triangle and form the 'soil line'. ρ_R and ρ_N from bare soils are approximately equal so the soil line generally has a slope (α_s) close to 1 and an ρ_N-intercept (β_s) near the origin (Rondeaux et al., 1996; it should be noted that sensors from

Table 1
The potential influence of atmospheric and sensor effects on ρ_R, ρ_N, and the NDVI

Source of variability	Potential effect on ρ_R	Potential effect on ρ_N	Potential effect on NDVI	Reference
Molecular scattering	+7%	+2%	−0.23 over densely vegetated targets	Tanre et al. (1992) El Saleous et al. (2000)
Ozone absorption	−15%	–	+0.06 over sparsely vegetated targets	As above
Aerosol scattering	+15%	+8%	−0.2 over densely vegetated targets	As above
Water-vapour absorption	−5%	−30%	−0.12 over sparsely vegetated targets	As above
Sensor calibration degradation	Effect is satellite-dependent but generally decreases ρ_R and ρ_N reflectance		Varies between satellites	Kaufman (1989) Price (1987)
Illumination angle due to orbital drift	Effect depends on the pre-processing (e.g., length of MVC period, accuracy of atmospheric corrections) and sensor calibration accuracy, and is of significance mainly over sparsely vegetated surfaces			Kaufmann et al. (2000) Bacour et al. (2006) Mitchell (1999)

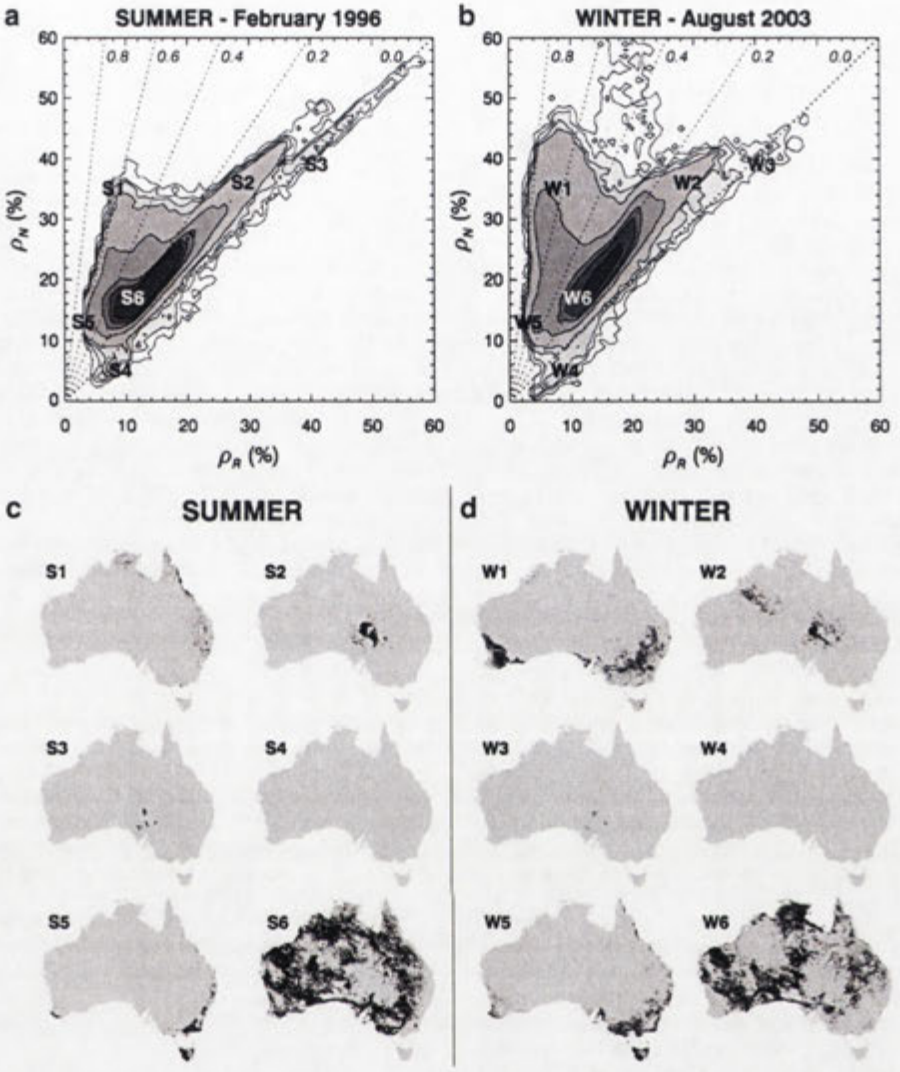

Fig. 1. The relationship between features of the vegetation cover triangle and the spatial distribution of their associated land-cover types for Australia. Plots a and b: reflectance density plots showing the characteristic vegetation cover triangle for a month in summer (a) and winter (b). These are derived from Australia-wide AVHRR images. Labels (e.g., S1,W1) indicate certain features within the triangle that have equivalent reflectance between the two months. NDVI isolines are displayed as grey dotted lines and are labelled in italics. The '0.0' isoline corresponds to the soil line (Note that pixel-density contour intervals are non-linear having the following steps: 2 [white], 5, 10, 20, 200, 800, 1300, and 3000 [darkest grey]. There are 10.8×10^4 land pixels in each 0.08° resolution image). Plots c and d: maps showing the spatial distributions of land-cover types associated with each feature labelled in plots a and b. Features S1 and W1 represent dense, bright vegetation and is mostly closed (>70% cover) forest in summer and closed grasslands in winter (that is, cereal crops or improved pasture). Feature 2 represents bright soils with sparse vegetation (open grasslands and shrublands with <30% cover) which occur in the most arid deserts. Feature 3 denotes bright, bare surfaces which are typically dry salt lakes and, in winter, includes snow cover. Feature 4 represents reflectance from water features such as water bodies and wet, bare soils. Feature 5 is the reflectance from dense, dark vegetation which typically originates from open (30–70% cover) evergreen forests with dense understories in relatively wet environments. Feature 6 is characterised by dark, moderately sparse vegetation on soils that are themselves moderately dark. This is the reflective characteristic of the majority of Australia's land cover, which typically consists of woodlands (<30% cover), shrublands, or grasslands (the last two both having <70% cover).

across different satellite programmes measure different red and NIR bandwidths resulting in variations in the soil-line position between sensors (Galvao et al., 1999)). Vegetation has a unique spectral signature as ρ_R from green foliage is small compared to ρ_N, with the difference between the two becoming more marked as vegetation cover increases (Huete, 1988, Oke, 1987). Reflectance from vegetated surfaces plots some distance above the soil line, with this distance increasing as canopy cover increases (Graetz & Gentle, 1982, Walker et al., 1986). The vegetation cover triangle is the data space bounded by the soil line and the reflectance from the densest canopies ('dense' is used throughout this article in reference to cover such that dense vegetation is at or near full cover and has the highest NDVI values; Fig. 1). In contrast, the reflectance from water and bare, wet surfaces plots below the dark end of the soil line (Fig. 1). This is because of the low albedo of water generally and because water absorbs proportionally more ρ_N than it does ρ_R (Oke, 1987; Richardson & Wiegand, 1977).

Red- and near-infrared-based vegetation indices are designed to capture various characteristics of the cover triangle, particularly the location of the soil line and the differences in ρ_R and ρ_N. The most commonly used vegetation index is the NDVI (Rouse et al., 1974), defined as:

$$\mathrm{NDVI} = \frac{\rho_N - \rho_R}{\rho_N + \rho_R}. \quad (1)$$

This index is based on the assumption that α_s is 1, β_s is 0, and that vegetation isolines converge at the origin (see Fig. 1). The NDVI is not a biophysical parameter and has no absolute range of values. Conversely, it is closely related to fractional green cover (0–1; Carlson & Ripley, 1997; Lu et al., 2003) and to the fraction of Photosynthetically Active Radiation absorbed by vegetation (fPAR, 0–0.95; Asrar et al., 1984). It has been used to make inferences about vegetation characteristics such as Leaf Area Index (e.g., McVicar et al., 1996; Pierce et al., 1993), canopy structure (e.g., Berry & Roderick, 2002), phenology (e.g., DeFries et al., 1995; Jolly et al., 2005; Guerschman et al., 2003), biomass (e.g., Baret et al., 1989), and vegetation type (e.g., Hill et al., 1999). The NDVI has also been related to vegetation-related phenomena—for example, landscape condition (Boer & Puigdefabregas, 2003; Holm et al., 2003); drought severity (McVicar & Jupp, 1998); biodiversity (Gould, 2000); carbon assimilation (Asrar et al., 1984); water availability (Wellens, 1997), and catchment energy and water balances (Szilagyi, 2000; Donohue et al., 2007a).

For time-series analyses using the NDVI, it is crucial that the position of the cover triangle—and the soil line in particular—be correctly located through time so that any detected changes in index values only relate to true changes in vegetation characteristics. Properly calibrated reflectance data should display no variability in the cover-triangle position. Several vegetation indices (e.g., SAVI and TSAVI) have been developed which allow the characteristics of the soil line, the index isolines, or both, to be individually specified (Huete, 1988; Baret & Guyot, 1991; Pickup et al., 1993; Qi et al., 1994; Yoshioka et al., 2000) and these indices lend themselves to time-series analyses using data that have not been adequately calibrated (e.g., Pickup et al., 1993). The approach behind such indices is to adapt the index structure to suit the characteristics of the reflectance data. The alternative approach presented in this paper is to adjust the reflectance data so the cover-triangle position is temporally fixed in red–NIR space prior to calculating the NDVI.

Invariant-target analysis identifies the combined effect of signal uncertainties and has the advantage that multiple-source uncertainties can be corrected without having to account for each source individually. Another approach to correcting reflectance data, one that is related to invariant-target analysis, is the end-member analysis presented by Hall et al. (1995). Although developed to make absolute corrections to reflectance data for measuring forest structural characteristics, Hall et al. (1995) proposed that the technique could also be used to correct for uncertainties in satellite reflectance data. End-member analysis requires independent measurements of surface targets that are known to uniquely occupy each apex of the cover triangle (the 'end members'). End-member reflectances are then used to correctly locate the entire cover triangle. In the next section we present the new method for calibrating remotely sensed red–NIR data that combines the invariant-target and end-member concepts to enforce a stationary cover triangle. In forcing this, the methodology produces data suitable for long-term time-series analyses of land-surface characteristics by minimising the relative temporal impacts of atmospheric and sensor effects on the resultant biophysical measurements.

2. Methods and materials

2.1. Approach

Conceptually, the method for calibrating AVHRR reflectance data presented here is an 'invariant-cover-triangle' approach. It utilises two features of the cover triangle: the soil line and the dark point. The latter represents the left-most extremity of the triangle where absorption of red light by vegetation is at a maximum (see Section 2.3.2). Using these two features, we linearly transform the reflectance data so the cover triangle is consistently located through time before calculating the NDVI and fPAR. We assume that, in the absence of atmospheric and sensor effects:

1. the NDVI is an appropriate index to use (i.e., the vegetation isolines converge at the origin);
2. the soil line is stationary and lies along the 1:1 line (i.e., α_s is 1 and β_s is 0); and
3. the dark point is stationary and is located at 2% ρ_R (i.e., dense green canopies can absorb a maximum of 98% of incident red light, see Section 2.3.2).

It is worth noting that this method presumes a global soil line and therefore can only be applied to areas where a wide range of (unvegetated) soil types are encompassed in the imagery.

In this section we describe the AVHRR reflectance data used here as a case study. We then describe the first step in this calibration methodology which has three components: a) identify the position of the observed soil line in red–NIR space; b) identify the position of the observed dark point in red–NIR space; and c) correct the reflectance data to account for the variability in these two features. In the second step, the NDVI is calculated from the corrected reflectances and converted to fPAR. Although it is very similar to the NDVI, we prefer fPAR because it is a biophysical attribute that directly links vegetation with surface energy and water fluxes (Asrar et al., 1984). The results in Section 3 are presented using a similar outline.

2.2. Data

Reflectance data from two AVHRR data products were used to construct the longest complete monthly time-series for Australia as practical; that is from July 1981 to current. The two data products are: i) the Pathfinder AVHRR Land (PAL) Global Area Coverage (GAC) data; and ii) the High Resolution Picture Transmission (HRPT) data. Data specifications, including the pre-processing undertaken by NASA (Kidwell, 1998) and CSIRO Marine and Atmospheric Research (King, 2003), are described in Table 2.

In the last 5 months of the PAL record, orbital drift of NOAA11 resulted in high Solar Zenith Angles (SZA). Consequently, data from these months were removed from analyses. Additionally, data for

Table 2
Specifications and pre-processing of the PAL and HRPT reflectance datasets used in this study

Specification	PAL	HRPT
Spatial resolution	0.08° at nadir (~8 km)	0.01° at nadir (~1.1 km)
Temporal resolution	1 month	1 month
Temporal extent	07/1981–04/1994, excluding portions of SE Australia for 05/1984–08/1984, 06/1988–07/1988, and 06/1993–07/1993	04/1992–12/2004, excluding 05/1993–08/1993, 05/1994–01/1995, and 05/2000–08/2000
Data-sensor lineage	07/1981–02/1985 NOAA7 03/1985–10/1988 NOAA9 11/1988–04/1994 NOAA11	04/1992–09/1994 NOAA11 02/1995–09/2000 NOAA14 10/2000–12/2004 NOAA16
Compositing method	Maximum NDVI	Maximum NDVI
Cloud removal	CLAVR (Stowe et al., 1991)	CLAVR (Stowe et al., 1991)
BRDF corrections	None	None
Atmospheric corrections	Molecular and ozone (Gordon et al., 1988)	None
Post-launch sensor calibration	Rao (1993)	Calwatch (Mitchell, 1999) NOAA11—Mitchell (1999) NOAA14—Vermote and El Saleous (see Mitchell, 1999) NOAA16—none applied (E. King, pers. comm.)

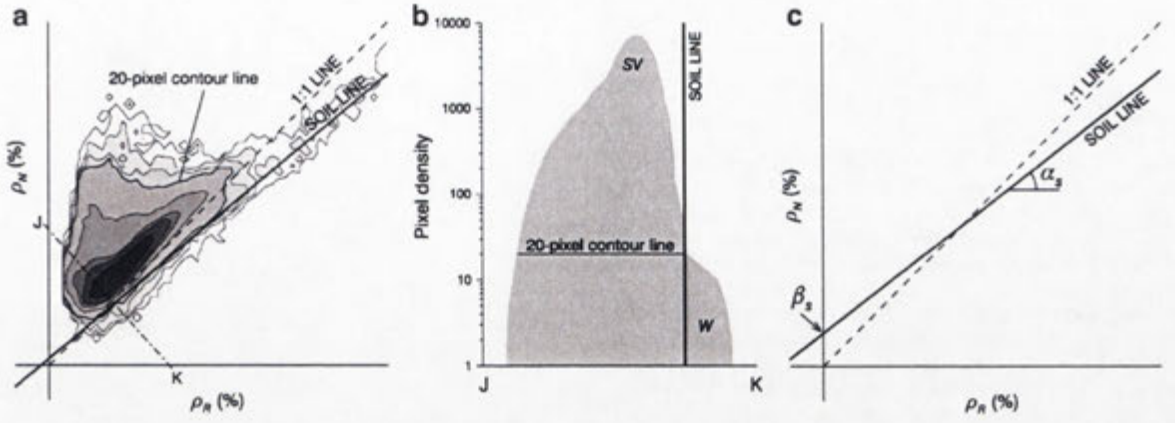

Fig. 2. Identification of the observed soil-line position. (a) is an example reflectance density plot, from December 2001, showing the location of the observed soil line. Note that pixel-density contour intervals are non-linear: 2 [white], 5, 10, 20, 200, 800, 1300, and 3000 [darkest grey]. The profile in (b) is of cross-section J–K from (a) and shows the placement of the soil line relative to the 20-pixel contour line. *SV* represents reflectance from sparse vegetation and *W* represents the water feature. (c) demonstrates the metrics used to describe the position of the observed soil line, which is described by its slope, α_s, and ρ_N-intercept, β_s.

June–August 1984, June–July 1988, and June–July 1993 were of low quality (e.g., areas of saturated reflectance values and/or remnant swathe boundaries) in south-eastern Australia and were masked out (see Donohue et al., 2007b). The original HRPT dataset was missing several months of data (September 1994–January 1995). An additional 14 monthly images (i.e., May–August 1993, April–September 1994, and May–August 2000) were entirely removed from the time-series due to spurious reflectance values in the south of Australia related to high SZA at the end of satellite operational lifespans. Both datasets have had the CLAVR algorithm (Stowe et al., 1991) applied prior to maximum value compositing in order to minimise the effect of clouds on the compositing process. The original reflectance data (ρ_R, ρ_N) were

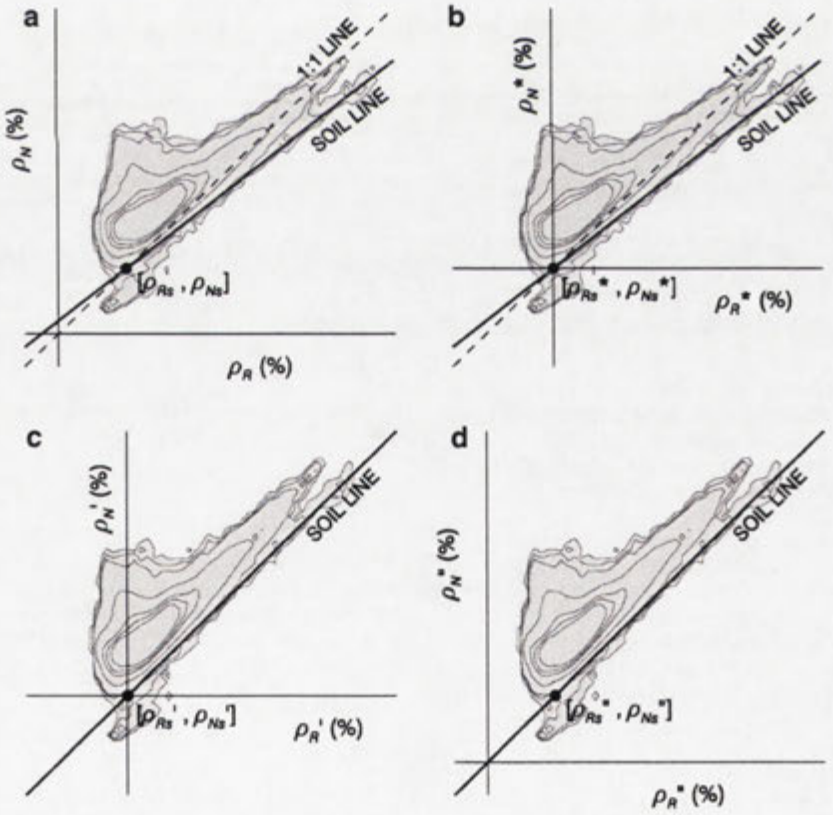

Fig. 3. Graphical representation of the geometric transformation used to produce reflectance data corrected for soil-line variability. (a) is the original reflectance data and shows the intercept between the soil line and the 1:1 line ($[\rho_{Rs}, \rho_{Ns}]$). (b) shows the data shifted so that the soil-line–1:1-line intercept is moved to the origin. In (c) the data are rotated to align the soil line with the 1:1 line. In (d) the data are shifted so that the soil-line–1:1-line intercept ($[\rho_{Rs}', \rho_{Ns}']$) has the same relative position as in the original reflectance coordinates.

used to calculate 'original' NDVI values (V_{orig}) for both the PAL and HRPT datasets using Eq. (1).

2.3. Correcting for soil-line and dark-point variability

2.3.1. Identifying the soil line

To correct for variations in the position of the cover triangle, the position of the soil line must be identified in an objective and repeatable manner. The method used to identify the observed soil-line position has three components. Firstly, an Australia-wide red–NIR density plot was generated for each month for both PAL and HRPT data (Fig. 2a).

Secondly, two features within each density plot were identified as anchor points for the ends of the observed soil line (Fig. 2a). The bright end of the soil line was anchored using the reflectance from dry salt lakes (e.g., feature 3 in Fig. 1). This feature provides a reliable reference point as it forms an easily identifiable, bare-soil feature quite distinct from other parts of the cover triangle. Surface moisture is known to alter reflectance from salt lakes (Mitchell et al., 1997) and for this reason they are not favoured as invariant geographic features. However, the salt-lake feature in reflectance space is formed by the reflectance from numerous dry salt lakes across Australia and is not affected by changes in surface moisture of any one lake. The dark end of the soil line was anchored using the top side of the water feature (e.g., feature 4 in Fig. 1). Variability in surface moisture causes instability in the shape of the water feature, which forms the lower edge of the cover triangle in the density plots. To avoid this soil-moisture-induced variability, the dark end of the soil line was anchored by aligning it against the 20-pixel contour line immediately above the water feature. This particular contour line was chosen as it is located at the very sharp threshold that delineates the water feature from the reflectance of sparse vegetation on moderately dark soils (Fig. 2b). Therefore this contour's location in this part of the triangle represents the reflectance from dry soils. Application of this method to other regions would require the reassessment of which contour line lies closest this threshold for each particular study area. These two anchoring features were easily identified in the monthly ρ_R–ρ_N density plots and provided a means for objectively and consistently identifying the soil-line position.

Thirdly and lastly, metrics describing the location of the soil line, now defined as a line that passes through the salt-lake feature and tangent to the 20-pixel contour line, were determined from the ρ_R–ρ_N density plots. These metrics, shown in Fig. 2c, include the soil-line slope (α_s) and ρ_N-intercept (β_s).

2.3.2. Identifying the dark point

As for the soil line, correcting for variability in the position of the dark point of the cover triangle required that the location of the observed dark point be identified in a consistent manner. We identify the dark point as the left-most extremity of the cover triangle and describe it simply as a red coordinate (see Fig. 4a).

There is a physical limitation to how much red light can be absorbed by green leaves, which lies between 90 and 95% (Hume et al., 2002; Jones, 1992). Due to the multiple scattering of light within canopies, vegetation can absorb more red light than individual leaves. We denote the threshold of minimum red reflectance from canopies as M (%). Kaufman (1989) reported that ρ_R from forest canopies is 1–3% and from pastures 2–4% and suggested setting M to 2%; accordingly, we set M to 2% here.

2.3.3. Correcting for soil-line and dark-point variability

To correct for the variability in the cover-triangle position, the original PAL and HRPT reflectance data were geometrically transformed, firstly so that the soil line was aligned with the 1:1 line and, secondly so that the dark point was 2% ρ_R for every month. This procedure follows the two-dimensional conformal transformation

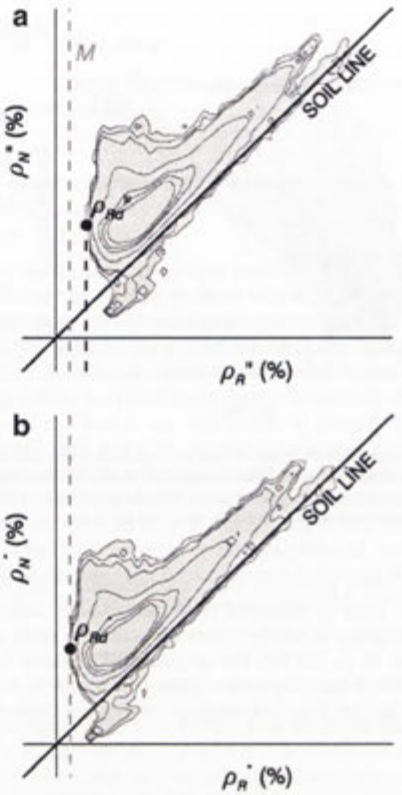

Fig. 4. Graphical representation of the transformation used to produce reflectance data corrected for dark-point variability. In (a) reflectance data corrected for soil-line variability (ρ_R^*, ρ_N^*), showing the location of the dark point (ρ_{Rd}^*) and the minimum red threshold (M). In (b), reflectances are shifted parallel to the soil line so that $\rho_{Rd}^* = M$.

described by Wolf (1974), assuming no rescaling was necessary. Using α_s, and β_s, we calculated the intercept between the soil line and the 1:1 line ($[\rho_{Rs}, \rho_{Ns}]$; Fig. 3a).

The ρ_R and ρ_N data were shifted so that $[\rho_{Rs}, \rho_{Ns}]$ was located over the origin (Fig. 3b):

$$\rho_R^* = \rho_R - \rho_{Rs} \tag{2a}$$

$$\rho_N^* = \rho_N - \rho_{Ns}. \tag{2b}$$

ρ_R^* and ρ_N^* were rotated to align the soil line with the 1:1 line (Fig. 3c):

$$\rho_R' = \rho_R^* \cos(\Theta) - \rho_N^* \sin(\Theta) \tag{3a}$$

$$\rho_N' = \rho_R^* \sin(\Theta) + \rho_N^* \cos(\Theta) \tag{3b}$$

where Θ is the difference between 45° and α_s, with α_s expressed in degrees. The rotated reflectance data (ρ_R', ρ_N') were shifted back from the origin so that $[\rho_{Rs}', \rho_{Ns}']$ occupied the same relative position it had in the original reflectances, producing reflectance data adjusted for soil-line variability:

$$\rho_R^e = \rho_R' + \rho_{Rs} \tag{4a}$$

$$\rho_N^e = \rho_N' + \rho_{Ns}. \tag{4b}$$

Soil-line-adjusted NDVI (V_{adj}) was calculated from ρ_R^e and ρ_N^e. The dark point $[\rho_{Rd}^e]$ was identified as the left-most extremity of the cover triangle plotted using the soil-line-adjusted reflectances (Fig. 4a). Dark-point values were measured to the nearest 1%. The dark point was anchored by shifting both ρ_R^e and ρ_N^e so that ρ_{Rd}^e was moved to M,

which was set to 2% (Fig. 4d). This yielded reflectance data corrected for both soil-line and dark-point variability (ρ^{*}_{R} and ρ^{*}_{N}):

$$\rho^{*}_{R} = \rho^{*}_{R} + M - \rho^{*}_{Rd} \quad (5a)$$

$$\rho^{*}_{N} = \rho^{*}_{N} + M - \rho^{*}_{Rd}. \quad (5b)$$

Note that ρ^{*}_{Rd} is present in both Eqs. (5a) and (5b) so that the data are shifted along the soil line.

Corrected NDVI (V_{cor}) was calculated from ρ^{*}_{R} and ρ^{*}_{N}.

2.4. Conversion of NDVI to fPAR

A preliminary fPAR (F_{pre}) was calculated from the corrected NDVI (V_{cor}) by linearly rescaling the NDVI using maximum and minimum thresholds (Roderick et al., 1999):

$$F_{pre} = \frac{(F_x - F_n)(V_{cor} - V_n)}{V_x - V_n} + F_n. \quad (6)$$

F_x and F_n are the maximum and minimum possible fPAR values and were set to 0.95 and 0.0, respectively. V_x and V_n are the corresponding maximum and minimum NDVI thresholds, respectively. V_x represents complete foliage cover where visible light absorption by canopy foliage is at a maximum and V_n represents zero green vegetation cover (e.g., bare soil) where visible light absorption by vegetation is minimal. F_{pre} was set to 0.95 when $V_{cor} > V_x$, and was set to 0.0 when $V_{cor} < V_n$.

Interim Biogeographic Regionalisation for Australia (IBRA) 5.1 (Environment Australia, 2000) regions were used to determine V_x and V_n. Six IBRA regions with very dense vegetation cover at some time throughout the year and six regions with minimal vegetation cover at some time of the year were chosen, based on *a priori* knowledge and interrogation of the NDVI database. We ensured that the 'maximum' regions included both native and agricultural vegetation and that the 'minimum' regions included both bright and dark soil backgrounds. A spatially averaged V_{cor} time-series was created for each maximum and minimum IBRA region. The highest (lowest) V_{cor} from each maximum (minimum) IBRA time-series was identified and these six values were averaged to produce one V_x (V_n) value for all Australia. This was done separately for the PAL and HRPT datasets.

In general, in the 20-month period when the two datasets overlap (Apr 1992–Apr 1993 and Sep 1993–Mar 1994), HRPT F_{pre} was lower than

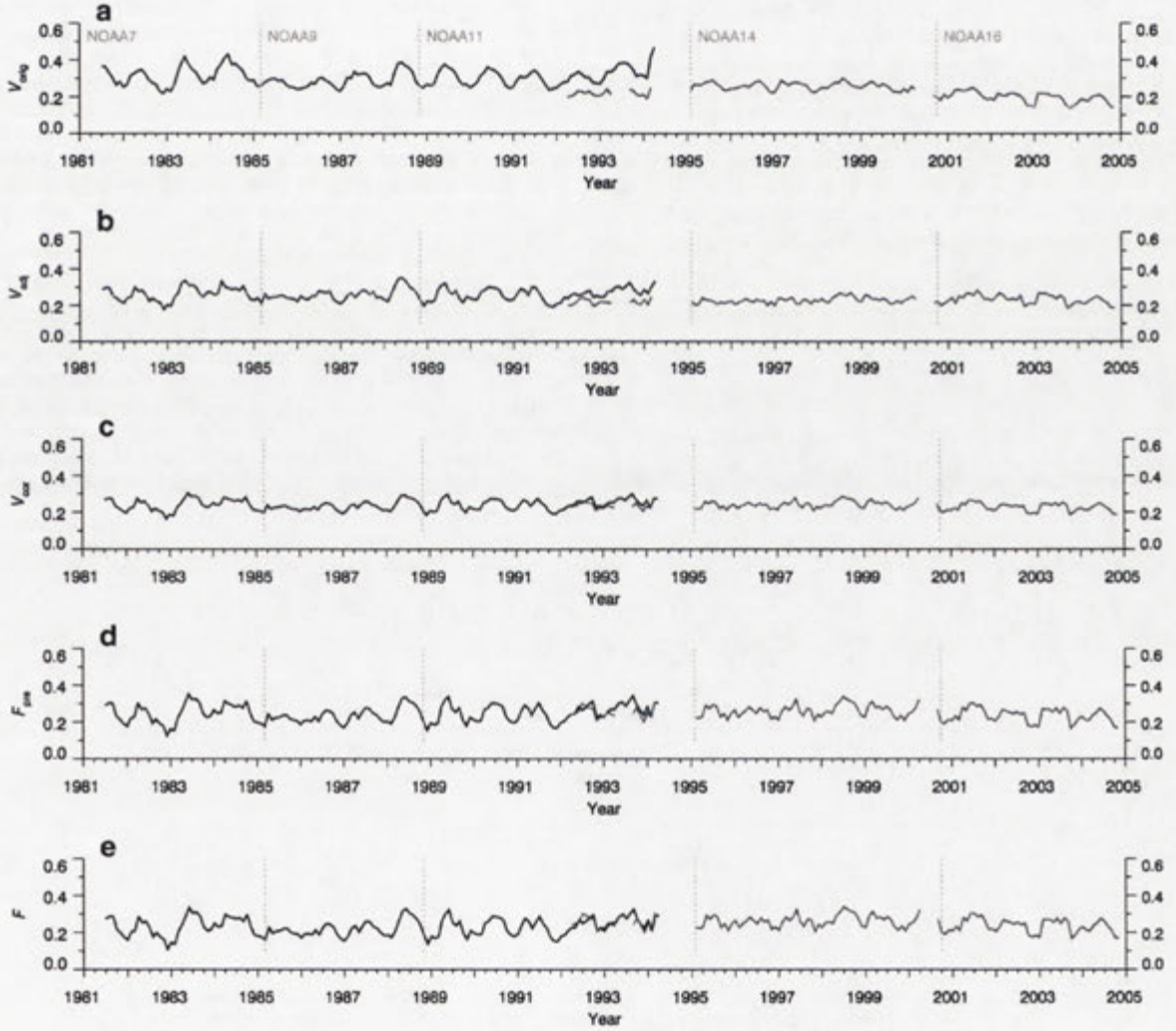

Fig. 5. The effects of the calibration process on calculated NDVI and fPAR. Plots a–e show the Australian-average PAL (black) and HRPT (grey) data in five stages of calibration. (a) shows the NDVI (V_{orig}) calculated from the original reflectance data (ρ_R and ρ_N). In (b) is the NDVI (V_{adj}) calculated from reflectances corrected for soil-line variability (ρ^{*}_{R} and ρ^{*}_{N}). (c) displays the NDVI (V_{cor}) calculated from reflectances corrected for both soil-line and dark-point variability (ρ^{*}_{R} and ρ^{*}_{N}). (d) shows the preliminary fPAR (F_{pre}) calculated from corrected NDVI (V_{cor}). Lastly, (e) is the final fPAR (F) calculated from the preliminary fPAR (F_{pre}) with offsets applied to PAL F_{pre}. The vertical dotted lines indicate satellite data acquisition periods.

Table 3
Comparison between the original NDVI and the final fPAR derived from the PAL and HRPT datasets

	Original NDVI (V_{orig})		Final fPAR (F)	
	PAL	HRPT	PAL	HRPT
Overall mean[a]	0.305 [0.290]	0.228 [0.217]	0.230	0.250
Mean seasonal amplitude[a,b]	0.113 [0.107]	0.068 [0.065]	0.132	0.100
Mean difference in overlap period[c]	0.100 [0.095]		−0.001	
Root mean square difference in overlap period[c]	0.103 [0.098]		0.027	

As the NDVI and fPAR values used here have slightly different scales (0.0–1.0 and 0.0–0.95, respectively), in order to allow direct comparison between these two variables the original NDVI are also presented in fPAR-equivalent units (that is, rescaled by multiplying by 0.95); these values are in square brackets.

[a] Calculated using the entire length of each dataset.

[b] The seasonal amplitude is the difference between the maximum and minimum value in each calendar year.

[c] Differences are calculated by subtracting the Australian-average HRPT from the Australian-average PAL for each month in the 20 month overlap period (Apr 1992–Apr 1993 and Sep 1993–Mar 1994).

PAL F_{pre}. Calculated globally (i.e., averaged over the whole continent), the difference between the average PAL and HRPT F_{pre} in the overlap period was 0.016 fPAR units. However, when calculated regionally (i.e., averaged per IBRA region, which range between 4×10^3 and 419×10^3 km^2), the differences varied between −0.026 and 0.133 fPAR units. To minimise any remaining differences between the two datasets, the difference between the two averages for the overlap period was calculated for every PAL-equivalent pixel in the image extent (i.e., PAL F_{pre} − HRPT F_{pre}). These 'offset' values were then subtracted from the PAL F_{pre} on a per-pixel basis, giving the final fPAR (F):

$$\text{for PAL data,} \quad F = F_{pre} - \text{offset} \tag{7a}$$

$$\text{for HRPT data,} \quad F = F_{pre}. \tag{7b}$$

3. Results

3.1. Original NDVI

The original, Australian-average monthly NDVI (V_{orig}) calculated from the original reflectance data for both datasets is shown in Fig. 5a. There are no obvious satellite-specific characteristics evident in the PAL V_{orig} time-series. According to Kaufmann et al. (2000), the corrections applied to the PAL data have removed enough of the sensor calibration variability that NDVI calculated from these data can be used for long-term time-series analyses. In contrast to this, there are satellite-specific characteristics present in the HRPT time-series, with NOAA14 V_{orig} being slightly higher than that from NOAA11 or NOAA16. This indicates that further sensor calibrations are required prior to time-series analyses using HRPT V_{orig}. Comparison between the datasets shows that the PAL V_{orig} is higher on average than that from HRPT and has larger seasonal amplitudes (Table 3). The root mean square difference (RMSD) between the two time-series' in the overlap period is 0.103 NDVI units (or 0.098 in fPAR-equivalent units). These distinct characteristics stem from the different data specifications and processing histories of the two datasets (Table 2). In their original form, it is clear that the PAL and HRPT V_{orig} are not equivalent representations of vegetation cover and are unsuitable as co-inputs to long-term time-series analyses.

3.2. Soil-line variability

The soil-line slope (α_s) and intercept (β_s) determined for each month of the AVHRR time-series is presented in Fig. 6. For nearly every month, α_s is less than 1 and β_s is between 0 and 4, indicating that the observed soil line is typically being rotated clockwise, with most movement occurring over bright targets. Fig. 6 also shows distinct differences in the soil-line metrics between the PAL and HRPT data, again demonstrating the inherent differences between the two datasets. Of particular interest is the contrast in the internal patterns. The PAL slopes and intercepts form a generally seamless time-series across three satellites whereas the HRPT data contain an abrupt change between the slopes of NOAA14 and 16.

The seasonality in α_s and β_s indicates that the causes of this variability are also seasonal, which points towards atmospheric effects and/or SZA effects. According to Tanre et al. (1992) and Kaufman (1989), water-vapour absorption effects are likely to be the most significant atmospheric variables over sparsely vegetated surfaces. Considering neither dataset had water-vapour corrections applied, that atmospheric water-vapour content is highly seasonal and decreases measured ρ_N, and that much of Australia is sparsely vegetated, water-vapour absorption is a possible cause of the variability in the soil line in the original reflectance data.

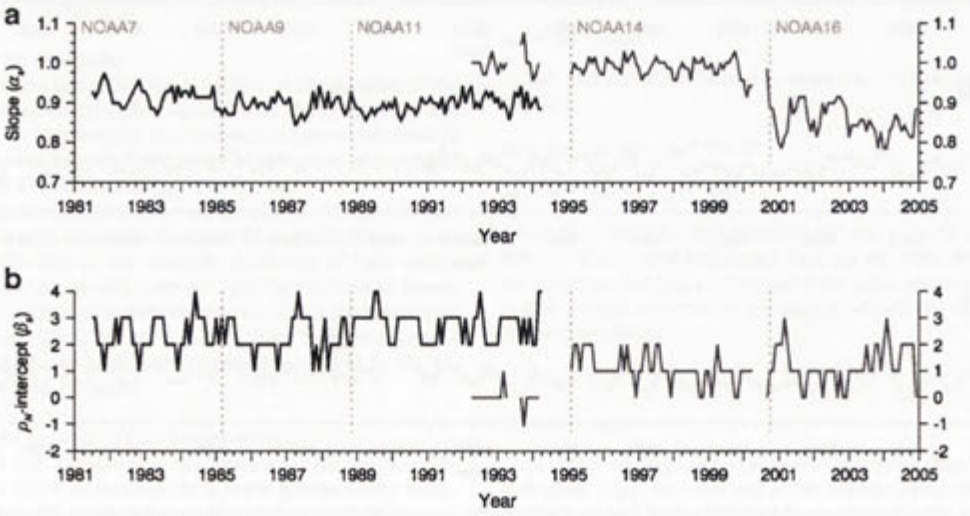

Fig. 6. Metrics describing the position of the observed soil line in ρ_R–ρ_N space. Metrics are the soil-line slope (α_s; plot a) and ρ_N-intercept (β_s; plot b) determined for both PAL (black) and HRPT (grey) datasets. The vertical dotted lines indicate satellite data acquisition periods.

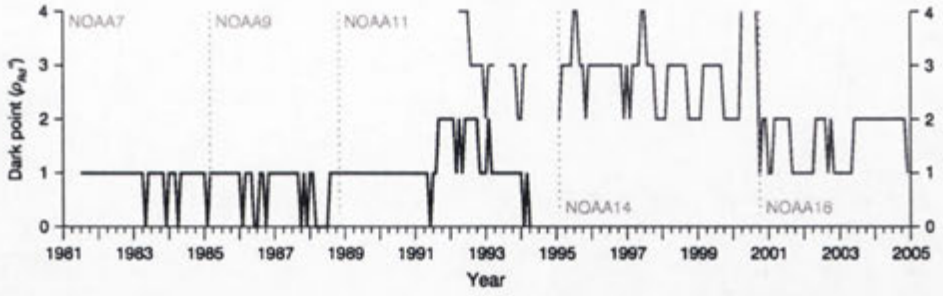

Fig. 7. Monthly position of the observed dark point. The PAL and HRPT dark-point coordinates are plotted in black and grey, respectively. The ρ_R–ρ_N contour plots were developed using data that had been rounded to the nearest integer and therefore the dark-point values are measured to the nearest 1%. The vertical dotted lines indicate satellite data acquisition periods.

The satellite-specific characteristics in α_s and β_s also suggest that some of the variability in the soil-line position is due to the effectiveness of post-launch calibrations. Both Kaufmann et al. (2000) and Tanre et al. (1992) report that the PAL calibrations are accurate and this is confirmed—in a relative sense—in Fig. 6. In contrast, the calibrations applied to the HRPT data have not been as effective and form one source of variability in the soil line that is addressed by this calibration methodology. The effect on the NDVI of removing soil-line variability from the reflectance data can be seen in Fig. 5b. The differences between the two datasets have been reduced and most of the satellite-specific differences within the HRPT V_{adj} have been removed.

3.3. Dark-point variability

There is a strong contrast in the dark-point location between the PAL and the HRPT data (Fig. 7). Corrections for molecular scattering generally decrease measured ρ_R (O'Brien et al., 2000) and those applied to the PAL data have produced a low and almost stationary dark point, located generally at 1% ρ_R*. The HRPT data have not been corrected for molecular scattering (Table 2) and consequently the dark point is high and quite variable, containing a strong seasonal pattern. This variability appears to be due to molecular scattering, which increase measured ρ_R over densely vegetated targets. The spike between 1991 and 1993 coincides with the Mount Pinatubo eruption (Robock, 2000) which suggests that the dark-point corrections are capturing some of the effects of tropospheric aerosol scattering. The HRPT dark-point values (Fig. 7) have satellite-specific characteristics stemming from the interplay between atmospheric and sensor calibration effects (Kaufmann et al., 2000).

An implication of the sensitivity of the NDVI to variations in reflectances (O'Brien et al., 2000, Roderick et al., 1996a) is that the closer the cover triangle is to the origin, the more NDVI isolines are traversed by any given fluctuation in reflectance (Fig. 1) and the greater the resulting variability in the NDVI. As the ρ_{Rd}* values for the PAL and the NOAA16 HRPT data are generally less than 2%, removal of dark-point variability from these data has effectively moved the cover triangle further away from the origin. This should have not only lowered V_{cor} relative to V_{adj} but also dampened the amplitude of the seasonal pattern in V_{cor}. Although subtle, these effects are present in Fig. 5c. Conversely, ρ_{Rd}* values of the NOAA11 and 14 HRPT data were already close to 2% and there is little discernable difference between V_{adj} and V_{cor} values for these datasets at this continent-wide scale. The dark-point corrections have brought the two datasets further into agreement in the overlap period.

3.4. Conversion of NDVI to fPAR

The main effect of the conversion of V_{cor} to F_{pre} has been to amplify the seasonal variation in the signal (Fig. 5d). The calculated minimum and maximum NDVI thresholds, V_s and V_n, were 0.67 and 0.09 for the PAL data and 0.64 and 0.09 for the HRPT, respectively. The technique of converting V_{cor} to F_{pre} rescales each dataset between two absolute and biologically meaningful thresholds and thereby standardises the data range of the two datasets. As such, this is an important step in the overall calibration methodology.

The calculated offset values (Fig. 8) indicate that differences still exist between the two datasets. That such differences remain means this methodology does not fully account for all non-target signal variability within the data and/or that there remain inherent differences between the two datasets unrelated to atmospheric conditions and calibration variability. The geographic patterns in the offset values generally match patterns of landscape complexity (heterogeneity of surface cover). One possible reason for this is that the combination of imprecise geolocation and the MVC procedure biases NDVI values over complex landscapes (Holben, 1986, Tan et al., 2006). As the PAL data were created using the GAC sub-sampling procedure (Cracknell, 1997), this bias is more pronounced in the PAL data.

The geolocation of the HRPT imagery used here is precise to within half a pixel (E. King, *pers. comm.*). Even this level of precision causes any given pixel to 'wander' around its true location in the landscape. If that pixel wanders over an area with relatively high NDVI then, when MVC is applied, the high NDVI value is preferentially selected as the composited value. Consequently, over boundaries between high and low NDVI targets, high NDVI values effectively spread out into the adjacent low

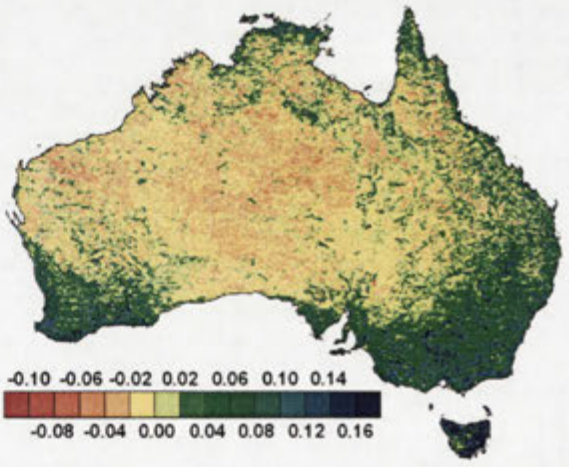

Fig. 8. The average difference in the overlap period between preliminary fPAR calculated from the PAL and HRPT datasets. The period of overlap is Apr 1992–Apr 1993 and Sep 1993–Mar 1994. The difference is calculated as PAL F_{pre} – HRPT F_{pre} and is calculated for every 0.08°pixel. The 0th, 5th, 95th, and 100th percentiles were −0.400, −0.030, 0.112 and 0.563, respectively. Values are in units of fPAR.

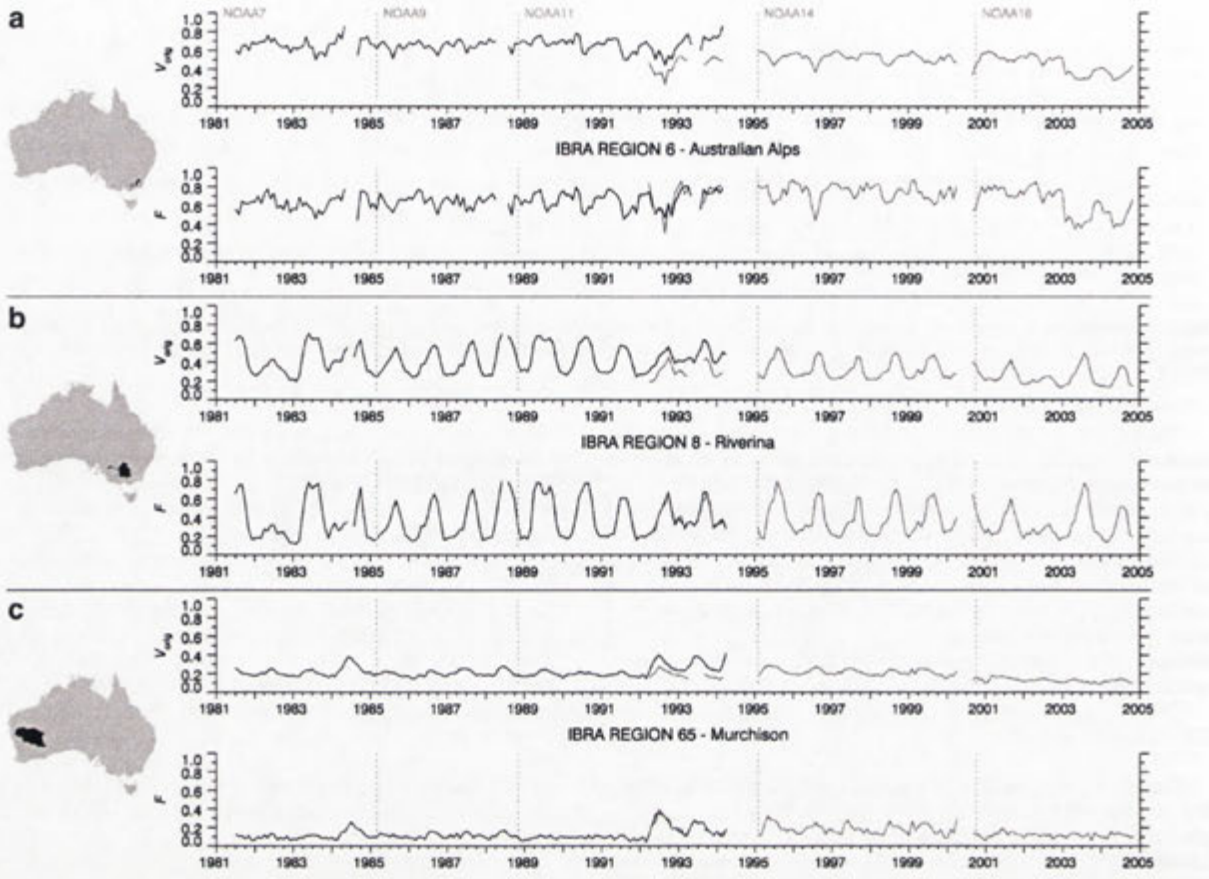

Fig. 9. Comparison of the original NDVI and the final fPAR for three IBRA regions. Plots a–c are the Australian Alps (8×10^3 km^2), the Riverina (96×10^3 km^2), and the Murchison (281×10^3 km^2) bioregions, respectively. Each plot shows a map of the IBRA region (left), the regionally averaged, monthly original NDVI (V_{orig}; top time-series in each plot) and final fPAR (F; bottom time-series in each) for both PAL (black line) and HRPT (grey line) data. The grey dotted lines indicate satellite data acquisition periods.

NDVI areas (Holben, 1986). In GAC-sub-sampled data, the average of four HRPT pixels (~1 km^2 each) is used to represent the value of one GAC pixel (~16 km^2). Even slight wanderings in the four-pixel averages caused by geolocation errors can alter the value of entire GAC cells. Further, resampling of the averaged HRPT values to the GAC grid can exacerbate the wandering effect of the original HRPT cells (King, 2003). This means that the effective spatial footprint of a high–low NDVI boundary is greater in GAC imagery than in the original HRPT imagery. The overall effect is that, with typical geolocation errors, maximum-value-composited PAL NDVI will tend to be higher than the equivalent HRPT NDVI over landscapes containing discontinuities between dense and sparse (or no) vegetation.

After the offset was applied, the final Australian-averaged fPAR (F) show extremely good agreement between the PAL and HRPT datasets (Fig. 5e and Table 3). The overall means and seasonal amplitudes are comparable and the RMSD in the overlap period is 0.027 fPAR units—an improvement from the original 0.098—a difference which is now only slightly greater than the best possible precision of AVHRR-derived NDVI (Roderick et al., 1996a), which is approximately 0.02. This is a pleasing result considering the inherent differences in the original data specifications (Table 2). There are no longer obvious differences between the two datasets nor between satellite periods within either dataset. The same conclusions are made when examining results at regional scales (Fig. 9) meaning that, even though the method requires the analysis area to be large enough to encompass the full range of soil types, the final fPAR can be applied at both small and large scales. It can be seen from Fig. 9 that the methodology is effective in regions with high vegetation cover (Fig. 9a), with strong seasonal cycles in cover (Fig. 9b), and with low and sporadic vegetation cover (Fig. 9c). The effects of vegetation disturbance (e.g., the widespread fires of January 2003 in southeast Australia; Fig. 9a) and of climate variability (e.g., the El Niño-related droughts of 1982/83 and 2002/03 in eastern Australia; Fig. 9b) are preserved in the final fPAR data. The invariant-cover-triangle method has produced, from two distinct datasets, one essentially equivalent dataset suitable for use as a single input in long-term time-series analyses of vegetation.

4. Discussion and conclusion

We demonstrated the invariant-cover-triangle calibration method using, as a case study, two distinct AVHRR datasets. Results indicate that the methodology is robust and effective when applied to AVHRR data that have had different degrees of corrections applied—that is, atmospheric corrections and sensor calibrations. We expect the methodology to be applicable to red–NIR reflectance data acquired from any one sensor, regardless of which corrections have been applied, whether none, partial, or full atmospheric corrections, and regardless of the accuracy of post-launch calibrations. However, due to the variance in spectral bandwidths of different sensors, this method cannot be expected to effectively harmonise red–NIR reflectances acquired from different sensors, unless a spectral translation is performed (e.g., Yoshioka et al., 2003) prior to the invariant-cover-triangle calibration.

The advantage of the approach we have outlined in this paper is that data with distinctly different correction histories can be rendered approximately equivalent and combined for the purposes of long-term time-series analyses.

One of the assumptions within this calibration methodology is that two features of the cover triangle—the soil line and the dark point—are temporally invariant in red–NIR reflectance space. Enforcing this stationarity therefore assumes an absence of trends in the spectral properties of bare soils and of dark, dense foliage across the study area (note that this is different from assuming the reflectance from these targets is constant). The difference between these assumptions in this invariant-cover-triangle approach and those inherent within traditional invariant-target approaches is significant. In the latter, reflectance from specific geographic targets and land-cover types are assumed constant whereas in the former all geographic locations and cover types are free from this constraint. In fact, the calibrated Australian AVHRR data used as a case study in this paper indicate that deserts and rainforests (which are commonly used invariant geographic targets) have all generally experienced long-term changes in fPAR over the analysis period (Donohue et al., 2007b; Schmidt et al. (2008) report similar results). The freedom of the cover-triangle approach from assumptions about ground target stability is a significant advantage when analysing long-term vegetation changes.

The invariant cover-triangle methodology performs a relative calibration and is designed to produce consistent, long-term vegetation information. It was not designed as a correction procedure *per se* and so doesn't quantify, or remove in an absolute sense, non-target signal variability. We haven't performed an assessment of the method's effectiveness in correcting for these uncertainties (as it is outside the scope of this paper) and we can only speculate about which are being removed. The methodology takes a 'lumped' approach, in that it removes the continentally averaged effects of scattering and absorption and of viewing angle variations. As such, it doesn't address the spatial variability in these effects. The results indicate that inter-sensor calibration discrepancies have been removed (Figs. 6 and 7). It seems reasonable, then, that sensor drift effects should also have been removed, although there is limited evidence of time-dependent trends in the soil-line and dark-point metrics (Figs. 6 and 7). We are confident that the dark-point corrections mimic Rayleigh corrections and are therefore removing much of the effect of molecular scattering (Fig. 7). The results suggest that the dark-point corrections are also removing some of the tropospheric aerosol scattering effects (Fig. 7) although evidence for this is less convincing. Finally, it is difficult to make conclusions from the results about the effectiveness of these corrections in removing water-vapour absorption, aerosol scattering, and viewing angle effects. Regardless, this technique has value because it uses two absolute and biologically meaningful reflectance features to remove the temporal effects of observation errors evident between each sensor in the time-series.

The example presented here used continental Australia as the study area, which spans 45° of longitude (110° E to 155° E) and 35° latitude (10° S to 45° S). We expect the invariant-cover-triangle method to be applicable to any study area that encompasses a sufficiently wide range of (unvegetated) soil types and that contains sufficient dark, dense vegetation cover so that both the soil line and dark point are identifiable in each image of the time-series. How large a study area must be to include these features depends on the spatial resolution of the sensor, the heterogeneity of cover types, and the range in the timing of growing seasons of vegetation within the imagery. In the absence of dry salt lakes within a study area, some other surface feature that is bright, spectrally invariant and which reflects approximately equal proportions of ρ_R and ρ_N (such as snow or water glint or perhaps concrete) must be present so that the soil line can be anchored consistently through time. The 20-pixel contour line chosen here to anchor the dark end of the soil line may not be the appropriate contour to use in other areas; an alternative region-specific value should be identified in each study. Setting M as 2% should be widely applicable, however the soil-line and dark-point metrics are specific to each case study.

The invariant-cover-triangle method lends itself to use in operational environments as it is simple, quick to implement (only requiring that an operator select the soil line and dark point), and does not require additional measured or modelled input data. The methodology can be further developed to be automatically implemented if the tasks of identifying the soil line and the dark point are automated, taking a similar approach to that of Fox et al. (2004). If AVHRR composite reflectance data are available in near-real-time, the invariant-cover-triangle methodology can be used for real-time applications since each new dataset can be immediately processed without the need for re-processing of the entire time-series or the need to wait for the publication of post-launch calibration coefficients.

Acknowledgements

We would like to thank Dr E. King (CSIRO Marine and Atmospheric Research) for providing us with the AVHRR data and metadata, T. Van Niel and Dr J.P. Guerschman (both from CSIRO Land and Water) and four anonymous reviewers for their many helpful comments that improved earlier drafts of this paper. IDL code of the invariant-cover-triangle methodology is available from the lead author, and the calibrated monthly Australian fPAR data are available at http://www-data.wron.csiro.au/rs/avhrr_fpar.

References

Asrar, G., Fuchs, M., Kanemasu, E. T., & Hatfield, J. L. (1984). Estimating absorbed photosynthetic radiation and leaf-area index from spectral reflectance in wheat. *Agronomy Journal, 76*, 300–306.

Bacour, C., Breon, F. M., & Maignan, F. (2006). Normalization of the directional effects in NOAA-AVHRR reflectance measurements for an improved monitoring of vegetation cycles. *Remote Sensing Environment, 102*, 402–413.

Baret, F., & Guyot, G. (1991). Potentials and limits of vegetation indexes for LAI and APAR assessment. *Remote Sensing Environment, 35*, 161–173.

Baret, F., Guyot, G., & Major, D. J. (1989). Crop biomass evaluation using radiometric measurements. *Photogrammetria, 43*, 241–256.

Berry, S. L., & Roderick, M. L. (2002). Estimating mixtures of leaf functional types using continental-scale satellite and climatic data. *Global Ecology and Biogeography, 11*, 23–39.

Boer, M. M., & Puigdefabregas, J. (2003). Predicting potential vegetation index values as a reference for the assessment and monitoring of dryland condition. *International Journal of Remote Sensing, 24*, 1135–1141.

Carlson, T. (2007). An overview of the "triangle method" for estimating surface evapotranspiration and soil moisture from satellite imagery. *SENSORS, 7*, 1612–1629.

Carlson, T. N., & Ripley, D. A. (1997). On the relation between NDVI, fractional vegetation cover, and leaf area index. *Remote Sensing Environment, 62*, 241–252.

Che, N., & Price, J. C. (1992). Survey of radiometric calibration results and methods for visible and near-infrared channels of NOAA-7, NOAA-9, and NOAA-11 AVHRRs. *Remote Sensing Environment, 41*, 19–27.

Cihlar, J., Ly, H., Li, Z. Q., Chen, J., Pokrant, H., & Huang, F. T. (1997). Multitemporal, multichannel AVHRR data sets for land biosphere studies—artefacts and corrections. *Remote Sensing Environment, 60*, 35–57.

Cracknell, A. P. (1997). *The Advanced Very High Resolution Radiometer*. London: Taylor and Francis.

DeFries, R., Hansen, M., & Townshend, J. (1995). Global discrimination of land cover types from metrics derived from AVHRR pathfinder data. *Remote Sensing Environment, 54*, 209–222.

Donohue, R. J., Roderick, M. L., & McVicar, T. R. (2007a). On the importance of including vegetation dynamics in Budyko's hydrological model. *Hydrology and Earth System Sciences, 11*, 983–995.

Donohue, R. J., Roderick, M. L., & McVicar, T. R. (2007b). Correcting long-term AVHRR reflectance data using the vegetation cover triangle. *CSIRO Land and Water Science Report 26/07*. Canberra: CSIRO Land and Water http://www.clw.csiro.au/publications/science/2007/sr26-07.pdf

El Saleous, N. Z., Vermote, E. F., Justice, C. O., Townshend, J. R. G., Tucker, C. J., & Goward, S. N. (2000). Improvements in the global biospheric record from the Advanced Very High Resolution Radiometer (AVHRR). *International Journal of Remote Sensing, 21*, 1251–1277.

Environment Australia (2000). *Revision of the Interim Biogeographic Regionalisation for Australia (IBRA) and development of version 5.1*. Canberra: Environment Australia.

Fox, G. A., Sabbagh, G. J., Searcy, S. W., & Yang, C. (2004). An automated soil line identification routine for remotely sensed images. *Soil Science Society of America Journal, 68*, 1326–1331.

Galvao, L. S., Vitorello, I., & Almeida, R. (1999). Effects of band positioning and bandwidth on NDVI measurements of tropical savannas. *Remote Sensing Environment, 67*, 181–193.

Gillies, R. R., & Carlson, T. N. (1995). Thermal remote-sensing of surface soil–water content with partial vegetation cover for incorporation into climate-models. *Journal of Applied Meteorology, 34*, 745–756.
Gordon, H. R., Brown, J. W., & Evans, R. H. (1988). Exact Rayleigh-scattering calculations for use with the Nimbus-7 Coastal Zone Color Scanner. *Applied Optics, 27*, 862–871.
Gould, W. (2000). Remote sensing of vegetation, plant species richness, and regional biodiversity hotspots. *Ecological Applications, 10*, 1861–1870.
Graetz, R. D., & Gentle, M. R. (1982). The relationships between reflectance in the Landsat wavebands and the composition of an Australian semi-arid shrub rangeland. *Photogrammetric Engineering & Remote Sensing, 48*, 1721–1730.
Graetz, R. D., Wilson, M. A., & Campbell, S. K. (1995). *Landcover disturbance over the Australian continent: A contemporary assessment*. Biodiversity Series, Paper 7 Sport and Territories: Canberra: Department of Environment.
Guerschman, J. P., Paruelo, J. M., & Burke, I. C. (2003). Land use impacts on the Normalized Difference Vegetation Index in temperate Argentina. *Ecological Applications, 13*, 616–628.
Gutman, G. G. (1999). On the use of long-term global data of land reflectances and vegetation indices derived from the Advanced Very High Resolution Radiometer. *Journal of Geophysical Research-Atmospheres, 104*, 6241–6255.
Hall, F. G., Shimabukuro, Y. E., & Huemmrich, K. F. (1995). Remote-sensing of forest biophysical structure using mixture decomposition and geometric reflectance models. *Ecological Applications, 5*, 993–1013.
Hill, M. J., Vickery, P. J., Furnival, E. P., & Donald, G. E. (1999). Pasture land cover in eastern Australia from NOAA-AVHRR NDVI and classified Landsat TM. *Remote Sensing Environment, 67*, 32–50.
Holben, B. N. (1986). Characteristics of maximum-value composite images from temporal AVHRR data. *International Journal of Remote Sensing, 7*, 1417–1434.
Holm, A. M., Cridland, S. W., & Roderick, M. L. (2003). The use of time-integrated NOAA NDVI data and rainfall to assess landscape degradation in the arid shrubland of Western Australia. *Remote Sensing Environment, 85*, 145–158.
Huete, A. R. (1988). A soil-adjusted vegetation index (SAVI). *Remote Sensing Environment, 25*, 295–309.
Hume, I. H., McVicar, T. R., & Roderick, M. L. (2002). Optical properties of leaves in the visible and near-infrared under beam and diffuse radiance. *Technical report 02/3. Cooperative Research Centre for Catchment Hydrology*. http://www.catchment.crc.org.au/pdfs/technical200203.pdf
Jolly, W. M., Nemani, R., & Running, S. W. (2005). A generalized, bioclimatic index to predict foliar phenology in response to climate. *Global Change Biology., 11*, 619–632.
Jones, H. G. (1992). *Plants and microclimate*. Second Edn Cambridge: Cambridge University Press.
Kaufman, Y. J. (1989). The atmospheric effect on remote sensing and its correction. In G. Asrar (Ed.), *Theory and applications of optical remote sensing* (pp. 336–428). New York: John Wiley.
Kaufman, Y. J., & Holben, B. N. (1993). Calibration of the AVHRR visible and near-IR bands by atmospheric scattering, ocean glint and desert reflection. *International Journal of Remote Sensing, 14*, 21–52.
Kaufman, Y. J., & Tanre, D. (1992). Atmospherically Resistant Vegetation Index (ARVI) for EOS-MODIS. *IEEE Transactions on Geoscience and Remote Sensing, 30*, 261–270.
Kaufmann, R. K., Zhou, L. M., Knyazikhin, Y., Shabanov, N. V., Myneni, R. B., & Tucker, C. J. (2000). Effect of orbital drift and sensor changes on the time series of AVHRR vegetation index data. *IEEE Transactions on Geoscience and Remote Sensing, 38*, 2584–2597.
Kauth, R. J., & Thomas, G. S. (1976). The tasselled cap – a graphic description of the spectral-temporal development of agricultural crops as seen by Landsat. *Proceedings of the Symposium on Machine Processing of Remotely Sensed Data* (pp. 44–51). West Lafayette: Purdue University.
Kidwell, K. B. (1998). *NOAA Polar Orbiter data user's guide (TIROS-N, NOAA-6, NOAA-7, NOAA-8, NOAA-9, NOAA-10, NOAA-11, NOAA-12, NOAA-13 and NOAA-14)*. Suitland: National Environmental Satellite Data and Information Service, NOAA.
King, E. A. (2003). The Australian AVHRR data set at CSIRO/EOC: Origins, processes, holdings and prospects. *CSIRO Earth Observation Centre Report 2003/04*. Canberra: CSIRO Earth Observation Centre http://www.eoc.csiro.au/tech_reps/2003/tr2003_04.pdf
Los, S. O., North, P. R. J., Grey, W. M. F., & Barnsley, M. J. (2005). A method to convert AVHRR Normalized Difference Vegetation Index time series to a standard viewing and illumination geometry. *Remote Sensing Environment, 99*, 400–411.
Lu, H., Raupach, M. R., McVicar, T. R., & Barrett, D. J. (2003). Decomposition of vegetation cover into woody and herbaceous components using AVHRR NDVI time series. *Remote Sensing Environment, 86*, 1–18.
McVicar, T. R., & Jupp, D. L. B. (1998). The current and potential operational uses of remote sensing to aid decisions on drought exceptional circumstances in Australia: A review. *Agricultural Systems, 57*, 399–468.
McVicar, T. R., Walker, J., Jupp, D. L. B., Pierce, L. L., Byrne, G. T., & Dallwitz, R. (1996). Relating AVHRR vegetation indices to in situ measurements of leaf area index. *Technical memorandum 96.5*. Canberra: CSIRO Division of Water Resources http://www.clw.csiro.au/publications/technical96/DWR_TR96-05.pdf
Mitchell, R. M. (1999). Calibration status of the NOAA AVHRR solar reflectance channels: CalWatch revision 1. *CSIRO Atmospheric Research Technical Paper No. 42*. Aspendale: CSIRO Atmospheric Research http://www.cmar.csiro.au/e-print/open/mitchellr_1999a.pdf
Mitchell, R. M., O'Brien, D. M., Edwards, M., Elsum, C. C., & Graetz, R. D. (1997). Selection and initial characterisation of a bright calibration site in Strzelecki desert, South Australia. *Canadian Journal of Remote Sensing, 23*, 342–353.
Nemani, R. R., Keeling, C. D., Hashimoto, H., Jolly, W. M., Piper, S. C., Tucker, C. J., Myneni, R. B., & Running, S. W. (2003). Climate-driven increases in global terrestrial net primary production from 1982 to 1999. *Science, 300*, 1560–1563.
O'Brien, D. M., Dilley, A. C., & Edwards, M. (2000). Interactions between surface and atmosphere in AVHRR shortwave channels. In T. R. McVicar (Ed.), *Land EnvSat Workshop – 10th Australian Remote Sensing and Photogrammetry Conference* (pp. 51–60). Adelaide: CSIRO Land and Water http://www.clw.csiro.au/publications/technical2000/tr36-00.pdf
Oke, T. R. (1987). *Boundary layer climates*, Second Edn. London: Routledge.
Pickup, G., Chewings, V. H., & Nelson, D. J. (1993). Estimating changes in vegetation cover over time in arid rangelands using Landsat MSS data. *Remote Sensing Environment, 43*, 243–263.
Pierce, L. L., Walker, J., Dowling, T. I., McVicar, T. R., Hatton, T. J., Running, S. W., & Coughlan, J. C. (1993). Ecohydrological changes in the Murray–Darling Basin.3. A simulation of regional hydrological changes. *Journal of Applied Ecology, 30*, 283–294.
Price, J. C. (1991). Timing of NOAA afternoon passes. *International Journal of Remote Sensing, 12*, 193–198.
Price, J. C. (1987). Calibration of satellite radiometers and the comparison of vegetation indexes. *Remote Sensing Environment, 21*, 15–27.
Qi, J., Chehbouni, A., Huete, A. R., Kerr, Y. H., & Sorooshian, S. (1994). A Modified Soil Adjusted Vegetation Index. *Remote Sensing Environment, 48*, 119–126.
Rao, C. R. N. (1993). Degradation of the visible and near-infrared channels of the Advanced Very High Resolution Radiometer on the NOAA-9 spacecraft: Assessment and recommendations for corrections. *NOAA Technical Report NESDIS-70* Washington, D.C.: NOAA/NESDIS.
Richardson, A. J., & Wiegand, C. L. (1977). Distinguishing vegetation from soil background information. *Photogrammetric Engineering & Remote Sensing, 43*, 1541–1552.
Robock, A. (2000). Volcanic eruptions and climate. *Reviews of Geophysics, 38*, 191–219.
Roderick, M., Smith, R., & Cridland, S. (1996a). The precision of the NDVI derived from AVHRR observations. *Remote Sensing Environment, 56*, 57–65.
Roderick, M., Smith, R., & Lodwick, G. (1996b). Calibrating long-term AVHRR-derived NDVI imagery. *Remote Sensing Environment, 58*, 1–12.
Roderick, M. L., Noble, I. R., & Cridland, S. W. (1999). Estimating woody and herbaceous vegetation cover from time series satellite observations. *Global Ecology and Biogeography, 8*, 501–508.
Rondeaux, G., Steven, M., & Baret, F. (1996). Optimization of soil-adjusted vegetation indices. *Remote Sensing Environment, 55*, 95–107.
Rouse, J. W., Haas, R. H., Schell, J. A., Deering, D. W., & Harlan, J. C. (1974). Monitoring the vernal advancement and retrogradation (greenwave effect) of natural vegetation. *NASA/GSFC Type III Final Report: Greenbelt*.
Running, S. W., & Nemani, R. R. (1988). Relating seasonal patterns of the AVHRR vegetation index to simulated photosynthesis and transpiration of forests in different climates. *Remote Sensing Environment, 24*, 347–367.
Schmidt, M., King, E. A., & McVicar, T. R. (2008). A method for operational calibration of AVHRR reflective time series data. *Remote Sensing of Environment, 112*, 1117–1129.
Stowe, L. L., McClain, E. P., Carey, R., Pellegrino, P., Gutman, G., Davis, P., Long, C., & Hart, S. (1991). Global distribution of cloud cover derived from NOAA/AVHRR operational satellite data. *Advances in Space Research, 11*, 51–54.
Szilagyi, J. (2000). Can a vegetation index derived from remote sensing be indicative of areal transpiration? *Ecological Modelling, 127*, 65–79.
Tan, B., Woodcock, C. E., Hu, J., Zhang, P., Ozdogan, M., Huang, D., Yang, W., Knyazikhin, Y., & Myneni, R. B. (2006). The impact of gridding artifacts on the local spatial properties of MODIS data: Implications for validation, compositing, and band-to-band registration across resolutions. *Remote Sensing Environment, 105*, 98–114.
Tanre, D., Holben, B. N., & Kaufman, Y. J. (1992). Atmospheric correction algorithm for NOAA-AVHRR products – Theory and application. *IEEE Transactions on Geoscience and Remote Sensing, 30*, 231–248.
Tucker, C. J. (1979). Red and photographic infrared linear combinations for monitoring vegetation. *Remote Sensing of Environment, 8*, 127–150.
Vermote, E., & Kaufman, Y. J. (1995). Absolute calibration of AVHRR visible and near-infrared channels using ocean and cloud views. *International Journal of Remote Sensing, 16*, 2317–2340.
Walker, J., Jupp, D. L. B., Penridge, L. K., & Tian, G. (1986). Interpretation of vegetation structure in Landsat MSS imagery – A case-study in disturbed semiarid Eucalypt woodlands. 1. Field data-analysis. *Journal of Environmental Management, 23*, 19–33.
Wellens, J. (1997). Rangeland vegetation dynamics and moisture availability in Tunisia: An investigation using satellite and meteorological data. *Journal of Biogeography, 24*, 845–855.
Wolf, P. R. (1974). *Elements of photogrammetry*. Kogakusha: McGraw Hill.
Yoshioka, H., Miura, T., & Huete, A. R. (2003). An isoline-based translation technique of spectral vegetation index using EO-1 Hyperion data. *IEEE Transactions on Geoscience Remote Sensing, 41*, 1363–1372.
Yoshioka, H., Miura, T., Huete, A. R., & Ganapol, B. D. (2000). Analysis of vegetation isolines in red–NIR reflectance space. *Remote Sensing Environment, 74*, 313–332.

CHAPTER 4

Climate-related trends in Australian vegetation cover as inferred from satellite observations, 1981–2006

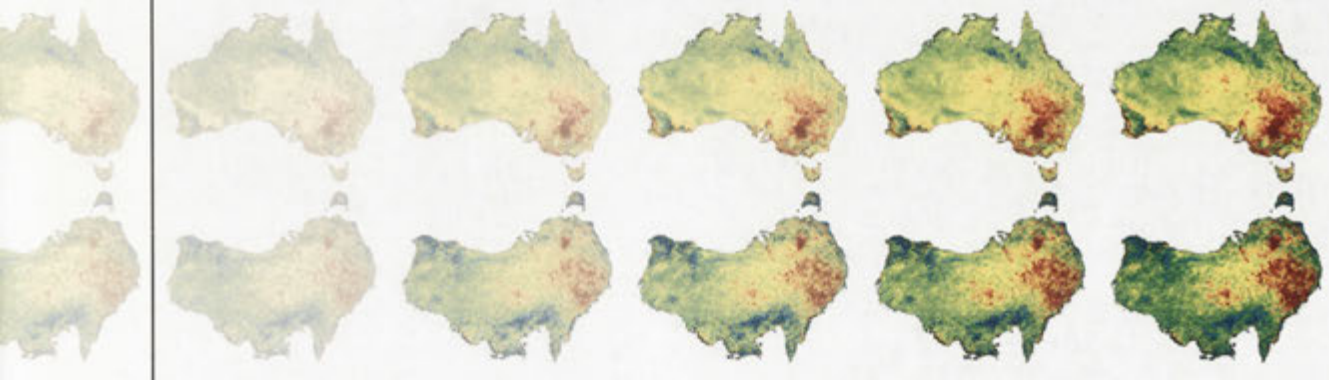

Global Change Biology (2009) 15, 1025–1039, doi: 10.1111/j.1365-2486.2008.01746.x

Climate-related trends in Australian vegetation cover as inferred from satellite observations, 1981–2006

RANDALL J. DONOHUE*†, TIM R. McVICAR* and MICHAEL L. RODERICK†
*CSIRO Land and Water and eWater CRC, GPO Box 1666, Canberra, ACT 2601, Australia, †Research School of Biological Sciences, The Australian National University, GPO Box 475, Canberra, ACT 2601, Australia

Abstract

Using Advanced Very High Resolution Radiometer data spanning 1981–2006 and calibrated for long-term analyses of vegetation dynamics, we examine whether vegetation cover has increased across Australia and whether there has been a differential response of vegetation functional types in response to changes in climatic growing conditions. Trends in vegetation cover are interpreted within Budyko's energy – water limitation framework. Results from an Australia-wide analysis indicate that vegetation cover (as described by the fraction of Photosynthetically Active Radiation absorbed by vegetation; fPAR) has increased, on average, by 0.0007 per year – an increase of ~ 8% over the 26 years. The majority of this change is due to a 0.0010 per year increase in persistent fPAR (representing nondeciduous perennial vegetation types; up 21%). In contrast, recurrent fPAR (representing deciduous, annual and ephemeral vegetation types) decreased, on average, by 0.0003 per year (down 7%), the trends of which are highly seasonal. Over the same period, Australian average annual precipitation increased by 1.3 mm yr^{-2} (up 7%). A site-based analysis using 90 long-term meteorological stations with minimal localized land-cover changes showed that energy-limited sites where total fPAR increased generally experienced decreases in precipitation, and water-limited sites that experienced decreases in cover were almost always associated with decreases in precipitation. Interestingly, where vegetation cover increased at water-limited sites, precipitation trends were variable indicating that this is not the only factor driving vegetation response. As Australia is a generally highly water-limited environment, these findings indicate that the effective availability of water to plants has increased on average over the study period. Results also show that persistent vegetation types have benefited more than recurrent types from recent changes in growing conditions. Regardless of what has been driving these changes, the overall response of vegetation over the past 2–3 decades has resulted in an observable greening of the driest inhabited continent on Earth.

Keywords: AVHRR, energy-limited, fPAR, NDVI, perennial, persistent, recurrent, CO_2, water-limited

Received 23 April 2008; revised version received 8 September 2008 and accepted 30 July 2008

Introduction

There is much concern about the expected impacts of climate change on the ecology and hydrology of the Earth (e.g., Pittock, 2003; IPCC, 2007). The response of vegetation to climatic changes will differ depending not only on how the climate changes but also on the environment the vegetation grows in and on the functional types that comprise the vegetation (Polley, 1997). At continental scales, vegetation responses are affected by which climatic factors represent the dominant limitation to plant growth (Forman, 1964; Nix, 1978). In a thermodynamic context, changes in climatic conditions can be categorized as those that affect the availability of energy and those that affect the availability of water (Budyko, 1974; Donohue *et al.*, 2007b). Using Budyko's (1974) dryness index, energy-limited conditions occur where $P > E_o$ and water-limited where $E_o > P$ (where P

Correspondence: Randall Donohue, CSIRO Land and Water and eWater CRC, GPO Box 1666, Canberra, ACT 2601, Australia, e-mail: Randall.Donohue@csiro.au

and E_o represent precipitation and potential evaporation, respectively).

In water-limited environments, vegetation growth generally responds to factors that alter the availability of water, such as changes in *P*. Similarly, changes in energy availability typically affect growth most in energy-limited environments. However, the increasing concentration of atmospheric CO_2 ($[CO_2]$) also affects the energy and water balances of vegetated landscapes by increasing the water-use efficiency of photosynthesis for the majority of plant species (Wong *et al.*, 1979; Farquhar, 1997). For vegetation, this latter effect is roughly equivalent to a proportional increase in the effective precipitation (Farquhar, 1997). With all else being equal, this is likely to induce an increase in CO_2 assimilation (Berry *et al.*, 2005) and vegetation cover (Specht, 1972; Woodward, 1987) in water-limited environments and an increase in run-off in energy-limited environments (e.g., McClelland *et al.*, 2004; Gedney *et al.*, 2006).

There is debate about how elevated $[CO_2]$ may differentially affect various plant functional types (e.g., Polley, 1997; Poorter & Navas, 2003). Elevated $[CO_2]$ generally increases plant assimilation rates (Drake *et al.*, 1997). However, studies of individual plants show that the growth of C3 species is enhanced more than that of C4 species particularly when water is limiting (Field *et al.*, 1992). This has led to some speculation that woody species may gain competitive advantages over nonwoody species in water-limited environments as $[CO_2]$ rises (see Polley, 1997). Indeed, Knapp & Soule (1996) and Morgan *et al.* (2007) attributed increases in the abundance of woody vegetation in rangelands to this differential effect of $[CO_2]$ and Berry & Roderick (2002a) estimated that evergreen vegetation cover has increased in abundance across Australia over the past two centuries in response to rising $[CO_2]$.

Satellite-based studies of vegetation change have the advantage that they provide observations that are spatially extensive and temporally frequent. Numerous satellite-based analyses of vegetation change have been undertaken using the Advanced Very High Resolution Radiometer (AVHRR) sensors because of the length of the data archive available (Table 1). Most commonly, these studies examined changes in the Normalized Difference Vegetation Index (NDVI) which is closely related to percent green cover, to the fraction of Photosynthetically Active Radiation absorbed by vegetation (fPAR) and therefore to gross primary productivity (Asrar *et al.*, 1984; Myneni *et al.*, 1995; Carlson & Ripley,

Table 1 Summary of Advanced Very High Resolution Radiometer (AVHRR)-based studies of long-term vegetation change

Study	Period	Region/latitudes	Variable*	Annual change	Percent change
Myneni *et al.* (1997, 1998)	1981–1991	Northern high latitudes (>45°N)	$NDVI_{GS}$	–	10–16
Kawabata *et al.* (2001)	1982–1990	Nth mid-high latitudes	$NDVI_A$	Positive	–
		Tropical latitudes		Positive	–
		Arid/semiarid sth latitudes		Negative	–
Zhou *et al.* (2001)	1981–1999	Eurasia	$NDVI_{GS}$	0.0017	12.4
		Northern America		0.0024	8.4
Tucker *et al.* (2001)	1982–1991	Eurasia	$NDVI_{GS}$	0.004	8.8
		Northern America		0.003	8.6
	1992–1999	Eurasia		0.004	6.5
		Northern America		0.005	10.1
Hicke *et al.* (2002)	1982–1999	Northern America	NPP_A	–	8
Nemani *et al.* (2003)	1982–1999	Global	NPP_A	–	6.2
Piao *et al.* (2003)	1982–1999	China	$NDVI_{GS}$	0.0013	–
Slayback *et al.* (2003)	1982–1999	Northern latitudes	$NDVI_{GS}$	0.0015–0.0045	5–10
Paruelo *et al.* (2004)	1981–2000	South America	$fPAR_A$	0.013	1.3
Goetz *et al.* (2005)	1981–2003	Canada and Alaska	$fPAR_{GS}$	0.002	–
		Tundra		0.002	–
		Forest		−0.00045	
Herrmann *et al.* (2005)	1981–2003	African Sahel	NDVI	Positive	–
Xiao & Moody (2005)	1982–1998	Above 23.5°N	$NDVI_A$	–	6.6–13.0
		23.5°S–23.5°N		–	3.9
Young & Harris (2005)	1982–1999	Global	$NDVI_A$	Positive	–
		Australasia		Positive	–

*NPP, net primary productivity; NDVI, Normalized Difference Vegetation Index; fPAR, fraction of Photosynthetically Active Radiation absorbed by vegetation; subscripts GS and A indicate growing season mean and annual mean, respectively.

1997). Several studies have used NDVI to model changes in net primary productivity (NPP). The removal of time-dependent artefacts – namely those stemming from variability in sensor calibration and viewing geometry – is crucial before the analysis of long-term trends using AVHRR data (Gutman, 1999). Eleven of the 13 studies summarized in Table 1 report positive trends in the NDVI – or in derived fPAR or NPP – regardless of the time period or region of analysis. Where changes were positive and the analysis period was >15 years, the magnitudes of change are in the order of 5–13%.

A recent examination of how the climate has changed across Australia – a generally highly water-limited landscape – indicates that, while trends are highly spatially variable, the average availability of water has increased over the past 25 or so years (Roderick & Farquhar, 2004; Nicholls, 2006; BOM, 2007). On average, this should have resulted in an increase in vegetation cover (Specht, 1981). One aim of this paper is to use satellite-based observations to test whether Australia has experienced an increase in vegetation cover and to interpret these changes within Budyko's (1974) energy–water limitation framework. Another aim is to test whether there has been a differential response of vegetation functional types to recent climatic changes. Analyses use both grid- and point-based monthly meteorological data, and the Australian monthly fPAR data of Donohue *et al.* (2008). To assess the responses of nondeciduous, evergreen vegetation from that of annual and ephemeral vegetation, the fPAR signal is split into the separate contributions from persistent and recurrent functional vegetation types. Trend analyses are performed firstly on the Australia-wide grids of P and total, persistent, and recurrent fPAR, and are then focused on sites with long-term (1981–2006) precipitation and pan evaporation observations in order to analyse fPAR trends in relation to changes in the climatic availability of water and energy.

Materials and methods

Meteorological data

Australia-wide monthly precipitation (P, mm month^{-1}) data were obtained from the Australian Bureau of Meteorology in the form of 0.05° resolution grids of total monthly precipitation from January 1981 to December 2006 (Jones *et al.*, 2006). These grids were converted to a 0.08° resolution to be compatible with the satellite data.

Site-based measures of monthly P and pan evaporation (E_p, mm month^{-1}) were compiled from the Monthly Australian Data Archive for Meteorology (MADAM) database (BOM, 2006). Data were extracted from MADAM only for those sites that had near-complete records between 1981 and 2006 for both P and E_p data. To determine whether a station record was near-complete, a simple rule set was followed: (i) each month needed at least 25 days of data to be considered complete, (ii) each year needed at least 9 complete months of data, and (iii) each station had to have at least 20 complete years of data to be included in the analysis. Remaining data gaps were filled with the long-term monthly means.

In these analyses, E_p was used as a proxy for available energy. A pan coefficient of 0.7 was applied to all E_p values before analyses (Linacre, 1994; making the assumption that the coefficient is the same across different climatic zones, see McVicar *et al.*, 2007) and all subsequent references to pan evaporation in this paper refer to converted pan values. The P and E_p time-series for each station were examined and stations found to have obvious temporal discontinuities were removed; there were seven such stations. Thirteen more stations with gaps in either P or E_p of 4 or more consecutive years at the beginning or end of the record were also removed. In total, 102 'long-term' stations remained.

Remotely sensed fPAR data

To analyse trends in vegetation cover, an Australian AVHRR-derived monthly fPAR dataset was used (Donohue *et al.*, 2008). This dataset spans the period July 1981–December 2006 and was derived from Pathfinder AVHRR Land (PAL; Kidwell, 1998) data pre-February 1992 and the CSIRO AVHRR Times Series (CATS [version 3.0]; King, 2003) data thereafter. These data have resolutions of 0.08° and 0.01°, respectively. For the analyses presented here, the CATS data were resampled to a PAL-equivalent resolution.

The AVHRR data were calibrated using the 'invariant-cover-triangle' method of Donohue *et al.* (2008) which is based on a simple biological framework that assumes the position of the vegetation cover triangle is invariant in red–near-infrared reflectance space. Any observed temporal variability in the position of the cover triangle is removed by geometrically transforming the observed reflectance data such that two features of the triangle – the soil line and the dark point – are stationary in reflectance space. fPAR is then calculated, via the NDVI, from calibrated reflectances. This procedure was applied separately to the PAL and the CATS data. These two datasets originally overlapped between 1992 and 1994, and a comparison in the overlap period showed that the calibrations improved the Australia-wide, root mean square difference between them from 0.098 to 0.027 fPAR units. Despite some differences in

the preprocessing histories of the two original datasets (i.e., sensor calibrations and atmospheric corrections, see Table 2 in Donohue *et al.*, 2008), this calibration procedure renders the two datasets approximately equivalent and suitable for use as a single input for time-series analyses.

Persistent and recurrent fPAR data

To examine fPAR changes in more detail, we derived the separate contributions of persistent and recurrent vegetation types, utilizing a similar approach to those of Roderick *et al.* (1999), Berry & Roderick (2002b), and Lu *et al.* (2003). Persistent vegetation is comprised of species that are active year-round and that display relatively little seasonal variation in canopy structure. Recurrent vegetation is comprised of species that operate in (often annual) cycles of activity and dormancy. While these two fPAR components can be broadly mapped to ecological functional types, their specific interpretation varies regionally. Generally, persistent fPAR represents nondeciduous, perennial species and recurrent fPAR represents the combined contributions of deciduous, annual and ephemeral species.

The persistent and recurrent components were derived using Roderick *et al.*'s (1999) approach. However, instead of calculating and offsetting a moving mean to estimate the persistent component, a moving minimum was used here as it better captures the baseline of the fPAR time-series signal (for a similar approach, see Gill *et al.*, 2006). As this derivation of persistent and recurrent fPAR is sensitive to dropouts in the time-series, the first step in the derivation was to remove major dropouts from each pixel's time-series. Dropouts were defined as a 1–2-month period where fPAR values were at least 0.1 units lower than each value either side of the dropout. Dropout values were replaced with the mean value of the two adjacent months. The second step was to construct a preliminary estimate of persistent fPAR (F_{p1}) as a 7-month moving minimum of total fPAR (F_t):

$$F_{p1}(t) = \min[F_t(t-3),..,F_t(t),..,F_t(t+3)], \quad (1)$$

where t denotes the month in the time-series. F_{p1} of the first and last 3 months of the time-series was estimated as the minimum value of those respective 3 months. F_{p1} was then smoothed using a 9-month moving average, yielding F_{p2}:

$$F_{p2}(t) = \frac{1}{9}[F_{p1}(t-4) + \cdots + F_{p1}(t) + \cdots + F_{p1}(t+4)]. \quad (2)$$

The widths of the moving minimum and average were chosen in order that F_{p2} was generally influenced by only one minimum value in any 12-month period, and that it still retained a slight annual cycle. Thirdly, a preliminary estimate of recurrent fPAR (F_{r1}) was calculated as the difference between F_t and F_{p2}:

$$F_{r1}(t) = F_t(t) - F_{p2}(t). \quad (3)$$

Where an F_{r1} value was negative, its absolute value was subtracted from F_{p2} to yield the final estimate of F_p:

$$F_p(t) = F_{p2}(t) - |F_{r1}(t)|, \quad \text{where } F_{r1}(t) < 0 \quad (4a)$$

$$F_p(t) = F_{p2}(t), \quad \text{where } F_{r1}(t) \geq 0. \quad (4b)$$

Lastly, F_r was calculated as

$$F_r(t) = F_t(t) - F_p(t). \quad (5)$$

Monthly F_t, F_p, and F_r were calculated for each terrestrial pixel and at each meteorological station. Examples of F_t and the derived F_p and F_r for three vegetation types are given in Fig. 1.

Trend analyses

All long-term change was assessed per-pixel using linear (ordinary least squares) regressions on a month-by-month basis (e.g., trend for January, February, etc.). As the regressions were linear, annual and seasonal P and E_p trends were calculated as the sum of the monthly P and E_p trends, respectively. For fPAR, the annual and seasonal trends were derived as the averages of monthly trends. Calculating trends per month has the advantage that results are less susceptible to biasing from whereabouts in the year that data gaps occur. This is particularly pertinent for the fPAR data we use here as most gaps occur in winter (see Donohue *et al.*, 2007a). Values of percent change were calculated as the overall change in the annual trend line compared with the 1981 annual average value. The analysis of trends has two distinct components – an Australia-wide analysis and a site-based analysis.

Australia-wide trend analysis. Monthly grids of P, F_t, F_p, and F_r were used to examine the Australian average trends as well as the geographic distribution of trends in these variables. We determined the monthly, seasonal, and annual trends in the four variables for every terrestrial pixel. Australia-wide trends were derived as the spatial averages of these trend grids.

Site-based trend analysis. As reliable, Australia-wide grids of E_p data were unavailable, a site-based trend analysis was performed so that changes in fPAR could be compared with changes in water and energy availability. Using the 102 long-term meteorological stations extracted from the MADAM database, we derived monthly time-series of F_t, F_p, and F_r as the average of a 3×3 cell window centred on each site. To isolate the response of vegetation to climatic dynamics

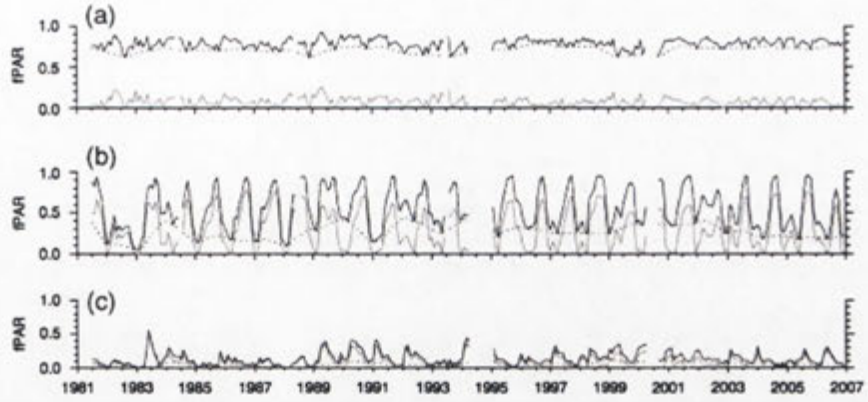

Fig. 1 Examples of the temporal decomposition of total fraction of Photosynthetically Active Radiation absorbed by vegetation (fPAR) (black line) into the persistent (dotted line) and recurrent (grey line) fPAR components. (a) Coffs Harbour (153.12°E, 30.31°S): the 1981–2006 average annual precipitation ($\overline{P}$) = 1623 mm yr^{-1} and pan evaporation ($\overline{E_p}$) = 1128 mm yr^{-1}; grazed pastures and open (50–80% cover) *Eucalyptus* forest. (b) Cowra (148.71°E, 33.81°S): $\overline{P}$ = 607 mm yr^{-1}, $\overline{E_p}$ = 967 mm yr^{-1}; grazed pastures and winter crops. (c) Longreach (144.28°E, 23.44°S): $\overline{P}$ = 404 mm yr^{-1}, $\overline{E_p}$ = 2155 mm yr^{-1}; low open (20–50% cover) *Astrebla* tussock grassland. Locations of these three sites are highlighted in Fig. 2. Meteorological and vegetation descriptions derived from BOM (2006) and NLWRA (2001), respectively.

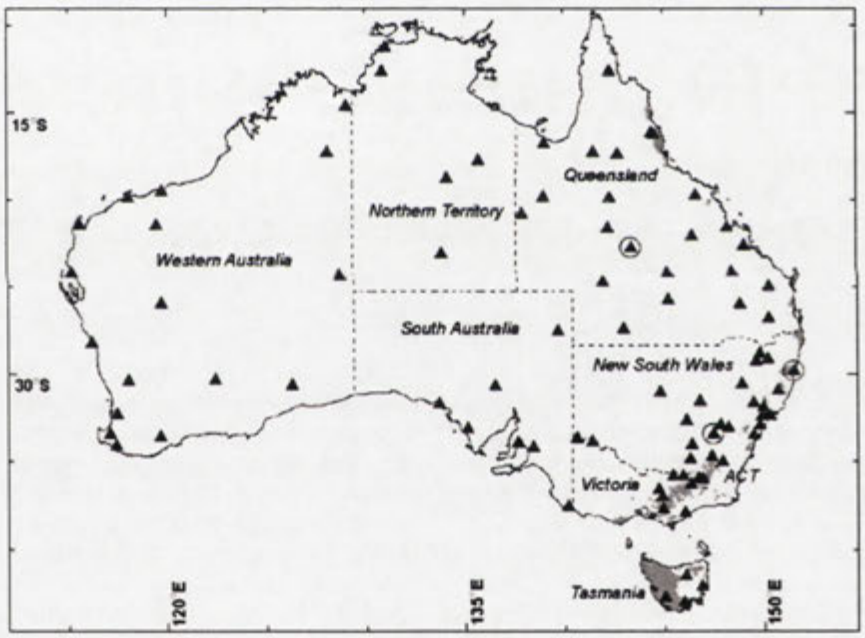

Fig. 2 Locations of the 90 sites used in the site-based trend analyses. Sites are shown as black triangles; those enclosed in circles are the three example sites in Fig. 1. Shaded in grey are regions of Australia that are energy-limited on an annual basis (from Raupach *et al.*, 2001).

from its response to land-use change, sites with apparent land-use changes in the fPAR signal were removed from the analysis. There were 10 such sites, which were typically located next to airports, within large cities, or in irrigation districts. Two additional sites were removed as they showed substantial but gradual increases in F_p without related changes in the meteorology and were known to be in regions undergoing timber plantation expansion (Parsons *et al.*, 2006). After removing these sites, a total of 90 long-term sites remained (Fig. 2). The annual averages and trends for P, E_p, F_t, F_p, and F_r were calculated for each site. To examine vegetation responses to climatic changes across these stations, we stratified the sites into

Table 2 Australia-wide trends in *P* and fPAR, 1981–2006

Variable	Average	Annual trend	Overall change*	Percent change*	*P*-value†
Precipitation (*P*)	480 mm yr^{-1}	+ 1.3 mm yr^{-2}	+ 33 mm yr^{-1}	+ 7.2	0.50
Total fPAR (F_t)	0.24	+ 0.0007 per year	+ 0.018	+ 7.8	0.28
Persistent fPAR (F_p)	0.13	+ 0.0010 per year	+ 0.026	+ 21.3	0.01
Recurrent fPAR (F_r)	0.11	−0.0003 per year	−0.008	−7.0	0.20

*Overall and percent change are made with reference to the average value at the start of the study period.
†Determined using a two-sided Kendall tau test (Kendall & Gibbons, 1990) performed on Australian-average annual values.

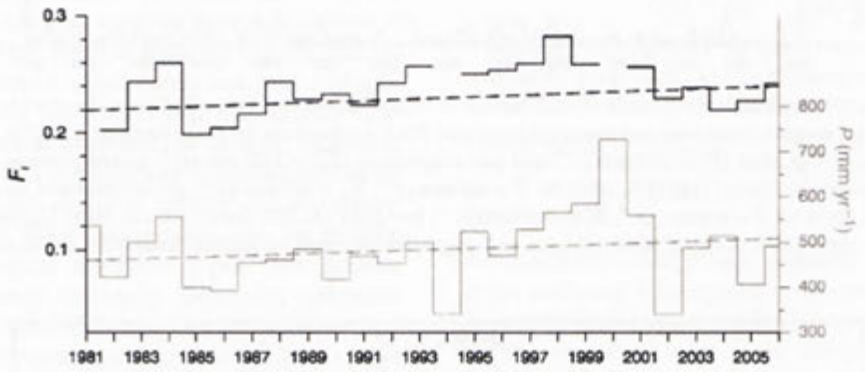

Fig. 3 Australia-wide annual F_t and *P*. In black are annual F_t data (solid line) and trend (dashed line; see Table 2 for slope coefficients). *P* data are in grey showing annual *P* (solid line) and trend (dashed line).

those that are energy- or water-limited over the long-term and into those sites that have positive or negative F_t trends.

Results

Australia-wide trend analysis

The Australia-wide estimates of trends in *P*, F_v, F_p, and F_r are presented in Table 2, with the accompanying Australian average monthly *P* and F_t time-series data shown in Fig. 3. Both *P* and F_t display positive trends over the analysis period with *P* increasing by 1.3 mm yr^{-2} (the overall change in *P*, denoted ΔP, is up ~ 7% over the 1981–2006 period) and F_t by 0.0007 per year (ΔF_t up ~ 8%). At an annual time-step, F_t is moderately correlated to *P* ($r^2 = 0.61$) and the temporal patterns also correspond (Fig. 3). Assuming that fPAR is approximately proportional to percent (green) cover (Carlson & Ripley, 1997; Lu *et al.*, 2003), this translates to an average 8% increase in vegetation cover across Australia during the period 1981–2006. The 0.0007 per year increase in F_t is comprised a 0.0010 per year increase in F_p but a 0.0003 per year decrease in F_r. This change in F_p is relatively large, representing a 21% increase in cover of persistent vegetation, which we broadly interpret as an increase in woody vegetation cover (a comparison of these results with those from field-based studies is provided in 'Discussion').

The distribution of *P* trends across Australia is shown in Fig. 4a. Broadly, there is a north-west to south-east gradient in *P* trends. Across much of the western half of the continent, as well as across the subtropical north, *P* increased over the study period. In contrast, and even though *P* has increased on average, there are widespread areas that have negative trends – most notably the east and south-east of Australia and the south-western coast of Western Australia. Similar trends in Australian *P* have been reported by Timbal & Jones (2008), Hendon *et al.* (2007), and Rotstayn *et al.* (2007). The broad spatial distribution of trends in the F_t component (Fig. 4b) largely follows that of *P*. There are, however, a few regions where fPAR has not responded directly to changes in *P*. For example, in many of the coastal areas in the south-west and south-east, F_t has increased (because of increases in F_p) even though *P* has declined.

The seasonal trends in *P* and the three fPAR components across Australia are shown in Figs 5 and 6. A notable feature in the patterns of seasonal trends (Fig. 5) is the substantial increases in summer *P* and F_v, especially across the north of the continent. The trends in autumn *P* are also striking, with enhanced *P* over the north and west and diminishing *P* in the east. It can be

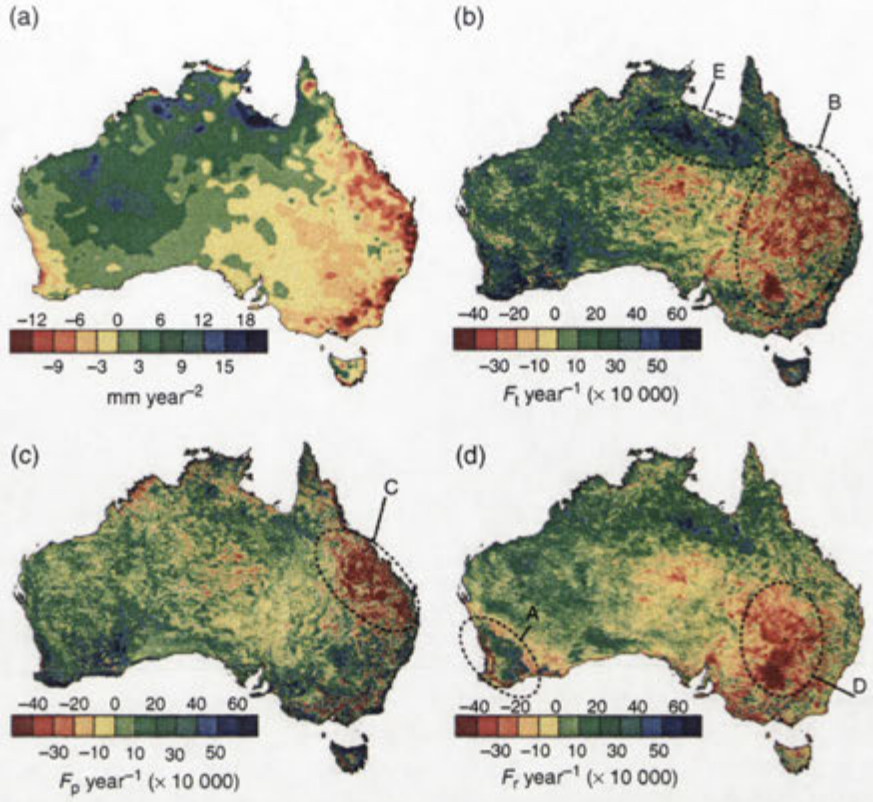

Fig. 4 Geographic distributions of trends in *P* and fPAR, 1981–2006: (a) precipitation (*P*), (b) total fPAR (F_t), (c) persistent fPAR (F_p), and (d) recurrent fPAR (F_r). Regions A–E are discussed in the main text.

seen that F_t, and particularly F_r (which, across the southern half of the continent, is predominantly comprised winter-growing vegetation), is highly sensitive to changes in autumn *P*. Averaged across Australia (Fig. 6) the seasonality of *P* and fPAR trends is also distinct. There is a moderate relationship between monthly trends in *P* and F_t ($r^2 = 0.52$), both of which display summer increases and autumn/winter decreases. Monthly trends in F_r are also seasonally variable, mirroring that of F_t and *P*, but with consistently negative trends outside the summer months. In contrast, Australia-wide trends in F_p are uniform throughout the year and are consistently positive (Fig. 6), again indicating a general increase in persistent vegetation cover.

Land use affects how vegetation will respond to changes in climate. An example of this is the south-western corner of Western Australia. This corner is a winter cereal-cropping zone (which is the distinct green triangular region, labelled 'A' in Fig. 4d) with forest cover along the coastal hinterland. In the cropping zone, where vegetation is managed to maintain annuals as the dominant functional type, changes in F_p have been moderate and reasonably uniform whereas F_r has responded directly to changes in *P* in which a west–east gradient in trends is evident (Fig. 4a). Outside of this cropping zone, where management does not restrict the growth of woody species, F_p has increased at the expense of F_r regardless of trends in *P*.

Another feature of interest in these trend images is the contrasting responses of F_p and F_r to changes in *P*. In Fig. 4b, a large area (labelled 'B') in the east of Australia has experienced decreasing F_t. Fig. 4c and d show that this area is split roughly into halves, with declines in the north-eastern half (region 'C' in Fig. 4c) caused by less F_p and somewhat more F_r, with the opposite effect in the south-western half (region 'D' in Fig. 4d). Ignoring for now the effects of land-cover change (land clearing has occurred during the study period in region 'C', Wilson *et al.*, 2002; DNRW, 2007), this pattern can be partly explained by which functional vegetation type dominates each area at the start of the study period. Region 'C' has higher woody overstorey cover on average than region 'D' (AUSLIG, 1990), and precipitation-induced decreases in total cover (i.e., ΔF_t) will be predominantly due to changes in overstorey cover (i.e., ΔF_p). Conversely, region 'D' typically supports grass-

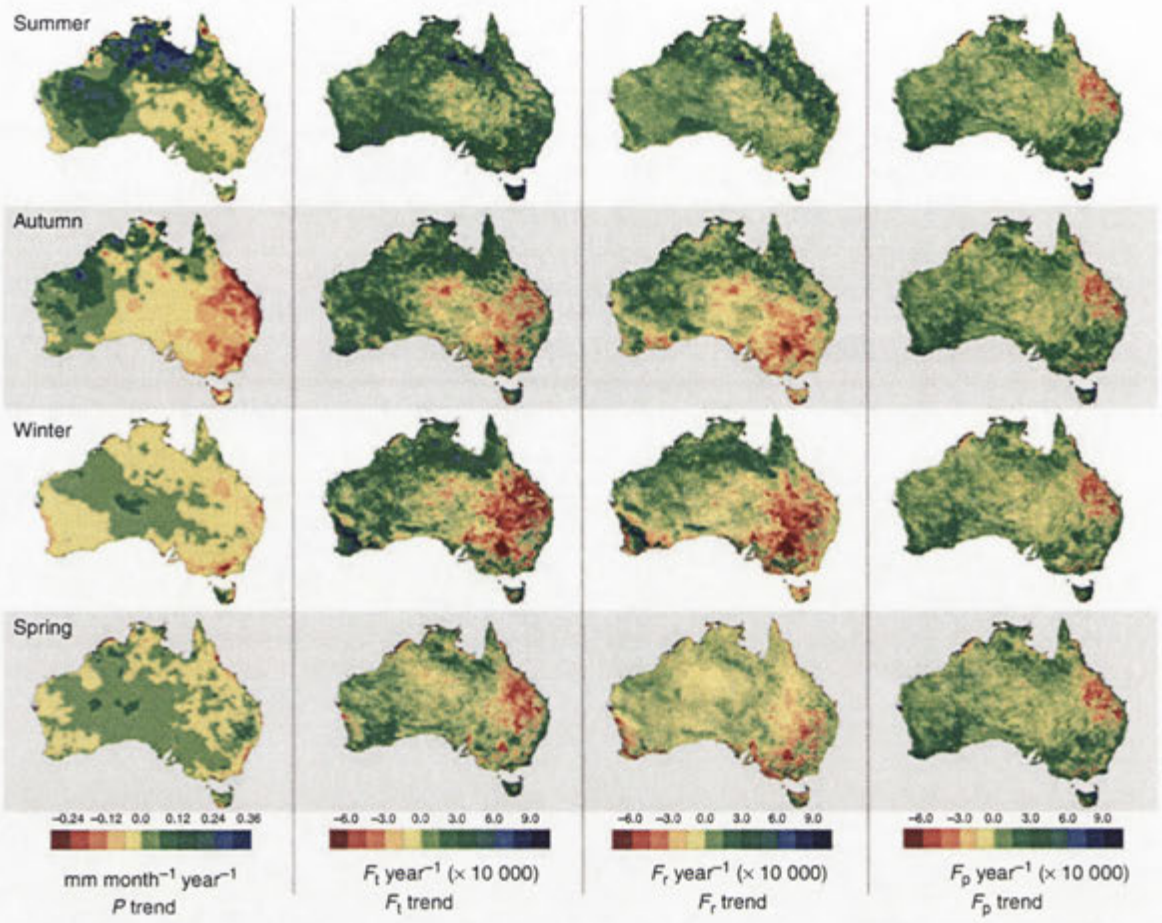

Fig. 5 Geographic distributions of seasonal trends in P and fPAR, 1981–2006. The left column shows the trends in P (expressed as yearly trends in the average monthly P for each season). The remaining columns (from left to right) contain the seasonal trends in F_t, F_r, and F_p. Summer is December–February, autumn is March–May, winter is June–August, and spring is September–November.

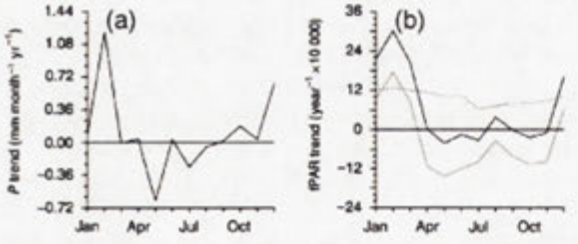

Fig. 6 Per-month trends in Australian average P and fPAR, 1981–2006. In (a) are the yearly trends in monthly P and (b) shows the yearly trends in monthly F_t, F_p, and F_r (black, dotted, and grey lines, respectively).

dominated ecosystems and decreases in total cover will occur generally because of decreases in grass cover, which are observed as decreases in F_r. This accords with the findings of Fensham *et al.* (2005). A possible climatic factor contributing to this pattern is the change in the seasonality of precipitation. Throughout eastern Australia, autumn P has been declining (Fig. 5). In water-limited environments with summer-growing periods (i.e., region 'C' in Fig. 4c), decreases in autumn P enhance the seasonality of F_t which, in turn, increases the proportion of F_r and may decrease the proportion of F_p. The opposite effect occurs in water-limited environments with winter-growing vegetation (i.e., region 'D' in Fig. 4d). Declines in autumn P have resulted in decreased seasonality of F_t and have decreased the proportion of F_p particularly in winter (Fig. 5).

Some of the regional patterns in fPAR trends also relate to local edaphic factors. For example, the blue 'strip' in the north-east (region 'E' in Fig. 4b) corresponds to the Mitchell Grass Downs bioregion (Environment Australia, 2000), which is defined by its deep cracking soils. Here, treeless grasslands support exten-

sive pastoralism, and the substantial increases in P have been expressed as changes in F_r.

These examples demonstrate some of the patterns of vegetation responses to climatic changes. F_t has responded to changes in total precipitation. Within this overall response, however, the regional patterns and the differential responses of F_p and F_r are further determined by: (1) which vegetation functional type is dominant at the start of the period of interest, (2) changes in the seasonality of precipitation relative to the growing season, (3) restrictions imposed by land use on which functional types are free to change, and (4) localized topographic and edaphic factors.

Site-based trend analysis

The averages of the trends in P, E_p and the three fPAR variables from the 90 stations in the site-based analysis are shown in Table 3. Because of a south-eastern bias in the distribution of these stations (Fig. 2), the average trend in annual P is approximately $-2\,\mathrm{mm\,yr^{-2}}$. Pan evaporation has also decreased. Also of interest is that F_t has increased on average across these sites. Again, this is largely a manifestation of increasing F_p (ΔF_p up 13%).

Figure 7 shows the site-based trends in fPAR grouped into sites that are energy- or water-limited over the long-term and into sites that have positive or negative F_t trends. There are few sites that are energy-limited and have experienced decreases in F_t (Fig. 7a). There are, however, a number of energy-limited sites that have positive F_t trends (ΔF_t up 11%; Fig. 7b). The trend in P is negative at nearly all of these sites and the overall trend in E_p is marginally negative. In general, increases in F_t in energy-limited environments are expected to be driven by rising energy availability, yet the observed E_p trends do not indicate that such a change has occurred at these sites. All of these sites are in coastal or mountainous regions and largely support forests, suggesting that the density of cover within forests has been increasing in these environments.

Table 3 Site-based trends in P, E_p, and fPAR, 1981–2006

Variable	Site-averaged, annual trend	Percent change*	P-value†
Precipitation (P)	$-2.1\,\mathrm{mm\,yr^{-2}}$	−2.6	0.85
Pan evaporation (E_p)	$-1.5\,\mathrm{mm\,yr^{-2}}$	−5.4	0.06
Total fPAR (F_t)	+ 0.0010 per year	+ 6.7	0.16
Persistent fPAR (F_p)	+ 0.0012 per year	+ 13.2	0.01
Recurrent fPAR (F_r)	−0.0002 per year	−4.0	0.53

*Percent of the average value at the start of the period.
†Determined using a two-sided Kendall tau test (Kendall & Gibbons, 1990) performed on Australian-average annual values.

Figure 7c shows that, of the 26 water-limited sites that have experienced decreases in F_t (ΔF_t down 10%), 25 sites are accompanied by negative P trends and most (18) have positive E_p trends. This decrease in F_t is the expected response of vegetation in water-limited environments when the availability of water declines. At these sites, P has decreased by approximately 16% and E_p is up by 5%.

In contrast, at the water-limited sites that have positive F_t trends (Fig. 7d), P has changed only a little overall (ΔP up 4%) while E_p has decreased an average of 8%. At these sites, F_t has increased on average by 18%, yet over a half of sites (27 of 48) experienced declines in P and most are clustered around the origin. These patterns indicate that changes in these two variables are not the dominant drivers of increases in vegetation cover at these sites. Figs 8 and 9 further explore the vegetation responses at these 48 sites. At 44 of the sites, the changes in F_t have been caused by increases in the persistent component (ΔF_p up 36%; Fig. 8) with a negligible overall contribution from the recurrent component (ΔF_r down 1%; Fig. 9). Such a large increase in F_t in response to a small increase in P highlights the sensitivity of vegetation to variations in moisture availability in water-limited environments.

Discussion

The satellite-observed changes in Australian vegetation between 1981 and 2006 reported here show that, on average, total fPAR (and therefore green cover) has increased by 8% across the continent. A number of field-based studies across Australia have also reported increases in vegetation cover, particularly woody cover. At the locations of these studies, our results generally show increases in persistent fPAR and are in broad agreement with the field-based observations ('broad' given the difficulty in comparing field-based studies with coarse resolution imagery and given the differences in study periods). Russell-Smith *et al.* (2004) and Brook & Bowman (2006) report the expansion of rainforest into open Eucalypt forest in northern and north-eastern Australia, and Butler *et al.* (2006) report the invasion of Eucalypt trees into montane grasslands in south-east Queensland. Increases in the cover of woody species have been observed in semiarid woodlands and shrublands in the west (Watson *et al.*, 2007), north (Fensham & Fairfax, 2003) and north-east of Australia (Fensham & Fairfax, 2005; Krull *et al.*, 2007). Most of these studies attribute observed vegetation changes to altered management regimes – notably fire regimes –

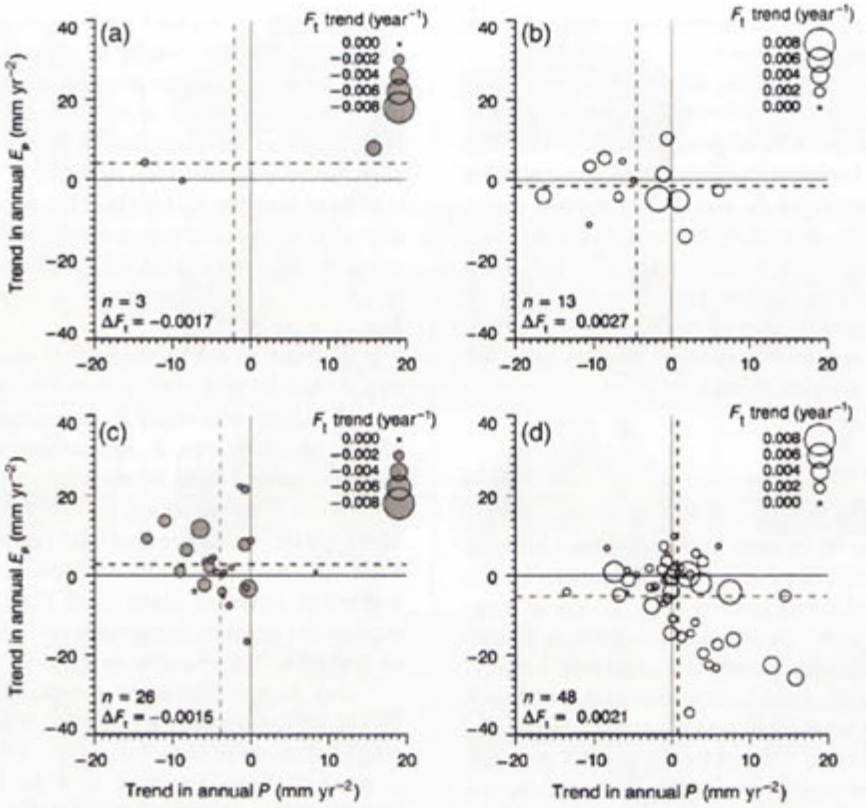

Fig. 7 Annual trends in P, E_p, and F_t at the 90 sites (Fig. 2), 1981–2006. The four graphs show sites that are energy-limited ($\overline{P} > \overline{E_p}$) (a and b) and water-limited ($\overline{P} < \overline{E_p}$) (c and d), and those with negative (a and c) and positive (b and d) trends in F_t. The x and y-axes of each plot are the annual trend in P and E_p, respectively. Dashed lines denote the means of the P and E_p trends for each subset of sites, n is number of sites in each subset and ΔF_t indicates the average trend in F_t for each subset.

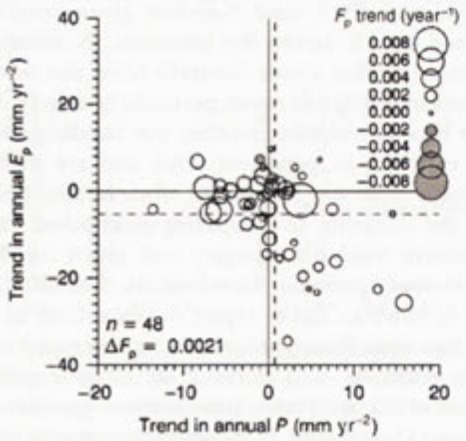

Fig. 8 Annual trends in P, E_p, and F_p at the 48 water-limited sites with increases in F_t, 1981–2006. These are the sites displayed in Fig. 7d but here the circle size denotes change in F_p. The x and y-axes are the annual trend in P and E_p, respectively. Dashed lines denote the means of the P and E_p trends and ΔF_p indicates the average trend in F_p.

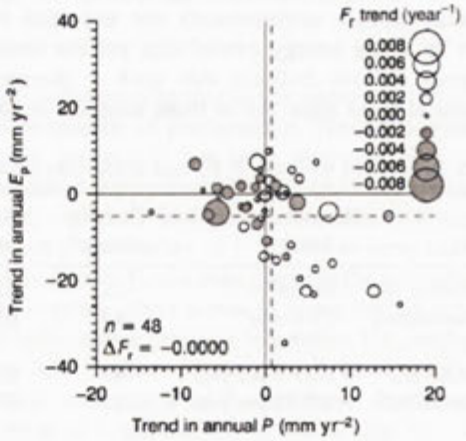

Fig. 9 Annual trends in P, E_p, and F_r at the 48 water-limited sites with increases in F_t, 1981–2006. These are the sites displayed in Fig. 7d but here the circle size denotes change in F_r. The x and y-axes are the annual trend in P and E_p, respectively. Dashed lines denote the means of the P and E_p trends and ΔF_r indicates the average trend in F_r.

over the past 50–100 years. In contrast, Eldridge & Stafford (1999) and Eldridge & Grant (2004) both report decreases in vegetation cover in the salt bush vegetation of the Western Riverina region in New South Wales, which lies within region 'D' in Fig. 4d, where both F_t and F_r has decreased. Also, over the last few decades, land clearing in Queensland has been substantial, with the highest rates having occurred within region 'C' in Fig. 4c (Wilson *et al.*, 2002; DNRW, 2007). Here trends in fPAR show a decrease in F_p and an increase in F_r.

According to Tables 2 and 3, the only statistically significant trends at the 95% level are those of F_p. However, in the context of this analysis, it is important to report all trends regardless of their statistical significance. The reason for this is three-fold. Firstly, the variables being analysed have different data characteristics. Those with inherently low temporal variance (i.e., F_p) are more likely to contain statistically significant trends than those with inherently high variance, such as P, F_t, and F_r (Weatherhead *et al.*, 1998). Secondly, even small changes in vegetation cover may have important implications for landscape functioning (e.g., a small change in cover – and therefore albedo – can greatly affect the surface radiation balance). Thirdly, if the independently determined pixel trends were the product of chance, there would be no discernable spatial patterns in the trend maps. The presence of ecologically meaningful patterns in these maps demonstrates that the trends are unlikely to be the result of random occurrence.

The observed 8% rise in Australian vegetation cover is within the range of values reported in similar studies from across the globe (Table 1). The majority of these studies are from energy-limited environments. By virtue of Australia's widespread aridity, our study is primarily an analysis of water-limited environments. As such, it is one of the few studies outside of Africa that specifically report long-term trends in vegetation growing in water-limited environments. One non-African study is that of Piao *et al.* (2005), who restricted their analysis to arid and semiarid China and found positive trends in P and in NDVI (up 9–14%) between 1982 and 1999. In a recent African study spanning 1982–2003, Herrmann *et al.* (2005) found positive trends in NDVI which were largely a response to increases in P; they also found a general 'background' greening trend unrelated to P trends. Our results concord with these findings, and further contribute to the body of literature reporting greening trends.

A novel aspect of our analysis is the assessment of trends of the persistent and recurrent fPAR components. The ecological interpretation of these fPAR components varies regionally. The most basic interpretation is that persistent fPAR corresponds to the 'baseline' vegetation cover and that recurrent represents the cyclical and episodic cover. Adding more ecological detail, we interpret persistent vegetation types as representing the cover of nondeciduous perennial species and recurrent vegetation types represent everything else (i.e., annual, ephemeral, and deciduous species) in the majority of Australian environments. Most ambiguity comes in relation to grasses. For example, some tropical perennial grasses are effectively deciduous as the foliage senesces annually (Shaw & Norman, 1970), and will therefore be classified as recurrent vegetation. Also, in landscapes with winter growth peaks, any change in the cover of summer-growing annual grasses will be interpreted as a change in persistent cover. The use of this persistent and recurrent framework is expected to be of limited use in landscapes with deciduous vegetation where discrimination between forest and nonforest is required. On the other hand, in water-limited environments largely devoid of native deciduous species, such as Australia, this is a valuable framework for differentiating functional vegetation types.

Quantitative validation of this method for decomposing the fPAR components has been performed by Gill *et al.* (2006), who assessed the accuracy of the methods of Roderick *et al.* (1999) and Lu *et al.* (2003), and a 'moving minimum' method similar to the one presented here. Gill *et al.* (2006) found that estimates of persistent fPAR made using the three methods were not significantly different from each other (at a 95% confidence level), and that there was a good correlation ($r^2 = 0.74$–0.79) with field-based measures of woody cover from across a range of vegetation types in north-eastern Australia.

Attribution of the drivers of the observed changes in fPAR is a considerable challenge. The Australia-wide results report the net effect on vegetation of all drivers including climatic variability and change, elevated [CO_2], land-cover and land-management changes, and disturbances. In the site-based analysis of fPAR trends, the site-selection process minimized the effects of land-cover changes and major disturbances, and so results from this analysis most directly reflect the influence of climate on vegetation. The key findings from the site-based analysis were that total cover has increased even though P has decreased across these sites, and that changes in growing conditions have favoured persistent vegetation types more than (and sometimes at the expense of) recurrent vegetation types. It is feasible that this is an observable CO_2 fertilization effect. For example, over the study period, [CO_2] has increased by 11% (ranging from approximately 340 to 378 ppm over the study period, Keeling & Whorf, 2005). If an increase in [CO_2] produces a proportional increase in effective P

(Farquhar, 1997), then the sites in Fig. 7d (i.e., water-limited sites with positive F_t trends) have undergone a change in effective P of 3.1 mm yr^{-2} (an overall increase in effective P of 15%) as opposed to the measured 0.7 mm yr^{-2}. Also, if rising [CO_2] preferentially favours woody species (Knapp & Soule, 1996; Polley, 1997; Morgan *et al.*, 2007), the CO_2-effect may explain why vegetation has responded predominantly through the persistent component, particularly where trends in actual P have been small or negative.

Land-use change and its effect on vegetation cover is another driver of the observed changes in fPAR. In Australia over the past two centuries, the predominant effect of land-use change has been to replace trees with grasses (Walker *et al.*, 1993; Graetz *et al.*, 1995). The result of such traditional land-use change is to decrease persistent vegetation cover and increase recurrent cover (Berry & Roderick, 2002a). In contrast, contemporary trends in land-use change have seen the expansion of plantations (Parsons *et al.*, 2006), large-scale revegetation activities, and the reintroduction of perennial vegetation into agricultural landscapes, all of which increase persistent cover and decrease recurrent. Our results indicate that, if land-use change is continuing as it has done traditionally (i.e., tree to grass), its net continent-wide effect is small compared with vegetation responses to climate. Alternatively, patterns of land-use change may have recently reversed direction (e.g., Kauppi *et al.*, 2006), the net effect of which may now be of increasing vegetation cover and would be in the same direction as climate-induced vegetation changes.

Several studies have estimated the effect of historical land-use change in Australia (predominantly the conversion of woodlands to grasslands) on surface water fluxes over the past 200 years (Pierce *et al.*, 1993; Gordon *et al.*, 2003; Berry & Roderick, 2004). Each indicated that, where such land-cover conversion occurred, annual average evapotranspiration decreased. It seems reasonable that the opposite effect should have occurred over the past 25 years across Australia in response to both the observed increases in F_t and F_p and the higher rates of P. The same can be expected of carbon assimilation rates (Monteith, 1972). We expect that the fPAR dataset used in these analyses will be valuable in analysing the effect of recent vegetation changes on Australia's energy, carbon, and water fluxes (e.g., Donohue *et al.*, 2007b) and that, from this, further insight can be gained into the potential impacts of climate change in water-limited environments.

Conclusion

Across the vast majority of Australia, vegetation productivity is limited by the availability of water and so understanding how changes in climatic conditions impact productivity is an important challenge. By presenting an observation-based analysis of changes in vegetation cover between 1981 and 2006, we found that vegetation cover across Australia has increased. On average, total cover (as described by total fPAR, F_t) has risen by 8% (0.0007 per year). Associated with this has been a 7% (1.3 mm yr^{-2}) rise in Australian precipitation (P). The spatial and seasonal patterns of trends in F_t generally correspond to those in P. These analyses have also shown that there has been a differential response of vegetation functional types to changes in climatic growing conditions. By splitting F_t into the persistent (F_p) and recurrent (F_r) fPAR functional components (generally distinguishing nondeciduous perennial species from deciduous, annual, and ephemeral species, respectively), results indicate that the observed Australia-wide increase in total cover has been predominantly due to a general 'background' increase in F_p (0.001 per year) and despite slight decreases in F_r (−0.0003 per year).

In a site-based analysis, vegetation trends in energy-limited and in water-limited environments were separately examined. Not surprisingly, vegetation cover was observed to change, on the whole, in accordance with changes in climatic limitations to growth (e.g., total cover decreased in water-limited environments when the availability of water decreased). Perhaps a little unexpectedly, at around one-third of all the water-limited sites (27 of 74), trends in P were negligible or negative yet F_t increased due to considerable increases in F_p (F_p up 36%), often at the expense of F_r. This suggests that factors other than changes in P are driving the observed increases in vegetation cover at these water-limited sites.

Observed increases in vegetation cover across Australia from both the grid- and site-based trend analyses indicates that the limitations to vegetation growth have eased during the study period which, for Australia, generally implies an effective increase in the availability of moisture to plants. Similar observations have been made in other water-limited environments across the globe (e.g., Nemani *et al.*, 2003; Herrmann *et al.*, 2005; Piao *et al.*, 2005). Here, we now also report that widespread changes in growing conditions across Australia have, on average, preferentially benefited persistent vegetation types over recurrent vegetation types. These findings are consistent with the expected effects of rising [CO_2] on vegetation cover in water-limited environments; however, the attribution of the drivers of these vegetation changes requires further research. Regardless of the causes, the degree of water-limitation experienced by vegetation across Australia has, on average, lessened over the past 2–3 decades, resulting

in an observable greening of the driest inhabited continent on Earth.

Acknowledgements

We would like to thank G. Farquhar, T. Van Niel, and J. P. Guerschman for helpful comments on drafts of this paper.

References

Asrar G, Fuchs M, Kanemasu ET, Hatfield JL (1984) Estimating absorbed photosynthetic radiation and leaf-area index from spectral reflectance in wheat. *Agronomy Journal*, **76**, 300–306.

AUSLIG (1990) *Atlas of Australian Resources (Vol. 6 Vegetation)*, 3rd edn. Australian Survey and Land Information Group, Canberra.

Berry SL, Farquhar GD, Roderick ML (2005) Co-evolution of climate, soil and vegetation. In: *Encyclopaedia of Hydrological Sciences*, Vol. 1 (ed. Anderson M), pp. 117–192. John Wiley, Indianapolis.

Berry SL, Roderick ML (2002a) CO_2 and land-use effects on Australian vegetation over the last two centuries. *Australian Journal of Botany*, **50**, 511–531.

Berry SL, Roderick ML (2002b) Estimating mixtures of leaf functional types using continental-scale satellite and climatic data. *Global Ecology and Biogeography*, **11**, 23–39.

Berry SL, Roderick ML (2004) Gross primary productivity and transpiration flux of the Australian vegetation from 1788 to 1988 AD: effects of CO_2 and land use change. *Global Change Biology*, **10**, 1884–1898.

BOM (2006) *Climate data: Australia CD-ROM, Version 2.2, December 2006*. Australian Government Bureau of Meteorology.

BOM (2007) *Timeseries—Australian climate variability and change*. Australian Government Bureau of Meteorology. http://www.bom.gov.au/cgi-bin/silo/reg/cli_chg/timeseries.cgi, accessed May 2007.

Brook BW, Bowman D (2006) Postcards from the past: charting the landscape-scale conversion of tropical Australian savanna to closed forest during the 20th century. *Landscape Ecology*, **21**, 1253–1266.

Budyko MI (1974) *Climate and Life*. Academic, New York.

Butler DW, Fairfax RJ, Fensham RJ (2006) Impacts of tree invasion on floristic composition of subtropical grasslands on the Bunya Mountains, Australia. *Australian Journal of Botany*, **54**, 261–270.

Carlson TN, Ripley DA (1997) On the relation between NDVI, fractional vegetation cover, and leaf area index. *Remote Sensing of Environment*, **62**, 241–252.

DNRW (2007) *Land cover change in Queensland 2004–2005: a Statewide Landcover and Trees Study (SLATS) report*. Department of Natural Resources and Water, Brisbane. http://www.nrw.qld.gov.au/slats/pdf/slats_0405.pdf.

Donohue RJ, Roderick ML, McVicar TR (2007a) *Correcting long-term AVHRR reflectance data using the vegetation cover triangle*. CSIRO Land and Water Science Report 26/07. CSIRO Land and Water, Canberra, 73 pp. http://www.clw.csiro.au/publications/science/2007/sr26-07.pdf.

Donohue RJ, Roderick ML, McVicar TR (2007b) On the importance of including vegetation dynamics in Budyko's hydrological model. *Hydrology and Earth System Sciences*, **11**, 983–995.

Donohue RJ, Roderick ML, McVicar TR (2008) Deriving consistent long-term vegetation information from AVHRR reflectance data using a cover-triangle-based framework. *Remote Sensing of Environment*, **112**, 2938–2949. doi: 10.1016/j.rse.2008.02.008.

Drake BG, Gonzalez-Meler MA, Long SP (1997) More efficient plants: a consequence of rising atmospheric CO_2? *Annual Review of Plant Physiology and Plant Molecular Biology*, **48**, 609–639. doi: 10.1146/annurev.arplant.48.1.609.

Eldridge D, Grant R (2004) *Rangeland Change in the Western Riverina Saltbush Range-Type*. Department of Infrastructure, Planning and Natural Resources, Sydney.

Eldridge DJ, Stafford MJ (1999) *Rangeland health in the western Riverina: 1990–1997. Report to the lower Murrumbidgee Lachlan resources management committee*. Department of Land and Water Conservation, Centre for Natural Resources.

Environment Australia (2000) *Revision of the Interim Biogeographic Regionalisation of Australia (IBRA) and the Development of Version 5.1—Summary Report*. Department of Environment and Heritage, Canberra.

Farquhar GD (1997) Carbon dioxide and vegetation. *Science*, **278**, 1411–1411.

Fensham RJ, Fairfax RJ (2003) Assessing woody vegetation cover change in north-west Australian savanna using aerial photography. *International Journal of Wildland Fire*, **12**, 359–367.

Fensham RJ, Fairfax RJ (2005) Preliminary assessment of gidgee (*Acacia cambagei*) woodland thickening in the Longreach district, Queensland. *Rangeland Journal*, **27**, 159–168.

Fensham RJ, Fairfax RJ, Archer SR (2005) Rainfall, land use and woody vegetation cover change in semi-arid Australian savanna. *Journal of Ecology*, **93**, 596–606.

Field CB, Chapin FS, Matson PA, Mooney HA (1992) Responses of terrestrial ecosystems to the changing atmosphere – a resource-based approach. *Annual Review of Ecology and Systematics*, **23**, 201–235.

Forman RTT (1964) Growth under controlled conditions to explain the hierarchical distributions of a moss, *Tetraphis pellucida*. *Ecological Monographs*, **34**, 1–25.

Gedney N, Cox PM, Betts RA, Boucher O, Huntingford C, Stott PA (2006) Detection of a direct carbon dioxide effect in continental river runoff records. *Nature*, **439**, 835–838.

Gill TK, Armston JD, Phinn SR, Pailthorpe BA (2006) *A comparison of MODIS time-series decomposition methods for estimating evergreen foliage cover*. Canberra. http://www.arspc.org/abstract/13.htm.

Goetz SJ, Bunn AG, Fiske GJ, Houghton RA (2005) Satellite-observed photosynthetic trends across boreal North America associated with climate and fire disturbance. *Proceedings of the National Academy of Sciences of the United States of America*, **102**, 13521–13525.

Gordon L, Dunlop M, Foran B (2003) Land cover change and water vapour flows: learning from Australia. *Philosophical Transactions of the Royal Society of London Series B – Biological Sciences*, **358**, 1973–1984.

Graetz RD, Wilson MA, Campbell SK (1995) *Landcover Disturbance over the Australian Continent: A Contemporary Assessment*.

Biodiversity Series, Paper 7. Department of Environment, Sport and Territories, Canberra.

Gutman GG (1999) On the use of long-term global data of land reflectances and vegetation indices derived from the Advanced Very High Resolution Radiometer. *Journal of Geophysical Research – Atmospheres*, **104**, 6241–6255.

Hendon HH, Thompson DWJ, Wheeler MC (2007) Australian rainfall and surface temperature variations associated with the Southern Hemisphere annular mode. *Journal of Climate*, **20**, 2452–2467.

Herrmann SM, Anyamba A, Tucker CJ (2005) Recent trends in vegetation dynamics in the African Sahel and their relationship to climate. *Global Environmental Change – Human and Policy Dimensions*, **15**, 394–404.

Hicke JA, Asner GP, Randerson JT *et al.* (2002) Satellite-derived increases in net primary productivity across North America, 1982–1998. *Geophysical Research Letters*, **29**, 1427, doi: 10.1029/2001GL013578.

IPCC (2007) Summary for policymakers. In: *Climate Change 2007: The Physical Science Basis. Contribution of Working Group I to the Fourth Assessment Report of the Intergovernmental Panel on Climate Change* (eds Solomon S, Qin D, Manning M *et al.*), pp. 1–18. Cambridge University Press, Cambridge.

Jones D, Wang W, Fawcett R, Grant I (2006) *The generation and delivery of level-1 historical climate data sets*. Australian Water Availability Project. Final Report. Australian Government Bureau of Meteorology.

Kauppi PE, Ausubel JH, Fang JY, Mather AS, Sedjo RA, Waggoner PE (2006) Returning forests analyzed with the forest identity. *Proceedings of the National Academy of Sciences of the United States of America*, **103**, 17574–17579.

Kawabata A, Ichii K, Yamaguchi Y (2001) Global monitoring of interannual changes in vegetation activities using NDVI and its relationships to temperature and precipitation. *International Journal of Remote Sensing*, **22**, 1377–1382.

Keeling CD, Whorf TP (2005) *Atmospheric CO_2 records from sites in the SIO air sampling network*. Carbon Dioxide Information Analysis Center, Oak Ridge National Laboratory, U.S. Department of Energy, Oak Ridge. http://cdiac.ornl.gov/trends/co2/sio-keel.html, accessed February 2008.

Kendall M, Gibbons JD (1990) *Rank Correlation Methods*, 5th edn. Oxford University Press, Oxford.

Kidwell KB (1998) *NOAA Polar Orbiter Data User's Guide (TIROS-N, NOAA-6, NOAA-7, NOAA-8, NOAA-9, NOAA-10, NOAA-11, NOAA-12, NOAA-13 and NOAA-14)*. National Environmental Satellite Data and Information Service, NOAA, Suitland.

King EA (2003) *The Australian AVHRR Data Set at CSIRO/EOC: Origins, Processes, Holdings and Prospects*. CSIRO Earth Observation Centre Report 2003/04. CSIRO Earth Observation Centre, Canberra. http://www.eoc.csiro.au/tech_reps/2003/tr2003_04.pdf.

Knapp PA, Soule PT (1996) Vegetation change and the role of atmospheric CO_2 enrichment on a relict site in central Oregon: 1960–1994. *Annals of the Association of American Geographers*, **86**, 387–411.

Krull E, Bray S, Harms B, Baxter N, Bol R, Farquhar G (2007) Development of a stable isotope index to assess decadal-scale vegetation change and application to woodlands of the Burdekin catchment, Australia. *Global Change Biology*, **13**, 1455–1468.

Linacre ET (1994) Estimating U.S. Class A pan evaporation from few climate data. *Water International*, **19**, 5–14.

Lu H, Raupach MR, McVicar TR, Barrett DJ (2003) Decomposition of vegetation cover into woody and herbaceous components using AVHRR NDVI time series. *Remote Sensing of Environment*, **86**, 1–18.

McClelland JW, Holmes RM, Peterson BJ, Stieglitz M (2004) Increasing river discharge in the Eurasian Arctic: consideration of dams, permafrost thaw, and fires as potential agents of change. *Journal of Geophysical Research*, **109**, D18102, doi: 10.1029/2004JD004583.

McVicar TR, Van Niel TG, Li LT, Hutchinson MF, Mu XM, Liu ZH (2007) Spatially distributing monthly reference evapotranspiration and pan evaporation considering topographic influences. *Journal of Hydrology*, **338**, 196–220.

Monteith JL (1972) Solar radiation and productivity in tropical ecosystems. *Journal of Applied Ecology*, **9**, 747–766.

Morgan JA, Milchunas DG, LeCain DR, West M, Mosier AR (2007) Carbon dioxide enrichment alters plant community structure and accelerates shrub growth in the shortgrass steppe. *Proceedings of the National Academy of Sciences*, **104**, 14724–14729.

Myneni RB, Hall FG, Sellers PJ, Marshak AL (1995) The interpretation of spectral vegetation indexes. *IEEE Transactions on Geoscience and Remote Sensing*, **33**, 481–486.

Myneni RB, Keeling CD, Tucker CJ, Asrar G, Nemani RR (1997) Increased plant growth in the northern high latitudes from 1981 to 1991. *Nature*, **386**, 698–702.

Myneni RB, Tucker CJ, Asrar G, Keeling CD (1998) Interannual variations in satellite-sensed vegetation index data from 1981 to 1991. *Journal of Geophysical Research – Atmospheres*, **103**, 6145–6160.

Nemani RR, Keeling CD, Hashimoto H *et al.* (2003) Climate-driven increases in global terrestrial net primary production from 1982 to 1999. *Science*, **300**, 1560–1563.

Nicholls N (2006) Detecting and attributing Australian climate change: a review. *Australian Meteorological Magazine*, **55**, 199–211.

Nix HA (1978) Determinants of environmental tolerance limits in plants. In: *Biology and Quaternary Environments* (eds Walker D, Guppy JC), pp. 195–206. Australian Academy of Science, Canberra.

NLWRA (2001) *Australian Native Vegetation Assessment 2001*. National Land and Water Resources Audit, Canberra.

Parsons M, Gavran M, Davidson J (2006) *Australia's Plantations 2006*. Australian Government Department of Agriculture, Fisheries and Forestry, Canberra.

Paruelo JM, Garbulsky MF, Guerschman JP, Jobbagy EG (2004) Two decades of Normalized Difference Vegetation Index changes in South America: identifying the imprint of global change. *International Journal of Remote Sensing*, **25**, 2793–2806.

Piao SL, Fang JY, Liu HY, Zhu B (2005) NDVI-indicated decline in desertification in China in the past two decades. *Geophysical Research Letters*, **32**, L06402, doi: 10.1029/2004GL021764.

Piao SL, Fang JY, Zhou LM *et al.* (2003) Interannual variations of monthly and seasonal Normalized Difference Vegetation Index (NDVI) in China from 1982 to 1999. *Journal of Geophysical Research – Atmospheres*, **108**, 4401, doi: 10.1029/2002JD002848.

Pierce LL, Walker J, Dowling TI, McVicar TR, Hatton TJ, Running SW, Coughlan JC (1993) Ecohydrological changes in the Murray-Darling Basin. 1. A simulation of regional hydrological changes. *Journal of Applied Ecology*, **30**, 283–294.

Pittock B (ed.) (2003) *Climate Change: An Australian Guide to the Science and Potential Impacts*. Australian Greenhouse Office, Canberra.

Polley HW (1997) Implications of rising atmospheric carbon dioxide concentration for rangelands. *Journal of Range Management*, **50**, 562–577.

Poorter H, Navas ML (2003) Plant growth and competition at elevated CO_2: on winners, losers and functional groups. *New Phytologist*, **157**, 175–198.

Raupach MR, Kirby JM, Barrett DJ, Briggs PR (2001) *Balances of water, carbon, nitrogen and phosphorus in Australian landscapes: (1) Project description and results*. 40/01. CSIRO Land and Water, Canberra.

Roderick ML, Farquhar GD (2004) Changes in Australian pan evaporation from 1970 to 2002. *International Journal of Climatology*, **24**, 1077–1090.

Roderick ML, Noble IR, Cridland SW (1999) Estimating woody and herbaceous vegetation cover from time series satellite observations. *Global Ecology and Biogeography*, **8**, 501–508.

Rotstayn LD, Cai WJ, Dix MR *et al.* (2007) Have Australian rainfall and cloudiness increased due to the remote effects of Asian anthropogenic aerosols? *Journal of Geophysical Research – Atmospheres*, **112**, D09202, doi: 10.1029/2006JD007712.

Russell-Smith J, Stanton PJ, Edwards AC, Whitehead PJ (2004) Rain forest invasion of eucalypt-dominated woodland savanna, iron range, North-Eastern Australia: II. Rates of landscape change. *Journal of Biogeography*, **31**, 1305–1316.

Shaw NH, Norman MJT (1970) Tropical and sub-tropical woodlands and grasslands. In: *Australian Grasslands* (ed. Moore RM), pp. 112–122. Australian National University, Canberra.

Slayback DA, Pinzon JE, Los SO, Tucker CJ (2003) Northern hemisphere photosynthetic trends 1982–99. *Global Change Biology*, **9**, 1–15.

Specht RL (1972) Water use by perennial evergreen plant communities in Australia and Papua New Guinea. *Australian Journal of Botany*, **20**, 273–299.

Specht RL (1981) Ecophysiological principles determining the biogeography of major vegetation formations in Australia. In: *Ecological Biogeography of Australia*, Vol. 1 (ed. Keast A), pp. 299–334. Dr W. Junk, The Hague.

Timbal B, Jones DA (2008) Future projections of winter rainfall in southeast Australia using a statistical downscaling technique. *Climatic Change*, **86**, 165–187. doi: 10.1007/s10584-007-9279-7.

Tucker CJ, Slayback DA, Pinzon JE, Los SO, Myneni RB, Taylor MG (2001) Higher northern latitude Normalized Difference Vegetation Index and growing season trends from 1982 to 1999. *International Journal of Biometeorology*, **45**, 184–190.

Walker J, Bullen F, Williams BG (1993) Ecohydrological changes in the Murray-Darling Basin. 1. The number of trees cleared over 2 centuries. *Journal of Applied Ecology*, **30**, 265–273.

Watson IW, Thomas PWE, Fletcher WJ (2007) The first assessment, using a rangeland monitoring system, of change in shrub and tree populations across the arid shrublands of Western Australia. *Rangeland Journal*, **29**, 25–37.

Weatherhead EC, Reinsel GC, Tiao GC *et al.* (1998) Factors affecting the detection of trends: statistical considerations and applications to environmental data. *Journal of Geophysical Research – Atmospheres*, **103**, 17149–17161.

Wilson BA, Neldner VJ, Accad A (2002) The extent and status of remnant vegetation in Queensland and its implications for statewide vegetation management and legislation. *Rangeland Journal*, **24**, 6–35.

Wong SC, Cowan IR, Farquhar GD (1979) Stomatal conductance correlates with photosynthetic capacity. *Nature*, **282**, 424–426.

Woodward FI (1987) *Climate and Plant Distribution*. Cambridge University Press, Cambridge.

Xiao J, Moody A (2005) Geographical distribution of global greening trends and their climatic correlates: 1982–1998. *International Journal of Remote Sensing*, **26**, 2371–2390.

Young SS, Harris R (2005) Changing patterns of global-scale vegetation photosynthesis, 1982–1999. *International Journal of Remote Sensing*, **26**, 4537–4563.

Zhou LM, Tucker CJ, Kaufmann RK, Slayback D, Shabanov NV, Myneni RB (2001) Variations in northern vegetation activity inferred from satellite data of vegetation index during 1981 to 1999. *Journal of Geophysical Research – Atmospheres*, **106**, 20069–20083.

CHAPTER 5

Assessing the ability of potential evaporation formulations to capture the dynamics in evaporative demand within a changing climate

Assessing the ability of potential evaporation formulations to capture the dynamics in evaporative demand within a changing climate

Randall J. Donohue[a,b *], Tim R. McVicar[a] and Michael L. Roderick[b,c]

[a] CSIRO Land and Water, GPO Box 1666, Canberra, 2601, ACT, Australia

[b] Research School of Biological Sciences, The Australian National University, Canberra, 0200, ACT, Australia

[c] Research School of Earth Sciences, The Australian National University, Canberra, 0200, ACT, Australia

* Corresponding Author:

E: randall.donohue@csiro.au

P: 61-2-6246-5803

Submitted to: Journal of Hydrology

Submission date: 20 November 2009

Keywords: Penman; Priestley-Taylor; Morton; albedo; wind speed; climate change.

5.1 Abstract

Rates of evaporative demand can be modelled using one of numerous formulations of potential evaporation. Physically, evaporative demand is driven by four key variables—net radiation, vapour pressure, wind speed, and air temperature—each of which have been changing across the globe over the past few decades. In this research we examine several formulations of potential evaporation, testing for how well each captures the dynamics in evaporative demand. We generated five daily potential evaporation datasets for Australia, spanning 1981-2006, using the: (i) Penman; (ii) Priestley-Taylor; (iii) Morton point; (iv) Morton areal; and (v) Thornthwaite formulations. These represent a range in how many of the key driving variables are incorporated within modelling. The testing of these formulations was done by analysing the spatial, annual, and seasonal trends in each against changes in precipitation (a proxy for actual evaporation), assuming that they should vary in an approximately inverse manner. Results show that only potential evaporation modelled with a 4-variable, fully physical formulation (i.e., Penman) displayed reasonable values of both rates *and* trends. An attribution analysis was performed using the Penman formulation to quantify the contribution each input variable made to overall trends in potential evaporation. Even though changes in air temperature played an important role in the overall magnitude of potential evaporation trends, it was the contribution of changes in vapour pressure, net radiation (primarily due to albedo) and wind speed that produced the complementary behaviour. This study highlights the need for spatially and temporally dynamic data describing all the key drivers of evaporative demand, especially the imperative for projections of each driving variable when estimating the possible affects of climatic changes on evaporative demand.

5.2 Introduction

Analyses of catchment hydrological dynamics require estimates of the supply of water and of the evaporative demand for water. Estimates of potential evaporation are generally used to represent evaporative demand. Conceptually, potential evaporation represents the maximum possible evaporation rate (e.g., Granger, 1989; Lhomme, 1999) and is the rate that would occur under given meteorological conditions from a continuously saturated surface (Thornthwaite, 1948). Notionally, the concept of potential evaporation is simple. However, the practical implementation of the concept is problematic and ambiguous due to the many ways potential evaporation can be, and has been, formulated. Here our focus is on how input variables are treated within several common formulations.

Even though potential evaporation is primarily driven by four meteorological variables (net radiation, vapor pressure, wind speed and temperature) it is a conceptual entity that can not be measured directly (Thornthwaite, 1948). Many different methods of estimating potential evaporation from one or more of these four variables have been developed according to local climatic conditions and the availability of suitable data (see Shuttleworth, 1993; Singh and Xu, 1997; Xu and Singh, 2000, , 2001). Some formulations, such as Thornthwaite's (1948), use a single variable (i.e., air temperature) that is related to potential evaporation rates via empirical relationships. These typically need to be recalibrated to maintain accuracy when applied outside the original spatial and temporal contexts (Xu and Singh, 2001). Other formulations, by assuming the surface is extensive and continually saturated, omit the effects of the 'advective' variables (i.e., wind speed and vapor pressure), and account only for the vertical heat and mass fluxes. Such formulations are often referred to as 'areal' or 'wet area' potentials and are best suited to energy-limited environments. Alternatively, fully physical models, such as the Penman and the Penman-Monteith equations (Penman, 1948; Monteith, 1981), are physically derived (except for any resistance terms) and explicitly incorporate all the driving variables. Although these formulations are universally applicable they are data intensive.

The relationship between potential evaporation and actual evaporation differs depending on what process is the dominant limit to evaporation. In water-limited landscapes, where the supply of energy exceeds the supply of water, the actual evaporation rate is

less than the potential rate and is largely determined by the supply of water. Alternatively, in energy-limited environments where the supply of water exceeds that of energy, actual evaporation rates closely follow those of potential (McIllroy and Angus, 1964; Budyko, 1974; Thornthwaite, 1948; Linacre, 2004).

This research was prompted by the need for spatially explicit potential evaporation data that are suitable for the analysis of long-term dynamics in evaporative demand. Widespread changes in climatic conditions have been reported, with long-term trends observed in global average air temperature (e.g., IPCC, 2007), vapour pressure (e.g., Durre et al., 2009), precipitation (e.g., New et al., 2001), net radiation (e.g., Wild, 2009), and wind speed (e.g., McVicar et al., 2008). This is no less true for Australia, where temperature and precipitation have been increasing on average over the past 3 or so decades (Bureau of Meteorology, 2007) as has vapour pressure (this study), whilst wind (Roderick et al., 2007; Rayner, 2007; McVicar et al., 2008) and net radiation (this study) have been decreasing. All these changes will have inevitably led to changes in evaporative demand. Given the extremely variable nature of the drivers of potential evaporation, any methods used to examine long-term analyses of evaporative demand need to be capable of accounting for the observed, and expected, changes in all relevant input variables (McKenney and Rosenberg, 1993) and should ideally be applicable in both water- and energy-limited environments.

Our aim is to test a variety of potential evaporation formulations, examining how well each captures the dynamics in evaporative demand. Towards this end, we generated datasets of daily potential evaporation—spanning Australia and extending from 1981 to 2006—using five formulations, namely the: (i) Penman (1948); (ii) Priestley-Taylor (1972); (iii) Morton (1983) point; (iv) Morton (1983) areal; and (v) Thornthwaite (1948) potential evaporation formulations. These were selected as they represent a range in how the key input variables are treated, varying from the fully physical, 4-variable Penman model to the empirical Thornthwaite model that contains only one variable (air temperature). We analysed the annual, seasonal and spatial trends of each formulation as well as attributing, for two of the formulations, how each input variable contributed to the overall trends. This allowed us to make an assessment of the suitability of each potential evaporation formulation for representing long-term dynamics in evaporative demand.

Potential evaporation can not be measured directly and so validating potential evaporation data both spatially and temporally is difficult. However, the input data used to generate potential evaporation estimates can be validated. Spatial surfaces of meteorological variables are increasingly being used in hydro-meteorological analyses. Little attention has been given to assessing the temporal accuracy of such surfaces. Prior to conducting analyses of potential evaporation dynamics, we undertook two rigorous tests of the temporal accuracy of the input surface data. In the first, which is reported in Donohue et al. (2009b), we compared surface-derived trends in the input variables with trends present in the underlying point data from which the surfaces were generated. In the second test, which is reported here, we use the input data and the Penpan model (Rotstayn et al., 2006) to estimate US Class A pan evaporation rates and trends, and compare these with rates and trends of observed pan evaporation.

This paper is organised as follows. In the next Section 'Materials and Methods' we describe: (i) the data used in these analyses and the validation performed to test their accuracy; (ii) the generation of Australia-wide daily net radiation surfaces; (iii) the five different potential evaporation formulations used; (iv) the calculation of trends in potential evaporation; and (v) an attribution analysis to quantify the contribution of each input variable to potential evaporation trends. Results are presented using this same structure, followed by a discussion of results. We then provide conclusions and recommendations. A more detailed description of the data, validation and methods is given in Donohue et al. (2009b).

5.3 Materials and Methods

5.3.1 Input data description and validation

Data in the form of daily grids were used for these analyses, spanning January 1981 through to December 2006 (see Table 1). This time-span was chosen to match that of the remotely sensed vegetation cover data of Donohue et al. (2008) from which estimates of albedo and surface emissivity were derived. Elevation was derived from the DEM-9S dataset of Geoscience Australia (2007). Meteorological data describing precipitation, air temperature and vapour pressure were sourced from Jones et al. (2006). A spatial dataset of daily wind speed was generated using the point-based wind data described by McVicar et al. (2008). Here, wind speed surfaces were derived from these

data using Triangular Irregular Networks (TINs). All input spatial data were converted to the same spatial resolution (0.05°), the same extent (112.0–154.0°E and 10.0–44.0°S) and to SI units prior to analyses.

Table 1. Input dataset specifications and sources for (A) grid-based data and (B) point-based data.

A	Input variable	Data origin	Units	Time-step	Cell size	Reference
	Precipitation (P)	Spline-interpolated point data	$mm.d^{-1}$	Daily	0.05°	Jones et al. (2009)
	Air temperature (max, T_x; min, T_n)	Spline-interpolated point data	K	Daily	0.05°	Jones et al. (2009)
	Vapour pressure (e_a)	Spline-interpolated point data	Pa	Daily	0.05°	Jones et al. (2009)
	Wind speed at 2m height (u_2)	TIN-interpolated point data	$m.s^{-1}$	Daily	0.05°	This study and McVicar et al. (2008)
	fPAR (F_t)	AVHRR* observations	—	Monthly	0.08°	Donohue et al. (2007)
	Red and NIR reflectance (ρ_R, ρ_N)	AVHRR* observations	%	Monthly	0.08°	Donohue et al. (2007)
	Elevation (z)	Spline-interpolated point data	m	—	9″	Geoscience Australia (2007)
B	**Input variable**	**Data origin**	**Units**	**Time-step**		**Reference**
	Precipitation (P)	Meteorological observations	$mm.mth^{-1}$	Monthly		Bureau of Meteorology (2006)
	Pan evaporation	Met. observations	$mm.mth^{-1}$	Monthly		Bureau of Meteorology (2006)
	Air temperature (T_x; T_n; dew point)	Met. observations	K	Monthly		Bureau of Meteorology (2006)
	Wind speed at 2m height (u_2)	Met. observations	$m.s^{-1}$	Monthly		Bureau of Meteorology (2006)

* Advanced Very High-Resolution Radiometer

Before generating the surfaces of potential evaporation, we tested the temporal accuracy of the input surfaces. This test entailed using these services to model Penpan evaporation (Rotstayn et al., 2006) and to compare these with observed point-based pan evaporation rates and trends. The Penpan model simulates US Class A pan evaporation rates. This provides a rigorous test of the data and gives a good indication of the accuracy of subsequently modelled potential evaporation data for two reasons: (i)

Roderick et al. (2007) have shown that the Penpan model can accurately reproduce both rates and trends in US Class A pan evaporation with high quality point-based input data; and (ii) pan evaporimeters integrate the effects of radiation, humidity, wind and air temperature on wet-surface evaporation rates (Stanhill, 2002), and so provide measurements of evaporation that are conceptually similar to potential (open water) evaporation rates (e.g., McVicar et al., 2007). Point-based pan evaporation observations were extracted from the Monthly Australian Data Archive for Meteorology database (Bureau of Meteorology, 2006). Only near-complete records for the study period were extracted, resulting in 102 sites (Figure 1). Corresponding Penpan values were extracted from the surfaces at these sites.

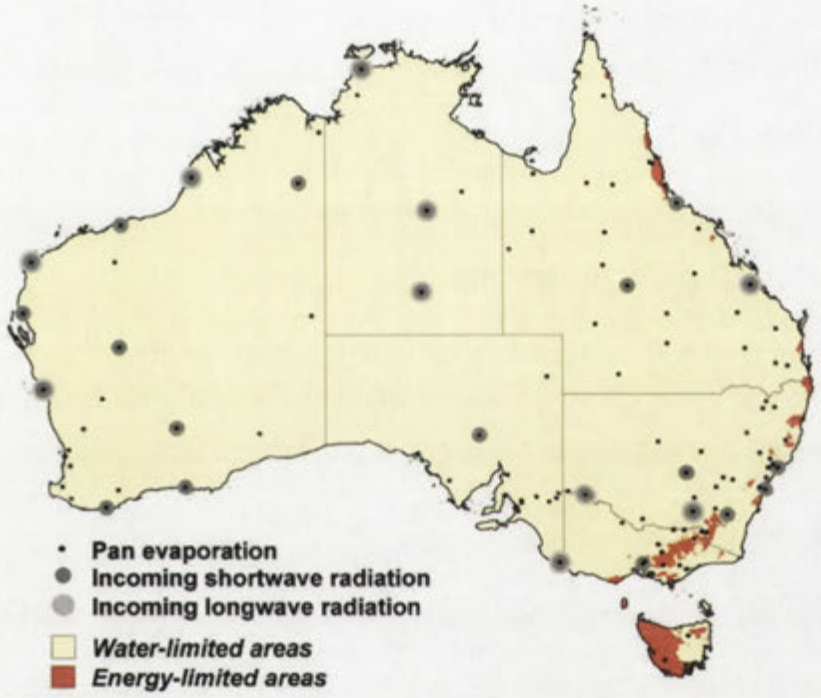

Figure 1. Distribution of stations with long-term radiation and pan evaporation observations. Also shown areas that are water/energy-limited on an annual average basis. Of the 102 pan evaporation stations, 96 lie within water-limited landscapes.

5.3.2 Modelling net radiation

Net radiation (R_n, W.m^{-2}) was modelled generally following the method of Allen et al. (1998) except for the following (see Donohue et al. (2009b) for a full description):

i) Top-of-atmosphere incoming radiation (R_o, W.m^{-2}) was calculated using the method of Iqbal (1983) and Roderick (1999);

ii) atmospheric transmissivity (τ_a) was estimated using a locally calibrated (McVicar and Jupp, 1999) version of the Bristow-Campbell (1984) relationship;

iii) actual surface albedo (α) was incorporated into the model and was estimated using calibrated Advanced Very High Resolution Radiometer (AVHRR) red (ρ_R, %) and near-infrared (ρ_N, %) monthly reflectances (Donohue et al., 2008), following Saunders (1990); and

iv) surface emissivity (ε_s) was incorporated into the model and was estimated as a function of monthly vegetation fractional cover (Donohue et al., 2008).

Modelled incoming short wave (R_{si}, W.m^{-2}) and incoming long wave (R_{li}, W.m^{-2}) radiation were validated using ground-based measurements. Monthly observations of these two variables originate from the daily radiation observations collected and published by the Bureau of Meteorology (which were subsequently summarised by Roderick and Farquhar (2006)). The R_{si} data came from 25 stations across Australia and the R_{li} from 10 stations (Figure 1).

5.3.3 Potential evaporation formulations

Five Australia-wide, datasets of daily potential evaporation were derived from the modelled R_n data and the grid-based data described in Table 1. These five datasets were generated using the formulations outlined in Table 2, which are described in detail in Donohue et al. (2009b).

Table 2. Five formulations used to generate potential evaporation datasets. 'Variables' refers to the input data required in each potential evaporation formulation.

Formulation	Notation	Units	Source	Variables
Penman	E_p	mm.d^{-1}	Penman (1948) as given by Shuttleworth (1993)	T_a, R_n, e_a, u_2
Morton point	E_{mp}	mm.d^{-1}	Morton (1983)	T_a, R_n, e_a
Morton areal	E_{ma}	mm.d^{-1}	Morton (1983)	T_a, R_n, e_a
Priestley-Taylor	E_{pt}	mm.d^{-1}	Priestley and Taylor (1972)	T_a, R_n
Thornthwaite	E_{th}	mm.d^{-1}	Thornthwaite (1948)	T_a

5.3.4 Analysis of trends

Long-term dynamics in potential evaporation were examined in terms of linear trends calculated using ordinary least squares regressions on a month-of-year basis (i.e., calculate the trend for all Januaries, then for all Februaries, etc.). Annual trends were calculated as the sum of the twelve monthly trends. Performing the trend analyses in

this manner minimises biases introduced by the timing of gaps within the data record, which is important in the case of the AVHRR-derived vegetation data (see Donohue et al., 2009a; Donohue et al., 2008). For the spatial data, regressions were performed for every pixel across Australia and Australia-wide trends were calculated as the spatial averages of all the pixel trends. Trends in point-based data were calculated in the same month-of-year manner. In this way, long-term changes in the radiation balance and in the five formulations of potential evaporation—including trends in the inputs variables used in each of the models—were calculated. Here we present trends in flux variables in units of $x.yr^{-2}$ (i.e., the change over time $[.yr^{-1}]$ in the rate $[x.yr^{-1}]$), or in units of $x.mth^{-1}.yr^{-1}$ (i.e., the change over time $[.yr^{-1}]$ in the rate $[x.mth^{-1}]$).

One way of testing the ability of each formulation of potential evaporation to realistically capture changes in evaporative demand in water limited environments is to compare the trends in potential evaporation with trends in precipitation. The pattern generally expected is an inverse relationship due to the feedbacks between evaporative demand and precipitation (e.g., Yang et al., 2006). That is, in water limited environments, an increase in precipitation should be associated with increased latent heat flux because of increases in surface moisture availability, and should be associated with decreased incoming shortwave radiation due to increased cloudiness and humidity. It has recently been shown that the role of changes in wind speed in these feedbacks does not produce a simple inverse relation (Shuttleworth et al., 2009) . Given this caveat, this test of inverse proportionality—though approximate—constitutes a useful means of examining potential evaporation dynamics.

5.3.5 Attribution of trends

Another means of examining the modelled trends in potential evaporation is to attribute the changes in potential evaporation to changes in the component input variables. This allows the effects of the assumptions in formulations (that is, which variables are implicitly held constant) to be quantified on the overall dynamics in potential evaporation. The attribution of trends was undertaken by performing partial differentiations on the input variables of both the Penman and the Priestley-Taylor formulations. These two formulations were chosen as representatives of a fully physically based model and of a radiation-based model, respectively. Attribution of the temperature-based Thornthwaite formulation is not needed, as any changes in E_{th} are

directly attributed to dT_a/dt. The potential evaporation equations that are differentiated below are outlined fully in Donohue et al. (2009b).

As per Roderick et al. (2007), the change in E_p can be attributed to changes in the radiative and aerodynamic components,

$$\frac{dE_p}{dt} = \frac{dE_{pR}}{dt} + \frac{dE_{pA}}{dt}. \tag{1}$$

Dynamics in the radiative component are due to changes in Δ (the slope of the saturated vapour pressure–temperature curve; $Pa.K^{-1}$)—which itself is a function solely of T_a—and to changes in R_n:

$$\frac{dE_{pR}}{dt} = \frac{\partial E_{pR}}{\partial \Delta}\frac{d\Delta}{dT_a}\frac{dT_a}{dt} + \frac{\partial E_{pR}}{\partial R_n}\frac{dR_n}{dt}; \tag{2}$$

where

$$\frac{\partial E_{pR}}{\partial \Delta}\frac{d\Delta}{dT_a}\frac{dT_a}{dt} = \frac{R_n\gamma}{(\Delta+\gamma)^2}\frac{d\Delta}{dT_a}\frac{dT_a}{dt}; \text{ and} \tag{3}$$

$$\frac{\partial E_p}{\partial R_n}\frac{dR_n}{dt} = \frac{\Delta}{\Delta+\gamma}\frac{dR_n}{dt}, \text{ respectively.} \tag{4}$$

In equation (4), γ is the psychrometric constant ($Pa.K^{-1}$). Given that D (the vapour pressure deficit; Pa) is the difference between e_s and e_a, and that e_s changes only with T_a, changes in the aerodynamic component are

$$\frac{dE_{pA}}{dt} = \frac{\partial E_{pA}}{\partial \Delta}\frac{d\Delta}{dT_a}\frac{dT_a}{dt} + \frac{\partial E_{pA}}{\partial u_2}\frac{du_2}{dt} + \frac{\partial E_{pA}}{\partial e_s}\frac{de_s}{dT_a}\frac{dT_a}{dt} + \frac{\partial E_{pA}}{\partial e_a}\frac{de_a}{dt}, \tag{5}$$

with the contributions from Δ, u_2, e_s, and e_a estimated as (where λ is the latent heat of vaporisation of water):

$$\frac{\partial E_{pA}}{\partial \Delta}\frac{d\Delta}{dT_a}\frac{dT_a}{dt} = \frac{-6430\gamma D(1+0.536u_u)}{(\Delta+\gamma)^2\lambda}\frac{d\Delta}{dT_a}\frac{dT_a}{dt}; \tag{6}$$

$$\frac{\partial E_{pA}}{\partial u_2}\frac{du_2}{dt} = \frac{3446.48\gamma D}{(\Delta+\gamma)\lambda}\frac{du_2}{dt}; \tag{7}$$

$$\frac{\partial E_{pA}}{\partial e_s}\frac{de_s}{dT_a}\frac{dT_a}{dt} = \frac{6430\gamma(1+0.536u_2)}{(\Delta+\gamma)\lambda}\frac{de_s}{dT_a}\frac{dT_a}{dt}\text{; and} \quad (8)$$

$$\frac{\partial E_{pA}}{\partial e_a}\frac{de_a}{dt} = \frac{-6430\gamma(1+0.536u_2)}{(\Delta+\gamma)\lambda}\frac{de_a}{dt}. \quad (9)$$

To bring the attribution back to the four key driving variables of potential evaporation (R_n, e_a, T_a, and u_2), the effect of dT_a/dt on dE_p/dt can be approximated as the sum of Equations (3), (6), and (8)—ignoring the effect of dT_a/dt on dR_n/dt and assuming both Δ and e_s are functions solely of T_a.

For Priestley-Taylor, the change in E_{pt} and its partial differentials can be similarly expressed:

$$\frac{dE_{pt}}{dt} = \frac{\partial E_p}{\partial \Delta}\frac{d\Delta}{dT_a}\frac{dT_a}{dt} + \frac{\partial E_p}{\partial R_n}\frac{dR_n}{dt}. \quad (10)$$

Again, ignoring the affect of dT_a/dt on dR_n/dt and assuming Δ is a function solely of T_a, the attribution of T_a and R_n can be expressed, respectively, as:

$$\frac{\partial E_{pt}}{\partial \Delta}\frac{d\Delta}{dT_a}\frac{dT_a}{dt} = \frac{1.26R_n\gamma}{(\Delta+\gamma)^2}\frac{d\Delta}{dT_a}\frac{dT_a}{dt}\text{; and} \quad (11)$$

$$\frac{\partial E_{pt}}{\partial R_n}\frac{dR_n}{dt} = \frac{1.26\Delta}{\Delta+\gamma}\frac{dR_n}{dt}. \quad (12)$$

In quantifying these partial differentials, the Australian average trend (1981–2006) is used to represent the derivative (i.e., dx/dt) and the Australian, long-term annual average value (1981–2006) is used to represent the coefficients.

5.4 Results

5.4.1 Input data validation

The comparison of values and trends in modelled Penpan evaporation (E_{pp}) with values and trends in pan observations (E_{pan}) provides a robust test of the input data (Figure 2).

Here, these comparisons are quantified by linear regressions. Figure 2a shows that, modelled E_{pp} values compare well with E_{pan} values, with a slope of 0.99, an r^2 of 0.92, and an RMSE (Root Mean Square Error) of 27 mm.mth^{-1}. A similar level of accuracy between modelled and observed values was attained by Roderick et al. (2007) using solely point-based data. The relation between trends in E_{pp} and E_{pan} has a slope of 0.43 and r^2 of 0.31 (Figure 2b). Trends in E_{pp} only moderately match those of pan observations presumably due to the compounding effect of the input variables' inability to perfectly capture temporal trends (see Donohue et al. (2009b)). However, the average Australian trend in E_{pp} from the grid is 0.0 mm.yr^{-2} (with a standard error of 2.3 mm.yr^{-2}) and is comparable to the average of the observed trends at the 102 points of Figure 2 which is -1.5 mm.yr^{-2} (with a standard error of 4.0 mm.yr^{-2}). Given that the modelled E_{pp} values reproduced E_{pan} values extremely well (Figure 2a) and reproduced temporal trends moderately well (Figure 2b), this test of the input data shows that the input data can be used with reasonable confidence to calculate the five formulations of potential evaporation.

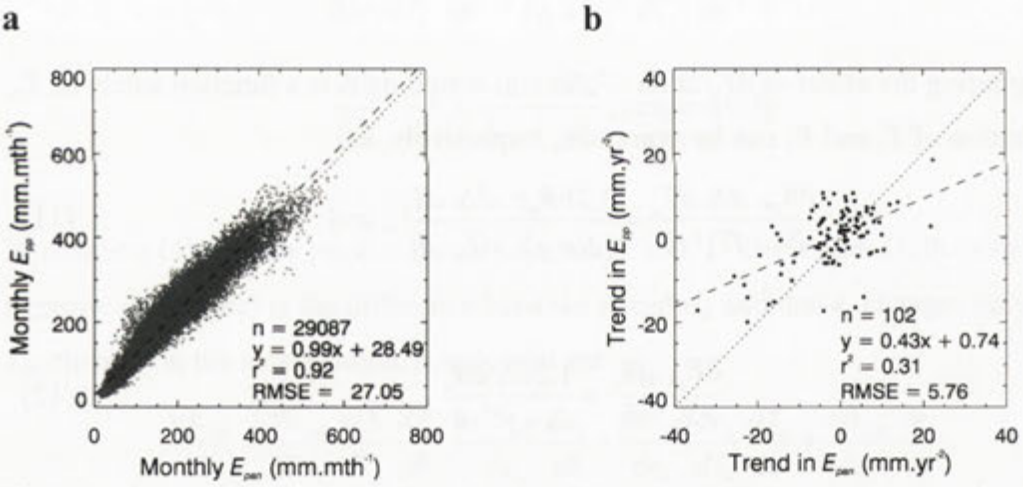

Figure 2. Comparison of observed pan evaporation and modelled Penpan evaporation at 102 sites across Australia. Plot (a) shows the monthly averages and (b) the annual trends. The dotted line is the 1:1 line, the dashed line is the equation of best fit (given on each plot), n is the number of observations, the offset and RMSE statistics are in ordinate units.

5.4.2 Net radiation validation

The use of McVicar and Jupp's (1999) locally calibrated coefficients within the Bristow-Campbell (1984) relation improved the accuracy of modelled R_{si} when compared to using the standard Bristow-Campbell formulation from r^2 and RMSE values of 0.72 and 43 W.m^{-2} to 0.93 and 18 W.m^{-2}, respectively (Figure 3a and b). Likewise, the addition of the local calibrations and the remotely sensed estimates of ε_s

improved R_{li} estimates from r^2 and RMSE values of 0.91 and 11 W.m^{-2} to 0.92 and 9 W.m^{-2}, respectively (Figure 3c and d).

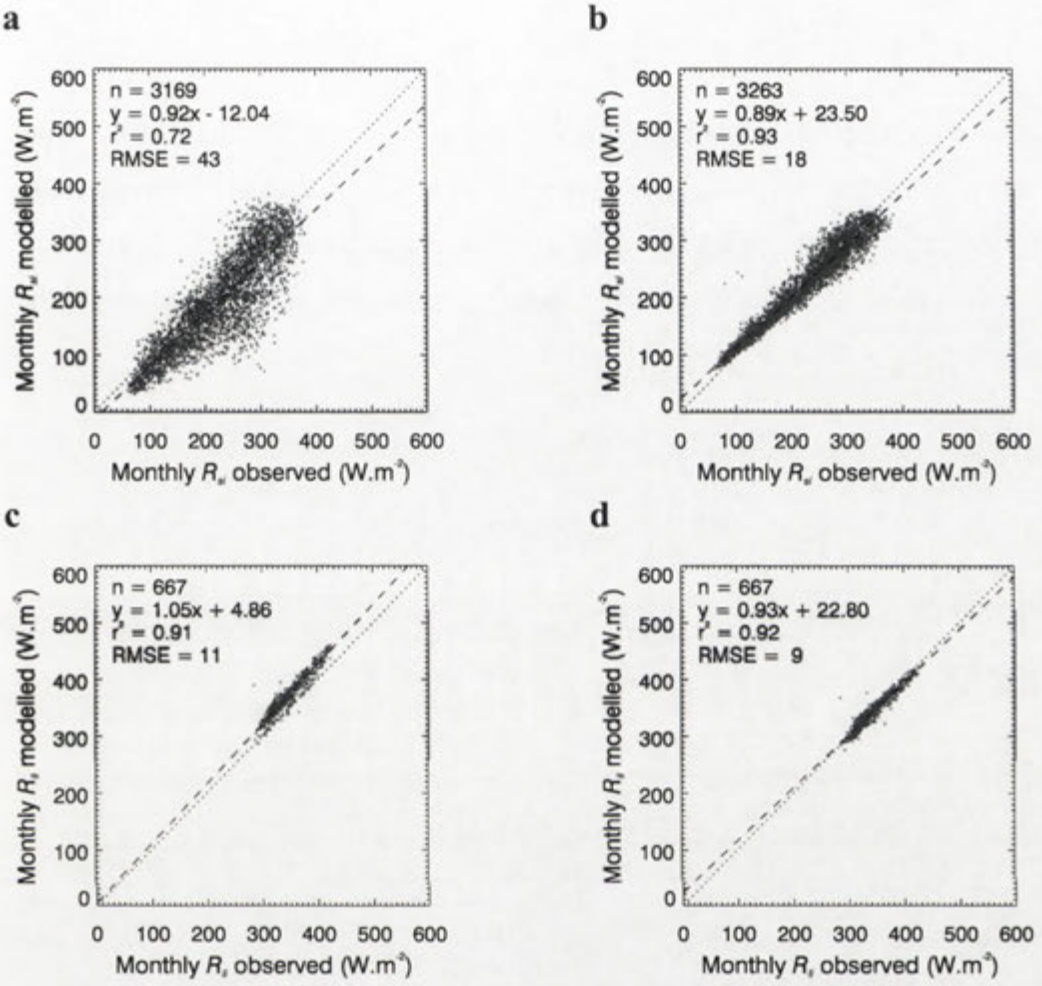

Figure 3. Comparison of observed and modelled monthly incoming radiation. Plot (a) shows incoming shortwave radiation (R_{si}) using the original Bristow-Campbell model; and (b) R_{si} using the Bristow-Campbell model calibrated with coefficients derived by McVicar and Jupp (1999). Plot (c) is the incoming longwave radiation (R_{li}) modelled using the standard FAO56 formulation (Allen et al. 1998); and (d) R_{li} modelled using the FAO56 formulation adapted to include the McVicar and Jupp (1999) coefficients and remotely sensed estimates of surface emissivity (ε_s). The dotted line is the 1:1 line, the dashed line is the equation of best fit (given on each plot), n is the number of observations, the offset and RMSE statistics are in ordinate units.

5.4.3 Potential evaporation formulations

Estimates of potential evaporation rates using the five formulations vary substantially in their magnitudes and ranges (Figure 4). Australian-average annual potential evaporation varies between 1765 and 3670 mm.yr^{-1}, whilst the smallest seasonal range is approximately 80 and the greatest is 300 mm.mth^{-1}. E_{mp} has the highest rate, and range, followed by E_p and E_{ma}. Pan evaporimeters, due to their 3-dimensional, above-ground geometry, are capable of absorbing more energy than can a flat surface (Linacre,

1994; McVicar et al., 2007; Rotstayn et al., 2006). Hence, E_{pan} should be higher than any rates of potential evaporation. Given this, and that the average E_{pp} value for Australia is 2894 mm.yr^{-1}, the values of E_{mp} seem unrealistically high, over-estimating potential rates by as much as 25%.

The values of E_p are estimates of open-water evaporation and the Penman formulation effectively has a surface resistance (r_s) of zero. E_{pt} and E_{ma} have similar average values and temporal patterns, each being less than E_p. The temperature-based E_{th} bears the least resemblance to any other formulation, both in terms of the seasonal range and the temporal pattern in values.

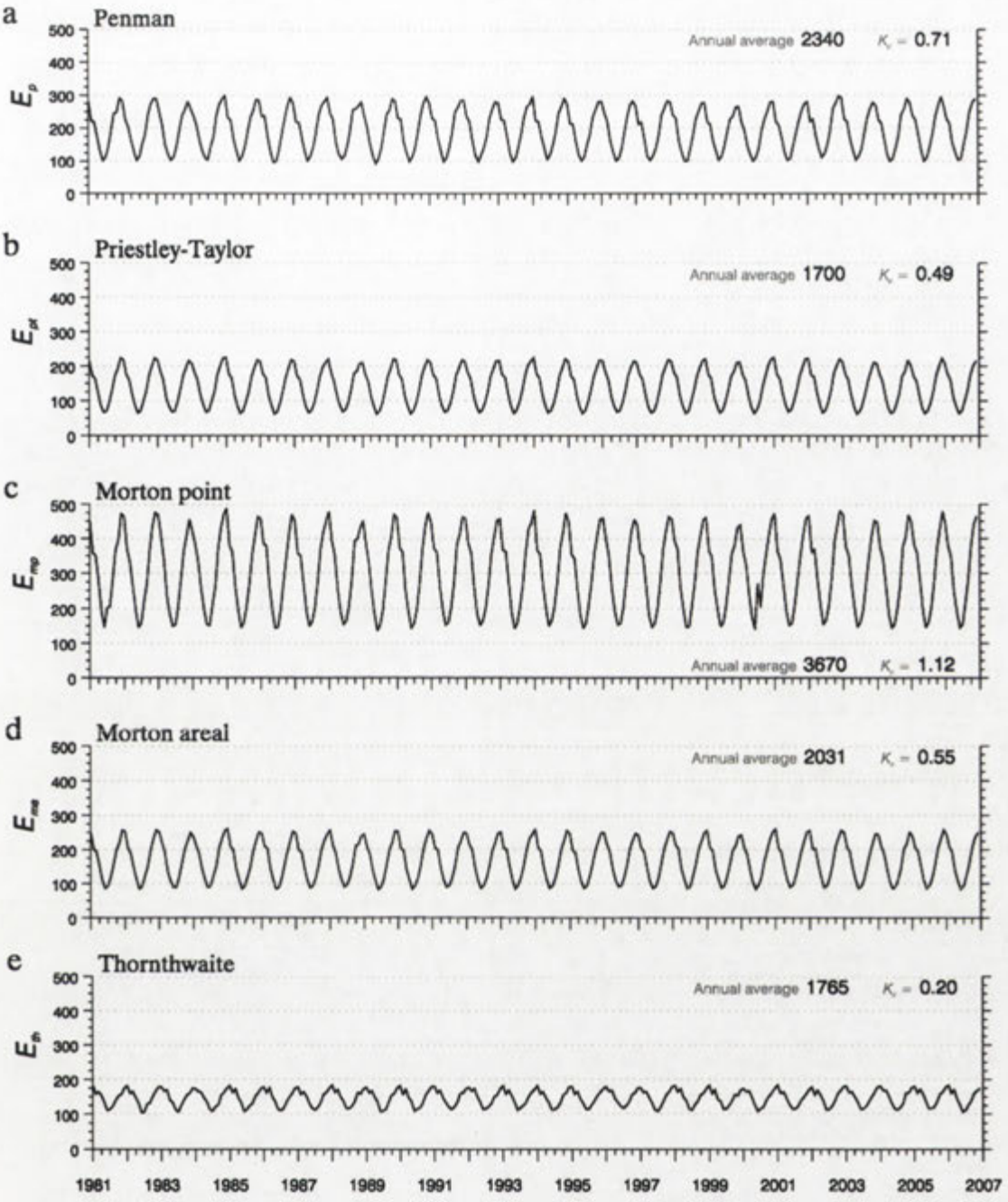

Figure 4. Australian-average monthly potential evaporation estimated using five formulations of potential evaporation. Ordinate units are mm.mth^{-1}. Annual averages are in mm.yr^{-1}. Australian average pan coefficients (K_p; e.g., E_p/E_{pan}) are also shown. These have been derived using E_{pan} observations at the 102 stations.

5.4.4 Analysis of trends

The Australia-wide trends in the inputs to the radiation modelling, as well as the modelled radiation components themselves, are shown in Table 3. Each component of the radiation balance has increased over the study period, with similar magnitude trends being experienced for both the two incoming components and for both the two outgoing components. As the combined trend in outgoing radiation is greater than that of

incoming radiation (almost 1.5 times greater), net radiation has decreased overall (down approximately 1% over the 26-year period). Differentiation of the outgoing short wave irradiance equation (see Donohue et al. (2009b)) indicates that 90% of the increase in R_{so} is due to the increase in α. If α was held constant in the modelling, the change in R_{so} would have been 0.01 $W.m^{-2}.yr^{-1}$ and R_n would have *increased* by an average of 0.028 $W.m^{-2}.yr^{-1}$. This result demonstrates the importance of understanding the role that even subtle changes in albedo can play in dynamics in the surface energy balance.

Table 3. Australian-average annual trends (1981–2006) in the variables used to calculate net radiation and the trends in the radiation components. Here the trend in R_n is calculated as the sum of the trends in incoming radiation minus the sum of those in outgoing radiation. P-values are determined using a two-sided Kendall tau test (Kendall and Gibbons, 1990) performed on Australian-average annual values.

Attribute	Trend		Standard error of trend		P-value
Albedo (α)	0.00037	yr^{-1}	0.0002		0.34
Minimum temperature (T_n)	0.007	$K.yr^{-1}$	0.01	K	0.98
Maximum temperature (T_x)	0.024	$K.yr^{-1}$	0.01	K	0.30
Air temperature (T_a)	0.016	$K.yr^{-1}$	0.01	K	0.47
Diurnal temperature range (T_r)	0.017	$K.yr^{-1}$	0.01	K	0.58
Actual vapour pressure (e_a)	0.88	$Pa.yr^{-1}$	1.4	Pa	0.30
Saturated vapour pressure (e_s)	3.08	$Pa.yr^{-1}$	1.7	Pa	0.55
Incoming shortwave (R_{si})	0.068	$W.m^{-2}.yr^{-1}$	0.07	$W.m^{-2}$	0.91
Incoming longwave (R_{li})	0.073	$W.m^{-2}.yr^{-1}$	0.06	$W.m^{-2}$	0.44
Outgoing shortwave (R_{so})	0.100	$W.m^{-2}.yr^{-1}$	0.05	$W.m^{-2}$	0.49
Outgoing longwave (R_{lo})	0.103	$W.m^{-2}.yr^{-1}$	0.04	$W.m^{-2}$	0.23
Net radiation (R_n)	-0.062	$W.m^{-2}.yr^{-1}$	0.05	$W.m^{-2}$	0.32

Annual Australia-average trends in potential evaporation (Table 4) show that E_{th} and E_{mp} have increased over the study period, E_{ma} has changed little and the trends for the remaining formulations have decreased over time. Despite the large error bounds of these trend estimates, the seemingly small changes in rates of potential evaporation can have important implications on the water balance in energy-limited catchments and in the more humid water-limited catchments (which are where the majority Australia's water supplies originate) over several decades. For comparison, the annual Australia-average (1981–2006) trends in P and E_{pp} are 1.3 and 0.0 $mm.yr^{-2}$, respectively (Table 4).

Table 4. Australian-average annual trends in potential evaporation (1981–2006). The equivalent trends in precipitation and Penpan evaporation are shown for reference. P-values are determined using a two-sided Kendall tau test (Kendall and Gibbons, 1990) performed on Australian-average annual values.

Formulation	Trend ($mm.yr^{-2}$)	Standard error of trend ($mm.yr^{-1}$)	P-value
Thornthwaite potential (E_{th})	0.6	1.3	0.39
Morton point potential (E_{mp})	0.2	1.3	0.49
Morton areal potential (E_{ma})	0.0	0.5	0.37
Priestley-Taylor potential (E_{pt})	-0.3	0.6	0.24
Penman potential (E_p)	-0.8	1.2	0.15
Precipitation (P)	1.3	2.1	0.41
Penpan potential (E_{pp})	0.0	2.3	0.44

Trends in the variables used to calculate potential evaporation are presented in Figure 5. Across most of eastern Australia, and across the far north, R_n has decreased over the study period (Figure 5a). Conversely, throughout the western interior R_n has increased. In general, R_n has increased where α has decreased, which—in many areas—has occurred where P has increased, and vice versa (see Figure 6f). The incorporation of remotely sensed α has a marked effect on R_n, as it has produced a fine scale patterning within the R_n trends governed by observed changes in land-surface properties. The effects of T_a on potential evaporation are expressed through R_n, e_s and Δ. Overall, T_a has increased across the majority of Australia, especially in the central-east (Figure 5b), the annual Australia-average trend is 0.016 $K.yr^{-1}$ (Table 3). Actual vapour pressure has increased by about 1.7% overall, at a rate of 0.88 $Pa.yr^{-1}$ (Table 3). The largest increases in e_a have occurred in the central-west of the country (Figure 5c), a region which has also experienced some of the largest increases in P (see Figure 6f). The average trend in u_2 is -0.01 $m.s^{-1}.yr^{-1}$ (down 13% over 26 years).

a – Net radiation (R_n)

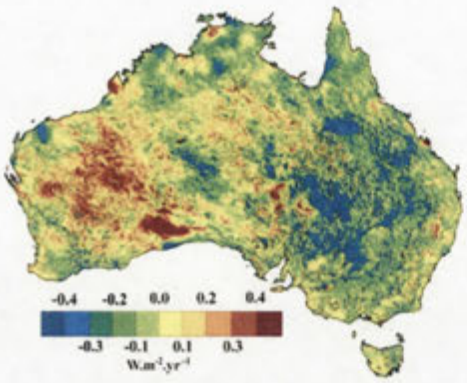

b – Mean air temperature (T_a)

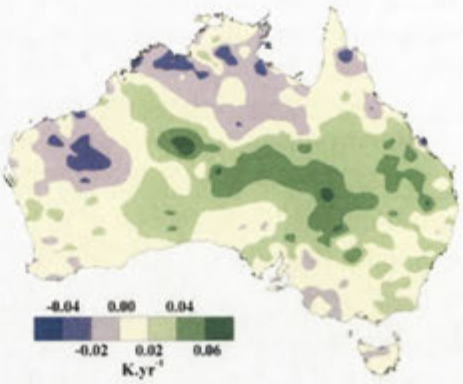

c – Actual vapour pressure (e_a)

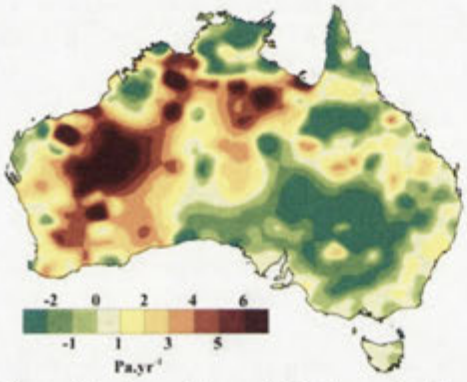

d – Wind speed (u_2)

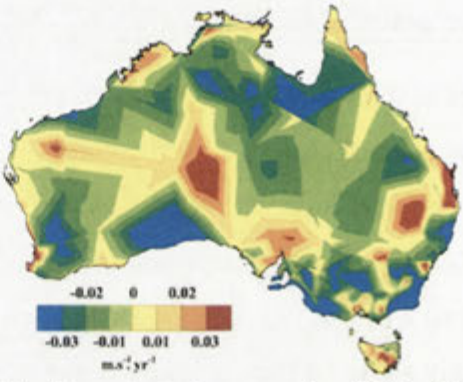

Figure 5. Annual trends in the variables used to calculate potential evaporation (1981–2006). (a) net radiation; (b) air temperature; (c) vapour pressure; and (d) wind speed.

Long-term trends in potential evaporation calculated using the five formulations can be seen in Figure 6a-e, with trends in P also being provided for context (Figure 6f). The spatial patterns in the trends of the Penman-based potential (Figure 6a) are dominated by changes in u_2, with decreases occurring across much of the north of Australia and increases in regions in the centre and the east (partially corresponding to where P has decreased). Morton point potential (Figure 6c) has a less distinct pattern and largely follows changes in R_n (and therefore in α). E_{mp} is also decreasing across the north, however this time it is primarily due to decreases in e_s. Patterns in E_{pt} and E_{ma} trends (Figure 6b and d) are very similar, generally following R_n trends, and the pattern in E_{th} trends (Figure 6e) are entirely a product of those in T_a.

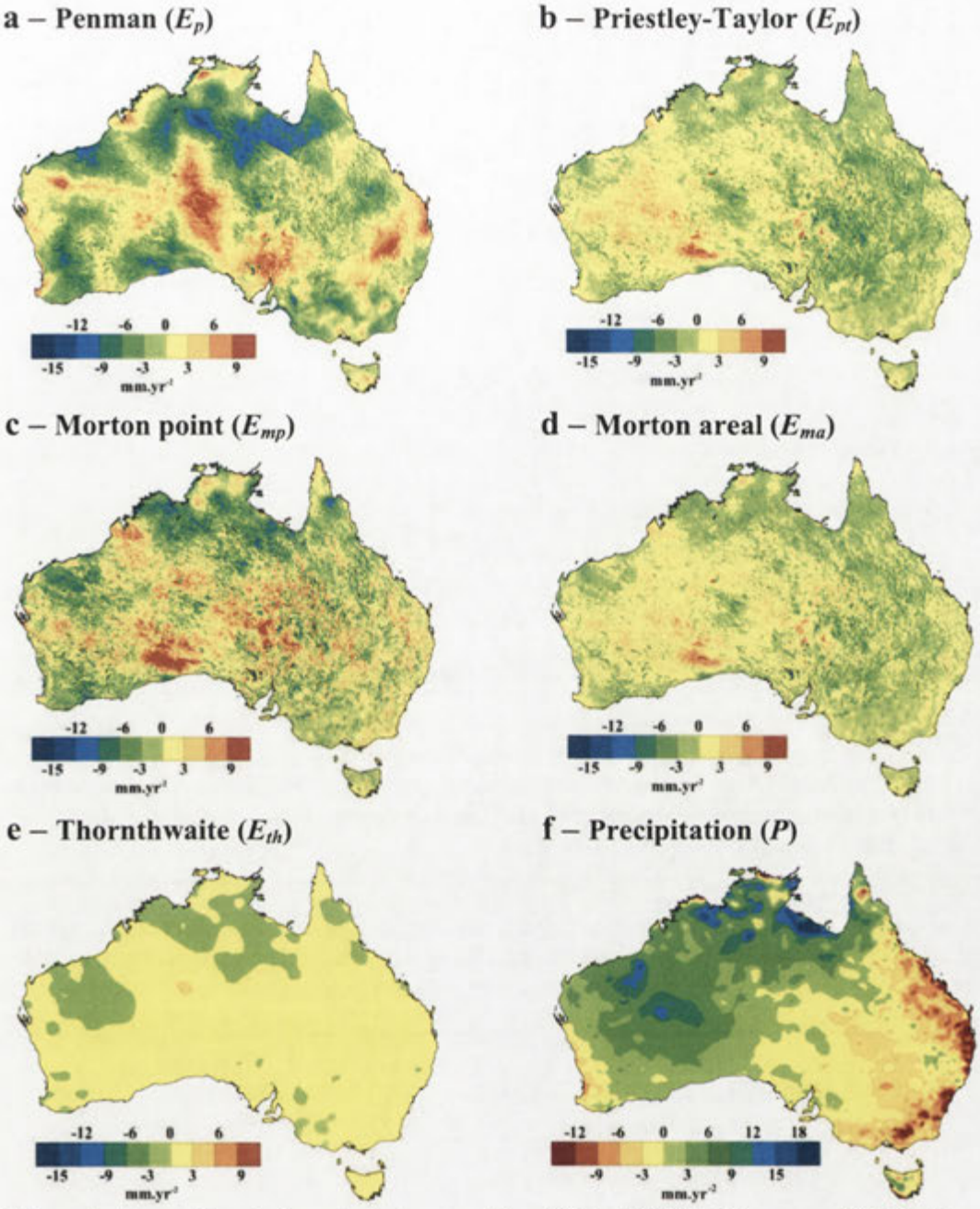

Figure 6. Annual trends in potential evaporation (1981–2006). (a) Penman; (b) Priestley-Taylor; (c) Morton point; (d) Morton areal; and (e) Thornthwaite formulations. Annual precipitation trends are also shown for reference (Donohue et al., 2009a)—note the reversed legend for precipitation.

Given that Australia is predominantly water-limited (Figure 1), and taking changes in P as a useful surrogate for changes in actual evaporation, we assess trends in potential evaporation as to whether they display an approximate complementary relation to trends in P. Figure 7 shows the per-month trends in potential evaporation and in P. In Figure 7a, two formulations (E_p and E_{mp}) have a distinct seasonal pattern with trends showing a sharp decrease in summer (DJF) and a slight increase in winter (JJA), and, for E_{mp}, large increases in spring (SON) values. Changes in E_{pt} and E_{ma} are similar and reasonably

uniform across all months (Figure 7a). Correlations between the per-month potential evaporation trends (Figure 7a) and the per-month P trends (Figure 7b) show a complementary relationship for the Penman formulation and, to a lesser extent, for E_{mp} (Table 5). Note that the seasonal pattern in P trends is present in the trends of Australian vegetation cover over the study period (Donohue et al., 2009a) and is mirrored by trends in α (Figure 7b). This seasonal assessment of complementarity provides a stronger test of the potential evaporation trends than does an assessment done purely on Australia-average annual trends.

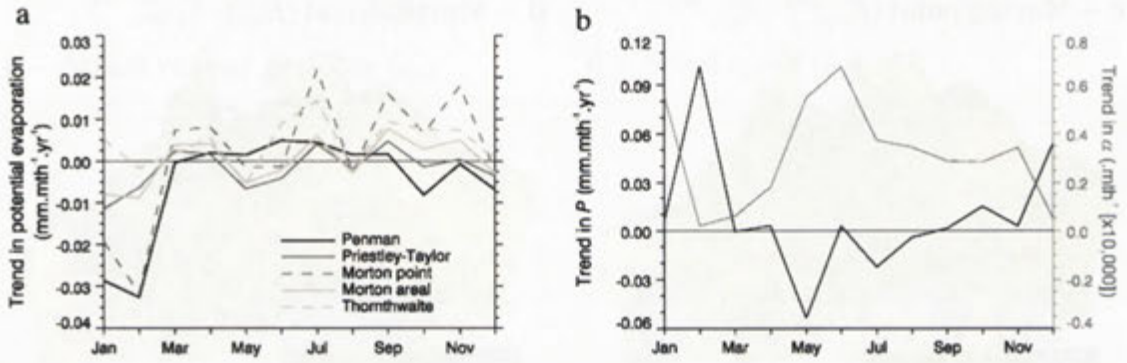

Figure 7. Monthly trends in Australia-wide potential evaporation (1981–2006). Plot (a) shows the monthly trends in potential evaporation and (b) the monthly trends in Australia-wide precipitation (black) and albedo (grey).

Table 5. Correlation between Australian-average per-month trends in precipitation and potential evaporation (1981–2006). P-values are determined using a two-sided Kendall tau test (Kendall and Gibbons, 1990) performed on Australian-average annual values; n = 12 in all cases.

Formulation	r	P-value
Penman potential (E_p)	-0.69	0.04
Priestley-Taylor potential (E_{pt})	-0.22	0.27
Morton point potential (E_{mp})	-0.60	0.13
Morton areal potential (E_{ma})	-0.37	0.22
Thornthwaite potential (E_{th})	-0.17	0.49

Figure 8 examines which formulations of potential have trends that are complementary with P trends at the 102 long-term pan evaporimeter locations across Australia. Only E_p and E_{mp} (Figure 8a and c) show a substantial negative relationship with changes in P (although each has a reasonable degree of scatter). E_{pt} and E_{ma} display little complementarity with P trends (Figure 8b and d) and E_{th} displays none at all (Figure 8e).

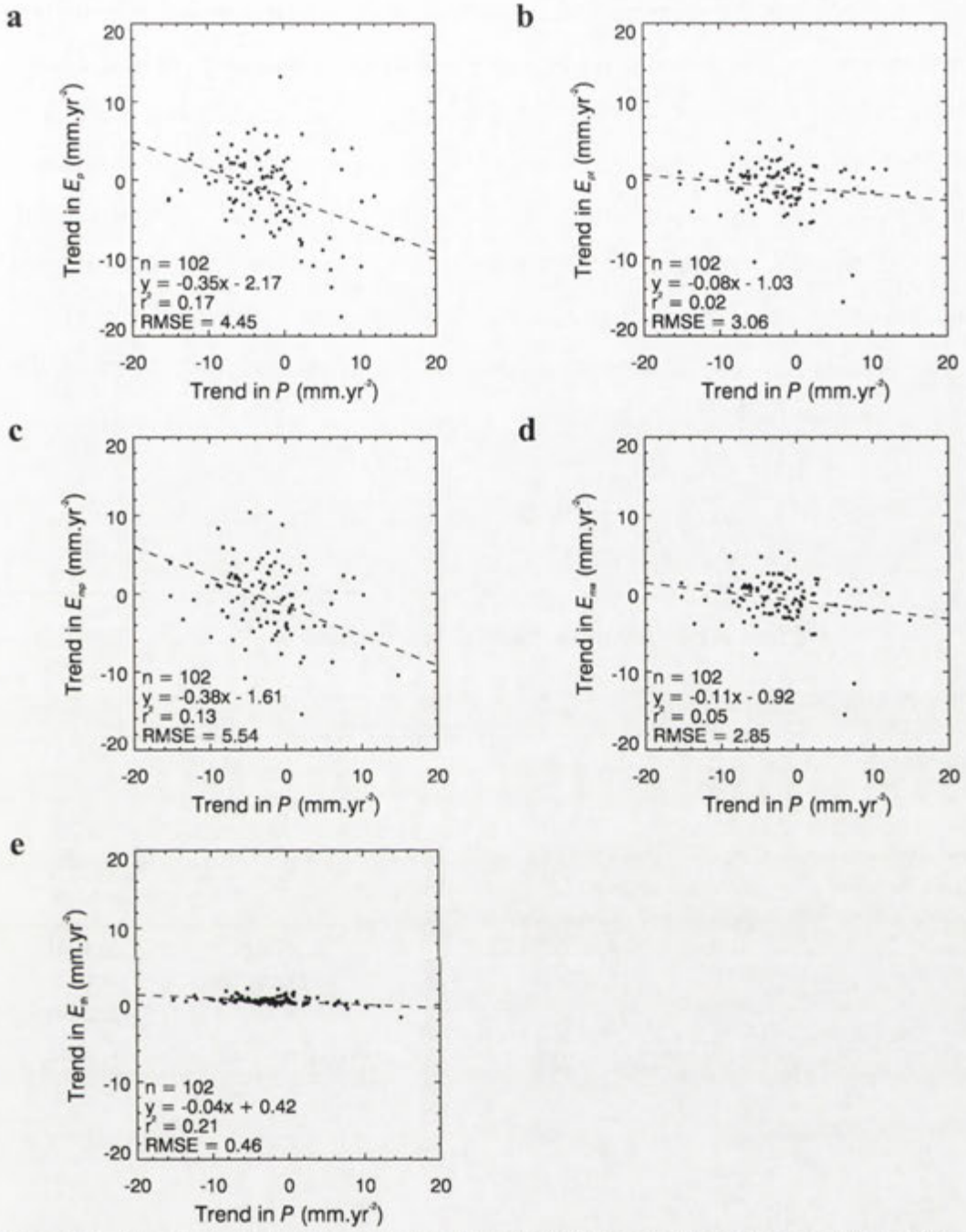

Figure 8. Comparison of annual trends of precipitation and potential evaporation (1981–2006) at the 102 stations. (a) Penman; (b) Priestley-Taylor; (c) Morton point; (d) Morton areal; and (e) Thornthwaite formulations of potential evaporation, respectively. The dashed line is the equation of best fit (given on each plot), n is the number of observations, the offset and RMSE statistics are in ordinate units.

5.4.5 Attribution of trends

The Australia-wide trend in Penman potential evaporation over 1981-2006 is -0.8 mm.yr^{-2} (see Table 4). Table 6 shows that the results of attributing the changes in E_p were, in order of magnitude, due to: (i) dT_a/dt (1.5 mm.yr^{-2}); (ii) du_2/dt (-1.3 mm.yr^{-2}); (iii) dR_n/dt (-0.6 mm.yr^{-2}); and (iv) de_a/dt (-0.4 mm.yr^{-2}). The spatial distributions of the

effects of each governing meteorological variable on dE_p/dt are shown in Figure 9. If u_2 was held constant (i.e., in the absence of available wind speed data), dE_p/dt would have been approximately 0.5 mm.yr^{-2}. Further, if both u_2 and α were held constant, dE_p/dt would have been around 1.0 mm.yr^{-2}. Albedo and wind speed have both substantially influenced potential evaporation trends and these results demonstrate the importance of treating these variables dynamically. Attribution of dE_p/dt on a per-month basis (Figure 10) indicates that the distinct seasonality in dE_p/dt is due to the combined effects of du_2/dt, de_a/dt, and dR_n/dt, as the monthly changes in dT_a/dt have had little impact on the monthly variability of dE_p/dt.

Table 6. Attribution of the changes in annual, Australia-wide Penman potential evaporation (1981–2006). All units are mm.yr^{-2}.

<table>
<tr><th colspan="6">Change in Penman potential evaporation $\frac{dE_p}{dt}$</th></tr>
<tr><td colspan="2">Radiative component $\frac{dE_{pR}}{dt}$</td><td colspan="4">Aerodynamic component $\frac{dE_{pA}}{dt}$</td></tr>
<tr><td rowspan="2">Saturation vapour pressure slope
$\frac{\partial E_{pR}}{\partial \Delta}\frac{d\Delta}{dT_a}\frac{dT_a}{dt}$</td><td rowspan="2">Net radiation
$\frac{\partial E_{pR}}{\partial R_n}\frac{dR_n}{dt}$</td><td rowspan="2">Saturation vapour pressure slope
$\frac{\partial E_{pA}}{\partial \Delta}\frac{d\Delta}{dT_a}\frac{dT_a}{dt}$</td><td rowspan="2">Wind speed
$\frac{\partial E_{pA}}{\partial u_2}\frac{du_2}{dt}$</td><td colspan="2">Vapour pressure deficit
$\frac{\partial E_{pA}}{\partial e_s}\frac{de_s}{dT_a}\frac{dT_a}{dt} - \frac{\partial E_{pA}}{\partial e_a}\frac{de_a}{dt}$</td></tr>
<tr><td>Saturated vapour pressure
$\frac{\partial E_{pA}}{\partial e_s}\frac{de_s}{dT_a}\frac{dT_a}{dt}$</td><td>Actual vapour pressure
$\frac{\partial E_{pA}}{\partial e_a}\frac{de_a}{dt}$</td></tr>
<tr><td rowspan="2">0.4</td><td rowspan="2">-0.6</td><td rowspan="2">-0.7</td><td rowspan="2">-1.3</td><td>1.8</td><td>-0.4</td></tr>
<tr><td colspan="2">1.4</td></tr>
<tr><td colspan="2">-0.2</td><td colspan="4">-0.6</td></tr>
<tr><td colspan="6">-0.8</td></tr>
</table>

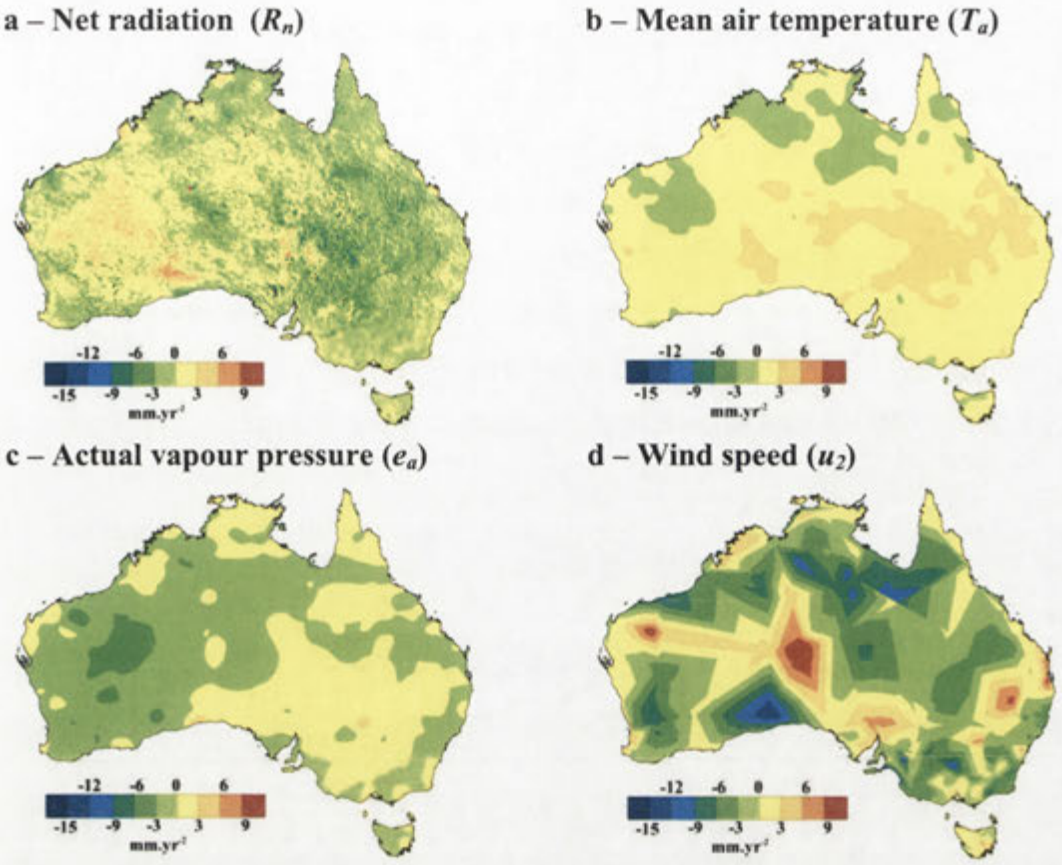

Figure 9. Attribution of the changes in Penman potential evaporation (1981–2006). (a) net radiation; (b) air temperature; (c) vapour pressure; and (d) wind speed.

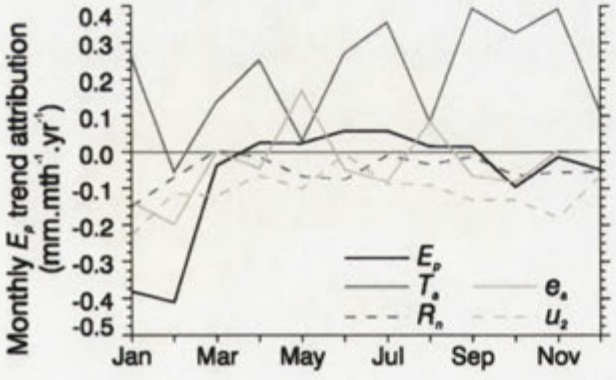

Figure 10. Attribution of the Australia-wide, monthly trends in Penman potential evaporation (1981–2006).

The Australia-wide Priestley-Taylor potential evaporation trend over 1981-2006 is -0.3 mm.yr^{-2} (see Table 4). Table 7 shows that changes in R_n account for -0.8 mm.yr^{-2} of the overall change, whilst dT_a/dt accounts for 0.5 mm.yr^{-2}. The spatial distributions of $\delta E_{pt}/\delta T_a \cdot dT_a/dt$ and $\delta E_{pt}/\delta R_n \cdot dR_n/dt$ are shown in Figure 11. The seasonal patterns in dE_{pt}/dt are indistinct (Figure 12) compared to those in dE_p/dt (Figure 10), but are most influenced by dR_n/dt. Given that 90% of the trend in R_{so} is due to changes in α, if the formulation of R_n assumed α was constant, then dE_{pt}/dt would be have been positive (~0.4 mm.yr^{-2}) and the spatial and monthly patterns would resemble those of the temperature-based potential evaporation formulation of Thornthwaite.

Table 7. Attribution of the changes in Australia-wide Priestley-Taylor potential evaporation (1981–2006) due to changes in Δ and net radiation. All units are mm.yr^{-2}.

Change in Priestley-Taylor potential evaporation $\frac{dE_{pt}}{dt}$	
Temperature $\frac{\partial E_{pt}}{\partial \Delta}\frac{d\Delta}{dT_a}\frac{dT_a}{dt}$	Net radiation $\frac{\partial E_{pt}}{\partial R_n}\frac{dR_n}{dt}$
0.5	-0.8
-0.3	

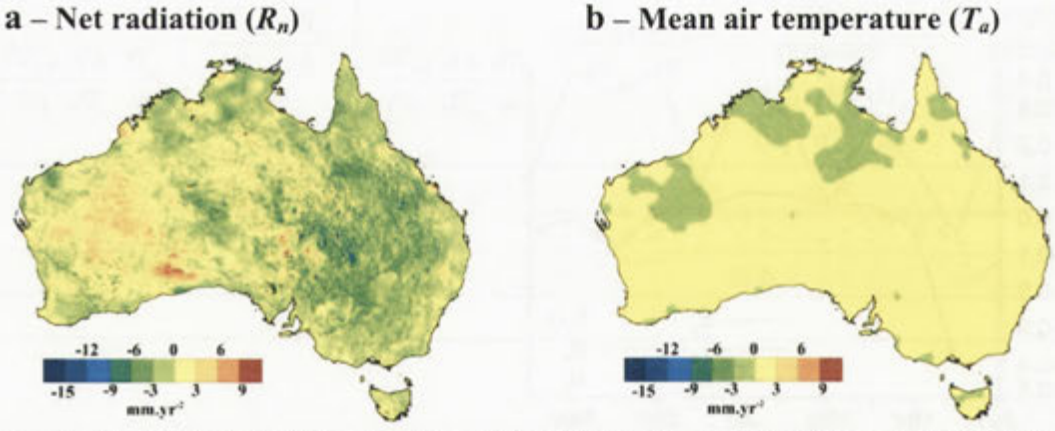

Figure 11. Attribution of the annual trends in Priestley-Taylor potential evaporation (1981–2006). (a) net radiation; and (b) air temperature.

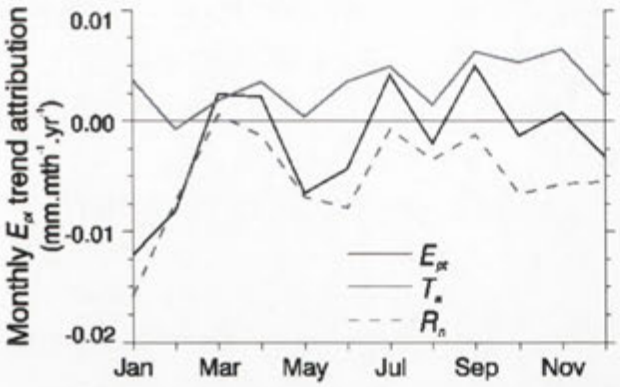

Figure 12. Attribution of the Australia-wide, monthly trends in Priestley-Taylor potential evaporation from 1981–2006.

5.5 Discussion

5.5.1 The availability and quality of appropriate input data

A critical requirement of being able to examine dynamics in evaporative demand, regardless of which formulation is used, is the availability of data describing all the relevant input variables. Recently Roderick et al. (2007) and McVicar et al. (2008) demonstrated that wind speed across Australia has been declining over the past three decades, and that this decline has been the main cause of the observed declines in pan evaporation (Roderick et al., 2007; Rayner, 2007). Donohue et al. (2009a) have found that, on average, Australian vegetation cover has been increasing since the early 1980s. The recent development and release of spatio-temporal u_2 and α data for Australia has been critical to the work presented here, which (to the best of our knowledge) is the first time the effect of observed spatial and temporal dynamics in these two variables on a number of potential evaporation formulations has been reported. Similar studies have been conducted, such as that of Xu et al. (2006), however these authors examined the temporal dynamics in FAO56 crop reference evaporation (Allen et al., 1998), in which α was treated as a constant.

The calculated trends in e_a and e_s need to be interpreted carefully as both have been calculated from measurements made at different times during the day. Trends in e_a are trends in 9am (local time) vapour pressure, not in daily integrals of vapour pressure. e_s has been calculated using daily T_x and T_n, the times of which are unknown and will differ from day-to-day (McVicar and Jupp, 1999). This means that e_a and e_s are not

concurrent measurements and consequently the effects of changes in the diurnal cycle of T_a and/or e_a may not necessarily be reflected in the calculated trends in D or e_s.

5.5.2 Difficulties in parameterising surface conditions in potential evaporation formulations

Conceptually, potential evaporation is the evaporation rate that occurs from a location where energy is the dominant limit to evaporation. This is widely interpreted as being the evaporation that would occur from a large, saturated surface. Technically, this should mean the surface is parameterised as actually being saturated (e.g., Shuttleworth, 1993), meaning $\alpha \leq 0.1$ (Oke, 1987). However, here we parameterised the surface with actual α values instead (McVicar et al., 2007), as enforcing a hypothetical saturated-surface α: (i) divorces the surface from the meteorological measurements made above the surface under non-saturated conditions; (ii) removes both temporal and spatial dynamics in surface conditions which is counter-intuitive when examining surface energy dynamics, and (iii) enables observed changes in energy availability (i.e., R_n) to be incorporated into estimates of potential evaporation. Thus, our concept of potential evaporation does not enforce an actual saturated surface; it estimates evaporation from a surface *as if* most of the energy absorbed at that surface was to be converted into latent heat under the extant surface and aerodynamic conditions.

The addition of measured α in the calculation of R_n is an important component of the net radiation model presented here. Australian-average α increased by approximately 6% over the past 26 years. On a per-pixel basis both increases and decreases in α have been observed. Previously Donohue et al. (2009a) found that vegetation cover across Australia changed considerably over the same period, generally increasing but with positive and negative trends across large areas of Australia. While the link between trends in α and vegetation cover are not straightforward (it is complicated by soil colour variations), it is reasonable that α has been, and is, changing. Although the magnitude of changes in R_n formulated with, and without, a dynamic α varies moderately (-0.062 versus 0.028 $W.m^{-2}.yr^{-1}$), the spatial and seasonal patterns introduced by measured α are important characteristics in a dynamic R_n model.

5.5.3 Findings and recommendations

The expectation in undertaking this research was that the fully physical formulations of potential evaporation, calculated using spatially and temporally dynamic input data, would yield the most realistic estimates of changes in potential evaporation. The results generally support this premise, as the greater the number of the four key variables used within a formulation, the more realistic the trends from that formulation became. E_p, which includes dynamic estimates of T_a, R_n, e_a, and u_2, has the most realistic temporal dynamics as it showed the greatest degree of complementarity with actual evaporation trends (as represented by dP/dt) when considering: (i) Australia-wide annual average trends (Table 4); (ii) spatial trends (Figure 6); (iii) seasonal trends (Figure 7); and (iv) trends at selected long-term meteorological stations (Figure 8). The E_p attribution analysis showed that, even though T_a and u_2 were the biggest contributors to the overall E_p trends (having similar but opposite magnitudes), it was R_n (due to $d\alpha/dt$), e_a, and u_2 that produced the seasonal complementarity in trends.

Morton point potential is a radiation-vapour pressure-temperature-based formulation—it does not explicitly include u_2 as a variable. Its rates of potential are extremely high (see Figure 4), over-estimating potential by up to one quarter of what seems reasonable (assuming potential evaporation rates should be no higher than E_{pan}). Despite this, E_{mp} still displays similar patterns in trends in potential as does the Penman model. Why the Morton point formulation captures trends but not actual values is unclear and, because of this, should be avoided as a means of estimating potential evaporation generally.

The radiation-temperature-based Priestley-Taylor formulation displays very weak complementarity with trends in actual evaporation (i.e., dP/dt) both spatially (Figure 6) and seasonally (Figure 7 and Table 5). The monthly pattern in E_{pt} trends (Figure 12) is mainly caused by dR_n/dt, which itself is primarily a product of $d\alpha/dt$. If E_{pt} was formulated with a static α, it would effectively mimic a temperature-based formulation under the climatic conditions of this study. However, considering the approximate similarity in modelled values between E_{pt} and E_p, for the application considered here E_{pt} is probably the optimal formulation for estimating *rates* in the absence of either e_a or u_2 data; it should not be used for examining *trends* in water-limited environments, however. The temperature-based Thornthwaite estimates of potential did not produce realistic values in either rates or trends of potential evaporation, and should not be used (Hobbins et al., 2008).

Overall our results indicate that the more variables that are held constant when estimating potential evaporation, the less realistic the results become. This concurs with previous findings globally (e.g., Chen et al., 2005; McKenney and Rosenberg, 1993; Shenbin et al., 2006; Garcia et al., 2004). We argue that Penman-based potential formulations should be the preferred means of examining long-term dynamics in potential evaporation.

This assessment of potential evaporation dynamics has been done only with respect to the inherent characteristics of the potential evaporation data itself. No analysis has been performed of the effects of the potential evaporation on the long-term dynamics of actual evaporation. The choice of which formulation to use and how it is parameterised can be crucial, for example: (i) in energy-limited catchments where actual evaporation is mainly determined by potential evaporation; (ii) in catchments that seasonally switch between energy- and water-limited states where actual evaporation follows potential for parts of the year (such catchments are important in Australia as these yield the majority of Australia's water supplies); or (iii) when actual evaporation is calculated as a fraction of potential regardless of the climate type (e.g., Guerschman et al., 2009; McVicar and Jupp, 2002).

The work presented here emphasises the fact that increases in mean air temperature over the past few decades does not necessarily mean that potential evaporation rates have also increased. Consideration of all the factors driving potential evaporation is critical, and will continue to be so as climate change continues. An important implication of this is that, to predict future potential evaporation rates, Generalised Circulation Models need the capacity to predict the dynamics in all the relevant variables with reasonable accuracy (Johnson and Sharma, 2009), including those in wind speed and albedo.

5.6 Summary and Conclusions

Evaporative demand is driven by four variables—net radiation, vapour pressure, wind speed, and air temperature. Analyses of long-term dynamics in potential evaporation, therefore, should ideally use a fully dynamic formulation where the effects of the variability in each of the driving variables are accounted for. Two key inputs used in the generation of potential evaporation data reported here are spatially and temporally

dynamic representations of albedo (allowing for a fully dynamic representation of net radiation) and wind speed. In Australia changes in wind speed and albedo have been observed since the early 1980s. The availability of these two datasets allowed the contribution of each of these variables on trends in potential evaporation to be quantified. We show that both these variables play important roles in evaporative demand dynamics.

We generated five daily potential evaporation datasets using the: (i) Penman; (ii) Priestley-Taylor; (ii) Morton point; (iv) Morton areal; and (v) Thornthwaite potential evaporation formulations. These models contain successively fewer input variables as one moves through the above list. Spatial, annual, and seasonal trends in each were assessed in terms of whether they displayed approximate complementary characteristics with trends in actual evaporation (using precipitation as a proxy for actual evaporation). We also examined the contribution that trends in each input variable made to the overall trends in a fully physical formulation (Penman) and in a radiation-based formulation (Priestley-Taylor) of potential evaporation. Attribution of the Penman formulation showed that the complementary nature of trends in Penman potential were due to the dynamics in radiation (and particularly albedo), vapour pressure and wind speed.

From first principles, fully physical formulations, such as Penman, are expected to best capture trends in potential evaporation, and our results confirmed this. Only the Penman formulation displayed realistic values of *both* potential evaporation rates *and* trends for the conditions tested, and this should be the model of choice when all input data are available. The trends in Morton point potential, a formulation which uses all variables except wind speed, were similar to those in the Penman model. However, its estimated rates of potential were unrealistically high—consequently, its use is not recommended. Both Priestly-Taylor and Morton areal formulations produced similar rates of potential, which were approximately similar to those from the Penman model. This, along with the simplicity of the Priestley-Taylor formulation, presents a strong argument for Priestley-Taylor being the best means of estimating potential evaporation *rates* when wind speed data are absent. Neither Priestley-Taylor nor Morton areal should be used to assess temporal dynamics. Finally, the Thornthwaite potential evaporation formulation, which contains only one input variable, was shown to be unsuitable for use.

5.7 Acknowledgements

We would like to thank David McJannet, Tom Van Niel and two anonymous reviewers for helpful comments that improved the manuscript. We are grateful to Michael Hutchinson of the Australian National University and to David Jones and Andrew Frost, both of the Bureau of Meteorology, for useful discussions on the accuracy of spline-interpolated data.

5.8 References

Allen RG, Pereira LS, Raes D and Smith M (1998) Crop evapotranspiration: guidelines for computing crop water requirements. FAO Irrigation and Drainage Paper 56. Food and Agriculture Organisation of the United Nations, Rome.

Bristow KL and Campbell GS (1984) On the relationship between incoming solar-radiation and daily maximum and minimum temperature. Agricultural and Forest Meteorology 31, 159-166.

Budyko MI (1974) Climate and life. edition. Academic, New York, 508 pp.

Bureau of Meteorology (2006) Climate Data: Australia CD-ROM, Version 2.2 December 2006. Australian Government Bureau of Meteorology

Chen D, Gao G, Xu CY, Guo J and Ren G (2005) Comparison of the Thornthwaite method and pan data with the standard Penman-Monteith estimates of reference evapotranspiration in China. Climate Research 28, 123-132.

Donohue RJ, McVicar TR and Roderick ML (2009a) Climate-related trends in Australian vegetation cover as inferred from satellite observations, 1981–2006. Global Change Biology 15, 1025-1039. DOI: 10.1111/j.1365-2486.2008.01746.x

Donohue RJ, McVicar TR and Roderick ML (2009b) Generating Australian potential evaporation data suitable for assessing the dynamics in evaporative demand within a changing climate. CSIRO: Water for a Healthy Country National Research Flagship, Canberra. Available at < http://www.clw.csiro.au/publications/waterforahealthycountry/2009/wfhc-evaporative-demand-dynamics.pdf >

Donohue RJ, Roderick ML and McVicar TR (2007) Correcting long-term AVHRR reflectance data using the vegetation cover triangle. CSIRO Land and Water Science Report 26/07. CSIRO Land and Water, Canberra, 73 pp. Available at < http://www.clw.csiro.au/publications/science/2007/sr26-07.pdf >

Donohue RJ, Roderick ML and McVicar TR (2008) Deriving consistent long-term vegetation information from AVHRR reflectance data using a cover-triangle-based framework. Remote Sensing of Environment 112, 2938-2949 DOI:10.1016/j.rse.2008.02.008.

Durre I, Williams Jr CN, Yin X and Vose RS (2009) Radiosonde-based trends in precipitable water over the Northern Hemisphere: An update. Journal of Geophysical Research - Atmospheres 114. D05112, doi:10.1029/2008JD010989.

Garcia M, Raes D, Allen R and Herbas C (2004) Dynamics of reference evapotranspiration in the Bolivian highlands (Altiplano). Agricultural and Forest Meteorology 125, 67-82.

Geoscience Australia (2007) GEODATA 9 Second Digital Elevation Model (DEM-9S) Version 2 Accessed May, 2008. Available at < http://www.ga.gov.au/meta/ANZCW0703005624.html >

Granger RJ (1989) An examination of the concept of potential evaporation. Journal of Hydrology 111, 9-19.

Guerschman JP, Van Dijk A, Mattersdorf G, Beringer J, Hutley LB, Leuning R, Pipunic RC and Sherman BS (2009) Scaling of potential evapotranspiration with MODIS data reproduces flux observations and catchment water balance observations across Australia. Journal of Hydrology 369, 107-119. DOI: 10.1016/j.jhydrol.2009.02.013

Hobbins MT, Dai AG, Roderick ML and Farquhar GD (2008) Revisiting the parameterization of potential evaporation as a driver of long-term water balance trends. Geophysical Research Letters 35, L12403. DOI: 10.1029/2008GL033840

IPCC (2007) Summary for Policymakers. In: Climate change 2007: the physical science basis. Contribution of Working Group I to the Fourth Assessment Report of the Intergovernmental Panel on Climate Change (eds Solomon S, *et al.*). Cambridge University Press, Cambridge.

Iqbal M (1983) An Introduction to Solar Radiation. edition. Academic Press, Ontario, 390 pp.

Johnson F and Sharma A (2009) Measurement of GCM skill in predicting variables relevant for hydroclimatological assessments. Journal of Climate In Press. DOI: 10.1175/2009JCLI2681.1.

Jones D, Wang W, Fawcett R and Grant I (2006) The generation and delivery of level-1 historical climate data sets. Australian Water Availability Project. Final Report. Australian Government Bureau of Meteorology.

Jones DA, Wang W and Fawcett R (2009) High-quality Spatial Climate Data Sets for Australia. Australian Meteorological and Oceanographic Journal In press.

Kendall M and Gibbons JD (1990) Rank correlation methods. 5th edition. Oxford University Press, Oxford.

Lhomme JP (1999) Towards a rational definition of potential evaporation. Hydrology and Earth System Sciences 1, 257-264.

Linacre ET (1994) Estimating U.S. Class A pan evaporation from few climate data. Water International 19, 5-14.

Linacre ET (2004) Evaporation trends. Theoretical and Applied Climatology 79, 11-21.

McIllroy IC and Angus DE (1964) Grass, water and soil evaporation at Aspendale. Agricultural Meteorology 1, 201-224.

McKenney MS and Rosenberg NJ (1993) Sensitivity of some potential evapotranspiration estimation methods to climate change. Agricultural and Forest Meteorology 64, 81-110.

McVicar TR and Jupp DLB (1999) Estimating one-time-of-day meteorological data from standard daily data as inputs to thermal remote sensing based energy balance models. Agricultural and Forest Meteorology 96, 219-238.

McVicar TR and Jupp DLB (2002) Using covariates to spatially interpolate moisture availability in the Murray-Darling Basin - A novel use of remotely sensed data. Remote Sensing of Environment 79, 199-212.

McVicar TR, Van Niel TG, Li LT, Hutchinson MF, Mu XM and Liu ZH (2007) Spatially distributing monthly reference evapotranspiration and pan evaporation considering topographic influences. Journal of Hydrology 338, 196-220.

McVicar TR, Van Niel TG, Li LT, Roderick ML, Rayner DP, Ricciardulli L and Donohue RJ (2008) Wind speed climatology and trends for Australia, 1975-2006: capturing the stilling phenomenon and comparison with near-surface reanalysis output. Geophysical Research Letters 35, L20403. DOI:10.1029/2008GL035627.

Monteith JL (1981) Evaporation and surface temperature. Quarterly Journal of the Royal Meteorological Society 107, 1-27.

Morton FI (1983) Operational estimates of areal evapo-transpiration and their significance to the science and practice of hydrology. Journal of Hydrology 66, 1-76.

New M, Todd M, Hulme M and Jones P (2001) Precipitation measurements and trends in the twentieth century. International Journal of Climatology 21.

Oke TR (1987) Boundary layer climates. Second edition. Routledge, London.

Penman HL (1948) Natural evaporation from open water, bare soil and grass. Proceedings of the Royal Society of London A 193, 120-145.

Priestley CHB and Taylor RJ (1972) On the assessment of surface heat flux and evaporation using large-scale parameters. Monthly Weather Review 100, 81-92.

Rayner DP (2007) Wind run changes: the dominant factor affecting pan evaporation trends in Australia. Journal of Climate 20, 3379-3394.

Roderick ML (1999) Estimating the diffuse component from daily and monthly measurements of global radiation. Agricultural and Forest Meteorology 95, 169-185.

Roderick ML and Farquhar G (2006) A physical analysis of changes in Australian pan evaporation. Land & Water Australia Project No. ANU49. CRC for Greenhouse Accounting, Research School of Biological Sciences, The Australian National University, Canberra.

Roderick ML, Rotstayn LD, Farquhar GD and Hobbins MT (2007) On the attribution of changing pan evaporation. Geophysical Research Letters 34, L17403, doi:17410.11029/12007GL031166.

Rotstayn LD, Roderick ML and Farquhar GD (2006) A simple pan-evaporation model for analysis of climate simulations: evaluation over Australia. Geophysical Research Letters 33, L17715, doi:17710.11029/12006GL027114.

Saunders RW (1990) The determination of broad-band surface albedo from AVHRR visible and near-infrared radiances. International Journal of Remote Sensing 11, 49-67.

Shenbin C, Yunfeng L and Thomas A (2006) Climatic change on the Tibetan Plateau: potential evapotranspiration trends from 1961–2000. Climatic Change 76, 291-319. DOI: 10.1007/s10584-006-9080-z.

Shuttleworth WJ (1993) Evaporation. In: Handbook of Hydrology (ed Maidment DR). McGraw-Hill, Sydney.

Shuttleworth WJ, Serrat-Capdevila A, Roderick ML and Scott RL (2009) On the theory relating changes in area-average and pan evaporation. Quarterly Journal of the Royal Meteorological Society 135, 1230-1247. DOI:10.1002/qj.434

Singh VP and Xu CY (1997) Evaluation and generalization of 13 mass-transfer equations for determining free water evaporation. Hydrological Processes 11, 311-323.

Stanhill G (2002) Is the Class A evaporation pan still the most practical and accurate meteorological method for determining irrigation water requirements? Agricultural and Forest Meteorology 112, 233-236.

Thornthwaite CW (1948) An approach toward a rational classification of climate. Geographical Review 38, 55-94.

Wild M (2009) Global dimming and brightening: A review. Journal of Geophysical Research - Atmospheres 114. D00D16, doi:10.1029/2008JD011470.

Xu CY, Gong LB, Jiang T, Chen DL and Singh VP (2006) Analysis of spatial distribution and temporal trend of reference evapotranspiration and pan evaporation in Changjiang (Yangtze River) catchment. Journal of Hydrology 327, 81-93.

Xu CY and Singh VP (2000) Evaluation and generalization of radiation-based methods for calculating evaporation. Hydrological Processes 14, 339-349.

Xu CY and Singh VP (2001) Evaluation and generalization of temperature-based methods for calculating evaporation. Hydrological Processes 15, 305-319.

Yang DW, Sun FB, Liu ZT, Cong ZT and Lei ZD (2006) Interpreting the complementary relationship in non-humid environments based on the Budyko and Penman hypotheses. Geophysical Research Letters 33, L18402, doi:18410.11029/12006GL027657.

CHAPTER 6

Can dynamic vegetation information improve the accuracy of Budyko's hydrological model?

Can dynamic vegetation information improve the accuracy of Budyko's hydrological model?

Donohue, R.J.[1,2*], Roderick, M.L.[2,3], and McVicar, T.R.[1]

[1]CSIRO Land and Water

[2]Research School of Biological Sciences, the Australian National University

[3]Research School of Earth Sciences, the Australian National University

* Corresponding Author:

E: randall.donohue@csiro.au

P: 61-2-6246-5803

Submitted to: Journal of Hydrology

Submission date: 20 November 2009

Key words: scale; fPAR; annual; perennial; evergreen; ecohydrology, stream flow.

6.1 ABSTRACT

This study examines whether the incorporation of dynamic, remotely sensed vegetation information into Budyko's hydrological model can improve that model's accuracy, particularly at finer spatial and temporal scales. Using numerous variables derived from three primary time-series variables (precipitation, potential evaporation and remotely sensed estimates of vegetation cover), linear 1-parameter models are developed to explain the variability in stream flow predictions not already captured by the Budyko model (the 'scatter'). Analyses are applied to 221 catchments across Australia and cover the period 1981 to 2006. At the annual average temporal scale, results show that vegetation-related variables are not the primary determinants of scatter at coarse spatial scales (i.e. continental), and that little improvement could be made on the original Budyko model. However, at medium spatial scales vegetation-related variables dominate models—most notably variables relating to dynamics in the cover of annual vegetation—reducing prediction error to 31% of average stream flow from the 42% error achieved using the original Budyko model. By contrast, at the annual time-scale the most important variables for explaining scatter relate to precipitation dynamics regardless of spatial scale. This is interpreted as the influence of non-steady-state conditions at this finer time-scale. Overall, vegetation information is shown to improve the accuracy of long-term annual average stream flow predictions as spatial scale decreases and that, at annual scales, the presence of non-steady-state conditions prohibits the exploration of the hydrological role of vegetation dynamics regardless of spatial scales of analysis.

6.2 INTRODUCTION

Numerous relationships have been developed that link long-term catchment average actual evaporation with long-term precipitation and potential evaporation, some of which have been in use for over a century. Building on the work of Schreiber (1904) and Ol'dekop (1911), Mikhail Budyko produced the most enduring and widely used frameworks for examining the catchment energy and water fluxes (Budyko, 1974). The long-term annual catchment average water balance can be defined as ($mm.yr^{-1}$)

$$P - Q - E_a = \Delta S_w \tag{1}$$

where P is precipitation, E_a is actual evaporation (which, by definition, includes transpiration) and Q is stream flow (all these are long-term averages and are in $mm.yr^{-1}$). ΔS_w (mm) is the change in stored water (i.e. soil and ground water stores). An equivalent formulation, but one that makes explicit the spatial and temporal scales of analyses, is (Donohue et al., 2007):

$$\frac{\overline{P} - \overline{E_a} - \overline{Q}}{\rho_w A} = \frac{1}{\rho_w}\left([S_w]\frac{\Delta z}{\tau} + z\frac{\Delta [S_w]}{\tau} \right). \tag{2}$$

Here $\overline{P}$, $\overline{E_a}$ and $\overline{Q}$ are in $kg.m^{-2}$ and denote the flux averaged over time period, τ (yr). ρ_w and is the density of liquid water ($kg.m^{-3}$); A is catchment area (m^2); z is the depth of water storage (m) and $[S_w]$ is the concentration of stored water ($kg.m^{-3}$). When a catchment is modelled individually, A defines the spatial scale of analysis, which Budyko ensured was as large as practical to minimise the effects of ground water fluxes as well as the effects of "local conditions" on E_a. The temporal scale is set by τ. To achieve steady state conditions (i.e., ΔS_w is zero), long-term averages are typically used (i.e., $\tau >> 1$ year).

Budyko (1974) defined the long-term climate dryness index, Φ, as the ratio of potential evaporation (E_p; $mm.yr^{-1}$) to P:

$$\Phi = \frac{E_p}{P}; \tag{3}$$

and the long-term evaporative index as

$$\varepsilon_o = \frac{E_a}{P}. \tag{4}$$

Actual evaporation asymptotically approaches the limits placed on evaporation by the supply of water and the evaporative demand for water as the climate becomes increasingly arid or humid, respectively. Budyko found empirically that the long-term evaporative index can be estimated as a curvilinear function of Φ:

$$\varepsilon_b = \left(\Phi \tanh \Phi^{-1} \left(1 - \cosh \Phi + \sinh \Phi\right)\right)^{0.5} \tag{5}$$

This relation has become known as the Budyko curve or model (Figure 1). Here ε_b denotes the evaporative index predicted using this curve. Many equivalent relations have subsequently been developed (e.g., Choudhury, 1999; Zhang et al., 2001; Fu, 1981; Yang et al., 2008).

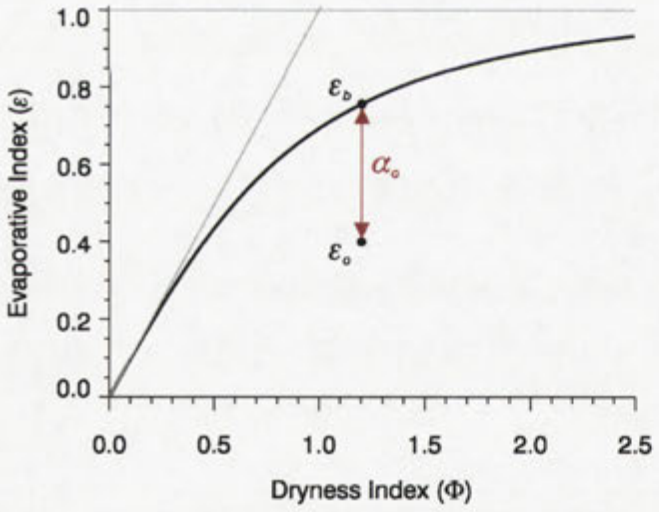

Figure 1. The Budyko curve demonstrating the derivation of observed 'Budyko scatter'. The black line shows the long-term annual average evaporative index as described by Budyko's curve. The horizontal and diagonal grey lines are the water and energy limits to evaporation, respectively. For a given dryness index value, ε_b is the evaporative index predicted by the curve, ε_o is the observed index value, and α_o is the observed scatter.

The original Budyko relation was developed for large spatial and temporal scales, that is, using large catchments (i.e., large A) and long-term averages (i.e., large τ). At these scales, Budyko showed that the curve estimated long-term E_a accurately (<10% error). In many circumstances, however, substantial variation around the curve has been

observed and many authors have examined the causes of this 'Budyko scatter' (e.g., Dooge et al., 1999; Hickel and Zhang, 2006; Koster and Suarez, 1999; Milly, 1994b; Porporato et al., 2004; Potter et al., 2005; Sankarasubramanian and Vogel, 2003; Yokoo et al., 2008; Zhang et al., 2008). We define the scatter as the difference between the observed and the Budyko-modelled evaporative indeces (see Figure 1):

$$\alpha_o = \varepsilon_o - \varepsilon_b . \tag{6}$$

Relatively more scatter is observed if shorter temporal scales are employed ($\tau \leq 1$ year) due generally to the absence of steady-state conditions (Zhang et al., 2008). Greater scatter is also observed at smaller spatial scales (A) where the influences of local factors start to dominate over those of climatic dryness (Budyko, 1974; Donohue et al., 2007; Oudin et al., 2008). To extend and adapt Budyko-type relations to be able to accurately estimate E_a and Q at finer spatial and temporal scales would greatly enhance our understanding of ecohydrological processes and would be of great practical value.

Several recent papers are of direct relevance to the current study. Yang et al. (2007) used the Fu equation (Fu, 1981), which has an adjustable parameter (w), to examine the role three catchment-based geophysical indices play in determining the position of the curve within the Φ–ε framework. The three indices were: (i) the relative infiltration capacity; (ii) the relative soil storage capacity; and (iii) the catchment-average slope. Using annual E_p, P and Q data, these three indices and step-wise regressions, Yang et al. (2007) developed a three-parameter, non-linear model to estimate w for each of the 108 catchments (they also tested a three-parameter linear model and found it produced similar results). Their approach didn't model the scatter itself but determined the optimal placement of the curve within each catchment's scatter. The authors did not directly compare the accuracy of the original Fu (1981) model against the accuracy of the three-parameter-adapted model, so it is difficult to gauge the improvement provided by the latter. However, statistics comparing annual observed and modelled Q using the three-parameter Fu model indicated that the coefficient of determination (r^2) was 0.62 and the Root Mean Square Error (RMSE) was 21 mm.yr^{-1} (which was approximately 30% of observed annual Q if the latter is taken to be 70 mm.yr^{-1}, see their Figure 7). Yang et al. (2009) repeated the analysis of Yang et al. (2007) replacing the relative soil storage capacity index with remotely sensed measures of fractional green vegetation

cover. They found that the accuracy of modelling E_a was essentially the same as in the original Yang et al., (2007) analysis.

Oudin et al. (2008) tested the impact land cover has on long-term annual average stream flow using the Budyko relation (as well as four other similar relations) adapted to include an adjustable parameter. Using land cover data describing five broad cover classes (i.e., forest, grassland, cropland, heathland, shrubland and non-vegetated) they calibrated the adjustable parameter to optimally fit the Budyko curve to Q associated with each land cover strata. One model was developed for all catchments (n = 1508) for each cover class. Results showed that the addition of the adjustable parameter, per se, did not improve model accuracy over the original Budyko model. However, recalibration of the model using the land cover data did improve Q predictions, from an RMSE of 65 to 53 $mm.yr^{-1}$. Of the five cover classes, it was found that forest cover improved predictions the least. Lastly, Oudin et al. (2008) showed that the influence of land cover data had the greatest impact in smaller catchments (i.e., less than ~1000km^2) and that it was difficult to improve the original Budyko model in large catchments by incorporating vegetation cover information.

Donohue et al. (2007) explored the relationships between vegetation dynamics and the observed Budyko scatter. They argued for a link between analysis scale (A and τ), vegetation-related processes and the scatter, and that, as the spatial and temporal scales of analysis decrease, the role vegetation dynamics play in determining the scatter may become more important. In particular, variations in rooting depth and in vegetation water use (which affect storage capacity and the rate of depletion of stored water, respectively) could violate steady-state conditions even across multiple years. Additionally, differences in the seasonal water use characteristics of perennial and annual vegetation types should alter values of ε_o for a given Φ, as per Zhang et al. (2001). Donohue et al. (2007) further hypothesised that remotely sensed measures of fPAR (the fraction of Photosynthetically Active Radiation absorbed by vegetation) should provide a useful surrogate for information describing the dynamics in ecohydrological properties of vegetation. fPAR is a unitless, biophysical parameter that is linearly related to the fractional green foliage cover (Asrar et al., 1984). The dynamics of perennial and annual vegetation functional types can be approximated by splitting total fPAR into its constituent persistent and recurrent components, respectively (e.g., Berry and Roderick, 2002; Gill et al., 2006; Donohue et al., 2007; Lu

et al., 2003; Roderick et al., 1999) . Thus Donohue et al. (2007) hypothesised that the incorporation of dynamic vegetation information (in the form of remotely sensed fPAR data) into the Budyko model might enhance the model's accuracy in small catchments and at short time-scales.

The aim of this paper is to test the hypothesis of Donohue et al. (2007). To do this we developed a database of monthly, catchment average values of three primary variables: precipitation, potential evaporation and total fPAR. From these we derived numerous secondary variables describing the long-term and annual averages, variability and seasonality of the primary parameters, as well as estimates of persistent and recurrent fPAR. Using these parameters along with the observed stream flow data, we developed linear models to describe the Budyko scatter at several different spatial and temporal scales. The models subsequently developed allowed us to assess the ecohydrological processes operating within and across the analysis catchments.

6.3 Data and methods

6.3.1 Input data

The primary data used in these analyses were monthly values of precipitation, potential evaporation, and total fPAR. Precipitation data and Penman's (1948) potential evaporation data originated from the 0.05° resolution, Australia-wide daily grids of Jones et al. (2007) and Donohue et al. (2009a), respectively. fPAR data were produced by Donohue et al. (2008) using monthly, 0.08° resolution AVHRR (Advanced Very High Resolution Radiometer) imagery. These data covered the period 1981–2006 and set the temporal bounds of analyses.

Monthly stream flow data used for modelling and validation came from the database of Peel et al. (2000), the coverage of which has subsequently been updated to the end of 2006. This database originally contained 331 catchments. Here, catchments not containing at a complete record for at least 10 years within the overall 26 year study period were discarded, leaving 221 catchments suitable for use in analyses (Figure 2). Monthly catchment-averages were calculated for all P, E_p and fPAR data. A summary of the long-term annual average potential evaporation, water flux and fPAR values for these catchments are given in Figure 3. These catchments were generally located in the

more humid regions of Australia (for comparison, the 1981–2006 Australia-wide annual average P is 475 mm.yr^{-1}). The long-term Budyko scatter of these catchments is shown in Figure 4. Most catchments have Φ greater than 1—highlighting the dominance of water-limited environments in Australia—and are generally located over the curve. A number of catchments plot well below the curve and therefore have relatively high stream flow.

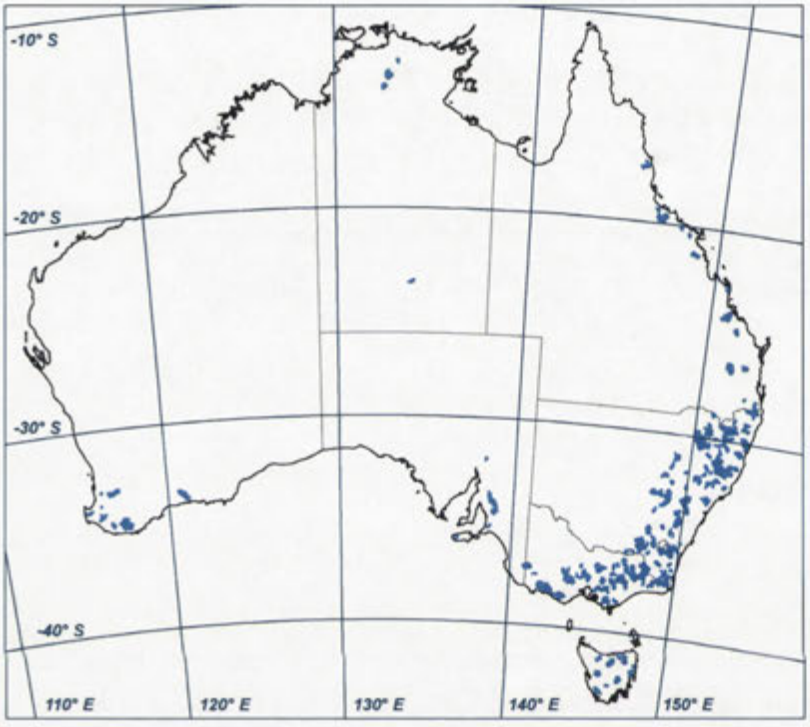

Figure 2. Locations of the 221 study catchments.

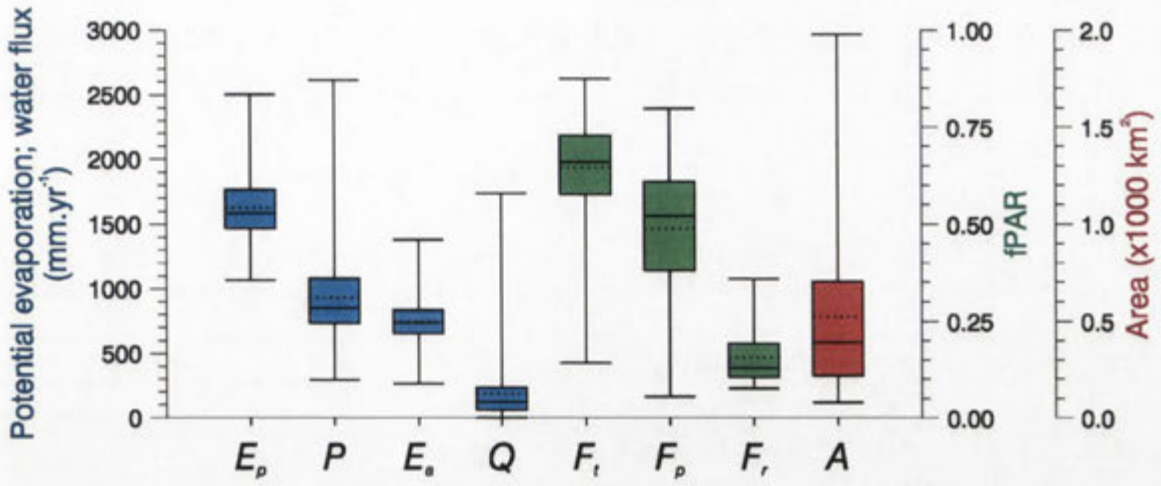

Figure 3. Summary of the long-term annual potential evaporation, average water fluxes, and fPAR values for the 221 study catchments. The box plots describe the maximum and minimum values, the inter-quartile range, and the median (solid centreline) and mean (dotted centreline) values. Total, persistent and recurrent fPAR are represented by F_t, F_p, and F_r, respectively.

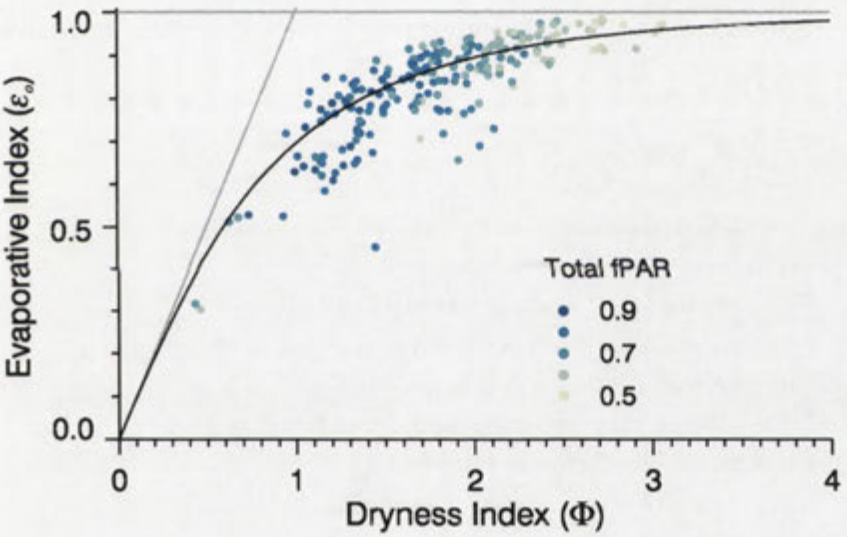

Figure 4. Long-term annual average Φ plotted against ε_o for each of the 221 study catchments. Each catchment's long-term average total fPAR is indicated by the shade of its data point.

A suite of derived variables were generated from the three primary monthly variables. Firstly, we decomposed total fPAR into its constituent persistent and recurrent components, using the method of Donohue et al. (2009b). Persistent fPAR represents the cover from perennial, non-deciduous vegetation types and recurrent fPAR represents that from annual, ephemeral and deciduous vegetation. For Australian landscapes, these approximately represent woody and non-woody vegetation types, respectively (Donohue et al., 2009b; Gill et al., 2009). Secondly, we generated calendar-year annual totals (or annual averages in the case of fPAR) and long-term annual averages of each

primary variable. Finally, we derived metrics describing the inter- and intra-annual variability in the above variables, as well as the Budyko indices (see Table 1 and Table 2). Catchment area and the number of years in each catchment's data record were also included in the modelling.

Table 1. Variables used in the analyses of long-term annual average scatter around the Budyko curve. Variables in bold are those used as independent variables in the regression analyses.

Variable	Units	Description
A	**km^2**	**Catchment area**
n	**years**	**Length of catchment's data record**
P	**mm.yr^{-1}**	**Long-term annual average precipitation**
E_p	**mm.yr^{-1}**	**Long-term annual average potential evaporation**
Q_b	mm.yr^{-1}	Long-term annual average stream flow derived using the Budyko curve
Q_o	mm.yr^{-1}	Long-term annual average stream flow, observed
Q_p	mm.yr^{-1}	Long-term annual average stream flow, predicted
E_a	mm.yr^{-1}	Long-term annual average actual evaporation (i.e., $P - Q$)
Φ	–	Long-term annual average dryness index (E_p/P)
ε_b	–	Long-term annual average evaporative index derived from the Budyko curve
ε_o	–	Observed long-term annual average evaporative index (E_a/P)
ε_p	–	Predicted long-term annual average evaporative index
α_o	–	Observed long-term annual average Budyko scatter ($\varepsilon_o - \varepsilon_b$)
α_p	–	Predicted long-term annual average Budyko scatter
F_t	**–**	**Long-term annual average total fPAR**
F_p	**–**	**Long-term annual average persistent fPAR**
F_r	**–**	**Long-term annual average recurrent fPAR**
σ_P	**mm.yr^{-1}**	**Inter-annual variation in precipitation**
σ_{Ep}	**mm.yr^{-1}**	**Inter-annual variation in potential evaporation**
σ_{Ft}	**–**	**Inter-annual variation in total fPAR**
σ_{Fp}	**–**	**Inter-annual variation in persistent fPAR**
σ_{Fr}	**–**	**Inter-annual variation in recurrent fPAR**
S_1	**months**	**Phase-offset between rainfall and potential evaporation seasonalities; calculated from long-term average monthly values as the difference in the timing between the annual peaks in precipitation and potential evaporation.**
S_2	**months**	**Phase-offset between rainfall and total fPAR seasonalities; calculated from long-term average monthly values as the difference in the timing between the annual peaks in precipitation and total fPAR.**

Table 2. Variables used in the analyses of annual scatter around the Budyko curve. Variables in bold are those used as independent variables in the regression analyses.

Variable	Units	Description
P'	**mm.yr^{-1}**	**Annual precipitation**
E_p'	**mm.yr^{-1}**	**Annual potential evaporation**
Q_b'	mm.yr^{-1}	Annual stream flow derived using the Budyko curve
Q_o'	mm.yr^{-1}	Annual stream flow, observed
Q_p'	mm.yr^{-1}	Annual stream flow, predicted
E_a'	mm.yr^{-1}	Annual actual evaporation (i.e., $P' - Q'$)
Φ'	–	Annual dryness index
ε_b'	–	Annual evaporative index derived using the Budyko curve
ε_o'	–	Observed annual evaporative index (E_a'/P')
ε_p'	–	Predicted annual evaporative index
α_o'	–	Observed annual scatter around the Budyko curve ($\varepsilon_o' - \varepsilon_p'$)
α_p'	–	Predicted annual scatter around the Budyko curve
F_t'	**–**	**Annual total fPAR**
F_p'	**–**	**Annual persistent fPAR**
F_r'	**–**	**Annual recurrent fPAR**
σ_P'	**mm.yr^{-1}**	**Intra-annual variation in precipitation**
σ_{Ep}'	**mm.yr^{-1}**	**Intra-annual variation in potential evaporation**
σ_{Ft}'	**–**	**Intra-annual variation in total fPAR**
σ_{Fp}'	**–**	**Intra-annual variation in persistent fPAR**
σ_{Fr}'	**–**	**Intra-annual variation in recurrent fPAR**
S_1'	**months**	**Phase-offset between rainfall and potential evaporation seasonalities; calculated from the current year's monthly values as the difference in the timing between the peaks in precipitation and potential evaporation.**
S_2'	**months**	**Phase-offset between rainfall and total fPAR seasonalities; calculated from the current year's monthly values as the difference in the timing between the annual peaks in precipitation and total fPAR.**
$\rho P'$	**mm.yr^{-1}**	**The previous year's P'**
$\rho F_t'$	**–**	**The previous year's F_t'**
$\rho F_p'$	**–**	**The previous year's F_p'**
$\rho F_r'$	**–**	**The previous year's F_r'**

6.4 Modelling the Budyko Scatter

6.4.1 Modelling framework

The modelling framework used for predicting Budyko scatter contained two scale hierarchies—one encompassing temporal scale and the other spatial scale. At each scale, the scatter was modelled using linear regressions (described in detail below); modelled scatter was then converted to stream flow units and validated against observed stream flow.

6.4.2 Temporal modelling scales

We modelled the Budyko scatter at two temporal scales—the long-term annual average time-step and the annual time-step. Analyses of long-term averages is the scale at which the Budyko relation was originally developed; this scale effectively removes temporal variation and focuses analyses solely on variability across different catchments. It is at the annual scale that temporal changes in ecohydrological processes can start to be examined. However, at the annual scale it is possible that non-steady-state conditions exist in many of the catchments (e.g., Donohue et al., 2007; Leblanc et al., 2009) in which case model results will reveal little apart from the variability of precipitation and associated water storage changes.

Long-term average analyses were conducted using the variables listed in Table 1. These are generally long-term annual average values of the primary variables, their inter-annual variability, and two seasonality indices that represent the timing differences in the long-term seasonal cycles in precipitation, potential evaporation and total fPAR. Each catchment's area (A) and data record length (n) were included in the long-term analyses to test whether catchment size and steady-state conditions, respectively, were influential in the prediction of stream flow. Variables used in the annual analysis (Table 2) include annual values of the primary variables, the intra-annual variability in these, the timing differences in each year's cycle in precipitation, potential evaporation and total fPAR, as well as the previous year's annual P and total, persistent and recurrent fPAR. These latter variables were included to capture some of the effect of non-steady state conditions.

6.4.3 Spatial modelling scales

Spatial scale is used here to refer to the breadth of climate and landscape characteristics covered by the catchments being analysed as opposed to the size of individual catchments. Three spatial scales were utilised. Firstly, the coarsest scale pools all 221 catchments from which one model was developed. The pooled catchments (Figure 2) spanned the Australian continent and encompassed all Australian climate types and broad vegetation groups.

Secondly, the medium scale grouped catchments according to their long-term seasonality phase-offset (S_l; see Table 1). There were 7 such phase-offset groups, containing between 14 and 51 catchments each (Figure 5). A model was developed for every offset group. The geographical extent of each group ranged between 300 and 3100 km. The seasonality offset grouping provides an intuitively meaningful, coarse-scale method of sub-setting the catchment database. This approach was used because of the important role played by variability in the supply of water and energy: the greater the variability, the greater the stream flow, all else being equal (Budyko, 1974; Hickel and Zhang, 2006; Milly, 1994b, 1994a; Porporato et al., 2004). This variability relates to inter-annual variability, intra-annual (seasonal) variability, intra-seasonal variability (i.e., storminess) as well as the temporal mismatch in the seasonal supply of water and energy.

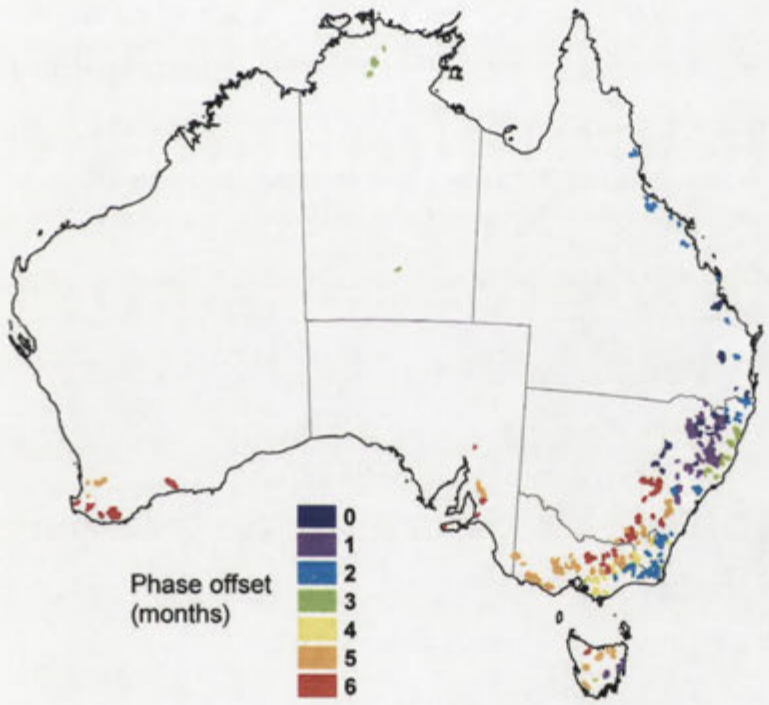

Figure 5. Study catchments grouped according to the phase-offset between the seasonal cycle in precipitation and potential evaporation.

Thirdly and finally, the finest modelling scale was individual catchments, which varied in length (and area) between approximately 16 km (100 km^2) and 65 km (2000 km^2). Thus 221 models were developed at this scale.

6.4.4 Linear regressions

Modelling of both the long-term and annual Budyko scatter was undertaken using linear least-square regressions. In each regression, the observed long-term or annual scatter (α_o or α_o', respectively) was set as the dependent variable and the independent variables were those highlighted in Table 1 or Table 2. To maximise model simplicity analyses were intentionally restricted to 1-parameter models. Scatter was modelled as

$$\alpha_p = mx + b \tag{7}$$

where x is the independent variable with the highest correlation with the observed scatter. Modelled evaporative index and, from this, modelled stream flow was calculated as follows:

$$\varepsilon_p = \alpha_p + \varepsilon_b \tag{8}$$

$$Q_p = P - \varepsilon_p P \tag{9}$$

(although the notation in the above formulations relate to long-term annual scatter, the same relations were used to model annual scatter). Metrics used to compare modelled and observed stream flow were the regression coefficient between observed and predicted stream flow, the Nash-Sutcliffe Efficiency (NSE see Nash and Sutcliffe, 1970) and the RMSE.

6.4.5 Summary of analyses

Thus the analyses performed were as follows.

1. Modelling long-term annual average scatter: pooled catchments.
2. Modelling long-term annual average scatter: catchments grouped by phase-offset.
3. Modelling annual scatter: pooled catchments.
4. Modelling annual scatter: catchments grouped by phase-offset.
5. Modelling annual scatter: individual catchments.

The next section outlines the results, which are presented in the same five-part structure as listed above. Alongside the description of results we provide some interpretations of the ecohydrological meaning of the established models. We then discuss these findings, and provide concluding remarks.

6.5 Results

6.5.1 Modelling long-term annual average scatter: pooled catchments

When all 221 catchments were pooled and the original Budyko model used for estimating long-term annual average Q from these catchments, the average error in predictions was 78 mm.yr^{-1} (Figure 6 and Table 3). This error is approximately 42% of the annual average stream flow for these catchments (187 mm.yr^{-1}). By incorporating the 1-parameter scatter model into the Budyko framework, the accuracy of modelled stream flow improved marginally, to 68 mm.yr^{-1} (which is 36% of Q_o). The variable most strongly related to the observed scatter was σ_P, the inter-annual variation in precipitation. That this is a climatic variable affirms the notion that, at coarse spatial scales, climate exerts the dominant influence on catchment hydrology (Donohue et al., 2007; Budyko, 1974). Several authors (previously noted) have demonstrated that variability in the supply of water and energy is a key cause of variations in stream flow, all else being equal—the greater the variability the greater the relative stream flow. We found σ_P to be inversely related to E_a (and therefore positively related to Q_o) at this spatial and temporal scale, which is in agreement with previous findings.

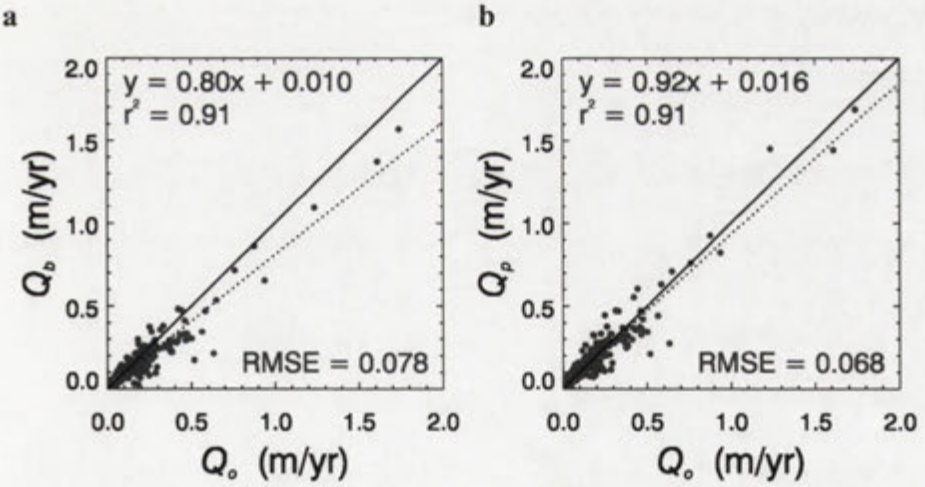

Figure 6. Plots comparing observed and modelled long-term annual average stream flow for the 221 catchments. Observed stream flow (Q_o) is compared with that predicted using the original Budyko model (Q_b, plot a) and with that predicted using the 1-parameter pooled scatter model (Q_p, plot b). The black line is the 1:1 line; the dotted line is the line of best-fit and is described by the linear equation.

Table 3. Metrics comparing observed and modelled long-term annual average stream flow for all 221 catchments. Stream flow is predicted using the original Budyko model (top row) and using the 1-parameter scatter model (bottom row). Slope describes the line of best-fit, NSE is the Nash-Sutcliffe Efficiency, RMSE is the root mean square error ($mm.yr^{-1}$). α_p, the predicted scatter, is unitless. Percent error is the percentage that the RMSE is of average stream flow (RMSE/Q_0 x100).

Model	Slope	NSE	RMSE	Equation	% Error
Original	0.80	0.88	78	—	42
Pooled	0.92	0.91	68	$\alpha_p = -0.0003\sigma_p - 0.02$	36

6.5.2 Modelling long-term annual average scatter: catchments grouped by phase-offset

Seven separate analyses were performed in modelling the long-term annual average scatter from the phase-offset catchment groups. The overall predictive error decreased from 42% to 31% of the mean stream flow (Figure 7) when modelled according to this grouping. This is an improvement over the long-term pooled model (36% error – see above) showing that finer spatial scale of modelling accommodated more of the regional-scale ecohydrological processes. This is further highlighted by the types of variables included in each phase-offset group (Table 4). Of the seven phase-offset analyses, six contained a vegetation-related variable.

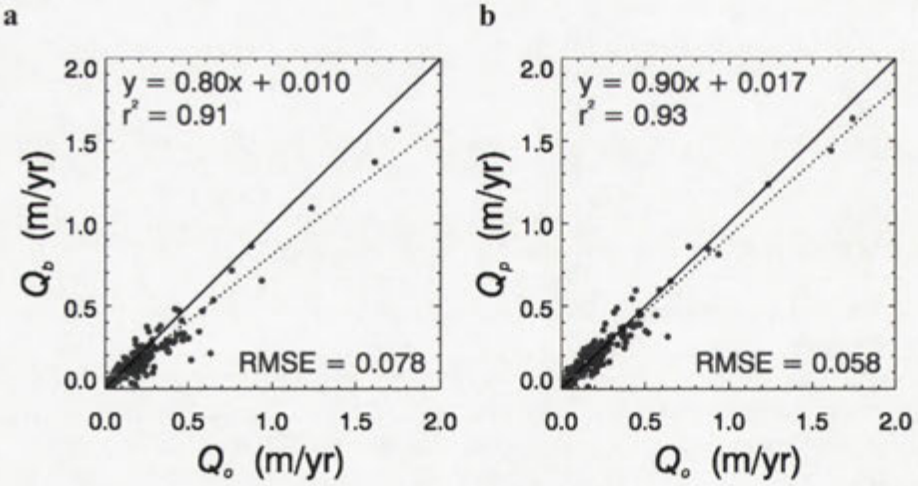

Figure 7. Plots comparing observed long-term annual average stream flow and stream flow estimated using the phase-offset models. Observed stream flow (Q_o) is compared with that predicted using the original Budyko model (Q_b, plot a) and with that predicted using the seven 1-parameter phase-offset scatter models (Q_p, plot b). The black line is the 1:1 line; the dotted line is the line of best-fit and is described by the linear equation.

Table 4. Metrics comparing observed and modelled long-term annual average stream flow for catchments grouped by phase-offset. Values in brackets are the equivalent values derived using the original Budyko model. N denotes the number of catchments in each group; Slope describes the line of best-fit; NSE is the Nash-Sutcliffe Efficiency; RMSE is the root mean square error ($mm.yr^{-1}$). α_p, the predicted scatter, is unitless. Percent error is the percentage that the RMSE is of average stream flow (RMSE/Q_0 x100).

Model	N	Slope	NSE	RMSE	Equation	% Error
Offset 0	18	0.80 (0.75)	0.75 (0.74)	31 (32)	$\alpha_p = 0.27F_r - 0.04$	38 (39)
Offset 1	37	0.78 (0.66)	0.83 (0.78)	33 (37)	$\alpha_p = 1.73\sigma_{Fr} - 0.06$	33 (37)
Offset 2	44	0.88 (0.75)	0.88 (0.77)	80 (110)	$\alpha_p = 0.00007A - 0.09$	34 (47)
Offset 3	18	0.84 (0.79)	0.72 (0.25)	88 (143)	$\alpha_p = 0.15F_t - 0.19$	23 (37)
Offset 4	14	0.40 (0.37)	0.33 (0.17)	59 (66)	$\alpha_p = 0.034S_2 - 0.05$	30 (37)
Offset 5	51	0.86 (0.74)	0.88 (0.83)	49 (59)	$\alpha_p = 1.16\sigma_{Fr} - 0.07$	30 (37)
Offset 6	39	0.85 (0.92)	0.82 (0.80)	37 (40)	$\alpha_p = -0.18F_r + 0.03$	33 (36)

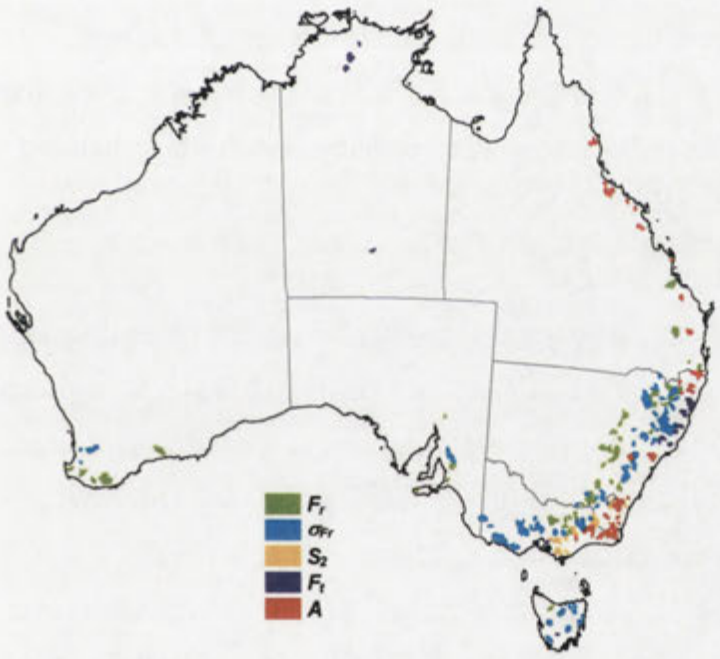

Figure 8. Distribution of the variables used within the long-term annual average phase-offset models. Note that, whilst the 0-month and 6-month models both contain the variable F_r, the former is positively correlated and the latter is negatively correlated to scatter, respectively.

As these analyses used long-term averages, the only source of variation in the analyses was space. The distribution of the identified variables has substantial spatial structure (Figure 8), namely that the same variables have been selected across contiguous offset groups (i.e. F_r for 0 and 6 month offset classes and σ_{Fr} for 1 and 5 month offset classes). This implies that the selection of variables is not random but that there are common processes operating across large areas. Making conclusions from these analyses about

what ecohydrological processes caused the scatter is challenging, partly because most offset groups encompass a wide range of climatic and ecological conditions. However, interpretation of some of the offset modelling results is plausible, as follows.

0-month and 1-month offset catchments

The models for the 0-month and 1-month offset catchment groups indicate that the higher the F_r and σ_{Fr}, respectively, the greater the α_o and therefore E_a. However, models of these two groups were unable to make substantial improvements to the estimation of stream flow compared to the original Budyko model (Table 4) and so little significance can be placed on the variables identified in each model.

2-month offset catchments

This is the only phase-offset group with a non-biological variable. All these catchments are near-coastal, and the group spans the 3,000 km length of the eastern coast of Australia. Here, the larger the catchment area the greater the relative E_a. What processes are operating differently in the larger catchments can not be ascertained from this analysis. This result is in contrast with that of Choudhury (1999) who concluded that analysis scale was inversely related to E_a.

3-month offset catchments

These are reasonably wet catchments mostly with late-summer rainfall (Sturman and Tapper, 2005). The few catchments in the far north (see Figure 8) have highly seasonal precipitation such that only relatively low levels of vegetation cover can be supported by the high precipitation and a relatively large proportion of precipitation becomes stream flow. In contrast, the eastern coast catchments receive more uniform precipitation throughout the year and support relatively high levels of vegetation cover. The identification of F_t in this analysis is probably more a reflection of the difference between precipitation seasonality between these two sub-groups of catchments.

4-month offset catchments

Catchments with a 4-month phase-offset are temperate, high precipitation catchments with moderate to high perennial vegetation cover. Precipitation generally peaks in spring (Sep–Nov, Sturman and Tapper, 2005). Here scatter is positively related to S_2, the phase offset between P and F_t. Those catchments where vegetation cover peaks in spring have relatively less E_a (and more Q_o) than those catchments where vegetation cover peaks earlier in the year. This may be related to water storage effects, where

those catchments that can store the spring rainfall within the rooting zone until the warmer late-summer months are the more productive catchments and have higher E_a.

5-month and 6-month offset catchments

The catchments within these two groups experience the classic Mediterranean-type climate with hot, dry summers and wet winters (Sturman and Tapper, 2005). These catchments largely support winter cereal cropping, which appear as low F_p and highly seasonal F_r, peaking in spring (Sep–Nov). Variations in F_r play an important role in these catchments as indicated by the two models (Table 4). The 6-month phase-offset grouping results indicate that α_o is inversely proportional to F_r. This is a similar result to that of Zhang et al. (2001) where catchments with greater proportions of grass cover than forest cover produced relatively more Q_o. Even though in the six-month offset grouping, Q_o is proportional to F_r this does not imply that the reverse is true, which is that F_p is proportional to E_a, as the Zhang et al. (2001) model does.

6.5.3 Modelling annual scatter: pooled catchments

Figure 9 and Table 5 show the results of the pooled catchment model estimates of annual stream flow, Q_o'. The original Budyko model used at this temporal scale is less effective (55% error) than when used at the long-term annual average scale (42% error). This is most likely due to non-steady-state conditions existing annually. The 1-parameter model performs a little better than the original model at the annual scale, with a relative error of 51%. As a major source of hydrological variation at this time-scale is ΔS_w, and as such changes are primarily a product of variability in precipitation, we find that σ_P' is the dominant variable in this model.

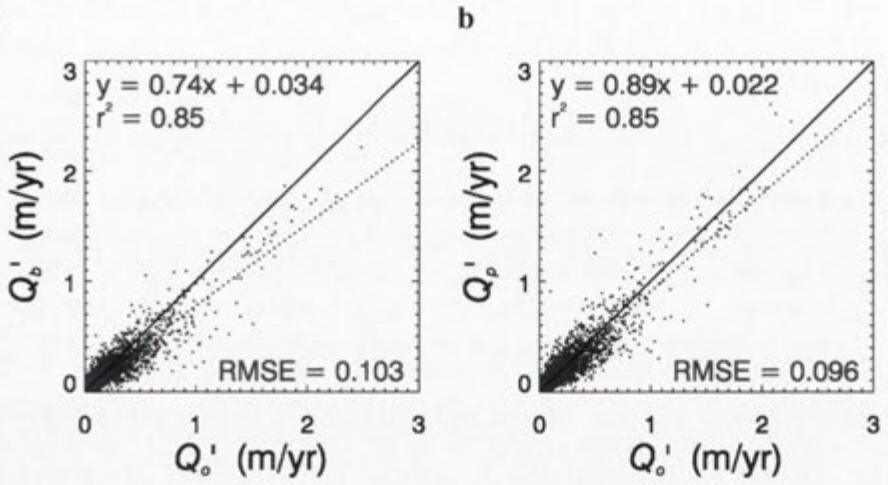

Figure 9. Plots comparing observed and modelled annual stream flow for the 221 catchments pooled. Observed stream flow (Q_o') is compared with that predicted using the original Budyko model (Q_b', plot a) and with that predicted using the 1-parameter pooled scatter model (Q_p', plot b). The black line is the 1:1 line; the dotted line is the line of best-fit and is described by the linear equation.

Table 5. Metrics comparing observed and modelled annual stream flow for all 221 catchments pooled. Stream flow is predicted using the original Budyko model (top row) and using the 1-parameter scatter model (bottom row). Slope describes the line of best fit, NSE is the Nash-Sutcliffe Efficiency, RMSE is the root mean square error ($mm.yr^{-1}$). α_p', the predicted scatter, is unitless. Percent error is the percentage that the RMSE is of average stream flow ($RMSE/Q_0'$ x100).

Model	Slope	NSE	RMSE	Equation	% Error
Original	0.74	0.83	103	—	55
Pooled	0.89	0.85	96	$\alpha_p' = -0.0009\sigma_p' - 0.04$	51

6.5.4 Modelling annual scatter: catchments grouped by phase-offset

The overall performance of the 7 phase-offset analyses performed at the annual scale (Figure 10 and Table 6) is approximately the same as that of the annual pooled analysis, with an overall error of around 50% of average Q. Six of the seven analyses identify precipitation variability (either σ_P' or $\rho P'$) as the most important variable. This is in contrast with the variables identified in the long-term phase-offset analyses, which had a range of variables, most of which were vegetation-related. In the annual offset-grouped catchment modelling, the addition of time an a source of variation has rendered (nearly) all variables the same, each presumably reflecting the now relatively important role played by ΔS_w—which is a product of precipitation variability in water-limited environments. Comparing the long-term phase-offset results (Table 4) with the annual

phase-offset results shows that the accuracy of the annual modelling is less, again this is likely due to ΔS_w.

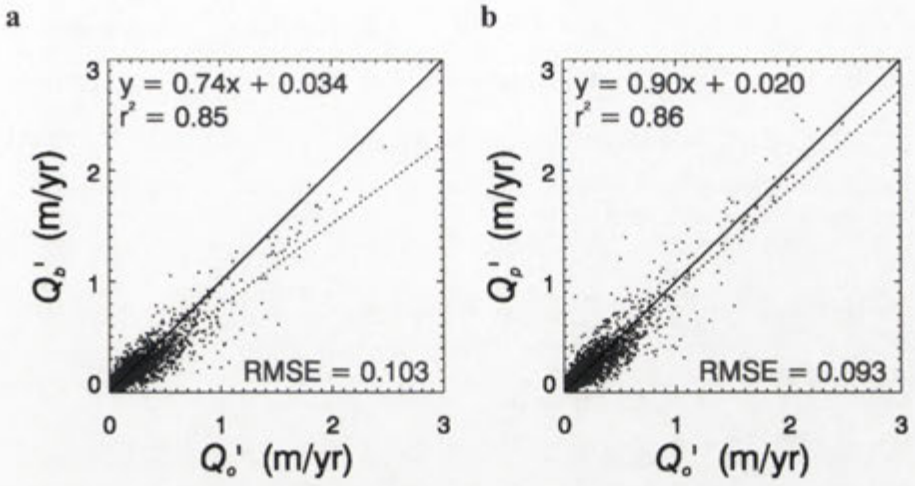

Figure 10. Plots comparing observed annual stream flow and stream flow estimated using the phase-offset models. Observed stream flow (Q_o') is compared with that predicted using the original Budyko model (Q_b', plot a) and with that predicted using the seven 1-parameter phase-offset scatter models (Q_p', plot b). The black line is the 1:1 line; the dotted line is the line of best-fit and is described by the linear equation.

Table 6. Metrics comparing observed and modelled annual stream flow for catchments grouped by phase-offset. Values in brackets are the equivalent values derived using the original Budyko model. N denotes the number of catchments in each group; Slope describes the line of best fit; NSE is the Nash-Sutcliffe Efficiency; RMSE is the root mean square error ($mm.yr^{-1}$). α_p', the predicted scatter, is unitless. Percent error is the percentage that the RMSE is of average stream flow (RMSE/Q_0'x100).

Model	N	Slope	NSE	RMSE	Equation	% Error
Offset 0	18	0.75 (0.64)	0.75 (0.71)	56 (59)	$\alpha_p' = -0.0008\sigma_p' + 0.06$	30 (32)
Offset 1	37	0.66 (0.61)	0.81 (0.78)	60 (66)	$\alpha_p' = -0.00009\rho P' + 0.10$	32 (35)
Offset 2	44	0.92 (0.69)	0.81 (0.78)	136 (147)	$\alpha_p' = -0.0007\sigma_p' + 0.02$	73 (79)
Offset 3	18	0.81 (0.65)	0.77 (0.67)	141 (168)	$\alpha_p' = -0.0008\sigma_p' + 0.01$	75 (90)
Offset 4	14	0.65 (0.59)	0.52 (0.47)	86 (90)	$\alpha_p' = -0.0011\sigma_p' + 0.06$	46 (48)
Offset 5	51	0.94 (0.84)	0.94 (0.93)	74 (81)	$\alpha_p' = -0.0013\sigma_p' + 0.05$	40 (43)
Offset 6	39	0.87 (0.91)	0.85 (0.84)	63 (65)	$\alpha_p' = -0.16\rho F_r' + 0.04$	34 (35)

6.5.5 Modelling annual scatter: individual catchments

At this spatial scale, a 1-parameter model was developed for each of the 221 catchments. The model equations and metrics comparing Q_o' and Q_p' are presented in

Appendix 1 (Table A1). Predicted stream flow is plotted against observed stream flow in Figure 11. There is a marked improvement in the accuracy of model estimates with a relative error of 28% compared to the original 55%. Whilst 56 models include a vegetation-related variable (Table 7), climate-related variables are the most prevalent. Precipitation variability remains the variable most correlated with the observed scatter showing that non-steady-state effects dominate the scatter in all analyses done at annual scales.

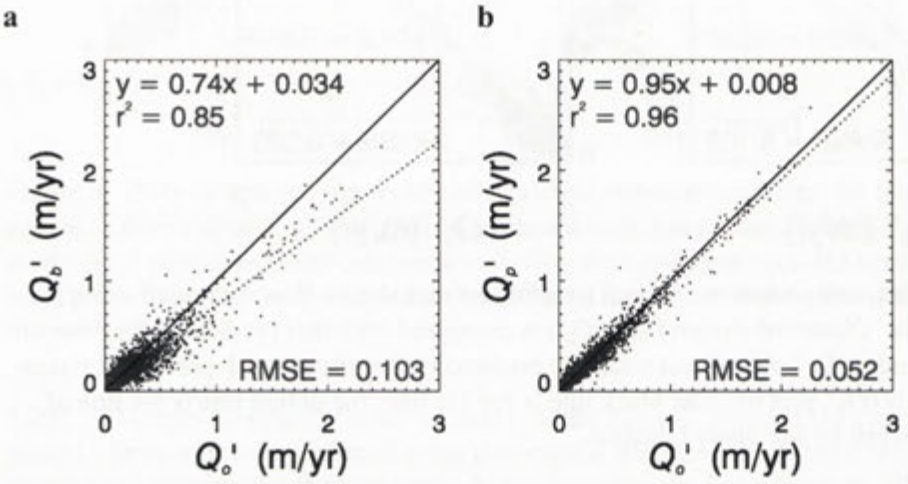

Figure 11. Plots comparing observed annual stream flow and stream flow estimated using individual catchment models. Observed stream flow (Q_o') is compared with that predicted using the original Budyko model (Q_b', plot a) and with that predicted using the 221 1-parameter phase-offset scatter models (Q_p', plot b). The black line is the 1:1 line; the dotted line is the line of best-fit and is described by the linear equation.

When individual catchments are modelled at the annual scale, the only source of variation encapsulated in each model is time. To examine the distribution of these models' variables is to examine whether there is a spatial pattern to the processes that cause the temporal dynamics in catchment fluxes. In Figure 12 the spatial distribution of model variables are displayed. It is apparent that there is no spatial pattern in the distribution of the dominant variables. We performed a simple analysis of the distribution of model variables and found no relationships with climatic zones (Stern et al., 2000), bioregions (DEWHA, 2008), vegetation cover types (Thackway et al., 2004), or land use (Stewart et al., 2001). This may indicate that there are no common temporal processes operating across any given region (instead they are highly localised) or, more probably, that the local ecohydrological processes are indistinct due to relatively large changes in the storage term at annual scales.

Table 7. The number of individual catchment models that incorporate each of the variables used in the analysis of annual Budyko scatter. The stream flow prediction errors, averaged for the models that use each variable, are given for the original Budyko model and for the 1-parameter scatter model. Errors are the percent that the average RMSE is of the average annual stream flow.

Variables	Number of models	% Error (original Budyko)	% Error (modelled scatter)
σ_P	55	60	31
ρP	34	48	30
P	26	88	33
E_p	20	101	35
S_1	17	60	35
σ_{Ep}	13	84	43
F_r	7	91	53
F_t	7	53	21
ρF_r	7	34	17
ρF_t	7	55	35
σ_{Fp}	7	78	46
σ_{Fr}	6	48	31
F_p	5	53	25
σ_{Ft}	4	31	18
ρF_p	3	48	30
S_2	3	50	24

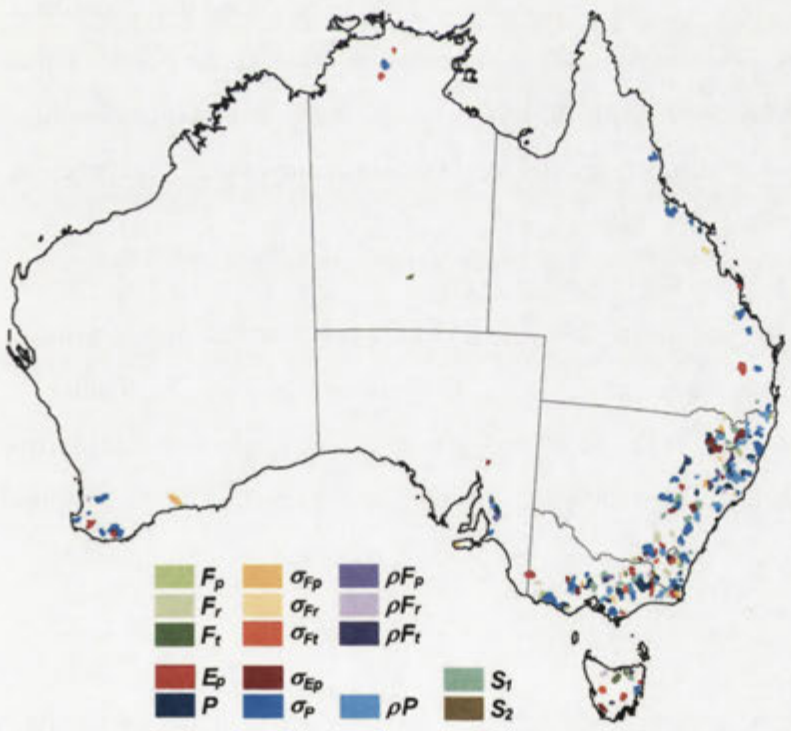

Figure 12. Distribution of the variables used within the annual individual catchment models.

6.6 Discussion

The spatial and temporal scales of analyses were key in interpreting how vegetation information relates to the observed Budyko scatter. Over a large area containing a wide range of climatic conditions, vegetation information was unable to improve predictions at either long-term or annual time scales—instead a climatic variable (σ_P) explained more of the scatter around the Budyko curve. Even this variable, though, made only small improvements indicating that Budyko's original model could not be improved upon substantially (as per Oudin et al., 2008). This implies that it is likely that no broad-scale vegetation-based ecohydrological relation exists that is generally applicable.

Vegetation information made the greatest contribution to the Budyko model at the coarse temporal scale (i.e., long-term annual average) and the moderate spatial scale (i.e., the phase-offset models). Here vegetation-related variables explained more of the scatter than did climatic ones, with F_r–related variables being more important than either F_t or F_p. This result relates to only to spatial variability, meaning that, as one moves from catchment to catchment, it is the changes in F_r that most determine the differences in those catchments' average scatter. Recurrent fPAR approximates the cover from non-forest vegetation types. Oudin et al. (2008) also found that non-forest cover has more influence on (spatial) hydrological variability than forest cover. These results have confirmed part of the hypothesis of this work—that the incorporation of vegetation information into the Budyko model might improve the model's accuracy at smaller *spatial* scales.

The results from both the long-term and the annual pooled catchment analyses were very similar (i.e., compare Figure 6 and Table 3 with Figure 9 and Table 5). Each identified σ_P as the variable most able to explain the scatter. This indicates that, across large enough areas, the drivers of variation in ε_o are similar irrespective of the temporal scale of analysis. However, of these two pooled models, that describing long-term variability was most accurate.

In contrast to the long-term analyses in which the model variables changed substantially across spatial scales, the variables in the annual analyses changed little with spatial scale (c.f. Table 5, 6 and 7). In all cases the variability in precipitation dominated modelling, leading to the conclusion that the effect of non-steady-state conditions is a more important source of variation at the annual scale than any ecological or geophysical

processes. In Donohue et al. (2007) we highlighted several studies (e.g., Talsma and Gardner, 1986; Calder et al., 1997) in which ΔS_w was shown to be large at annual scales (sometimes greater than P itself) and Leblanc et al. (2009) recently showed that over the Murray Darling Basin (~$1x10^6$ km^2) annual storage can vary by up to twice the basin-average stream flow. Donohue et al. (2007) suggested that, as vegetation in drier landscapes is the integrated response of all processes that determine the availability of water (e.g., Eagleson, 1982; Specht, 1972), dynamic measures of vegetation attributes might contain some information about ΔS_w and that incorporating vegetation dynamics into the Budyko model might lessen the requirement for steady state conditions. These results have shown this not to be true and hence partially disprove the hypothesis of this work—that the incorporation of vegetation information into the Budyko model might improve the model's accuracy at smaller *temporal* scales. This does not mean that vegetation processes are not important in determining hydrological variability at annual or finer time-scales, but that the role of such processes can not be clearly observed until steady state conditions are established. Additionally, it is still plausible that vegetation information might improve Budyko model accuracy at annual scales if steady state conditions could be established within the modelling.

Even though the annual time-step models' variables were reasonably constant across spatial scales, the predictive accuracy of these models did change, increasing as the spatial scale became finer. The accuracy of the annual 1-parameter models increased by 4%, 5% and 27% for the pooled, phase-offset, and individual catchment models, respectively, over the original Budyko model. This pattern was also found in the annual average analyses and seems to be a general phenomenon. The individual catchment modelling provided the greatest predictive accuracy out of all the models (a predictive error of 52 $mm.yr^{-1}$ or 28% of average stream flow). This is a logical result as developing a model per catchment maximised the ability of analyses to incorporate localised processes.

It should be emphasised that the models developed in the individual catchment analyses describe only temporal dynamics. As if to emphasise this point, the spatial distribution of individual catchment model variables appears to be random (see Figure 12). This may be a true reflection of the distribution of temporal drivers of hydrological variability but it is likely that this randomness is due to non-steady-state conditions masking the true nature of the underlying drivers of variability.

Despite constraining the scatter models to include only one parameter, the interpretation of these models is difficult. These models remain empirical, revealing only which variables are most correlated to the scatter. Nor do they identify whether a combination of processes are operating. Further, many of the variables used here are highly correlated, most particularly precipitation and fPAR. Whilst we attempted some interpretation, a physically based model that incorporates dynamics of water storage is required to properly identify the drivers of the Budyko scatter.

6.7 Conclusions

We tested the hypothesis that the incorporation of remotely sensed fPAR data into Budyko's hydrological model would increase the model's accuracy, especially at smaller spatial and temporal scales. This was achieved by developing, at several temporal and spatial scales, linear 1-parameter models that predicted the 'Budyko scatter'—the observed variability in actual evaporation and stream flow not accounted for by the original model formulation. Using only three primary time-series variables of monthly precipitation, potential evaporation and total fPAR, we developed numerous secondary variables describing the averages, variability and seasonality in these primary variables, including in the persistent (perennial vegetation cover) and recurrent (annual vegetation cover) components of total fPAR. Linear regressions were performed to ascertain which of the secondary variables explained most of the Budyko scatter. Thus, in combining Budyko's original model with the linear models of scatter, we were able to predict stream flow using three primary time-series variables that are easily derived from available spatio-temporal datasets.

A database of 221 catchments from across Australia with long-term stream flow records was used. Models of scatter were developed at two different temporal scales (long-term annual averages, which approximate steady-state conditions, and annual values) and at three spatial scales ranging from coarse scale (all catchments pooled), moderate scale (catchments stratified by the temporal differences in the seasonality of precipitation and potential evaporation) to fine scale (individual catchment models).

Models in which all catchments were pooled showed that variability in precipitation best explained the observed scatter in both annual average and annual data. The

predictive error of the annual average model was less than the annual model (36 and 50% of average stream flow, respectively). When modelling long-term scatter, a decrease in spatial scale, using the climate-phase-offset stratification, showed that vegetation-related variables best explained the scatter in six out of the seven models, and improved model accuracy by 10% compared to the original Budyko model. The vegetation characteristics shown to be of greatest importance related to recurrent fPAR (~annual vegetation cover). At the long-term temporal scale, these analyses confirm the hypothesis that vegetation information can increase the accuracy of the Budyko model at smaller spatial scales.

By contrast, when modelling annual scatter, at all spatial scales the dominant model variables related to variation in precipitation. Vegetation-related variables were rarely identified as being important. Consequently, these analyses disprove the hypothesis that vegetation information may increase the accuracy of the Budyko model at finer temporal scales. This result is interpreted as being due to the effect of changes in stored water—a source of variability that dynamic vegetation information could not explain. However, further research is required to conclude whether vegetation information may be effective in describing annual Budyko scatter if steady state conditions were to be established at that time-scale.

Using these results to identify which ecohydrological processes most affect the scatter is difficult. Part of this difficulty is the source of variation. In the annual average modelling the source of variation was space only—such models (which include the original Budyko model) described the spatial variability in average catchment behaviour. In most of the annual models the source of variation was both space and time making model interpretation extremely difficult. The exception to this was the individual catchment modelling in which only temporal processes were captured. To gain substantial insight into the ecohydrological processes causing the Budyko scatter—and most particularly the temporal processes—a physically based model that can incorporate vegetation information and account for non-steady-state conditions is needed.

6.8 Acknowledgements

We would like to thank Lu Zhang, Tom Van Niel for comments that improved earlier drafts of this manuscript.

6.9 References

Asrar G, Fuchs M, Kanemasu ET and Hatfield JL (1984) Estimating absorbed photosynthetic radiation and leaf-area index from spectral reflectance in wheat. Agronomy Journal, 76, 300-306.

Berry SL and Roderick ML (2002) Estimating mixtures of leaf functional types using continental-scale satellite and climatic data. Global Ecology and Biogeography, 11, 23-39.

Budyko MI (1974) Climate and life. edition. Academic, New York, 508 pp.

Calder IR, Rosier PTW, Prasanna KT and Parameswarappa S (1997) Eucalyptus water use greater than rainfall input-a possible explanation from southern India. Hydrology and Earth System Sciences, 1, 249-256.

Choudhury BJ (1999) Evaluation of an empirical equation for annual evaporation using field observations and results from a biophysical model. Journal of Hydrology, 216, 99-110.

DEWHA (2008) Interim Biogeographic Regionalisation for Australia (IBRA), version 6.1 (sub-regions). Australian Government Department of the Environment, Water, Heritage and the Arts, Canberra. Accessed 2 June 2009. Available at < http://www.environment.gov.au/metadataexplorer/explorer.jsp >

Donohue RJ, McVicar TR and Roderick ML (2009a) Assessing the ability of potential evaporation formulations to capture the dynamics in evaporative demand within a changing climate. Journal of Hydrology, Submitted manuscript.

Donohue RJ, McVicar TR and Roderick ML (2009b) Climate-related trends in Australian vegetation cover as inferred from satellite observations, 1981–2006. Global Change Biology, 15, 1025-1039. DOI: 10.1111/j.1365-2486.2008.01746.x

Donohue RJ, Roderick ML and McVicar TR (2007) On the importance of including vegetation dynamics in Budyko's hydrological model. Hydrology and Earth System Sciences, 11, 983-995.

Donohue RJ, Roderick ML and McVicar TR (2008) Deriving consistent long-term vegetation information from AVHRR reflectance data using a cover-triangle-based framework. Remote Sensing of Environment, 112, 2938-2949 DOI:10.1016/j.rse.2008.02.008.

Dooge JCI, Bruen M and Parmentier B (1999) A simple model for estimating the sensitivity of runoff to long-term changes in precipitation without a change in vegetation. Advances in Water Resources, 23, 153-163.

Eagleson PS (1982) Ecological optimality in water-limited natural soil-vegetation systems .1. theory and hypothesis. Water Resources Research, 18, 325-340.

Fu BP (1981) On the calculation of the evaporation from land surface (in Chinese). Scientia Atmospherica Sinica, 5, 23-31.

Gill TK, Armston JD, Phinn SR and Pailthorpe BA (2006) A comparison of MODIS time-series decomposition methods for estimating evergreen foliage cover. Canberra. < http://www.arspc.org/abstract/13.htm >.

Gill TK, Phinn SR, Armston JD and Pailthorpe BA (2009) Estimating tree-cover change in Australia: challenges of using the MODIS vegetation index product. International Journal of Remote Sensing, 30, 1547-1565. 10.1080/01431160802509066

Hickel K and Zhang L (2006) Estimating the impact of rainfall seasonality on mean annual water balance using a top-down approach. Journal of Hydrology, 331, 409-424.

Jones D, Wang W and Fawcett R (2007) Climate data for the Australian Water Availability Project. Final Milestone Report. Australian Government Bureau of Meteorology.

Koster RD and Suarez MJ (1999) A simple framework for examining the interannual variability of land surface moisture fluxes. Journal of Climate, 12, 1911-1917.

Leblanc MJ, Tregoning P, Ramillien G, Tweed SO and Fakes A (2009) Basin-scale, integrated observations of the early 21st century multiyear drought in southeast Australia. Water Resources Research, 45.

Lu H, Raupach MR, McVicar TR and Barrett DJ (2003) Decomposition of vegetation cover into woody and herbaceous components using AVHRR NDVI time series. Remote Sensing of Environment, 86, 1-18.

Milly PCD (1994a) Climate, interseasonal storage of soil-water, and the annual water-balance. Advances in Water Resources, 17, 19-24.

Milly PCD (1994b) Climate, soil water storage, and the average annual water balance. Water Resources Research, 30, 2143-2156.

Nash J and Sutcliffe J (1970) River flow forecasting through conceptual models - Part I - A discussion of principles. Journal of Hydrology, 10, 282-290.

Ol'dekop EM (1911) On evaporation from the surface of river basins. Transactions on meteorological observations., 4.

Oudin L, Andreassian V, Lerat J and Michel C (2008) Has land cover a significant impact on mean annual streamflow? An international assessment using 1508 catchments. Journal of Hydrology, 357, 303-316.

Peel MC, Chiew FHS, Western AW and McMahon TA (2000) Extension of unimpaired monthly streamflow data and regionalisation of parameter values to estimate streamflow in ungauged catchments. National Land and Water Resources Audit, Canberra. Available at < http://audit.ea.gov.au/anra/water/docs/national/Streamflow/Streamflow.pdf >

Penman HL (1948) Natural evaporation from open water, bare soil and grass. Proceedings of the Royal Society of London A, 193, 120-145.

Porporato A, Daly E and Rodriguez-Iturbe I (2004) Soil water balance and ecosystem response to climate change. American Naturalist, 164, 625-632.

Potter NJ, Zhang L, Milly PCD, McMahon TA and Jakeman AJ (2005) Effects of rainfall seasonality and soil moisture capacity on mean annual water balance for Australian catchments. Water Resources Research, 41. DOI: 10.1029/2004WR003697.

Roderick ML, Berry SL, Saunders AR and Noble IR (1999) On the relationship between the composition, morphology and function of leaves. Functional Ecology, 13, 696-710.

Sankarasubramanian A and Vogel RM (2003) Hydroclimatology of the continental United States. Geophysical Research Letters, 30.

Schreiber P (1904) Über die Beziehungen zwischen dem Niederschlag und der Wasserführung der Flüsse in Mitteleuropa. Meteorologische Zeitschrift, 21.

Specht RL (1972) Water use by perennial evergreen plant communities in Australia and Papua New Guinea. Australian Journal of Botany, 20, 273-299.

Stern H, de Hoedt G and Ernst J (2000) Objective classification of Australian climates. Australian Meteorological Magazine, 49, 87-96.

Stewart JB, Smart RV, Barry SC and Veitch SM (2001) 1996/97 Land Use of Australia - Final Report for Project BRR5. National Land and Water Resources Audit, Canberra.

Sturman A and Tapper N (2005) The Weather and Climate of Australia and New Zealand. 2nd edition. Oxford University Press, Melbourne, 541 pp.

Talsma T and Gardner EA (1986) Soil-water extraction by a mixed Eucalypt forest during a drought period. Australian Journal of Soil Research, 24, 25-32.

Thackway R, Donohue RJ and Smart R (2004) Integrated Regional Vegetation Information - A compilation of vegetation types for National Action Plan and Natural Heritage Trust regions. Bureau of Rural Sciences, Canberra.

Yang DW, Shao WW, Yeh PJF, Yang HB, Kanae S and Oki T (2009) Impact of vegetation coverage on regional water balance in the nonhumid regions of China. Water Resources Research, 45.

Yang DW, Sun FB, Liu ZY, Cong ZT, Ni GH and Lei ZD (2007) Analyzing spatial and temporal variability of annual water-energy balance in nonhumid regions of China using the Budyko hypothesis. Water Resources Research, 43. DOI: 10.1029/2006WR005224

Yang HB, Yang DW, Lei ZD and Sun FB (2008) New analytical derivation of the mean annual water-energy balance equation. Water Resources Research, 44.

Yokoo Y, Sivapalan M and Oki T (2008) Investigating the roles of climate seasonality and landscape characteristics on mean annual and monthly water balances. Journal of Hydrology, 357, 255-269.

Zhang L, Dawes WR and Walker GR (2001) Response of mean annual evapotranspiration to vegetation changes at catchment scale. Water Resources Research, 37, 701-708.

Zhang L, Potter N, Hickel K, Zhang YQ and Shao QX (2008) Water balance modeling over variable time scales based on the Budyko framework - Model development and testing. Journal of Hydrology, 360, 117-131. DOI: 10.1016/j.jhydrol.2008.07.021

Appendix 1. Model equations of the annual individual catchment scatter models.

Table A1. Metrics comparing observed and modelled annual stream flow for each of the 221 catchments. Values in brackets are the equivalent values derived using the original Budyko model. Slope describes the line of best fit; NSE is the Nash-Sutcliffe Efficiency; RMSE is the root mean square error ($mm.yr^{-1}$). α_p', the predicted scatter, is unitless. The percent error is the percentage that the RMSE is of average stream flow ($RMSE/Q_0' \times 100$).

Catch. No.	Catchment Name	Equation	Slope	NSE	RMSE ($mm.yr^{-1}$)	% Error
60046	Todd River (Wigley Gorge)	$\alpha_p' = -1.49\ F_t' + 0.12$	0.94 (0.05)	0.90 (-0.73)	9 (40)	31 (138)
110003	Barron River (Picnic Crossing)	$\alpha_p' = -0.0009\ \sigma_P' + 0.04$	0.97 (0.65)	0.89 (0.69)	99 (166)	21 (36)
111007	Mulgrave River (Peets Bridge)	$\alpha_p' = -0.0006\ \sigma_P' + 0.10$	0.90 (0.70)	0.90 (0.82)	174 (227)	16 (21)
112003	North Johnstone River (Glen Allen)	$\alpha_p' = -0.001\ \sigma_P' + 0.03$	1.04 (0.67)	0.92 (0.60)	139 (314)	15 (34)
117002	Black River (Bruce Highway)	$\alpha_p' = -0.65\ F_t' + 0.33$	0.98 (0.72)	1.00 (0.90)	13 (59)	9 (40)
119003	Haughton River (Powerline)	$\alpha_p' = -0.002\ \sigma_P' + 0.05$	1.00 (0.34)	0.93 (0.22)	53 (176)	31 (102)
121002	Elliott River (Guthalungra)	$\alpha_p' = -0.0022\ \sigma_P' + 0.03$	0.94 (0.30)	0.93 (0.08)	64 (228)	29 (104)
122003	Proserpine River (Peter Faust Dam)	$\alpha_p' = 0.0001\ P' - 0.09$	0.51 (1.04)	0.56 (-0.14)	100 (161)	70 (112)
125002	Pioneer River (Sarich'S)	$\alpha_p' = -2.69\ \sigma_{Fr}' + 0.21$	0.85 (0.84)	0.90 (0.85)	80 (96)	33 (39)
129001	Waterpark Creek (Byfield)	$\alpha_p' = 0.0009\ E_p' - 1.64$	0.89 (0.62)	0.91 (0.76)	117 (187)	29 (46)
130319	Bell Creek (Craiglands)	$\alpha_p' = -0.69\ F_r' + 0.12$	0.68 (0.36)	0.43 (0.01)	30 (40)	111 (148)
132001	Calliope River (Castlehope)	$\alpha_p' = -0.0011\ \sigma_P' + 0.05$	0.91 (0.47)	0.82 (0.54)	23 (38)	33 (54)
135002	Kolan River (Springfield)	$\alpha_p' = -0.0024\ \sigma_P' + 0.16$	0.90 (0.32)	0.86 (0.43)	42 (85)	45 (92)
136202	Barambah Creek (Litzows)	$\alpha_p' = -0.0008\ \sigma_P' + 0.08$	0.89 (0.82)	0.91 (0.73)	25 (44)	36 (64)
136315	Boyne River (Carters)	$\alpha_p' = -0.0001\ E_p' + 0.29$	0.80 (1.08)	0.79 (0.04)	12 (26)	66 (142)
143110	Bremer River (Adams Bridge)	$\alpha_p' = -0.021\ S_l' + 0.04$	0.78 (0.54)	0.76 (0.63)	61 (75)	44 (54)
145102	Albert River (Bromfleet)	$\alpha_p' = -0.001\ \sigma_P' + 0.12$	1.00 (0.78)	0.98 (0.87)	34 (87)	15 (38)
201001	Oxley River (Eungella)	$\alpha_p' = -0.0001\ \rho P' + 0.08$	0.97 (0.85)	0.98 (0.93)	64 (111)	11 (19)
201900	Tweed River (Uki)	$\alpha_p' = -0.69\ F_p' + 0.62$	0.97 (1.17)	0.99 (0.69)	25 (158)	7 (44)
203005	Richmond River (Wiangaree)	$\alpha_p' = -0.0001\ \rho P' + 0.18$	0.87 (0.76)	0.93 (0.86)	64 (90)	22 (31)
203010	Leycester River (Rock Valley)	$\alpha_p' = -0.0002\ \rho P' + 0.19$	0.77 (0.64)	0.90 (0.77)	84 (126)	27 (40)

Table A1. Continued...

Catch. No.	Catchment Name	Equation	Slope	NSE	RMSE ($mm.yr^{-1}$)	% Error
203030	Myrtle Creek (Rappville)	$\alpha_p' = -0.0002\ \rho P' + 0.17$	0.78 (0.62)	0.88 (0.77)	68 (93)	36 (50)
204025	Orara River (Karangi)	$\alpha_p' = -0.0012\ \sigma_P' + 0.12$	0.92 (0.69)	0.94 (0.85)	122 (189)	19 (30)
204030	Aberfoyle River (Aberfoyle)	$\alpha_p' = -0.0002\ \rho P' + 0.20$	0.50 (0.53)	0.65 (0.37)	46 (62)	48 (65)
204031	Mann River (Shannon Vale)	$\alpha_p' = -0.0002\ \rho P' + 0.25$	0.59 (0.52)	0.70 (0.41)	46 (65)	42 (59)
204033	Timbarra River (Billyrimba)	$\alpha_p' = -0.0002\ \rho P' + 0.20$	0.76 (0.61)	0.87 (0.73)	51 (74)	31 (45)
204034	Henry River (Newton Boyd)	$\alpha_p' = -0.0001\ \rho P' + 0.15$	0.82 (0.79)	0.91 (0.64)	24 (48)	27 (54)
204036	Cataract Creek (Sandy Hill)	$\alpha_p' = -0.0002\ \rho P' + 0.21$	0.70 (0.55)	0.85 (0.70)	66 (94)	34 (49)
204041	Orara River (Bawden Bridge)	$\alpha_p' = -0.0013\ \sigma_P' + 0.05$	0.90 (0.62)	0.92 (0.71)	77 (145)	22 (41)
204055	Sportsmans Creek (Gurranang Siding)	$\alpha_p' = -0.0017\ \sigma_P' + 0.11$	0.98 (0.63)	0.93 (0.74)	49 (94)	23 (44)
204056	Dandahra Creek (Gibraltar Range)	$\alpha_p' = -0.0004\ P' + 0.17$	0.94 (0.37)	0.92 (-0.15)	116 (448)	19 (74)
204067	Gordon Brook (Fine Flower)	$\alpha_p' = -0.0017\ \sigma_P' + 0.08$	0.90 (0.52)	0.83 (0.59)	93 (146)	38 (60)
205002	Bellinger River (Thora)	$\alpha_p' = -0.0002\ P' + 0.18$	0.91 (0.55)	0.91 (0.53)	92 (206)	20 (44)
205006	Nambucca River (Bowraville)	$\alpha_p' = -0.0001\ \rho P' + 0.18$	0.88 (0.91)	0.92 (0.74)	75 (132)	25 (44)
206009	Tia River (Tia)	$\alpha_p' = -0.0003\ \rho P' + 0.31$	0.65 (0.50)	0.81 (0.63)	59 (83)	35 (49)
206014	Wollomombi River (Coninside)	$\alpha_p' = -0.25\ F_p' + 0.16$	0.70 (0.63)	0.78 (0.48)	34 (52)	40 (61)
206018	Apsley River (Apsley Falls)	$\alpha_p' = -0.0001\ \rho P' + 0.16$	0.62 (0.68)	0.71 (-0.09)	36 (70)	58 (112)
206025	Salisbury Waters (Near Dangar Falls)	$\alpha_p' = -0.18\ \rho F_t' + 0.17$	0.50 (0.53)	0.66 (0.25)	41 (61)	71 (105)
207006	Forbes River (Birdwood(Filly Flat))	$\alpha_p' = -0.0003\ P' + 0.28$	0.85 (0.48)	0.90 (0.58)	109 (218)	26 (51)
207013	Ellenborough R (below Bunnoo R Jnc.)	$\alpha_p' = -0.0001\ \rho P' + 0.24$	0.85 (0.83)	0.90 (0.71)	75 (124)	23 (39)
207014	Wilson River (Avenel)	$\alpha_p' = -0.0025\ \sigma_P' + 0.17$	0.90 (0.58)	0.94 (0.74)	75 (156)	20 (42)
207015	Hastings River (Mount Seaview)	$\alpha_p' = -2.69\ \rho F_r' + 0.25$	0.73 (0.51)	0.88 (0.69)	92 (147)	31 (49)
208005	Nowendoc River (Rocks Crossing)	$\alpha_p' = -0.0002\ \rho P' + 0.22$	0.83 (0.74)	0.90 (0.68)	39 (71)	23 (42)
208006	Barrington River (Forbesdale Causeway)	$\alpha_p' = -0.0002\ P' + 0.17$	0.68 (0.42)	0.68 (0.24)	142 (216)	32 (48)
208007	Nowendoc River (Nowendoc)	$\alpha_p' = -0.0002\ P' + 0.22$	0.76 (0.49)	0.79 (0.64)	74 (97)	32 (42)
208009	Barnard River (Barry)	$\alpha_p' = -0.0091\ \sigma_{Ep}' + 0.51$	0.60 (0.45)	0.74 (0.43)	79 (117)	28 (42)
208026	Myall River (Jacky Barkers)	$\alpha_p' = -0.0002\ \rho P' + 0.21$	0.61 (0.55)	0.75 (0.67)	64 (75)	39 (45)
209002	Mammy Johnsons River (Crossing)	$\alpha_p' = 3.19\ \sigma_{Fr}' - 0.17$	0.57 (0.52)	0.63 (0.57)	107 (116)	39 (43)
209006	Wang Wauk River (Willina)	$\alpha_p' = -0.0016\ \sigma_P' + 0.08$	0.82 (0.65)	0.92 (0.79)	41 (66)	17 (28)

Table A1. Continued...

Catch. No.	Catchment Name	Equation	Slope	NSE	RMSE ($mm.yr^{-1}$)	% Error
210014	Rouchel Brook (Rouchel Brook)	$\alpha_p' = -0.0001\ \rho P' + 0.14$	0.62 (0.64)	0.79 (0.73)	48 (55)	37 (43)
210022	Allyn River (Halton)	$\alpha_p' = 2.32\ \rho F_r' - 0.32$	0.86 (0.54)	0.91 (0.25)	58 (165)	16 (46)
210040	Wybong Creek (Wybong)	$\alpha_p' = -0.14\ \rho F_t' + 0.12$	0.62 (0.63)	0.66 (0.17)	22 (34)	67 (103)
210042	Foy Brook (Ravensworth)	$\alpha_p' = -0.0004\ P' + 0.27$	0.77 (0.38)	0.78 (0.52)	47 (70)	42 (62)
210048	Wollombi Brook (Paynes Crossing)	$\alpha_p' = -0.0001\ \rho P' + 0.16$	0.82 (0.82)	0.94 (0.65)	26 (61)	26 (60)
210061	Pages River (Blandford (Bickham))	$\alpha_p' = -0.0072\ \sigma_P' + 0.30$	0.73 (0.41)	0.86 (0.59)	51 (87)	44 (75)
210082	Wollar Creek (Goulburn River)	$\alpha_p' = 0.0001\ P' - 0.04$	0.55 (1.31)	0.60 (-8.65)	9 (45)	53 (266)
210091	Merriwa River (Merriwa)	$\alpha_p' = 0.52\ \sigma_{Fp}'$	0.65 (0.59)	0.76 (-0.94)	13 (39)	40 (121)
211014	Wyong River (Yarramalong)	$\alpha_p' = -0.0015\ \sigma_P' + 0.14$	0.87 (0.66)	0.91 (0.81)	69 (99)	34 (48)
212018	Capertee River (Glen Davis)	$\alpha_p' = -0.009\ S_l' + 0.06$	0.73 (0.70)	0.38 (-1.83)	15 (33)	60 (131)
212045	Coxs River (Island Hill)	$\alpha_p' = -0.0002\ \rho P' + 0.26$	0.58 (0.49)	0.75 (0.54)	62 (85)	56 (77)
215002	Shoalhaven River (Warri)	$\alpha_p' = -0.002\ \sigma_P' + 0.07$	0.94 (0.50)	0.86 (0.49)	32 (60)	27 (51)
215004	Corang River (Hockeys)	$\alpha_p' = -0.042\ S_l' - 0.09$	0.56 (0.31)	0.73 (-0.86)	79 (209)	28 (73)
215008	Shoalhaven River (Kadoona)	$\alpha_p' = -0.027\ S_l' + 0$	0.74 (0.50)	0.85 (0.41)	51 (103)	30 (60)
216009	Buckenbowra River (Buckenbowra No.3)	$\alpha_p' = -0.0018\ \sigma_P' + 0.04$	0.87 (0.44)	0.83 (0.33)	63 (124)	30 (60)
218001	Tuross River (Tuross Vale)	$\alpha_p' = -0.0002\ \rho P' + 0.05$	0.76 (0.48)	0.87 (0.27)	58 (140)	27 (65)
218007	Wadbilliga River (Wadbilliga)	$\alpha_p' = -0.0003\ P' + 0.10$	0.91 (0.38)	0.94 (0.12)	52 (193)	22 (82)
219017	Double Creek (near Brogo)	$\alpha_p' = -0.0041\ \sigma_P' + 0.15$	0.86 (0.42)	0.93 (0.48)	50 (139)	29 (81)
220003	Pambula River (Lochiel)	$\alpha_p' = -0.0057\ \sigma_P' + 0.24$	0.94 (0.37)	0.96 (0.46)	40 (141)	24 (84)
220004	Towamba River (Towamba)	$\alpha_p' = -0.0004\ P' + 0.33$	0.89 (0.43)	0.90 (0.63)	40 (77)	35 (67)
221002	Wallagaraugh River (Princes Highway)	$\alpha_p' = -2.9\ \sigma_{Fp}' + 0.07$	0.75 (0.49)	0.84 (0.69)	48 (67)	36 (51)
221201	Cann River (West Branch) (Weeragua)	$\alpha_p' = 2.14\ F_r' - 0.18$	0.44 (0.48)	0.56 (0.23)	42 (56)	40 (53)
221210	Genoa River (The Gorge)	$\alpha_p' = -0.0008\ E_p' + 1.14$	0.40 (0.51)	0.57 (0.26)	46 (61)	63 (84)
222004	Little Plains River (Wellesley (Rowes))	$\alpha_p' = -0.0002\ \rho P' + 0.15$	0.88 (0.64)	0.59 (0.35)	31 (39)	34 (43)
222007	Wullwye Creek (Woolway)	$\alpha_p' = 0.32\ F_r' - 0.02$	0.84 (0.81)	0.74 (-0.61)	11 (27)	77 (189)
222009	Bombala River (The Falls)	$\alpha_p' = -0.0069\ \sigma_P' + 0.16$	0.98 (0.27)	0.97 (-0.11)	24 (154)	13 (84)
222015	Jacobs River (Jacobs Ladder)	$\alpha_p' = 0.0002\ P' - 0.19$	0.78 (1.13)	0.80 (0.57)	30 (44)	13 (20)
222017	Maclaughlin River (The Hut)	$\alpha_p' = -0.006\ \sigma_P' + 0.20$	0.88 (0.23)	0.86 (0.30)	33 (74)	50 (113)

Table A1. Continued...

Catch. No.	Catchment Name	Equation	Slope	NSE	RMSE ($mm.yr^{-1}$)	% Error
222202	Brodribb River (Sardine Creek)	$\alpha_p' = -0.0002\ \rho P' + 0.15$	0.92 (0.82)	0.58 (0.38)	37 (45)	29 (36)
222206	Buchan River (Buchan)	$\alpha_p' = -0.0009\ E_p' + 1.25$	1.08 (1.04)	0.91 (-0.13)	10 (37)	11 (39)
222213	Suggan Buggan River (Suggan Buggan)	$\alpha_p' = -0.0001\ \rho P' + 0.13$	1.01 (1.21)	0.75 (-0.45)	21 (50)	17 (41)
223202	Tambo River (Swifts Creek)	$\alpha_p' = 0.0002\ P' - 0.10$	0.63 (1.48)	0.59 (-3.89)	18 (63)	32 (114)
224201	Wonnangatta River (Waterford)	$\alpha_p' = -0.0001\ \rho P' + 0.09$	0.73 (0.78)	0.81 (0.75)	39 (44)	19 (21)
225213	Aberfeldy River (Beardmore)	$\alpha_p' = -0.0028\ \sigma_P' + 0.19$	0.99 (0.56)	0.95 (0.39)	20 (71)	8 (29)
225218	Freestone Creek (Briagolong)	$\alpha_p' = -0.0072\ \sigma_P' + 0.23$	0.68 (0.18)	0.74 (0.22)	59 (103)	65 (113)
225219	Macalister River (Glancairn)	$\alpha_p' = -0.86\ \sigma_{Fl}' - 0.02$	0.97 (0.76)	0.80 (0.20)	56 (113)	14 (29)
226204	La Trobe River (Willow Grove)	$\alpha_p' = 2.22\ \sigma_{Fr}' - 0.13$	0.92 (0.67)	0.92 (-0.17)	14 (54)	6 (24)
226410	Traralgon Creek (Koornalla)	$\alpha_p' = -0.0002\ \rho P' + 0.21$	0.74 (0.91)	0.90 (0.19)	24 (68)	14 (40)
227200	Tarra River (Yarram)	$\alpha_p' = 1.12\ \sigma_{Fl}' - 0.08$	0.80 (0.69)	0.85 (0.67)	29 (44)	25 (37)
227202	Tarwin River (Meeniyan)	$\alpha_p' = -0.0027\ \sigma_P' + 0.10$	0.93 (0.71)	0.91 (0.84)	30 (39)	14 (18)
228203	Eumemmering Creek (Lyndhurst)	$\alpha_p' = -0.0002\ \rho P' + 0.07$	0.87 (0.65)	0.93 (0.50)	21 (58)	12 (34)
228212	Bunyip River (Tonimbuk)	$\alpha_p' = 0.0002\ P' - 0.12$	0.56 (1.15)	0.65 (-1.62)	50 (136)	27 (74)
229215	Woori Yallock Creek (Woori Yallock)	$\alpha_p' = -0.0002\ \rho P' + 0.20$	0.98 (0.80)	0.95 (0.87)	30 (48)	11 (18)
230205	Maribyrnong River (Emu Creek Junction)	$\alpha_p' = -0.009\ S_l' + 0.06$	0.89 (0.82)	0.85 (0.62)	19 (30)	34 (54)
231213	Lerderderg River (Sardine Cr)	$\alpha_p' = 0.54\ \rho F_t' - 0.34$	0.75 (0.64)	0.74 (0.28)	54 (90)	34 (56)
233215	Leigh (Mount Mercer)	$\alpha_p' = -0.0026\ \sigma_{Ep}' + 0.19$	0.84 (0.94)	0.82 (0.64)	18 (26)	24 (35)
234200	Woady Yallock (Pitfield)	$\alpha_p' = -0.0001\ \rho P' + 0.11$	0.88 (0.87)	0.83 (0.25)	13 (28)	33 (71)
234203	Pirron Yallock Creek (Pirron Yallock)	$\alpha_p' = -0.0002\ P' + 0.17$	0.92 (0.77)	0.90 (0.55)	19 (42)	20 (45)
235203	Curdies River (Curdie)	$\alpha_p' = -0.0002\ P' + 0.17$	0.96 (0.78)	0.90 (0.70)	21 (35)	19 (31)
235211	Kennedys Creek (Kennedys Creek)	$\alpha_p' = -0.2\ F_p' + 0.18$	0.96 (0.99)	0.93 (0.15)	17 (59)	13 (43)
236203	Mount Emu Creek (Skipton)	$\alpha_p' = -0.0025\ \sigma_P' + 0.11$	0.84 (0.75)	0.87 (0.35)	12 (28)	33 (76)
236205	Merri River (Woodford)	$\alpha_p' = -0.0011\ \sigma_P' + 0.08$	0.90 (0.88)	0.88 (0.37)	14 (32)	25 (57)
236212	Brucknell Creek (Cudgee)	$\alpha_p' = -0.0027\ \sigma_P' + 0.10$	0.94 (0.68)	0.90 (0.81)	21 (29)	17 (24)
237200	Moyne River (Toolong)	$\alpha_p' = -0.0039\ \sigma_P' + 0.15$	0.95 (0.62)	0.90 (0.62)	17 (34)	25 (50)
237205	Darlot Creek (Homerton Bridge)	$\alpha_p' = 0.18\ F_p' - 0.07$	0.83 (0.69)	0.89 (0.78)	15 (20)	20 (27)
237206	Eumeralla River (Codrington)	$\alpha_p' = -0.0019\ \sigma_P' + 0.09$	0.89 (0.75)	0.85 (0.58)	17 (29)	29 (49)
238223	Wando River (Wando Vale)	$\alpha_p' = -0.41\ F_r' + 0.13$	0.75 (0.52)	0.86 (0.61)	18 (31)	24 (41)

Table A1. Continued...

Catch. No.	Catchment Name	Equation	Slope	NSE	RMSE ($mm.yr^{-1}$)	% Error
239519	Mosquito Creek (Struan)	$\alpha_p' = -0.0003\ E_p' + 0.53$	0.77 (0.69)	0.64 (-0.41)	10 (21)	39 (82)
302200	Swan River (The Grange)	$\alpha_p' = -0.0079\ \sigma_P' + 0.17$	0.82 (0.35)	0.81 (0.13)	58 (126)	31 (67)
302208	Meredith River (Swansea)	$\alpha_p' = -0.008\ \sigma_P' + 0.13$	0.94 (0.39)	0.90 (0.03)	39 (123)	20 (64)
304201	Jordan River (Mauriceton)	$\alpha_p' = 0.0003\ E_p' - 0.35$	0.99 (0.69)	1.00 (-0.06)	1 (33)	3 (99)
304206	Tyenna (Newbury)	$\alpha_p' = -0.89\ \rho F_t' + 0.52$	0.89 (1.44)	0.97 (-0.57)	9 (73)	1 (9)
307201	Davey River (below Crossing River)	$\alpha_p' = -0.0109\ \sigma_{Ep}' + 0.47$	1.03 (1.00)	0.88 (-1.45)	50 (223)	3 (13)
314207	Leven River (below Bannons Bridge)	$\alpha_p' = 0.74\ \rho F_r' - 0.10$	0.93 (0.88)	0.93 (0.88)	60 (80)	7 (9)
318852	Meander River (Strathbridge)	$\alpha_p' = -0.68\ F_t' + 0.34$	0.95 (0.70)	0.95 (0.31)	38 (141)	10 (35)
318900	Break O'Day River (Killymoon Br.)	$\alpha_p' = 0.0008\ E_p' - 0.88$	0.89 (0.76)	0.83 (0.76)	50 (60)	22 (27)
319201	Great Forester River (2Km)	$\alpha_p' = 0.93\ \rho F_t' - 0.78$	0.94 (0.66)	0.89 (0.19)	45 (123)	11 (31)
319204	Pipers River (below Yarrow Creek)	$\alpha_p' = 0.66\ F_t' - 0.57$	0.85 (0.64)	0.95 (0.33)	25 (93)	9 (33)
401009	Maragle Creek (Maragle)	$\alpha_p' = 0.94\ \sigma_{Ft}' - 0.03$	0.85 (0.91)	0.75 (0.41)	39 (61)	28 (43)
401012	Murray River (Biggara)	$\alpha_p' = -0.017\ S_2' - 0.10$	0.80 (0.62)	0.70 (-0.68)	67 (160)	18 (42)
401013	Jingellic Creek (Jingellic)	$\alpha_p' = -0.72\ \rho F_r' + 0.08$	0.89 (0.69)	0.76 (0.49)	37 (55)	26 (38)
401015	Bowna Creek (Yambla)	$\alpha_p' = 0.28\ F_p' - 0.05$	0.73 (0.83)	0.77 (0.17)	19 (37)	46 (89)
401203	Mitta Mitta River (Hinnomunjie)	$\alpha_p' = 0.0002\ P' - 0.21$	0.84 (1.65)	0.74 (-2.25)	32 (116)	12 (43)
401210	Snowy Creek (Below Granite Flat)	$\alpha_p' = -0.0001\ \rho P' + 0.11$	0.96 (0.86)	0.74 (0.68)	81 (91)	17 (19)
401212	Nariel Creek (Upper Nariel)	$\alpha_p' = 1.17\ \rho F_r' - 0.32$	0.98 (0.75)	0.81 (-1.00)	67 (218)	13 (41)
402204	Yackandandah Creek (Osbornes Flat)	$\alpha_p' = -0.0004\ E_p' + 0.62$	0.83 (1.07)	0.80 (0.42)	48 (82)	23 (39)
402206	Running Creek (Running Creek)	$\alpha_p' = -0.0006\ E_p' + 0.95$	0.79 (1.22)	0.78 (-1.10)	59 (184)	23 (71)
403205	Ovens River (Bright)	$\alpha_p' = -0.025\ S_1' + 0.18$	0.90 (0.89)	0.87 (0.60)	65 (114)	15 (26)
403213	Fifteen Mile Creek (Greta South)	$\alpha_p' = -1.09\ \rho F_r' + 0.12$	0.88 (0.85)	0.90 (0.81)	45 (65)	17 (25)
403214	Happy Valley Creek (Rosewhite)	$\alpha_p' = -0.0006\ E_p' + 0.95$	0.70 (1.03)	0.78 (-0.43)	53 (136)	28 (71)
403224	Hurdle Creek (Bobinawarrah)	$\alpha_p' = 1.09\ F_t' - 0.79$	0.85 (0.87)	0.76 (0.61)	49 (63)	27 (34)
403226	Boggy Creek (Angleside)	$\alpha_p' = -1.93\ \sigma_{Fr}' + 0.14$	0.84 (0.79)	0.84 (0.69)	54 (74)	21 (29)
405209	Acheron River (Taggerty)	$\alpha_p' = -0.0001\ \rho P' + 0.05$	0.92 (0.73)	0.88 (0.40)	61 (139)	13 (30)
405214	Delatite River (Tonga Bridge)	$\alpha_p' = -0.029\ S_1' + 0.16$	0.74 (0.78)	0.83 (0.71)	53 (69)	18 (24)

Table A1. Continued…

Catch. No.	Catchment Name	Equation	Slope	NSE	RMSE ($mm.yr^{-1}$)	% Error
405219	Goulburn River (Dohertys)	$\alpha_p' = -0.0001\ P' + 0.09$	0.90 (0.64)	0.91 (0.40)	50 (130)	11 (29)
405226	Pranjip Creek (Moorilim)	$\alpha_p' = -0.014\ S_l' + 0.04$	0.70 (0.60)	0.85 (0.71)	22 (31)	30 (43)
405228	Hughes Creek (Tarcombe Road)	$\alpha_p' = -0.25\ \rho F_l' + 0.12$	0.83 (0.81)	0.89 (0.69)	25 (44)	16 (29)
405237	Seven Creeks (Euroa Township)	$\alpha_p' = -0.32\ \rho F_p' + 0.06$	0.97 (0.83)	0.94 (0.62)	25 (63)	12 (30)
406213	Campaspe River (Redesdale)	$\alpha_p' = -0.0002\ P' + 0.13$	0.90 (0.62)	0.87 (0.76)	31 (44)	27 (38)
406214	Axe Creek (Longlea)	$\alpha_p' = -0.0027\ \sigma_P + 0.08$	0.77 (0.55)	0.85 (0.67)	17 (26)	30 (47)
407220	Bet Bet Creek (Norwood)	$\alpha_p' = -0.0027\ \sigma_P' + 0.08$	0.71 (0.52)	0.73 (0.60)	21 (25)	41 (48)
407221	Jim Crow Creek (Yandoit)	$\alpha_p' = -1.89\ \sigma_{Fp}' + 0.08$	0.62 (0.52)	0.64 (0.47)	51 (62)	43 (52)
408202	Avoca River (Amphitheatre)	$\alpha_p' = -0.96\ \sigma_{Fp}' + 0.03$	0.82 (0.45)	0.85 (0.53)	20 (35)	31 (55)
410038	Adjungbilly Creek (Darbalara)	$\alpha_p' = -0.0008\ E_p' + 1.23$	0.66 (0.84)	0.63 (0.32)	50 (68)	26 (35)
410044	Muttama Creek (Coolac)	$\alpha_p' = -0.43\ F_r' + 0.14$	0.61 (0.47)	0.57 (0.32)	26 (33)	50 (63)
410047	Tarcutta Creek (Old Borambola)	$\alpha_p' = -0.003\ \sigma_P' + 0.11$	0.95 (0.69)	0.62 (0.43)	32 (39)	33 (40)
410048	Kyeamba Creek (Ladysmith)	$\alpha_p' = -0.0075\ \sigma_P' + 0.24$	0.77 (0.33)	0.90 (0.41)	19 (47)	31 (76)
410057	Goobarragandra River (Lacmalac)	$\alpha_p' = -0.0002\ \rho P' + 0.10$	0.98 (0.64)	0.72 (-0.39)	71 (159)	19 (42)
410061	Adelong Creek (Batlow Road)	$\alpha_p' = -0.001\ E_p' + 1.53$	0.65 (0.68)	0.74 (0.29)	48 (79)	21 (34)
410096	Mountain Creek (Thomond North)	$\alpha_p' = -0.0065\ \sigma_{Ep}' + 0.46$	0.87 (0.62)	0.64 (-0.10)	34 (60)	21 (37)
410097	Billabong Creek (Aberfeldy)	$\alpha_p' = 0.28\ \rho F_t' - 0.16$	0.76 (0.62)	0.66 (0.58)	29 (33)	47 (54)
410141	Micaligo Creek (Michelago)	$\alpha_p' = -0.0005\ E_p' + 0.83$	0.88 (0.95)	0.83 (-2.44)	10 (48)	40 (190)
410705	Molonglo River (Burbong Bridge)	$\alpha_p' = -0.018\ S_l' + 0.08$	0.94 (0.65)	0.73 (-0.42)	20 (47)	42 (98)
410730	Cotter (Gingera)	$\alpha_p' = 0.0002\ P' - 0.21$	0.74 (1.01)	0.73 (0.55)	54 (70)	20 (26)
410731	Gudgenby (Tennent)	$\alpha_p' = -0.0004\ E_p' + 0.73$	0.84 (1.22)	0.59 (-2.91)	26 (83)	41 (131)
410734	Queanbyan (Tinderry)	$\alpha_p' = 1.89\ \sigma_{Fr}' - 0.09$	0.83 (0.94)	0.82 (-0.13)	26 (65)	33 (83)
410736	Orroral (Crossing)	$\alpha_p' = 0.0002\ P' - 0.13$	0.63 (1.62)	0.65 (-4.17)	30 (115)	31 (119)
412063	Lachlan River (Gunning)	$\alpha_p' = -0.0059\ \sigma_P' + 0.2$	0.73 (0.25)	0.75 (0.27)	35 (60)	39 (67)
412066	Abercrombie River (Hadley No.2)	$\alpha_p' = -0.004\ \sigma_P' + 0.15$	0.89 (0.50)	0.88 (0.63)	31 (54)	28 (49)
412068	Goonigal Creek (Gooloogong)	$\alpha_p' = -0.006\ S_l' + 0.04$	0.79 (0.79)	0.25 (-0.70)	19 (28)	86 (127)
412071	Canomodine Creek (Canomodine)	$\alpha_p' = -0.0004\ E_p' + 0.81$	0.83 (0.30)	-0.36 ()	18 (62)	90 (312)
412073	Nyrang Creek (Nyrang)	$\alpha_p' = -0.0019\ \sigma_{Ep}' + 0.19$	0.91 (1.06)	0.62 (-3.03)	11 (39)	69 (245)

Table A1. Continued...

Catch. No.	Catchment Name	Equation	Slope	NSE	RMSE ($mm.yr^{-1}$)	% Error
412076	Bourimbla Creek (Cudal)	$\alpha_p' = -0.0042\ \sigma_P' + 0.11$	0.39 (0.15)	0.44 (0.10)	107 (135)	80 (100)
412096	Pudmans Creek (Kennys Creek Road)	$\alpha_p' = -0.6\ F_r' + 0.15$	0.60 (0.39)	0.66 (0.31)	36 (52)	35 (51)
412110	Bolong River (Giddigang Creek)	$\alpha_p' = -0.0046\ \sigma_P' + 0.19$	0.63 (0.31)	0.66 (0.41)	63 (84)	49 (65)
415207	Wimmera River (Eversley)	$\alpha_p' = -0.0079\ \sigma_{Ep}' + 0.57$	0.86 (0.34)	0.91 (0.14)	13 (42)	15 (49)
416008	Beardy River (Haystack)	$\alpha_p' = -0.012\ S_1' + 0.04$	0.74 (0.68)	0.85 (0.77)	22 (28)	31 (40)
416020	Ottleys Creek (Coolatai)	$\alpha_p' = 0.29\ \sigma_{Fp}' + 0.02$	0.73 (0.86)	0.81 (0.45)	15 (26)	42 (73)
416022	Severn River (Fladbury)	$\alpha_p' = -0.0045\ \sigma_{Ep}' + 0.29$	0.76 (0.80)	0.85 (0.33)	21 (45)	26 (56)
416023	Deepwater River (Bolivia)	$\alpha_p' = -0.0048\ \sigma_{Ep}' + 0.31$	0.81 (0.89)	0.88 (0.45)	22 (48)	28 (60)
416036	Campbells Creek (Near Beebo)	$\alpha_p' = -0.15\ F_r' + 0.04$	1.08 (1.11)	0.93 (0.48)	6 (18)	32 (96)
418005	Copes Creek (Kimberley)	$\alpha_p' = -0.01\ S_1' + 0.03$	0.61 (0.55)	0.77 (0.70)	34 (38)	39 (44)
418015	Horton River (Rider (Killara))	$\alpha_p' = -0.0045\ \sigma_{Ep}' + 0.32$	0.66 (0.55)	0.77 (0.58)	21 (28)	31 (41)
418016	Warialda Creek (Warialda No.2)	$\alpha_p' = 0.011\ S_2'$	0.95 (0.82)	0.89 (0.61)	12 (23)	26 (49)
418017	Myall Creek (Molroy)	$\alpha_p' = 0.06$	0.78 (0.85)	0.80 (0.40)	15 (27)	42 (75)
418021	Laura Creek (Laura)	$\alpha_p' = -0.5\ F_t' + 0.35$	0.61 (0.41)	0.67 (0.52)	46 (55)	47 (56)
418025	Halls Creek (Bingara)	$\alpha_p' = -0.0001\ \rho P' + 0.09$	0.77 (0.72)	0.68 (0.39)	22 (31)	46 (64)
418027	Horton River (Horton Dam Site)	$\alpha_p' = -0.025\ S_1' - 0.04$	0.76 (0.45)	0.76 (0.15)	67 (127)	32 (60)
418032	Tycannah Creek (Horseshoe Lagoon)	$\alpha_p' = 0.0001\ P' - 0.02$	0.90 (1.44)	0.91 (-0.66)	9 (38)	24 (102)
419010	Macdonald River (Woolbrook)	$\alpha_p' = -0.0002\ P' + 0.16$	0.74 (0.57)	0.79 (0.71)	50 (59)	34 (41)
419029	Halls Creek (Ukolan)	$\alpha_p' = -0.83\ \sigma_{Fr}' + 0.08$	0.64 (0.59)	0.73 (0.53)	26 (34)	53 (69)
419035	Goonoo Goonoo Creek (Timbumburi)	$\alpha_p' = -0.21\ \rho F_p' + 0.13$	0.64 (0.65)	0.75 (0.44)	32 (49)	52 (79)
419044	Maules Creek (Damsite)	$\alpha_p' = 0.0001\ P' - 0.07$	0.75 (1.74)	0.78 (-2.30)	15 (62)	36 (148)
419047	Ironbark Creek (Woodsreef)	$\alpha_p' = -0.0033\ \sigma_{Ep}' + 0.25$	0.61 (0.70)	0.79 (0.50)	21 (33)	42 (66)
419053	Manilla River (Black Springs)	$\alpha_p' = -0.0031\ \sigma_{Ep}' + 0.24$	0.60 (0.67)	0.66 (0.34)	28 (39)	52 (73)
419054	Swamp Oak Creek (Limbri)	$\alpha_p' = -0.009\ S_1' + 0.06$	0.69 (0.72)	0.79 (0.50)	30 (46)	38 (58)
419072	Baradine Creek (Kienbri No.2)	$\alpha_p' = 0.0001\ P' - 0.02$	0.43 (0.84)	0.49 (-2.39)	16 (43)	101 (270)
420010	Wallumburrawang Creek (Bearbung)	$\alpha_p' = 0.0001\ P' - 0.03$	0.62 (1.22)	0.67 (-2.20)	14 (44)	67 (211)
421018	Bell River (Newrea)	$\alpha_p' = -0.011\ S_1' + 0.03$	0.82 (0.68)	0.83 (0.69)	18 (24)	32 (42)
421026	Turon River (Sofala)	$\alpha_p' = -0.0078\ \sigma_{Ep}' + 0.53$	0.60 (0.48)	0.79 (0.64)	45 (59)	49 (64)

Table A1. Continued...

Catch. No.	Catchment Name	Equation	Slope	NSE	RMSE ($mm.yr^{-1}$)	% Error
421048	Little River (Obley No.2)	$\alpha_p' = -0.0035\ \sigma_P' + 0.12$	0.66 (0.26)	0.70 (0.35)	47 (68)	70 (101)
421050	Bell River (Molong)	$\alpha_p' = -0.0024\ \sigma_P' + 0.08$	0.65 (0.40)	0.71 (0.49)	48 (63)	47 (62)
421055	Coolbaggie Creek (Rawsonville)	$\alpha_p' = -0.0015\ \sigma_P' + 0.05$	0.55 (0.40)	0.67 (0.55)	22 (26)	63 (74)
421056	Coolaburragundy River (Coolah)	$\alpha_p' = -0.0002\ \rho P' + 0.17$	0.54 (0.48)	0.70 (0.40)	25 (35)	31 (43)
421068	Spicers Creek (Saxa Crossing)	$\alpha_p' = -0.0003\ E_p' + 0.62$	1.05 (1.33)	0.61 (-8.36)	8 (42)	74 (389)
421076	Bogan River (Peak Hill No.2)	$\alpha_p' = -0.0014\ \sigma_P' + 0.06$	0.84 (0.47)	0.85 (0.62)	14 (22)	51 (81)
421084	Burrill Creek (Mickibri)	$\alpha_p' = -0.0021\ \sigma_P' + 0.09$	0.83 (0.36)	0.87 (0.49)	17 (34)	51 (102)
421101	Campbells River (Ben Chifley Dam)	$\alpha_p' = -0.024\ S_1' + 0.11$	0.84 (0.69)	0.88 (0.29)	23 (57)	24 (59)
426504	Finniss River (4Km East Of Yundi)	$\alpha_p' = -0.0045\ \sigma_P' + 0.19$	1.07 (0.65)	0.72 (0.31)	35 (55)	26 (41)
505504	North Para River (Turretfield)	$\alpha_p' = 0.24\ \rho F_p' - 0.03$	1.13 (1.08)	0.92 (0.86)	7 (9)	28 (35)
505532	Light River (Mingays Waterhole)	$\alpha_p' = 0.0001\ P' - 0.03$	0.94 (1.55)	0.92 (0.20)	4 (15)	35 (132)
506500	Wakefield River (Near Rhynie)	$\alpha_p' = -0.0001\ \rho P' + 0.06$	1.22 (1.25)	0.82 (0.45)	7 (13)	42 (78)
507500	Hill River (Andrews)	$\alpha_p' = -0.009\ S_2' + 0.02$	1.08 (1.12)	0.91 (0.72)	5 (10)	29 (59)
507501	Hutt River (Near Spalding)	$\alpha_p' = -0.0013\ \sigma_P' + 0.05$	1.03 (0.90)	0.94 (0.86)	5 (9)	25 (45)
509503	Kanyaka Creek (Sth Of Hawker)	$\alpha_p' = -0.0017\ \sigma_{Ep}' + 0.14$	0.76 (0.40)	0.49 (-0.66)	4 (7)	174 (304)
513501	Rocky River (Flinders Chase(Ki))	$\alpha_p' = -1.53\ \sigma_{Fp}' + 0.06$	0.88 (0.81)	0.78 (0.51)	25 (37)	33 (49)
601001	Young River (Neds Corner)	$\alpha_p' = 0.27\ \sigma_{Fp}'$	0.60 (0.75)	0.63 (0.28)	4 (6)	95 (143)
603004	Hay River (Sunny Glen)	$\alpha_p' = -0.0021\ \sigma_P' + 0.11$	0.99 (0.62)	0.84 (0.28)	13 (27)	25 (51)
603136	Denmark River (Mt Lindesay)	$\alpha_p' = -0.0004\ E_p' + 0.63$	0.74 (0.78)	0.81 (-0.76)	14 (43)	27 (83)
604001	Kent River (Rocky Glen)	$\alpha_p' = -0.0022\ \sigma_P' + 0.09$	0.93 (0.48)	0.82 (0.32)	9 (17)	32 (60)
606001	Deep River (Teds Pool)	$\alpha_p' = -0.001\ \sigma_P' + 0.13$	0.91 (0.85)	0.86 (-1.34)	16 (68)	18 (77)
608151	Donnelly River (Strickland)	$\alpha_p' = -0.0006\ E_p' + 0.97$	0.83 (0.68)	0.87 (0.68)	21 (34)	16 (26)
610001	Margaret River (Willmots Farm)	$\alpha_p' = -0.0018\ \sigma_P' + 0.12$	0.98 (0.63)	0.90 (0.74)	26 (42)	13 (21)
611111	Thomson Brook (Woodperry Homestead)	$\alpha_p' = -0.0014\ \sigma_P' + 0.07$	0.94 (0.61)	0.96 (0.75)	12 (29)	10 (25)
613002	Harvey River (Dingo Rd)	$\alpha_p' = -0.73\ \rho F_r'$	0.78 (0.65)	0.86 (0.11)	30 (75)	13 (33)
614196	Williams River (Saddleback Rd Br)	$\alpha_p' = -0.0031\ \sigma_P' + 0.07$	0.97 (0.31)	0.95 (-0.45)	6 (34)	12 (68)
3080003	Franklin River (Mt Fincham)	$\alpha_p' = -1.05\ \sigma_{Ft}' + 0.05$	0.83 (0.83)	0.88 (0.31)	99 (240)	5 (13)
3180010	North Esk River (Ballroom)	$\alpha_p' = 0.03\ S_1' - 0.21$	0.86 (0.82)	0.84 (0.17)	39 (91)	10 (23)

Table A1. Continued…

Catch. No.	Catchment Name	Equation	Slope	NSE	RMSE ($mm.yr^{-1}$)	% Error
3190200	Brid River (Of Tidal Limit)	$\alpha_p' = 0.37\ F_t' - 0.34$	0.94 (0.76)	0.82 (-0.12)	37 (93)	13 (33)
8140159	Seventeen Mile Creek (Waterfall View)	$\alpha_p' = 0.0005\ E_p' - 1.21$	0.72 (0.46)	0.81 (0.49)	39 (64)	31 (51)
8200045	South Aligator River (El Sharana)	$\alpha_p' = -0.0018\ \sigma_P' + 0.11$	0.75 (0.33)	0.63 (-0.51)	94 (191)	32 (65)
8210007	Magela Creek (Bowerbird Waterhole)	$\alpha_p' = 0.0019\ E_p' - 4.48$	0.76 (0.26)	0.83 (-0.66)	116 (364)	24 (77)
			0.81 (0.69)	*0.80 (0.12)*	*41 (80)*	

CHAPTER 7

Conclusions and recommendations

7.1 The value of spatio-temporal ecohydrological data

Arguably the most critical component of the body of research presented in this thesis is the generation of Australia-wide monthly grids of fPAR and potential evaporation data. Without these datasets the testing of Hypotheses I and II would have been difficult and of questionable value.

Two papers, and consequently two chapters of this thesis, are devoted to describing the generation of key datasets and to testing their fitness-for-purpose. In Chapter 3, a monthly, Australia-wide fPAR dataset is described which was developed specifically for examining the short- and long-term dynamics in vegetation-related characteristics, having been generated using an biophysical approach (as apposed to an atmospheric radiative transfer approach). Whilst the AVHRR instruments are relatively primitive and the resulting data require substantial corrections before application, the data's great value lies in their record length. The AVHRR-derived fPAR dataset of Chapter 3 is the longest, near-complete records of monthly vegetation cover for Australia and represents the first freely available dataset that describes both persistent and recurrent fPAR. Likewise, the potential evaporation data of Chapter 5 are significant. The reliability of the potential evaporation data have been thoroughly tested with respect to the accuracy of the input data and to the dynamics in the potential evaporation data themselves. The research of Chapter 5 represents the first time that a suit of potential evaporation datasets for Australia have been available—a suit that includes the fully physical Penman dataset parameterised with wind and albedo observations. Both these core datasets are freely available on-line and constitute a significant contribution to Australia's natural resource information base.

The value of having spatially and temporally explicit input data of climate and vegetation cover can not be over-stated. They enabled all analyses to be framed in fully dynamic terms and brought rigour to the analyses in which they were used. In particular, the significance and novelty of the vegetation trends work of Chapter 4 is due entirely to the underlying fPAR data. More generally, analyses of Hypotheses I and II provided new insights simply because of the availability of persistent and recurrent fPAR components. This thesis as a whole demonstrates the enormous value to ecohydrology of, and the richness of information contained within, relatively few time-series variables—namely, precipitation, potential evaporation and total fPAR. This

research has also demonstrated that if such variables are unavailable for a location or time period, they can be routinely—even operationally—generated if the underlying meteorological and remotely sensed data are available.

Perhaps the greatest limitation of the fPAR data produced in Chapter 3 is that angle of view effects have not been entirely removed. For some months and regions, where these effects were obvious, data from entire regions have been removed. Where they weren't obvious, these errors remain incorporated into the fPAR data. Such effects are most pronounced in winter months and at high latitudes, so that data covering Tasmania in particular are of low quality. Due to the relative correction methodology applied, these effects have not been quantified.

One main improvement could be made to the method used to generate the potential evaporation datasets is the temporal accuracy of the input air temperature and vapour pressure grids. These proved to be only of moderate accuracy and, just as the temporal accuracy of the wind speed grids were improved by using TIN interpolations, the air temperature and vapour pressure grids also could be recreated using a temporally accurate spatial interpolation technique. Another change that could be made to the methods—an interesting analysis in itself—would be to incorporate into the net radiation model the forcing effect of rising CO_2 concentrations. Currently it is assumed that CO_2-related long-wave irradiance is constant. It would be interesting to quantify this effect and it could prove to be an important effect to incorporate into estimates of Penman potential evaporation, especially for climate-change-related analyses.

7.2 Vegetation responses to climatic dynamics

The analyses in Chapter 4 of long-term vegetation dynamics are an assessment of the response of vegetation cover to perturbations in climatic forcings. As such it contributes towards the filling-in of coloured areas in Table 1 below (which is a summary of Table 1 of the first chapter). These tables were developed as a framework for building understanding of the dynamics between ecohydrological forcings and responses. In order to simplify the complexities in vegetation–water systems, the role of system feedbacks were ignored. This is an essential simplification if detailed systems understanding is to progress. However, in reality it is extremely difficult to identify and isolate individual forcings and to remove the effects of feedbacks from observational

data. Thus, the testing of Hypothesis I—and therefore the analyses of Chapter 4—was aimed at identifying the *net* response of fPAR to all perturbations (and inherently includes the effects of feedbacks).

Table 1. The relative certainties with which the dynamics between climate and vegetation variables are understood within water-limited environments. Those variables whose interactions are relatively well understood are highlighted in yellow and those relatively poorly understood are in red.

Change in forcing variable	WATER-LIMITED Change in response variable due to change in forcing variable		
	F_t	F_p	F_r
P			
E_p			
CO_2			

Hypothesis I was accepted because the net response of vegetation cover to changes in climatic forcings across Australia over the past 2–3 decades has been an increase in F_t. It was also shown that F_p has increased whilst F_r has decreased. Whilst the decreases in F_r were closely tied to changes in P seasonality, the increases in F_p were more uniform geographically and seasonally, and were not predominantly linked to changes in P or E_p. It is likely that this is, at least in part, a manifestation of the CO_2-fertilisation effect on vegetation in water-limited landscapes. These analyses have increased understanding of the response of the fPAR variables, as no previous studies have shown a differential response between persistent (perennial) and recurrent (annual) vegetation across an entire continent.

Notwithstanding the 'lumped' approach of these analyses (i.e., examining the net effect of all forcings and feedbacks), several inferences can be made from the testing of Hypothesis I about the role of individual forcings and responses, as per Table 1. Firstly, the dominant fPAR response has been to annual and seasonal perturbations in P. Thus understanding of the response of the three fPAR components to variations in P has been improved, particularly with respect to the responses of F_p and F_r. Secondly, there was little evidence that fPAR has responded to variations in evaporative demand (i.e., potential evaporation) in water-limited environments, which suggests a lack of sensitivity of fPAR to this forcing under such conditions (fPAR did respond to changes

in E_p in the few energy-limited areas studied). Thirdly, analyses revealed possible evidence of a CO_2-fertilisation effect, although further analyses are required to confirm this. Thus some minor gains in understanding of the response of fPAR to perturbations in CO_2 have been made. These three inferences are summarised in Table 2.

Table 2. The relative gains in the understanding of the dynamics between climatic forcings and vegetation cover responses in water-limited environments as per the analyses of Chapter 4. Purple indicates the greatest gains in understanding, and blue lesser gains. The arrows indicate the *net* response in fPAR to observed changes in all forcings across Australia over the past 2-3 decades.

Change in forcing variable	**WATER-LIMITED** Change in response variable due to change in forcing variable		
	F_t	F_p	F_r
P			
E_p			
CO_2			
Net effect of changes in all forcing variables	↑	↑	↓

The observed increases in fPAR show that the overall system response to changes in all forcings has been a shift in the dynamic equilibrium to a 'greener', more perennial cover of vegetation. In Chapter 1 it was hypothesised that, in water-limited environments, vegetation will respond to perturbations in system forcings in such a way as to maximise its water use over the long term in order to maximise its energy up-take. Given this, and that the effective availability of water across Australia has generally increased, it can be inferred from these results that this increase in total cover, and the shift away from annual towards perennial vegetation cover types, has enabled vegetation to maximise (and in many cases increase) its water use under the new dynamic equilibrium.

One challenge of great scientific and practical importance is to quantify the effects of changes in atmospheric CO_2 concentrations on ecohydrological processes. The fPAR data and analysis frameworks established in Chapter 4, as well as a potential evaporation data of Chapter 5, provide opportunities to pursue this in the future. The first step would be to quantify the relationship between changes in CO_2 and the

response to this of vegetation cover (including both persistent and recurrent) in water-limited environments. The second, and considerably harder step, would be to quantify the CO_2 effect on the catchment water fluxes in the midst of a changing climate. Such analyses could also be extended to energy-limited environments in the future. It is likely that a physically-based model will be required to achieve this which accounts for changes in, and interactions between, all the key ecohydrological variables (i.e., P, E_p, E_a, Q, CO_2, and the three fPAR variables), including changes in the seasonality of these.

7.3 Understanding vegetation dynamics as an ecohydrological forcing

The research of Chapter 2 and 6 established and tested the second hypothesis of this thesis, that the incorporation of vegetation dynamics into Budyko's hydrological model will improve that model's accuracy especially at smaller spatial and temporal scales. If this hypothesis was to be accepted, then the hydrological responses to vegetation forcings could have been examined and quantified. In turn, this would have provided a means of populating Table 1 of Chapter 1 (summarised in Table 3 below) and thereby would have substantially enhanced understanding of vegetation–water dynamics.

Table 3. The relative certainties with which the influence of perturbations in climate and vegetation forcings on water balance variables are understood. Those variables whose responses are relatively well understood are highlighted in yellow and those moderately well understood are in orange.

Change in forcing variable	WATER-LIMITED Change in response variable due to change in forcing variable	
	E_a	Q
P		
E_p		
F_t		
F_p		
F_r		

Whilst Hypothesis II was shown to hold true at the long-term annual scale (i.e., 26-year averages), it did not hold at the annual time-scale. It is at this annual scale that the biggest advances in vegetation-water systems understanding are expected to be made,

and it is information gleaned at this annual scale that is expected to be of greatest practical use. This hypothesis proposed that data describing vegetation dynamics should contain information about perturbations in all forcings, one of which is changes in stored water. Given this, an adapted Budyko model that contains dynamic vegetation information should work effectively under non-steady state conditions (i.e., at annual and sub-annual time-scales). Results showed that this is not the case and consequently Hypothesis II is rejected. A number of implications stem from this result.

Firstly, the analyses of Chapter 6 have marginally increased understanding of the role of vegetation as an ecohydrological forcing and consequently the uncertainties associated with Table 3 remain more or less unchanged.

Secondly, year to year changes in stored water can be much larger than are often expected and assuming steady state conditions at annual time-scales (e.g., Koster and Suarez, 1999; Zhang et al., 2008) should be done with great care.

Thirdly, the annual dynamics in stored water are not reflected in the annual dynamics in fPAR. A number of explanations for this are possible. 1) The annual changes in stored water are so large that vegetation cover can not respond quickly enough to such system perturbations. This seems unlikely, however, as vegetation cover across Australia generally responds to changes in the supply of water within around two months (Pook, 1984 and related papers). 2) Vegetation cover is capable of responding to such large changes in annual storage but that it is prevented from doing so by other limiting processes, such as nutrient availability or disturbances. 3) The observed annual changes in stored water may be in storages that can not be accessed by vegetation.

Fourthly, to continue examining the role of vegetation as an ecohydrological forcing at annual time-scales, steady state conditions need to first be established within the analyses. Even though Hypothesis II was disproven at this time scale, there is still reason to expect an improvement in the performance of an adapted Budyko model at annual scales when using vegetation information *if water storage changes can be accounted for*. One way to accomplish this for large catchments may be to use remotely sensed gravimetric data (e.g., Leblanc et al., 2009). Hence, the same recommendation stemming from the testing of the first hypothesis may provide a means of further testing the second hypothesis—which is to develop a simple physically based ecohydrological

model that operates at a monthly time-step, that incorporates remotely sensed fPAR data, *and* that accounts for changes in water storage. Only then might firm conclusions be made about which vegetation processes are affecting water balances, and only then are results likely to take on significance in practical management applications. The principles of vegetation optimality may provide the means of capturing the ecohydrological effects of vegetation dynamics without requiring great model complexity, nor of being restricted to any particular environment type, nor requiring detailed process knowledge of CO_2 fertilisation effects.

7.4 Recommendations

Several opportunities exist for extending the research presented in this thesis and relate generally to ways of improving the datasets created in the course of research or to ways of further exploring and extending the investigating the long-term dynamics and interactions in the key ecohydrological variables. Recommendations for future research are listed below.

- Remove viewing angle effects from the cover-triangle-corrected fPAR data, which would reduce the frequency and extent of data gaps, and increase confidence in the data over high latitudes.
- Obtain the underlying 9 am and 3 pm air temperature measurements from which spatial datasets can be created. This would avoid the problem of having vapour pressure and air temperature data that were measured at different times of the day.
- Generate grids of minimum and maximum air temperate and of actual vapour pressure using an alternative spatial interpolation technique that better reflects trends in the underlying data.
- Incorporate into the net radiation model the effects of increasing CO_2 concentrations on the incoming long-wave radiation flux. Then the trends in net radiation and in Penman potential evaporation can be re-examined to gauge the effects of CO_2 forcing alone on energy availability and evaporative demand.
- Attribute the changes in vegetation cover (perennial and annual) to the individual drivers of vegetation dynamics.
- Conduct analyses of long-term trends in stream flow so that trends in catchment water balances and catchment vegetation cover can be examined together.

- Explore the possibilities of using the fPAR and potential evaporation data from this research to quantify the effect of rising CO_2 levels on i) perennial and annual vegetation cover, and ii) actual evaporation and stream flow. This could eventually be extended to cover energy-limited landscapes.
- The albedo data produced as a part of the dynamic net radiation model showed some interesting trends that may potentially be of great significance. These have not been explored and may provide a fruitful research focus.
- Develop a simple monthly, physically based ecohydrological model that incorporates P, E_p and remotely sensed fPAR and that accounts for changes in water storage. Ideas around this are currently being explored.

7.5 References

Koster RD and Suarez MJ (1999) A simple framework for examining the interannual variability of land surface moisture fluxes. *Journal of Climate*, 12, 1911-1917.

Leblanc MJ, Tregoning P, Ramillien G, Tweed SO and Fakes A (2009) Basin-scale, integrated observations of the early 21st century multiyear drought in southeast Australia. *Water Resources Research*, 45.

Pook EW (1984) Canopy dynamics of Eucalyptus-maculata Hook.1. Distribution and dynamics of leaf populations. *Australian Journal of Botany*, 32, 387-403.

Zhang L, Potter N, Hickel K, Zhang YQ and Shao QX (2008) Water balance modeling over variable time scales based on the Budyko framework - Model development and testing. *Journal of Hydrology*, 360, 117-131. DOI: 10.1016/j.jhydrol.2008.07.021